THEORETICAL STUDY OF DICHALCOGENIDES AS BUILDING BLOCKS FOR EFFICIENT SELF-HEALING MATERIALS

DIKALKOGENUROETAN OINARRITUTAKO MATERIAL AUTOKONPONGARRIEN AZTERKETA TEORIKOA

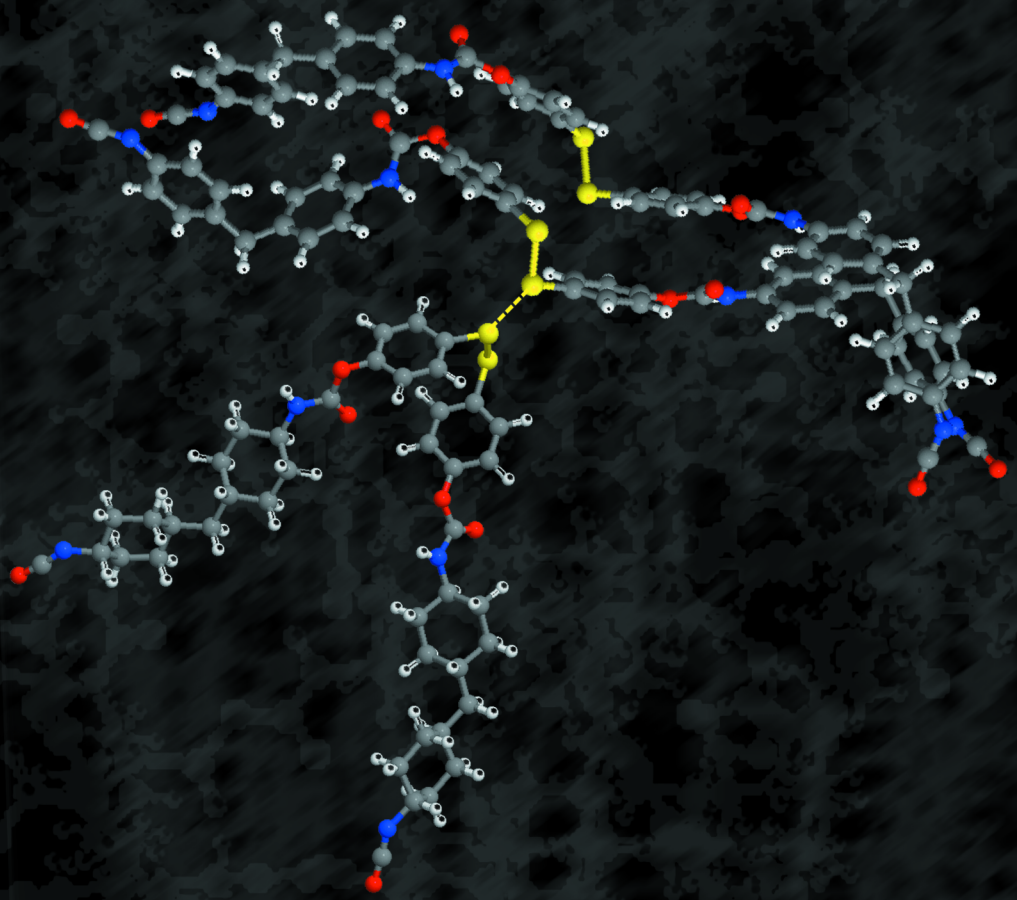

MIKEL IRIGOYEN URTASUN

2021

eman ta zabal zazu

UPV EHU

NAZIOARTEKO BIKAINTASUN CAMPUSA

CAMPUS DE EXCELENCIA INTERNACIONAL

Theoretical Study of Dichalcogenides as Building Blocks for Efficient Self-Healing Materials
Dikalkogenuroetan Oinarritutako Material Autokonpongarri Eraginkorren Azterketa Teorikoa

Thesis
Author: Mikel Irigoyen Urtasun
Directors: Jon M. Matxain and Fernando Ruipérez
Donostia - San Sebastian

June 10, 2021

"What is broken may never break, but rises again healed and recovered"

Acknowledgements

Ha llegado el momento que parecía que nunca iba a llegar. Casi 4 años después aquí estoy, intentando encontrar las palabras para describir lo que siento. En fin.

En primer lugar, me gustaría agradecer a todo el grupo por la acogida que me habéis brindado desde antes incluso de empezar este trayecto, habéis conseguido que me sienta como en casa en muchos momentos, ¡y eso no tiene precio! Pero especialmente agradecer a quién me ha enseñado que se puede ser cientifíco y disfrutar de la vida, y sobre todo a los que me han aguantado estos 4 años en el día a día, en los cafés... gracias por aguantar mis lloros y mis quejas, y los días que me despertaba con el pie izquierdo... pero sobre todo gracias por ser tan maravillosos como sois, y por aportar luz en los días oscuros, he tenido mucha suerte al poder compartir este viaje con vosotros.

Hace ya 9 años que llegué a esta ciudad, pero ahora que llega el momento de decir "adios"... Me ha costado, pero creo que me llevo un pedazo de Donosti en mí para siempre. He podido conocer gente maravillosa que me ha acogido tanto, y tan bien, que casi he sentido la necesidad de robar unas setas cada vez que iba al pueblo... casi!! Creo que no me equivoco si digo que Antiguo es mi segunda casa, y por éllo tengo que estar agradecido! No me puedo olvidar de los que empezasteis hace ya 9 años esta andadura conmigo, y aunque no todos sigáis por estos lares, si he llegado a sentirme parte de Donosti es, en gran parte, gracias a vosotros... preparad unas cervezas con hielos que la tesis me ha dado mucha sed!

A todos los que me han acompañado durante estos años, ya sea de una forma u otra, y especialmente a los que lo habéis hecho los últimos tiempos, ¡¡GRACIAS!!. Y qué decir de la gente de BISKARRET, cabrones, me habéis hecho olvidarme de la tesis cuando más necesitaba hacerlo, y darme un empujón cuando lo he necesitado, pero sobre todo, habéis hecho que me lo haya pasado de puta madre. Los que siempre habéis estado, cómo los que estáis ahora, espero que tengáis tantas ganas de celebrarlo como yo..... No voy a nombraros por que no es necesario, pero que sepais que os quiero mucho a todos, ¡CABRONES!

Agradecer también a toda mi familia, que de una forma u otra todos han aportado algo a lo largo de mi vida que me ha hecho ser lo que soy hoy en día, y estar orgulloso de quién soy y de dónde vengo. Aitatxi, has acabado saliendo en la tele antes que yo!!!

Fernando, perro del infierno!! espero no haberte provocado muchos infartos a lo largo de estos 4 años jejeje. Ahora en serio, creo que he tenido una suerte increible al haber tenido la oportunidad de trabajar contigo, pero aun más importante, de haberte conocido. Me has hecho crecer mucho como científico, pero tambien como persona, e incluso has

llegado a ampliar mi espectro musical!!! Pero, para mi, lo más importante es que me has entendido en todo momento, cuando he tenido dudas, cuando he estado más, y menos motivado, cuando estaba que no estaba, cuando estaba al limite y hasta cuando estaba a 1000 kms, y todo éllo sin llegar a sentir nunca ninguna sensación de obligación... creo que has entendido cómo soy (y mira que eso es dificil), y me has dejado hacer... Espero que estés contento conmigo, por que yo lo estoy, y mucho, contigo. Que sepas que no te pienso perdonar ni las birras ni el concierto que tenemos pendiente, aun que si quieres te perdono que me corrigieras todas las comas... jejej En definitiva, he aprendido mucho contigo y de ti, y siempre te estaré agradecido. ¡MENOS CIENCIA Y MÁS PERSONAS!

Txoni!! ¿Cuántos años han pasado desde que mandamos el primer cálculo juntos? Más de 5... y aquí seguimos... pero sin duda no estaría aquí si desde el primer momento no hubieras apostado por mí, cuando ni siquiera yo mismo era capaz de dar un duro por mi mismo, y no hay palabras para describir lo agradecido que te estoy por éllo. Han sido muchas horas compartidas, y espero que sean muchas más, ya sean de trabajo, de charla, de comida, de viaje o con unas cervezas, o todas éllas!! Gracias por todo lo que has hecho por mi, si me pongo a enumerarlo no acabaría y eso los dos lo sabemos. Ha sido un auténtico placer trabajar y aprender de un jefe como tú, pero sobre todo, de un amigo como tú, y dudo mucho que muchos en la posición en la que estoy ahora puedan decir lo que yo acabo de decir. Desde que te conocí mi vida cambió por completo, y desde entonces, en todo momento he sentido que estabas ahí para lo que hiciera falta, he sentido tus ánimos y tu apoyo incondicional, y joder Txoni, milesker denagatik, bihotzez!

No podían faltar unas lineas para tí tambien... Creo que esta tesis ha estado prácticamente igual de influenciada por tí que por mí, por tu ausencia y tu presencia, pero sobre todo por todo lo que me has ayudado y apoyado, no creo que la hubiera podido acabar si no lo hubiera tenido. Creo que ya lo sabes todo. Gracias, de corazón.

Y por último, dos de los pilares de mi vida... Andrea, qué te puedo decir que no sepas, eres increible y me siento afortunado de haber podido compartir toda una vida contigo alrededor, aun que me jodieras los legos... Sé que podría haber hecho las cosas de otra manera, quizás mejor, quizás peor... pero no creo que eso importe demasiado ahora mismo, pues siempre hemos encontrado la manera de entendernos, y ojalá que siga siendo así, Te quiero mucho enana!

¿Y qué decir de ti, viejo? Quizás no lo diga o no se me note demasiado, pero eres un referente para mí. He aprendido muchas cosas de tí sin las que no hubiera podido llegar hasta dónde he llegado, pero por muchos títulos que tenga aún no te llego a la suela de los borzegis. Dame tiempo, que llegaré. Por todo lo que has hecho estos 27 años para que yo esté aquí, gracias, este trabajo es por y para tí, Aita.

Technical and human support provided by IZO-SGI, SGIker (UPV/EHU, MICINN, GV/EJ, ERDF and ESF) is gratefully acknowledged for assistance and generous allocation of computational resources. Financial support comes from Eusko Jaurlaritza through projects PI2017-11 and IT588- 13, and the Spanish Gobernment through project CTQ2015-67660-P.

Publication List

1. **M. Irigoyen**, A. Fernandez, A. Ruiz, F. Ruipérez, J. M. Matxain, "Diselenide Bonds as an Alternative to Outperform the Efficiency of Disulfides in Self-Healing Materials" J. Org. Chem., 2019, 84 (7), pp 4200–4210. DOI: 10.1021/acs.joc.9b00014

2. A. Erice, I. Azcune, A. Ruiz de Luzuriaga, F. Ruipérez, **M. Irigoyen**, J. M. Matxain, J. M. Asua, H. J. Grande, A. Rekondo, "Effect of Regioisomerism on Processability and MechanicalProperties of Amine/Urea Exchange Based Poly(urea-urethane)Vitrimers" ACS Applied Polymer Materials, Online (2019). DOI: 10.1021/acsapm.9b00589

3. **M. Irigoyen**, J. M. Matxain, F. Ruipérez, "Effect of Molecular Structure in the Chain Mobility of Dichalcogenide-Based Polymers with Self-Healing Capacity", Polymers, 11 (12), 1960 (2019). DOI: 10.3390/polym11121960

4. Kathryn O'Harra, Naroa Sadaba, **Mikel Irigoyen**, Fernando Ruipérez, Roberto Aguirresarobe, Haritz Sardon, Jason Bara "Nearly Perfect 3D Structures Obtained by Assembly of Printed Parts of Polyamide Ionene Self-Healing Elastomer", ACS Appl. Polym. Mater., 2, 11, 4352–4359 (2020). DOI: https://doi.org/10.1021/acsapm.0c00799

5. **M. Irigoyen**, J. M. Matxain, F. Ruipérez, "Theoretical Protocol To Study The Self-Healing Character Applied to Real PU and PHMA Polymers" To be submitted.

Contents

Bibliography 171

Part I

Theoretical Study of Dichalcogenides as Building Blocks for Efficient Self-Healing Materials

Chapter 1

Introduction

The foundations of modern chemistry were laid in the 18th century by french chemist Antoine Lavoisier, who showed how chemistry could be understood in terms of finite and measurable quantities of reactants, and helped to provide the tools and conceptual basis for more accurate analysis. After that, it became possible to establish the composition of different compounds by carefully weighing both the reactants and the product(s) they form when chemically united; union that is made in the process called chemical reaction. Since then, chemists have been able to synthesize a myriad of already known and brand new chemical compounds.

1.1 Reversible Chemistry

Traditionally, the synthesis of organic compounds has been centered in kinetically controlled reactions [1], which lead to the formation of irreversible covalent bonds. In this kind of synthetic chemistry, the choose of the reagents (or catalysts) and reaction conditions is made very carefully with the aim of effectively producing a single product. In essence, a more favorable energetic pathway to the formation of a particular product, rather than other possible products, is usually the objective. For example, A goes to C rather than to B in Figure 1.1. The irreversible nature of the reaction guarantees that, once the particular product is formed, it is not possible either for the starting materials to be reformed from it or for it to be converted into another product (at least under the conditions of the reaction).

Recently, however, there has been a resurgence of interest in a branch of chemistry where the covalent bond has the ability to be formed and broken, and indeed, reformed reversibly under equilibrium control [2]. If the

equilibration process is sufficiently fast, then this so-called dynamic covalent chemistry leads to the efficient formation of products under thermodynamic control, for example, A gives B rather than C (Figure 1.1). In such reactions, it is the relative stabilities of the resulting products (ΔG_B^0 compared with ΔG_C^0 in Figure 1.1) and not the relative magnitudes ($\Delta G_B^{\neq}$ versus $\Delta G_C^{\neq}$) of the transition states to the different products (B and C) that controls the proportions of the products, so that, the proportions of the products can be controlled. Thus, the search of bonds capable of break and reform, namely, reversible bonds, has become a cornerstone in the field of reversible chemistry.

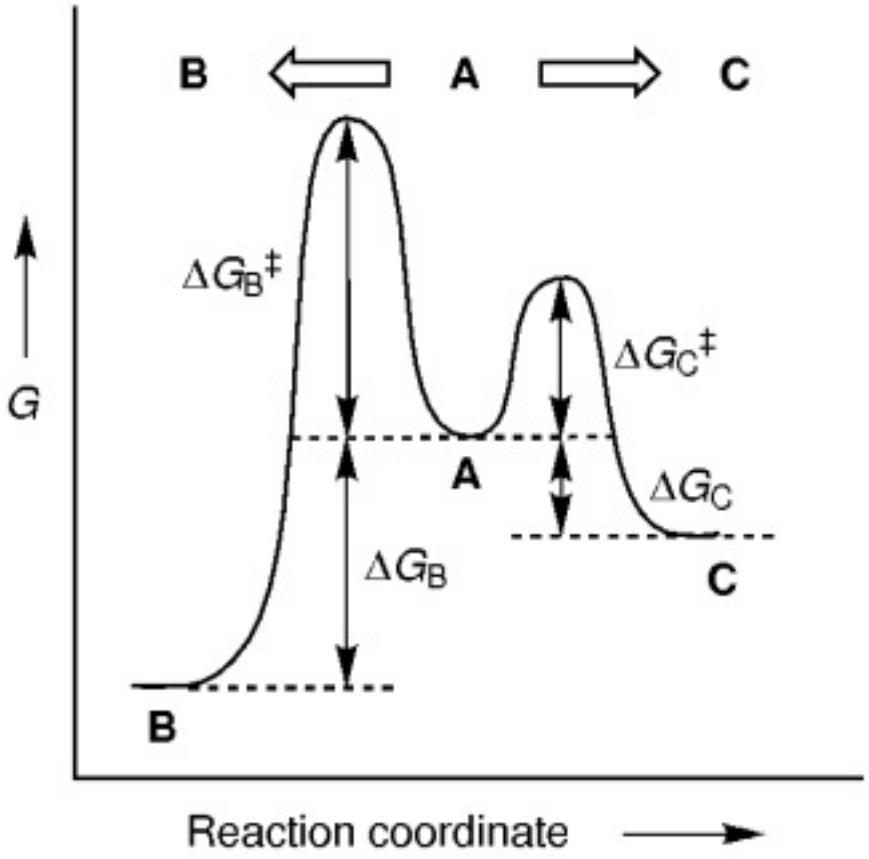

Figure 1.1: Free energy profile illustrating kinetic (A→C) versus thermodynamic (A→B) control of the product distribution. Most covalent chemistry is irreversible and so occurs under kinetic control while most supramolecular and dynamic covalent chemistry is reversible and so occurs under thermodynamic control.

A reversible bond is defined as a chemical linkage that can cleavage and re-form under equilibrium conditions, which may enable materials to be adaptable by means of structure modification to favor a more thermodynamically stable state determined by a stimulus [3, 4, 5]. There is a range of different dynamic covalent bonds, but in general, all reversible reactions can

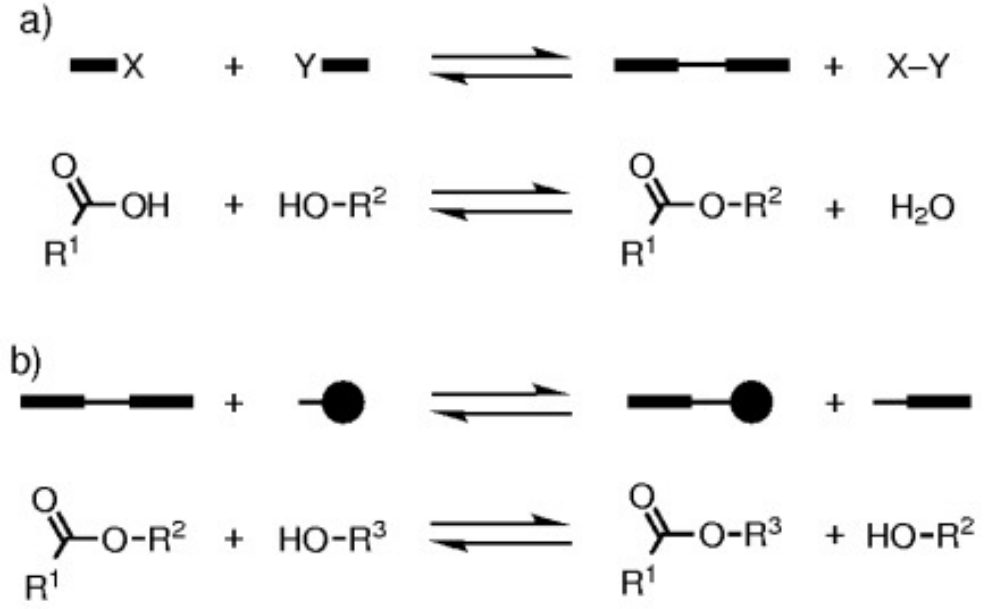

Figure 1.2: Two possible types of reversible reaction: a) involving the formation/scission of a new type of bond (for example, ester formation/cleavage) and b) involving a direct exchange reaction (for example, transesterification).

be assigned to one of two different categories: a) making/breaking of the reversible bond, where the reversible process involves formation/scission of one type of bond from/to another in a mechanism that involves the generation of a condensation product with loss of a small molecule; an example is the reaction of a carboxylic acid and an alcohol to yield an ester and water (Figure 1.2 a), and b) a direct exchange reaction, where the reversible covalent bond is of the same type in both starting material and product; an example is transesterification (Figure 1.2 b), wherein an ester and an alcohol are in equilibrium with a different ester and alcohol. Other examples [2] of dynamic covalent functionalities include acetals, borazaaromatic anhydrides, borate esters, disulfides, hydrazones, imines, oximes, and olefins (metathesis). The fact that the bonds being broken and reformed are the same means that the energetic difference between the products and the reactans is very low, if any.

One of the most appealing applications emerging from reversible chemistry is the ability of some materials to autorepair and heal the suffered damage by themselves and, in that manner, being able to recover the original properties [6, 7, 8, ?, 9]. Thus, the reorganization of the chemical bonds leads to a reconnection of the damaged parts, resulting in a partial or complete recovery of the material. This is the origin of the concept of self-healing materials.

1.2 Self-healing Materials

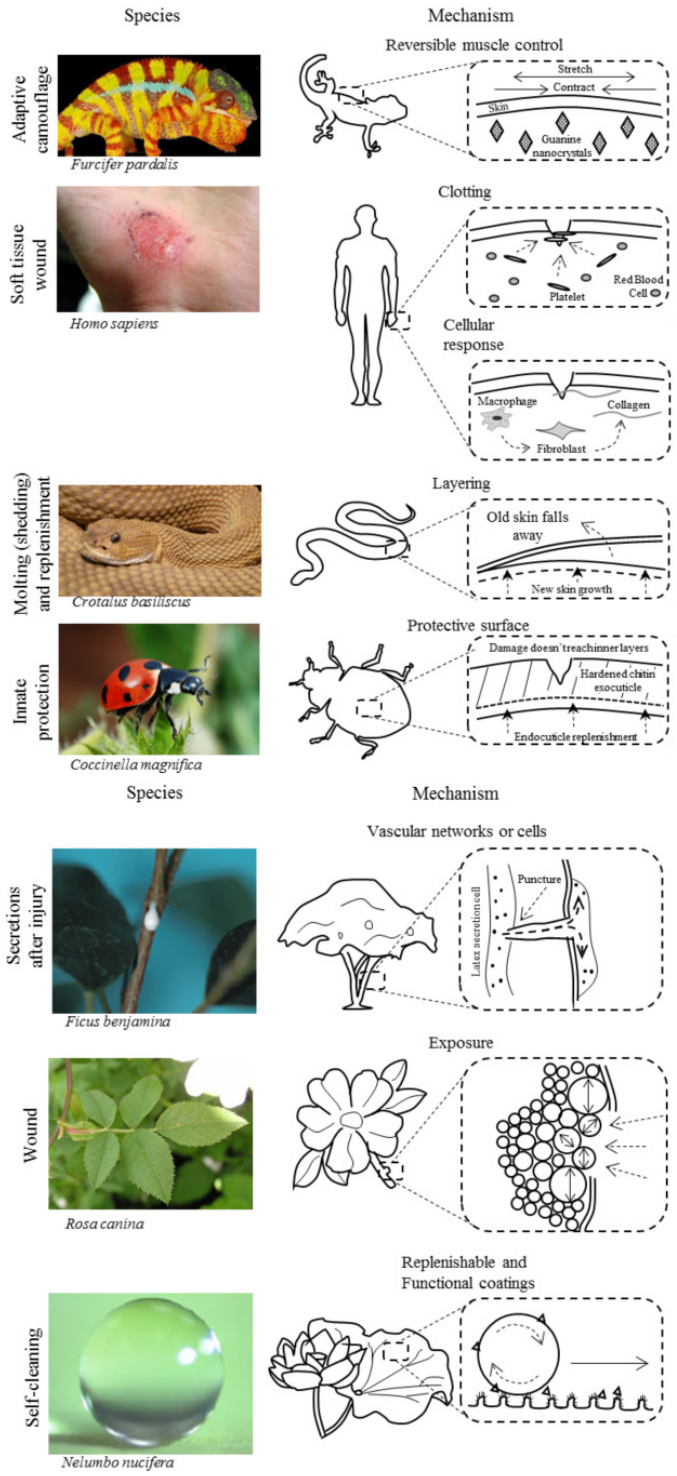

Figure 1.3: Examples of self-healing in nature, top belonging to fauna and bottom to flora. Image taken from reference [10]

Biological materials are evolutionary-optimized functional systems and, amongst their vast range of functionalities, one of the most outstanding is the self-healing ability [10]. Some examples of this feature are depicted in Figure 1.3, where a set of living organisms (including both fauna and flora) present the ability of self-heal via a big variety of methods. Thus, in nature, it is clear that the self-healing process may occur at both the molecular level (repair of DNA) and the macroscopic level (merging of broken bones or healing of small cuts in the skin).

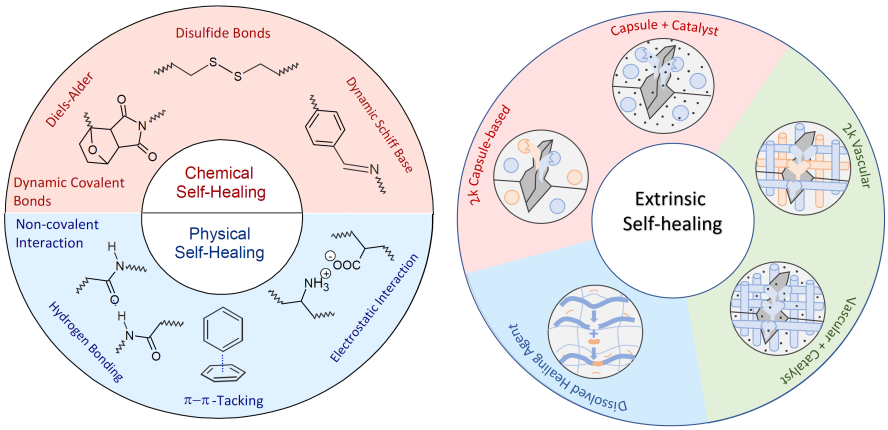

Figure 1.4: Schematic representation of the different self-healing agents. Left: intrinsic, including both chemical and physical self-healing. Right: extrinsic self-healing.

Inspired by this relevant feature, extensive effort has been carried out to develop self-healing materials, among them, self-healing polymers[1] in particular, due to their wide field of functionalities and applications [6, 11, 12, 13]. The ability of self-healing materials to regain, autonomously or externally assisted, their initial properties is primarily affected by the selection of the healing agents. Inspired by the biological systems, intrinsic, capsule-based and vascular methods (both being considered extrinsic, as an external stimuli is needed in order to trigger the self-healing process) are the main approaches used in order to impart self-healing functionalities to materials or structures. Many different chemistries have been used for that purpose (as depicted in Figure 1.4), including Diels-Alder reaction [14, 15, ?], siloxane exchange [16, 17], transesterification [18, 19] or disulfides [20, 21], and the use of both steric [22, 23, 24, 25] and electronic effects, for example [26, 27, 28, 29, 30, 31]. Based on the reversibility process, two main approaches may be devised among the intrinsic self-healing materials depending on the nature of the interaction: the first one involves weak, non-

[1]Healing of a polymeric material can refer to the recovery of properties such as fracture toughness, tensile strength, surface smoothness, barrier properties and even molecular weight.

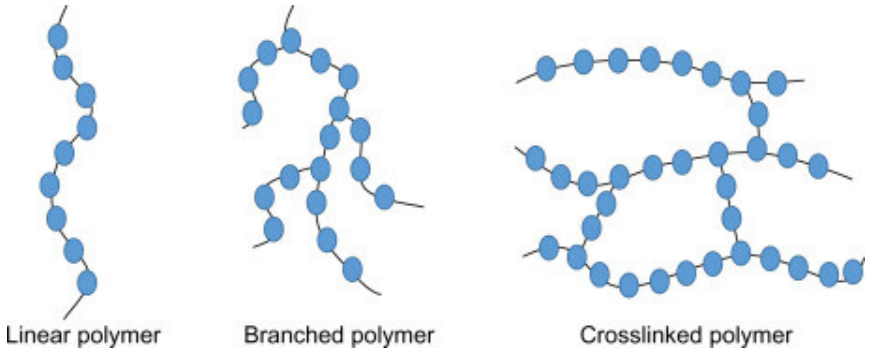

Figure 1.5: Schematic representation of the different types of polymers according to their linkage structure.

covalent interactions, such as hydrogen bonds [?], $\pi - \pi$ stacking [32] or metal-ion interactions [33], and the second one involves dynamic covalent bonds [34, 35, 36], with the main difference between these two approaches being that the use of covalent networks may provide the material with higher mechanical strength and stability.

Recently, polymer science has reached a point where it is possible to synthesize "smart" polymers that possess the remarkable, bio-inspired ability of regaining their initial properties completely, ideally without external input. These polymers constitute one of the most important categories of self-healing materials, that of the intrinsic or remendable healing polymers. In this case, repair is achieved through the inherent reversibility of bonding in the matrix phase, which acts as a healing agent. An ideal self-healing material is capable of continuously sensing and responding to damage over the lifetime of the polymeric components, and restoring the material's performance without negatively affecting the initial materials properties. This is expected to make the materials safer, more reliable and durable while reducing costs and maintenance. Successful development of self-healing polymeric materials offers great opportunities for broadening the applications of these lightweight materials into the manufacture of structural and critical components.

Nevertheless, synthesizing polymers in which the matrix phase is solely composed by the healing agent may not be the way forward, as the processability and the mechanical properties of the material could hinder its future applications. So that, for introducing the self-healing character in the polymers without affecting massively their mechanical properties, the introduction of a healing agent, such as a dynamic covalent bond, as a crosslinker (see Figure 1.5) between the main polymeric chains could be a good solution trying to find a balance between these two contrasting effects [37].

However, many reversibly covalently crosslinked polymers have inherent low reactivities that require external stimulation, such as heat or UV irradiation. Thus, in order to achieve a reversible covalent self-healing material which is autonomous or needs weak stimulations, an appropriate choice of this covalent bond is a key feature [23, 38, ?]. In this sense, disulfide bonds appear as good candidates to introduce a healing functionality at lower temperatures while keeping a reasonably level of bond strength.

1.3 Dichalcogenide-Based Self-Healing Materials

The chemistry of disulfides is very versatile. Due to the dynamics and reversibility of the S-S bond cleavage (to generate sulfenyl radicals), disulfide compounds play a crucial role in several fields such as physiological chemistry, where disulfide bridges are involved in folding, conformational stability and biological activity of proteins by means of thiol-disulfide exchange reactions with the thiol moiety in cystein residues [39, 40, 41], or synthetic chemistry [42]. Besides, it is noteworthy their use in materials science as highly versatile precursors for the synthesis of colloidal nanocrystals [43] or as crosslinking groups that result from the vulcanization of rubber, in analogy to the role of disulfides in proteins, strongly affecting the rheology of the material [44].

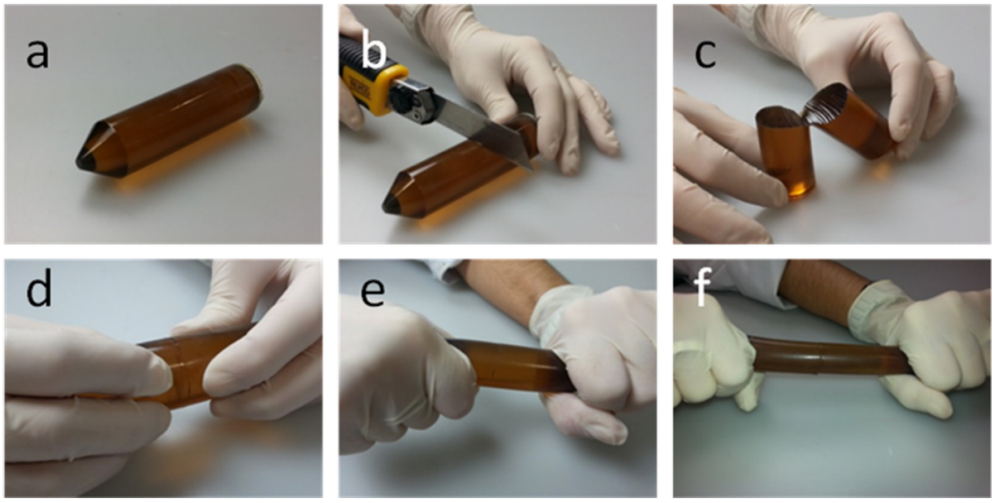

Figure 1.6: Graphic representation of the self-healing process of a dichalcogenide based polyurethane, known as "Terminator" (taken from ref [?]).

Several disulfide compounds are shown to exchange in the presence of catalysts [45, 46] or under UV irradiation [47] but, in order to improve their performance, it would be desirable to have this exchange at room temperature and without external stimuli. Therefore, disulfide bonds with lower

bond dissociation energies are necessary to prepare self-healing materials under mild conditions. This is the case of aromatic disulfides, in which metathesis has been reported to happen at room temperature, both in solution [48] and in the solid state [49].

Following this approach, a very successful work has appeared recently in the literature, where bis(4-aminophenyl) disulfide is used as a dynamic crosslinker for the design of self-healing poly(urea-urethane) elastomers, which show quantitative healing efficiency at room temperature without the need of any catalyst or external intervention [50] (see Figure 1.6). The high healing efficiency is explained in terms of the constant exchange of aromatic disulfides at room temperature, which is further improved by the generation of hydrogen bonds among urea moieties, contributing up to a 50% of the healing efficiency.

It is known that, in the case of polyurethanes (PUs), the mechanical properties are greatly affected by supramolecular interactions, as hydrogen bonds, as well as by the packaging of the hard segments [31, 51, 52, 53], so tuning these features could provide the materials with a reasonable level of mechanical strenght for their further application. In this vein, Kim et. al. [54] and Takahashi et. al. [55] studied a set of disulfide materials with different hard segments (or hardeners, see Figure 1.7) and crosslinkers, in order to check for the self-healing properties at different temperatures. The formers obtained a self-healing thermoplastic polyurethane (TPU) at room temperature (IP) with mechanical properties such as robustness, stretchability, and durability, surpassing those of room-temperature self-healable materials to date, while the latter used different crosslinkers, in order to study the effect of different packagings.

In addition to sulfur, the study of selenium is relevant, since it may replace sulfur in proteins and other biological systems [56, 57]. Nevertheless, the inherent atomic differences, such as size or electronegativity, are responsible of the different behavior observed in Se-based compounds, such as an enhancement on chemical reactivity in S_N2 reactions [58] or the enhanced stability of the selenyl radicals compared to sulfenyl radicals in compounds with significative strain [59]. More interestingly, it has been observed that selenium confers resistance to inactivation by oxidation in some biological compounds [60].

The chemistry of diselenides can be also used to design brand new self-healing materials. So are the combination of selenium and sulfur or nitrogen [61, 62], whose bond dissociation energies (BDEs) suggest that they could also be used in reversible chemistry due to the dynamic character of the bonds, even at milder conditions. For example, Ji et. al. [63] were able to synthesize aliphatic diselenide compounds capable of self-healing in a process triggered by visible light and UV irradiation, yet no reaction

happened in the dark. Similarly, Pan et. al. [64] demonstrated the healing and reprocessing behavior of aliphatic diselenides containing polymer networks upon UV irradiation. Recently, in a combined experimental and computational study, the ability of aromatic diselenides to exchange faster than their disulfide counterparts, at room temperature and without the need of any external stimulus, was reported [65].

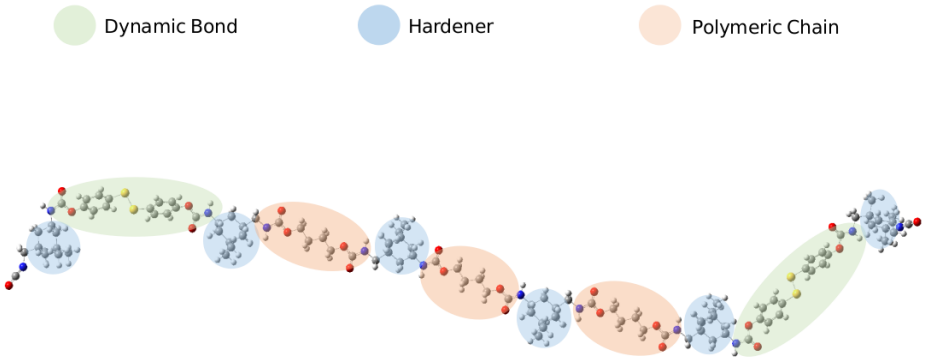

Figure 1.7: Schematic representation of the different components of the IP polymer, with the dynamic bond in green, the polymeric chain in red and the hardener in blue.

1.4 Reaction Mechanism and Theoretical Studies

Thus, it is clear that the study of the mechanism of such an important and highly applicable process is of paramount importance to achieve a better understanding of the reaction at the molecular level, which may lead to an improvement of the self-healing capacity of the materials by predicting new bonds which experience exchange without the presence of catalyst or UV irradiation. Apart from several theoretical works dealing with the dissociation of the disulfide bond [66, 67, 68], the first computational study exploring the reaction mechanism involved in disulfide-based self-healing materials was performed by Matxain and Ruipérez [69]. Contrary to what was believed, a [2+1] radical-mediated mechanism (see Figure 1.8) is found to be responsible for the self-healing reaction, and not the expected [2+2] metathesis mechanism. In the [2+1] mechanism, the first step is the generation of sulfenyl radicals by cleavage of the S-S bond, that may attack other disulfide bonds that are found in the vicinity, via a three-membered transition state, producing a new radical in a single-displacement reaction and another disulfide compound and, therefore, leading to the interchange of sulfur atoms in the process. The formation of the sulfenyl radicals has been recently confirmed experimentally [70], supporting the theoretical findings. Another experimental confirmation can be found in the work of Odriozola et. al. where a fiber-glass containing disulfides was hit by a hammer changing the colour of the material, and recovering its original colour after 24

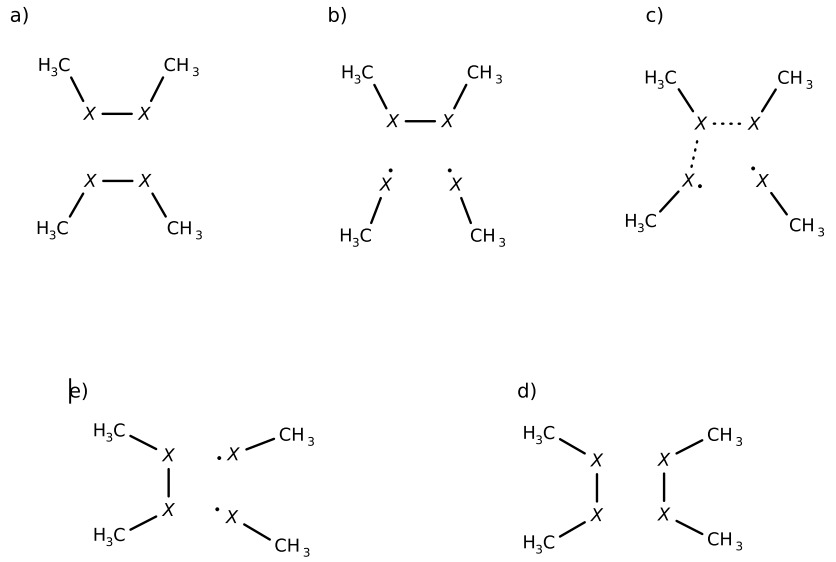

Figure 1.8: Schematic representation of the [2+1] radical mediated reaction mechanism, a) two dichalcogenide bonds prior to the exchange reaction b) the breaking of the dichalcogenide bonds, forming chalcogenyl radicals c) the attack of a chalcogenyl radical to a neighbouring dichalcogenide bond, via a three-membered transition state d) the formation of a new dichalcogenide bond by exchange of chalcogenide atoms e) formation of another dichalcogenide bond.

hours at room temperature, with calculations showing that the sulfenyl radicals where responsible of the colour [71].

In the work of Matxain and Ruipérez [69] it is highlighted the relevance of the chemical structure of the disulfide in the self-healing process, and three features are analyzed. Firstly, the breaking of the S-S bond, which is the first step of the reaction. Since the process should occur at room temperature, a thermal dissociation implies low bond dissociation energies (BDE) and photodissociation should be effective by using visible light. Secondly, low energy barriers are mandatory in order to facilitate the reaction in a reversible manner. Finally, that study also showed that hydrogen bonding has a structural role in the process, as it may keep the disulfides close enough to undergo the reaction. Nevertheless, the small models used did not allow to perform a deeper analysis of this feature.

In a subsequent work, the same authors [72] used bigger models in order to study the effect of non-covalent interactions on these systems, including hydrogen bonding, by means of classical molecular dynamics simulations. The authors reported that the influence of the $\pi - \pi$ interactions among phenyl rings are irrelevant in comparison to the hydrogen bonding (see Figure 1.9). Moreover, they reported that the number of hydrogen bonds

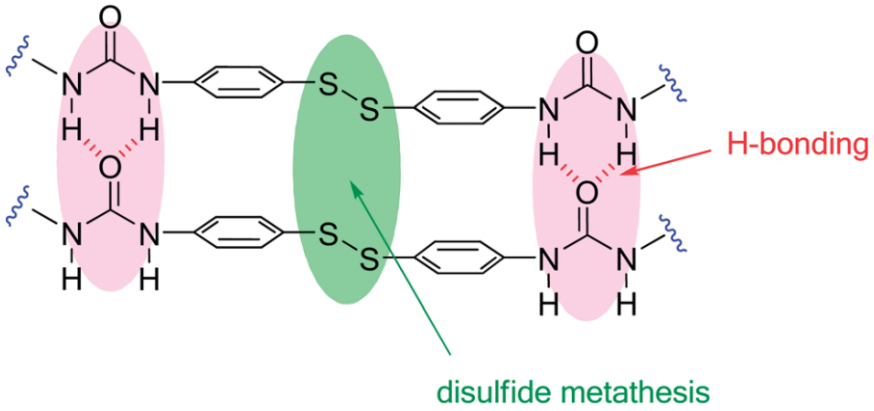

Figure 1.9: A picture highlighting the different factors affecting the self-healing process for the aromatic disulfides, with the dynamic disulfide bond in green and the hydrogen bonds formed by the interaction of the urea moieties coloured in red. Image taken from ref. [?].

formed is also a key factor, as they directly affect the mobility of chains, in such a way that both an excessively large and small number of hydrogen bonds is detrimental for the self-healing process, since the chains may be either too rigid, avoiding the contact among disulfides, or too mobile, resulting in a smaller ratio of disulfides close enough to react. With all this, they were able to establish a theoretical protocol for studyting the self-healing character of dichalcogenide-based materials (The author highly recommends reading the Appendix "Theoretical Protocol", where the theoretical protocol is explained in detail).

1.5 Motivation and Goals of the Thesis

At this point, it is clear that the simoultaneous design of dynamic networks combined with reasonable mechanical properties has become the landmark of the field of self-healing materials [73], and theoretical chemistry could be a very powerful tool to achieve this goal, as it helps understanding and rationalising experimentals results, as well as designing brand new polymeric materials. Up to now, theoretical chemistry has helped understanding the reaction mechanism leading to the dichalcogenide exchange reaction, as well as to highlight the relevance of the chemical structure around the dynamic bond in the exchange process. Moreover, computational chemistry is able to study not only systems of few atoms, but systems with thousands of atoms too, which makes of it a very useful tool to study the dynamics of the bulky materials. So that, the main goal of this thesis will be the multiscale study of dichalcogenide-based self-healing materials.

The specific goals of this thesis are:

- In the third chapter, the study of the nature of the dynamic bond and its chemical sorroundings by means of quantum chemistry, mainly focused on thermal and photodissociation and the exchange reaction kinetics.
- In the fourth chapter, the study of the dynamic behaviour of the bulk material. For that, the protocol for building the models will be assessed, and then the dynamics of a set of substituted dichalcogenides will be compared and analyzed by means on molecular dynamics.
- In the fifth chapter, using the previously developed theoretical protocol to evaluate the self-healing capacity of dichalcogenide-based materials, we will analayze some experimental systems [54, 55] in two-fold aim: i) test the validity of the theoretical protocol and ii) rationalise the observed experimental features.

Finally, the major conclusions will be detailed in the sixth chapter.

Chapter 2

Theory and Methods

2.1 Introduction to Quantum Chemistry

The theory of quantum mechanics arised in the twenties of the 20th century [74, 75, 76], and its development supposed a revolution in the understanting of the microscopic world, as it changed completely the viewpoint of physicists at that time. For example, before its development, all the attempts to explain the structure and stability of atoms failed until Bohr explained the structure of the simplest atom, hydrogen, by stating that electrons were fixed in stationary orbits around the nucleus, associated with definite energies. Based on Planck's theory of radiation, electrons can only gain or loose energy by jumping from one allowed orbit to another absorbing or emitting radiation. At the beginning, the theory was only of interest for physicists, but soon it was extended to chemistry, giving birth to the concept of quantum chemistry. Over the years, quantum chemistry has become a very important tool for chemists, as it helps to calculate, understand and predict molecular properties.

The theoretical methods of quantum chemistry are based on the Schrödinger equation [77], which is a differential equation in space and time, and depends on the mass and velocity of the particles. This equation, in its time-dependent form reads as:

$$i\hbar\frac{\delta}{\delta t}\Psi(r,R,t) = \hat{H}\Psi(r,R,t) \tag{2.1}$$

When it comes to stationary states, the time dependence disappears, with the stationary Scrödinger equation now reading:

$$\hat{H}(r,R) = E\Psi(r,R) \tag{2.2}$$

where the Hamiltonian operator, $\hat{H}$, corresponds to the total energy of the system, Ψ is the wavefunction, which depends on the position of both the nuclei and electrons, and contains all the measurable information about the system. Finally, E is the energy associated to the wavefunction.

For a system with N electrons and M nuclei, the non-relativistic Hamiltonian includes the kinetic energy of nuclei ($\hat{T}_n$) and electrons ($\hat{T}_e$), the electron-nucleus attraction ($\hat{V}_{ne}$) as well as the repulsion between electrons ($\hat{V}_{ee}$) and nuclei ($\hat{V}_{nn}$):

$$\hat{H} = \hat{T}_e + \hat{T}_n + \hat{V}_{ne} + \hat{V}_{ee} + \hat{V}_{nn} \tag{2.3}$$

which, in atomic units, is expressed as follows:

$$\hat{H} = \sum_{i=1}^{N}\left[\frac{-\nabla_i^2}{2} + \sum_{A=1}^{M}\frac{-Z_A}{|\vec{r}_i - \vec{R}_A|}\right] + \sum_{i>j}^{N}\frac{1}{|\vec{r}_i - \vec{r}_j|} + \sum_{A=1}^{M}\frac{-\nabla_A^2}{2m_A} + \sum_{A>B}^{M}\frac{-Z_A Z_B}{|\vec{R}_A - \vec{R}_B|} \tag{2.4}$$

This complex equation can only be exactly solved for a one-electron system (e.g., the hydrogen atom), due to the electron-electron interaction term ($|\vec{r}_i - \vec{r}_j|$) and approximations must be done.

2.2 Solving the Schrödinger Equation

2.2.1 Born-Oppenheimer Approximation

The Born-Oppenheimer approximation [78] is based on the fact that the nuclei are much heavier than the electrons (the mass of the proton and neutron is about 1800 times larger than the electron mass). Therefore, the motion of the electrons is several orders of magnitude faster than the motion of nuclei, that is, on the time scale of the electron motion, nuclei can be considered as stationary objects, while electrons are assumed to respond instantaneously to changes in the nuclear configuration and, thus, the nuclei can be considered to move in the mean field generated by the electrons.

As a consequence, the nuclear and electronic parts of the Schrödinger equation can be treated separately and the molecular equation is transformed into the electronic and nuclear Schrödinger equations. In the electronic equation, the nuclear kinetic energy term ($\hat{T}_n$) is neglected, the nuclear repulsion term ($\hat{V}_{nn}$) is constant and the interaction between nuclei and electrons ($\hat{V}_{ne}$) depends parametrically on the coordinates of the fixed nuclei. Therefore, a simplified Schrödinger equation which does not treat nuclear motion is solved for electrons only.

$$\hat{H}_e\Psi_e = (\hat{T}_e + \hat{V}_{ee} + \hat{V}_{en} + \hat{V}_{nn})\Psi_e = E_e\Psi_e \tag{2.5}$$

The obtained electronic wavefunction Ψ_e explicitly depends on the electronic coordinates and depends parametrically on the nuclear coordinates:

$$\hat{H}_e\Psi_e(\{r_i\};\{R_\alpha\}) = E_e(\{R_\alpha\})\Psi_e(\{r_i\};\{R_\alpha\}) \tag{2.6}$$

Under the same assumptions made to formulate the electronic problem, it is possible to write down the equations for the nuclear motion. As the electrons move much faster than the nuclei, the latter are considered to move in the mean field generated by the former. In other words, the electronic energy E_e, added to the internuclear repulsion $\hat{V}_{nn}$, provides the potential energy surface V_N for the nuclei. Then, the nuclear part of the Schrödinger equation reads as

$$(\hat{T}_n + E_e + \hat{V}_{nn})\Psi_n(\{R_\alpha\}) = E_{tot}(\{R_\alpha\}) \tag{2.7}$$

The potential energy surface of the system represents the central quantity to obtain information about the roto-vibrational levels, equilibrium geometries and chemical reactivity and, therefore, transition state (TS) geometries.

A transition state of a chemical reaction is a first-order saddle point on the potential energy surface. Like the minima, the first order saddle points are stationary points with all forces equal to zero. However, unlike the minima, one of the second derivatives in the first order saddle point is negative. Thus, the transition state structure associated with the first-order saddle point has one imaginary frequency and the normal mode of vibration associated with this negative frequency emulates the motion of the atoms along the reaction coordinate.

The energy of transition state structures is important to determine the energy barrier for the reaction and, thus, the reaction rate. In 1889, the Arrhenius equation [79] was proposed to determine energies for reaction barriers. However, this equation derives from empirical observations and the mechanical basis was not understood. Thus, in 1935, the Transition State Theory and the Eyring equation were developed [80]. Transition State Theory explains the reaction rates of elementary chemical reactions. It details a hypothetical transition state that exists between reactants and products during a chemical reaction. This theory is used to explain how chemical reactions take place and led to the Eyring equation:

$$k = \frac{k_B T}{h} e^{-\frac{\Delta G^{\ddagger}}{RT}} \tag{2.8}$$

where $\Delta G^{\ddagger}$ is the Gibbs free energy difference between the TS and reactants, k is the reaction rate constant, T is the absolute temperature, k_B is the Boltzmann constant, h is the Planck's constant, and R is the universal gas constant. The lifetime of the reactants can be then calculated as the inverse of the reaction rate constant. While Arrhenius equation is useful only in gas phase reactions, the Eyring equation can be applied in the study of gases, condensed and mixed phase reactions. However, it is important to emphasize that the Eyring model is an approximation to calculate reaction rate constants and then lifetimes, consequently, the data obtained from this equation should be taken qualitatively.

2.2.2 *Ab Initio* Methods

Besides the Born-Oppenheimer approximation, further approximations have to be performed in order to solve the molecular Schrödinger equation. These approximations are the origin of the field of quantum chemistry, in such a way that quantum chemical models differ in the nature of these approximations and span a wide range, both in terms of reliability and cost.

The most representative approximation is the Hartree-Fock (HF) method [81, 82] which, when applied to the many-electron Schrödinger equation, leads to an important class of quantum chemical models, the molecular orbital (MO) models, and also provides the foundation for both simpler and more complex models. In the Hartree-Fock method, in order to fulfill the Pauli exclusion principle, the wavefunction is an antisymmetrized determinantal product (the so-called Slater determinant) of one-electron orbitals, which depends explicitly on the $3N$ coordinates of the electrons, in an N-electron system. In this approximation, each electron moves independently

in an average field created by the rest of the electrons and nuclei, leading to a set of uncoupled single-particle equations, the Hartree-Fock equations [83]. Using the variational principle, we ensure that the obtained wavefunction is the best, that is, the one that yields the lowest energy of the system.

HF models provide with a reasonably good description of equilibrium geometries and conformations, except when transition metals are involved. However, they behave poorly in accounting for the thermochemistry of reactions involving explicit bond breaking and forming. The failures can be traced back to the incomplete description of the electron correlation, that is, the way in which the motion of one electron affects the motions of the rest of the electrons. In order to allow for electron correlation, several quantum chemical methods have been developed. Among them, three fundamental approaches must be underlined: (i) configuration interaction (CI) [84, 85, 86] (ii) Møller-Plesset perturbation theory [87] (MPn, where n is the order of the perturbation) and (iii) coupled-cluster approaches (CC) [88, 89, 90, 91], which extend the flexibility of the HF method by mixing ground- and excited-state wavefunctions, that is, using several Slater determinants obtained from a permutation of electron occupancies among all the molecular orbitals available. These approaches are significantly more expensive than HF but provide excellent descriptions of thermochemistry.

A conceptually different methodology to include electron correlation is Density Functional Theory (DFT), which is based on the electron density, $\rho(\vec{r})$, as opposed to the many-electron wavefunction, Ψ [92, 93]. This is the main difference that makes DFT to be more cost-efficient: the simplest wavefunctions depends on $3N$ spatial coordinates, whereas the probability distribution of electrons in space depends only on three coordinates.

2.3 Density Functional Theory

There are, nevertheless, similarities between wavefunction-based and electron density-based approaches. First, the essential building blocks of a many-electron wavefunction are the one-electron orbitals, which are analogous to the orbitals used in DFT. Second, both the electron density and the wavefunction are constructed from a self-consistent field (SCF) approach. This procedure is an iterative process where an approximate Hamiltonian is constructed to solve the Schrödinger equation and to obtain a set of molecular orbitals that are used to construct another Hamiltonian and obtain a set of new, more accurate set of MOs until the process reaches convergence. The SCF procedure leads to the MOs that minimize the energy.

2.3.1 Time-Independent Density Functional Theory

Hohenberg and Kohn [94] proved that the electronic properties of a system with a non-degenerate ground state are uniquely determined by the electron density $\rho(\vec{r})$. Hence, the ground state energy E_0, defined as the sum of the kinetic energy (T), electron-electron repulsion (E_{ee}) and nucleus-electron attraction (E_{ne}) is a functional of ρ:

$$E_0[\rho] = T[\rho] + E_{ee}[\rho] + E_{ne}[\rho] \tag{2.9}$$

Since $T[\rho]$ and $E_{ee}[\rho]$ are unknown, they are usually gathered in the so-called Hohenberg-Kohn functional, $F_{HK}[\rho]$:

$$F_{HK}[\rho] = T[\rho] + E_{ee}[\rho] \tag{2.10}$$

Besides, they also established a variational principle for the energy functional, analogous to that for wavefunctions. Thus, knowing the exact form of the $E[\rho]$ functional, one can search for the ground state density.

However, since the exact form of the functional is not known, Kohn and Sham [95] developed an approach to determine the electronic density in the ground state, using a non-interacting reference system. They showed that the exact ground state electronic energy E_0 of an N-electron molecule with a ground-state electron density ρ is given by

$$E_0 = -\frac{1}{2}\sum_{i=1}^{N} < \psi_i(1)|\nabla_i^2|\psi_i(1) > + \int v(r)\rho(1)d\vec{r}_1 + \\ + \frac{1}{2}\int\int \frac{\rho(1)\rho(2)}{r_{12}} d\vec{r}_1 d\vec{r}_2 + E_{xc}[\rho] \tag{2.11}$$

where $v(r) = -\sum_\alpha \frac{Z_\alpha}{r_{1\alpha}}$ is the external potential due to the nuclei, ψ_i are the Kohn-Sham orbitals, and $E_{xc}[\rho]$ is the exchange-correlation energy. In the Kohn-Sham procedure, the exact ground state ρ can be found from the Kohn-Sham orbitals according to,

$$\rho = \sum_{i=1}^{N} |\psi_i|^2 \tag{2.12}$$

and the Kohn-Sham orbitals are found by solving the one-electron equations

$$\hat{F}_{KS}(1)\psi_i(1) = \epsilon_i\psi_i(1) \tag{2.13}$$

where the Kohn-Sham operator $\hat{F}_{KS}$ is defined as:

$$\hat{F}_{KS} = -\frac{1}{2}\nabla_1^2 - v(1) + \sum_{j=1}^{n}\hat{J}_j(1) + V_{xc}(1) \tag{2.14}$$

where $\hat{J}$ is the Coulomb operator and V_{xc} is called the exchange-correlation potential, defined as:

$$V_{xc} = \frac{\delta E_{XC}[\rho]}{\delta\rho} \tag{2.15}$$

Thus, $\hat{F}_{KS}$ is like the Fock operator in Hartree-Fock equations, except that the exchange operators are replaced by V_{xc}. As it was previously stated, these equations are self-consistently (iteratively) solved. Starting from a guess density, $\hat{F}_{KS}$ is built and the set of equations are solved. This process is repeated until convergence is achieved.

The physical significance of the Kohn-Sham orbitals is still under debate. Some authors claim that they only allow obtaining the exact ρ. Likewise, the Kohn-Sham orbital energies should not be confused with molecular orbital energies. However, other authors, based on the fact that the exact Kohn-Sham orbital energy for the HOMO is just the negative ionization potential [96, 97], and that the set of Kohn-Sham equations are analogous to the HF equations, they associate to the KS orbitals a similar physical significance as the HF canonical orbitals. Besides, some publications show that the results obtained from molecular orbitals using DFT are quite similar to those obtained from standard MO-LCAO methods [96, 98].

Still, besides for the uniform electron gas, exact E_{xc} and V_{xc} are unknown, even though the Kohn-Sham formalism is, in principle, exact. So that, approximations need to be made in order to make DFT a practical tool. Those approximations are known as Density Functional Approximations (DFAs). The first implemented approximation is the so-called Local Density Approximation (LDA) [99], where each volume element with local density $\rho(\vec{r})$ is considered to be a homogeneus electron gas. Yet, this approximation would be accurate given a slowly variant density in the space, which generally is

not the case. So, a more sophisticated method is needed in order to account for the inhomogeneous character of the electron density. For that, the gradient of the density ($\nabla\rho(r)$) is included. This approximation is known as Generalized Gradient Approximation (GGA), and made DFT a new player in the field of computational chemistry, as its correlation-exchange functionals are, in general, accurate enough for most chemical applications. Further improvements can be made by introducing the Laplacian of the density, $\nabla^2\rho(r)$, which are known as meta-GGA functionals, or even a fraction of Hartree-Fock exchange can be included into the functionals, as it occurs in the so called hybrid functionals, which are a combination of Hartree-Fock exchange and DFT correlation. Among the hybrid functionals, both local and range-separated functionals can be found. In the former the amount of HF exchange depends on local properties of each particular system and, in the latter, the Coulomb operator is split into a long-range and a short-range part. For a more detailed read on DFAs, see Appendix I.

2.3.2 Time-Dependent Density Functional Theory

The time-dependent generalization of the density functional theory formalism, TDDFT [100], offers a rigorous procedure to calculate the dynamic response of the charge density that, combined with linear response theory, allows to compute vertical electronic spectra of molecules [101, 102, 103, 104, 105]. TDDFT has been applied to very different systems, i.e. for metal-containing, organic [106, 107, 108] or inorganic compounds [109, 110], as well as for extended systems, becoming a very powerful tool to calculate excitation energies (see [101, 111] for reviews).

A stationary action principle may be derived, analogous to the minimun energy principle of Hohenberg-Kohn theory, and this can be used, together with appropiate assumptions concerning v-representability, to derive the time-dependent Kohn-Sham equation:

$$\left[-\frac{1}{2}\nabla^2 + v(r,t) + \int \frac{\rho(r't)}{|r-r'|}dr' + v^{\sigma}_{xc}(r,t)\right]\psi_{j\sigma}(r,t) = i\frac{\partial}{\partial t}\psi_{j\sigma}(r,t) \tag{2.16}$$

where $v^{\sigma}_{xc}(r,t)$ is formally the functional derivative of the exchange-correlation action, A_{xc}, in analogy of the Kohn-Sham exchange-correlation term in time-independent DFT, E_{xc}:

$$v^{\sigma}_{xc}(r,t) = \frac{\delta A_{xc}[\rho_\sigma]}{\delta\rho_\sigma(r,t)} \cong \frac{\delta E_{xc}[\rho^t_\sigma]}{\delta\rho^t_\sigma(r)} \tag{2.17}$$

where $\rho_\sigma^t(r)$ is the $\rho_\sigma(r,t)$ function evaluated at a fixed time. Since the dynamic polarizability, $\bar{\alpha}(\omega)$, describes the response of the dipole moment to a time-dependent electric field, it may be calculated from the response of the charge density obtained from time-dependent density functional theory, that is, using time-dependent density functional response theory. This allows the determination of the electronic excitation spectrum in the usual dipole approximation because, according to the sum-over-states relation,

$$\bar{\alpha}(\omega) = \sum_l \frac{f_l}{\omega_l^2 - \omega^2} \tag{2.18}$$

the poles of the dynamic polarizability determine the excitation energies, ω_l, while the residues, f_l, determine the corresponding oscillator strenghts [101]. The transition energies may be obtained by solving a matrix eigenvalue problem:

$$\Omega F_l = \omega_l^2 F_l \tag{2.19}$$

where Ω is defined in the references [101, 102] and the oscillator strengths, f_l, are obtained from the eigenvectors F_l. For more information see references [112, 113].

2.4 *Ab Initio* Molecular Dynamics

The aim of molecular dynamics (MD) is to model the detailed microscopic dynamical behavior of different types of systems as found in chemistry, physics or biology. Is a technique to investigate equilibrium and transport properties of many-body systems.

One of the most important questions in MD is the description of interatomic interactions. Typically, the full interaction is split into two-body and many-body contributions, short-range and long-range terms, electrostatic and not electrostatic interactions, etc., which have to be represented by suitable functional forms [114, **?**]. After decades of research, very elaborate interaction models, including the non-trivial aspect of representing these potentials analitically, were devised [114, 115, 116, 117].

Using a fixed predefined potential may only be convenient for the system for which it has been parametrized, as a small chemical change in that system would demand a reparametrization of the functional. Besides, since each different atom or molecule gives raise to a myriad of different interatomic

interactions, this implies that all of them have to be parametrized for each system. Moreover, it must be taken into account the electronic structure and the chemical bonding pattern, that may change qualitatively during the simulation. As a result, a systematic study would require a titanic effort if no suitable set of consistent potentials is already available. Thanks to the development and growth of computational capacity, it is possible nowadays to perform dynamic simulations computing the electronic structure "on the fly". This is the origin of the *ab initio* molecular dynamics (AIMD), an extension of classical MD to include first-principles derived potential functions for the interactions.

Thus, the main feature of AIMD is the computation of the interatomic forces acting on the nuclei from electronic structure calculations that are performed "on the fly" as the molecular dynamics trajectory is generated. In this way, the electronic variables are considered to be active and as explicit degrees of freedom in the course of the simulation, in spite of being integrated out beforehand and represented by fixed interaction potentials. This implies that, given an approximate solution of the many-electron problem, even systems in which electronic structure changes dramatically during the simulation can be handled easily by molecular mechanics. Therefore, one has to choose a particular approximation in order to solve the time dependent Schrödinger equation

$$i\hbar\frac{\partial}{\partial t}\Psi(r,R,t) = \hat{H}\Psi(r,R,t) \tag{2.20}$$

In quantum mechanics, the Hamiltonian operator ($\hat{H}$) acts on the wavefuntion (Ψ) in the same way as the Lagrangian operator ($\mathscr{L}$) acts on the position of the particles in the framework of classical mechanics. Taking this into account, different approaches have been developed throughout the years, such as Car-Parrinelo molecular dynamics (CPMD) [118], who introduced an algorithm in which the separate tasks of following the nuclear motion and finding the electronic ground state for fixed nuclear positions are treated in a unified way through an extended Lagrangian, making use of the time-scale separation of the fast electronic and slow nuclear motion. Thus, the two-component quantum/classical problem is mapped onto a two-component purely classical problem with two separate energy scales. Another approach is the so called Born-Oppenheimer Molecular Dynamics (BOMD), which is the method of choice in this work and will be described in detail in the following section.

2.4.1 Born Oppenheimer Molecular Dynamics

The main idea of this approximation is to straightforwardly solve the static

electronic structure problem in each MD step given a set of fixed nuclear positions at that particular time. BOMD follows the adiabatic time evolution of a system, dividing time into series of time steps. In order to solve the equations of motion, electrons are treated quantum mechanically (solving the electronic equation by means of DFT) and nuclei classically. Thus, one has to solve the static electronic structure problem in each MD step given the set of fixed nuclear positions at that instance of time. Hence, the electronic structure part is reduced to solving the time-independent Schrödinger equation, followed by the propagation of the nuclei via classical MD.

The Kohn-Sham energy depends only on the nuclear positions and defines the hypersurface for the movement of the nuclei. Thus, the Lagrangian for BO dynamics is:

$$\mathscr{L} = \frac{1}{2}\sum_{\alpha} M_\alpha \dot{R}_\alpha^2 - \underset{\{\phi_i\}}{min} E^{KS}[\{\phi_i\}; R] \tag{2.21}$$

and the minimization of the Kohn-Sham energy is constraint to orthogonal sets of $\{\phi_i\}$. The equations of motion are:

$$M_\alpha \ddot{R}_\alpha(t) = -\nabla_\alpha \left[\underset{\{\phi_i\}}{min} E^{KS}[\{\phi_i\}; R]\right] \tag{2.22}$$

where the electronic ground state has to be reached in each MD step according to Eq. 2.22.

The molecular dynamics simulations carried out in this work have been performed at constant temperature, in such a way that the average temperature of the system is fixed, but a fluctuation of the temperature with a canonical distribution is allowed. In the framework of statistical mechanics, all ensembles can be formally obtained from the microcanonical (NVE) ensemble, where particle number, volume and energy are thermodynamic control variables. Although the temperature is not a control variable, it is evident that the possibility to control the average temperature (obtained from the average kinetic energy of the nuclei) is very appealing. This can be achieved using a thermostat to impose temperature instead of energy as external control parameter, thereby the canonical ensemble (NVT) is generated. A deterministic algorithm for achieving temperature control was devised by Nosé and Hoover [119, 120] where the system is in thermal contact with a heat bath by adding an artificial variable associated with an artificial mass.

Finally, the time step employed is an important control parameter for a simulation. The maximum time-step is determined by the rate of the fastest process in the system, i.e. typically an order of magnitude smaller than the fastest process. Molecular vibrations typically occur in the range of $10^{-12} - 10^{-15}$ seconds, so time-steps of the order of femtoseconds are required to model such motions with enough accuracy.

2.5 Molecular Dynamics

One of the principal tools in the theoretical study of molecules is the method of molecular dynamics simulations. This computational method calculates the time dependent behavior of a molecular system. Like Monte Carlo methods [121, 122, 123, 124], MD provides a means to sample the potential energy surface of a molecule but in addition, this computational method calculates the time dependent behavior of the system. Classical MD simulations are now routinely used to investigate the structure, dynamics and thermodynamics of molecules and materials [125].

Molecular dynamics simulations are based on Newton's second law or equation of motion,

$$\overrightarrow{F} = m\overrightarrow{a} \tag{2.23}$$

where $\overrightarrow{F}$ is the force exerted on the particle, m is its mass and $\overrightarrow{a}$ is its acceleration. From a knowledge of the force on each atom, it is possible to determine the acceleration of each atom in the system. Integration of the equations of motion then yields a trajectory that describes the positions, velocities and accelerations of the particles as they vary with time. From this trajectory, the average values of properties can be determined. The method is deterministic; once the positions and velocities of each atom are known, the state of the system can be predicted at any time in the future or the past. More precisely, the trajectory is obtained by solving the differential equations embodied in Newton's second law

$$\frac{F_{xi}}{m_i} = \frac{d^2x_i}{dt^2} \tag{2.24}$$

This equation describes the motion of a particle of mass m_i along one coordinate (x_i) with F_{xi} being the force on the particle in that direction. The force can also be expressed as the gradient of the potential energy (U), as shown in equation 2.25.

$$\overrightarrow{F_i} = -\overrightarrow{\nabla}_i U \tag{2.25}$$

Combining equations 2.24 and 2.25, equation 2.26 is obtained, where U is the potential energy of the system. Newton's equation of motion can then relate the derivative of the potential energy to the changes in position as a function of time.

$$\frac{-dU}{dx_i} = m_i \frac{d^2 x_i}{dt^2} \tag{2.26}$$

The initial distribution of velocities is usually determined from a random distribution with the magnitudes conforming to the required temperature and corrected so there is no overall momentum (P) as expressed in equation 2.27.

$$P = \sum_{i=1}^{N} m_i v_i = 0 \tag{2.27}$$

Usually, the velocities v_i are chosen randomly from a Maxwell-Boltzmann or Gaussian distribution at a given temperature, which gives the probability (p_{ix}) that an atom i has a velocity v_x in the x direction at a temperature T (Eq. 2.28). Here k_B is the Boltzman constant.

$$p(v_{ix}) = \left(\frac{m_i}{2\pi k_B T}\right)^{1/2} e^{\left(-\frac{1}{2}\frac{m_i v_{ix}^2}{k_B T}\right)} \tag{2.28}$$

The temperature can then be calculated if we consider that, at thermal equilibrium, the average kinetic energy per degree of freedom can be expressed as in equation 2.29, where v_α is the α component of the velocity of a given particle. We can use this relation to define an instantaneous temperature at time t, $T(t)$, as shown in Equation 2.30.

$$\langle \frac{1}{2} m v_\alpha^2 \rangle = \frac{1}{2} k_B T \tag{2.29}$$

$$T(t) = \sum_{i=1}^{N} \frac{m_i v_i^2(t)}{k_B N_f} \tag{2.30}$$

where N_f is the number of degrees of freedom, which is $3N-3$ for a system of N particles with fixed total momentum. The relative fluctuations in the p temperature will be of order $\frac{1}{N_f}$. As N_f is typically on the order of $10^2 - 10^3$, the statistical fluctuations in the temperature are on the order of 5-10%

2.5.1 Integration Algorithms

The potential energy is a function of the atomic positions (3N) of all the atoms in the system (N). Due to the complicated nature of this function, there is no analytical solution to the equations of motion, they must be solved numerically. Numerous numerical algorithms have been developed for integrating the equations of motion. The algorithm must conserve energy and momentum, should be computationally efficient and permit long integration time steps [126, 127]. All integration algorithms assume that the positions, velocities and accelerations can be approximated by a Taylor series expansion (Equations 2.31, 2.32 and 2.33):

$$r(t+\delta t) = r(t) + v(t)\delta t + \frac{1}{2}a(t)\delta t^2 + \frac{1}{3!}b(t)\delta t^3 + ... \tag{2.31}$$

$$v(t+\delta t) = v(t) + a(t)\delta t + \frac{1}{2}b(t)\delta t^2 + ... \tag{2.32}$$

$$a(t+\delta t) = a(t) + b(t)\delta t + ... \tag{2.33}$$

where r is the position, v is the velocity (the first derivative of r with respect to time), a is the acceleration (second derivative of r with respect to time), $b(t)$ is the third derivative and δt the time step in the Molecular Dynamics simulation.

2.5.2 Force Fields

A force field (FF) is a mathematical expression describing the dependence of the energy of a system on the coordinates of its particles. It consists of an analytical form of the interatomic potential energy, U(r_1, r_2, ..., r_N), and a set of parameters entering into this form. The parameters are typically obtained either from *ab initio* or semi-empirical quantum mechanical calculations or by fitting to experimental data such as neutron, X-ray and electron diffraction, NMR, infrared, Raman and neutron spectroscopy, etc.

Molecules are simply defined as a set of atoms that is held together by simple elastic (harmonic) forces and the FF replaces the true potential with a simplified model valid in the region being simulated. Ideally, it must be simple enough to be evaluated quickly, but sufficiently detailed to reproduce the properties of interest of the system studied. There are many force fields available in the literature, having different degrees of complexity, and oriented to treat different kinds of systems. However, a typical expression for a FF may look like this:

$$U = \sum_{bonds} \frac{1}{2} k_b (r - r_0)^2 + \sum_{angles} \frac{1}{2} k_a (\theta - \theta_0)^2 + \sum_{torsions} \frac{V_n}{2} \left[1 + cos(n\phi - \delta)\right] + \sum_{improper} V_{imp} + \sum_{LJ} 4\epsilon_{ij} \left(\frac{\sigma_{ij}^{12}}{r_{ij}^{12}} - \frac{\sigma_{ij}^{6}}{r_{ij}^{6}} \right) + \sum_{elec} \frac{q_i q_j}{r_{ij}} \tag{2.34}$$

where the first four terms refer to intramolecular or local contributions to the total energy (bond stretching, angle bending, and dihedral and improper torsions), and the last two terms serve to describe the repulsive and Van der Waals interactions (in this case by means of a 12-6 Lennard-Jones potential) and the Coulombic interactions.

2.6 Basis Sets

As it has been mentioned before, the Schrödinger equation can only be analytically solved for hydrogen-like atoms. In other cases, this equation has to be solved approximately and one of the approximations inherent in all *ab initio* methods is the introduction of a basis set. Expanding an unknown function, such an orbital, in a set of known functions is not an approximation if the basis set is complete. However, a complete basis set means that an infinite number of functions must be used, which is impossible. Thus, an unknown orbital can be represented as a function in the infinite coordinate system spanned by the complete basis set. When a finite basis set is used, only the components of the orbital along those coordinate axes corresponding to the selected basis functions can be represented. The smaller the basis set, the poorer the representation of the orbital. The type of basis functions used also influence the accuracy.

Two types of basis functions are commonly used in electronic structure calculations: Slater Type Orbitals (STO) [128] and Gaussian Type orbitals (GTO) [129]. STOs have the following functional form:

$$\chi_{\zeta,n,l,m}(r,\theta,\phi) = NY_{l,m}(\theta,\phi)r^{n-1}e^{-\zeta r} \tag{2.35}$$

where N is a normalization constant and $Y_{l,m}$ are spherical harmonic functions. The exponential dependence on the nucleus-electron distance mimics the exact orbitals of hydrogen atoms and ensures rapid convergence with increasing number of functions. However, the calculation of three- and four-centre two-electron integrals cannot be performed analytically. GTOs, on the other hand, can be written in terms of polar or Cartesian coordinates:

$$\begin{aligned}\chi_{\zeta,n,l,m}(r,\theta,\phi) &= NY_{l,m}(\theta,\phi)r^{2n-2-l}e^{-\zeta r^2} \\ \chi_{\zeta,l_x,l_y,l_z}(x,y,z) &= Nx^{l_x}y^{l_y}z^{l_z}e^{-\zeta r^2}\end{aligned} \tag{2.36}$$

The r^2 dependence in the exponential makes GTOs inferior to the STOs in two respects: GTOs have problems representing the proper behavior near the nucleus and fall off too rapidly far from the nucleus. These considerations indicate that more GTOs are necessary to achieve a certain accuracy compared to STOs. Usually, the STO orbitals are modeled by a linear combination of three GTOs (STO-3G).

The most important factor is the number of functions to be used. A minimal basis set that only contains one basis function for each occupied atomic orbital is defined as a basis set of single-ζ quality. This minimal description of the orbitals is inadequate and needs to be improved. Thus, the basis can be split and, if all basis functions are doubled, i.e. two basis functions per atomic orbital, the basis set has a double-ζ quality. Similarly, the triple-ζ and quadruple-ζ types consist of further splittings.

Further improvement of the basis set can be done by adding polarization functions, that consist of higher angular momentum functions. Polarization functions are essential to describe the electron correlation. For molecules where the charge distribution is more diffuse, such in anions, diffuse functions are needed for a better description of the electron distribution.

Chapter 3

Quantum Chemical Study of Dichalcogenides as Building Blocks for Efficient Self-Healing Materials

Abstract

Self-healing materials are a very promising kind of materials due to their capacity to repair themselves. Among others, dichalcogenide-based materials are being widely studied due to their dynamic covalent bond nature. Recently, the reaction mechanism occurring in these materials was characterized both theoretically and experimentally. In this vein, a theoretical protocol was established in order to predict further improvements. Among these improvements, the use of diselenides instead of disulfides appears to be one of the paths to enhance these properties. Nevertheless, the physicochemical aspects of these improvements are not completely clear. In this work, the self-healing properties of several disulfides, diselenides and mixed S-Se materials have been considered by means of computational simulations. Among all the tested species, diphenyl-diselenide based materials appear to be the most promising ones due to the decrease on the reaction barriers, instead of weaker diselenide bonds, as thought up to now. Moreover, the radical formation needed in this process would also be enhanced by the fact that these species are able to absorb visible light. In this manner, at room conditions, selenyl radicals would be formed by both thermal dissociation and photodissociation. This fact, together with the lower energetic barriers needed for the diselenide exchange, makes diphenyl diselenides ideal for self-healing materials.

3.1 Introduction

The reasons of the good performance of disulfide-containing materials have been recently unveiled by means of several computational studies. First, Matxain and Ruipérez [69] explored the reaction mechanism involved in aromatic disulfide-based self-healing materials, such as those developed by Rekondo et al. [130]. Contrary to what was believed, a [2+1] radical-mediated mechanism (see Figure 3.1) was found to be responsible for the self-healing reaction, and not the expected [2+2] metathesis mechanism. In the [2+1] mechanism, the first step is the generation of sulfenyl radicals by cleavage of the S-S bond, which may further attack other disulfide bonds that are found in the vicinity. This process takes place via a three-membered transition state, producing a new radical in a single-displacement reaction and another disulfide compound and, therefore, leading to the interchange of sulfur atoms in the process. The formation of the sulfenyl radicals has been recently confirmed experimentally [70], supporting the theoretical findings. Another experimental confirmation can be found in the work of Ruiz de Luzuriaga et al., where a fiber-glass containing disulfide was hit by a hammer changing the color of the material, and recovering its original color after 24 hours at room temperature. Theoretical calculations showed that the sulfenyl radicals where responsible of the color [71].

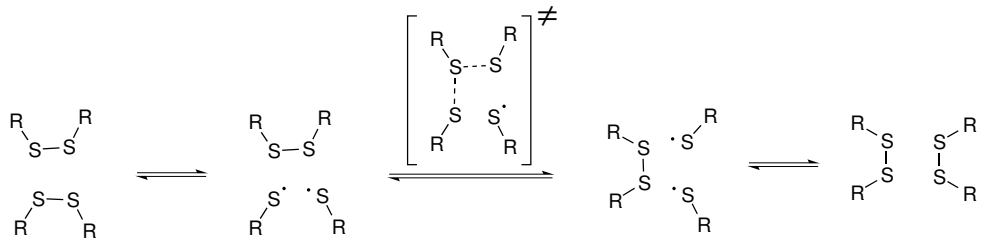

Figure 3.1: Schematic representation of the [2+1] radical mediated reaction mechanism.

This radical formation was favoured by weakening of the S-S bond due to amino groups linked to the diphenyl disulfides. This weakening explains that in some cases there is no need of heating the material to undergo the self-healing process, since a small amount of radicals may be formed at room temperature, which are the responsible for the self-healing capacity. Having this in mind, Matxain and Ruipérez further studied the possibility of lowering the S-S bond strength by two different strategies: including an amino group in between the disulfides and the phenyl groups, and removing the phenyl groups so that the disulfides are directly attached to the urea moieties [131]. In all cases, urea and urethane were considered to be the possible connection between the crosslink and the polymer. The authors concluded that the inclusion of these amino groups linked to the disulfide

indeed decreased the S-S bond strength, favouring in this way the radical formation. However, the calculated energy barriers were unfavourable compared to those of the diphenyl disulfide cases. Moreover, these authors also studied the self-healing process via the photodissociation mechanism, where the radicals are formed after the absorption of UV light by the material. In the excited state, an electron is promoted to the antibonding S-S bond, consequently decreasing the bond order and leading to the dissociation of the disulfide bond. In all the studied cases, this process needed UV light. Thus, it would be desirable to find out materials that could lead to this process via visible light, meaning that no external influence would be necessary.

In the mentioned works, small models were used to study the reactivity of the species. Nevertheless, these models were too small to study another important structural feature of these materials, namely, hydrogen bonding and other weak interactions among chains. In order to consider this, Formoso et al. [72] used bigger models to study the effect of non-covalent interactions on these systems, including hydrogen bonding, by means of classical molecular dynamics simulations. The authors reported that the number of hydrogen bonds formed is a key factor, as they directly affect the mobility of chains, in such a way that both an excessively large and small number of hydrogen bonds is detrimental for the self-healing process, since the chains may be either too rigid, avoiding the contact among disulfides, or too mobile, resulting in a smaller ratio of disulfides close enough to react.

Based on these works, the authors proposed a theoretical protocol to estimate the self-healing capacity of disulfide-based materials, depending on three parameters directly related to the previously discussed features: i) the radical formation probability (ρ); ii) the reaction rate constant (k) and iii) the probability of finding two disulfide bonds close enough to react (ω). However, several questions still remain unanswered. For instance, why diselenides apparently improve the self-healing capacity of these materials? Is it possible to find out disulfides or diselenides that are able to absorb visible light? Would it be possible to obtain self-healing properties in materials that do not contain ureas linked to the dichalcogenides? With the aim of answering partially or totally these questions, in this work we have focused on several materials containing S-S, Se-Se and mixed S-Se bonds. Concretely, aromatic chalcogenides, diphenyl diamine chalcogenides and aliphatic chalcogenides have been studied using the theoretical methods of quantum chemistry to be considered as an alternative to the disulfide bond for the self-healing process. The X-X (X = S, Se) bond dissociation energy, photodissociation, hydrogen bonds and reaction barriers will be studied for all these systems, in order to determine their theoretical self-healing capacity, with the aim of predicting new materials with improved properties.

3.2 Computational Details

All geometry optimizations were carried out in gas phase within density functional theory (DFT) [94, 95], by using the long-range corrected ωB97XD functional [132] combined with the 6-31+G(d,p) basis set [133]. Harmonic vibrational frequencies were obtained by analytical differentiation of gradients, in order to determine whether the structures found were minima or transition states. The frequencies were then used to evaluate the zero-point vibrational energy (ZPVE) and the thermal (T = 298 K) vibrational corrections to the enthalpy (H) and Gibbs free energy (G) in the harmonic oscillator approximation. Single point calculations using the 6-311++G(2df,2p) basis set [134] were performed on the optimized structures to refine the electronic energy. In order to understand the photodissociation process, Time-Dependent Density Functional Theory (TDDFT) [100] was used together with the 6-31+G(d,p) basis set. All DFT calculations were carried out using the GAUSSIAN16 package [135].

Ab initio Born–Oppenheimer Molecular Dynamics (BOMD) calculations were further carried out for the optimized species in order to determine their thermal stability, using the PBE functional [136, 137] combined with a DZP quality basis set and the RI formalism with the corresponding auxiliary basis sets [138, 139, 140]. The calculations were carried out at 298 K by means of the Nose–Hoover thermostat. All these simulations were as long as 40.000 a.u. (9.651 ps), with a time step of 40 a.u. (1.93 ps), and were performed using the TURBOMOLE package [141].

The analysis of the population of the natural orbitals was carried out using the Natural Bonding Orbital (NBO) method [142, 143, 144].

3.3 Results

In this chapter, a set of selenium-containing homonuclear (Se-Se) and heteronuclear (Se-S) dynamic covalent bonds has been computationally studied and compared to the well-known disulfide (S-S) bond, in the pursuit of new molecules that may improve the performance of disulfides in self-healing materials. Hence, both the thermal and photodissociation of these dynamic bonds, as well as the barriers of the exchange reaction have been computed using theoretical methods of quantum chemistry. To this end, molecular models have been constructed by the combination of three dynamic bonds (Se-Se, S-Se and S-S) and three backbones directly attached to the dynamic bond, labeled as PD (diphenyl), PA (diphenyl amino) and PF (phenyl-free). Besides, seven functionals groups (R_1 - R_7) linked to

the backbone have been also considered, generating a total of 63 molecular systems (see Figure 3.2). The three backbones are amino derivatives, since it was previously observed that this group is able to effectively weaken the disulfide bond, [69, 131] and are classified as phenyl derivatives (PD-XX), phenyl amino derivatives, including an extra amino group inserted between the phenyl ring and the dynamic bond (PA-XX), and phenyl-free derivatives (PF-XX), with X = S, Se. Thus, all functional groups are linked to the backbone by an amino group (-NH-) except for urethane (R_2), which is linked by the oxygen atom.

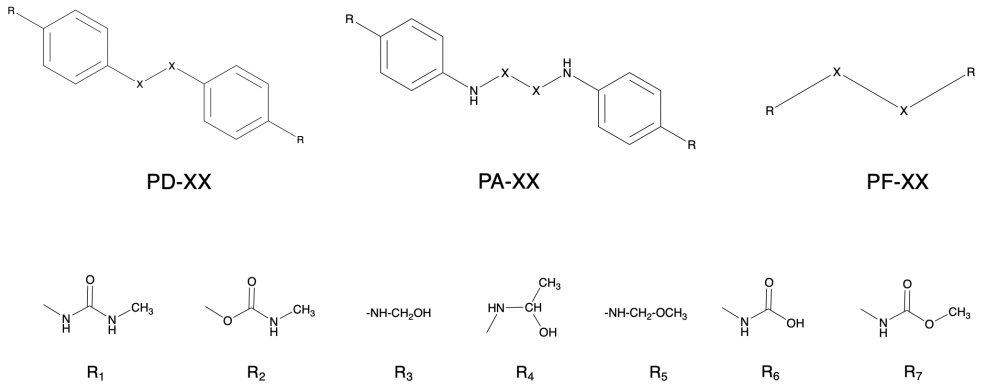

Figure 3.2: Models used in this work for X = S, Se. The substituents in *para* position are: urea (R_1), urethane (R_2), primary alcohol (R_3), secondary alcohol (R_4), ether (R_5), acid (R_6) and ester (R_7).

The results are organized as follows: i) the formation of sulfenyl and/or selenyl radicals will be discussed using the bond dissociation energy (BDE) of the X-X bond, and the role of the hydrogen bonding in this process will be considered as well; ii) the photodissociation process of the same bond and iii) the height of the barrier of the exchange reaction, which provides and estimation of the reaction rate constant.

3.3.1 Thermal Dissociation

In this section, the dissociation of all the model compounds is analyzed by means of the BDE, which is estimated as the variation of enthalpy in the process represented in Eq. 3.1.

$$RX - XR \xrightarrow[heat]{h\nu} 2RX^{\cdot} \tag{3.1}$$

Quantum molecular dynamics (QMD) have also been performed in order to estimate the probability to generate radicals (ρ), using the following

parameter (Eq. 3.2):

$$\rho = \frac{N_{X-X}}{N_{tot}} \tag{3.2}$$

which is defined as the number of simulation steps where the X-X bond distance is longer than a certain threshold value (N_{X-X}) for which the bond may be considered dissociated (and the radical formed), divided by the total number of simulation steps, N_{tot}. The threshold for the bond distances is determined after the inspection of the transition states of the exchange reaction (that will be analyzed hereafter) and corresponds to 2.30, 2.56 and 2.45 Å for S-S, Se-Se and S-Se molecular systems, respectively.

Table 3.1: Bond dissociation energy (BDE) of the X-X bond and interaction energy between two dichalcogenide units (RX-XR) due to the presence of hydrogen bonds, ΔH^{HB}, in kcal/mol, calculated at the ωB97XD/6-311++G(2df,2p)//ωB97XD/6-31+G(d,p) level of theory. ρ is the probability to generate sulfenyl and selenyl radicals obtained from QMD simulations.

		S-S			Se-Se			Se-S		
Model	R	BDE	ΔH^{HB}	ρ	BDE	ΔH^{HB}	ρ	BDE	ΔH^{HB}	ρ
PD-XX	R_1	48.55	30.40	0.0051	47.78	24.92	0.0122	44.03	32.21	0.0058
	R_2	51.99	33.64	0.0010	49.90	26.08	0.0040	47.05	17.45	0.0007
	R_3	45.36	23.46	0.0209	41.73	16.74	0.0081	41.12	31.38	0.0261
	R_4	37.66	37.35	0.0310	43.01	12.27	0.0094	40.79	32.76	0.0103
	R_5	47.86	18.38	0.0101	41.75	16.64	0.0041	41.41	18.42	0.0062
	R_6	45.27	32.73	0.0222	46.18	17.76	0.0009	44.18	23.52	0.0020
	R_7	41.57	33.91	0.0045	43.37	21.55	0.0000	43.53	20.31	0.0173
PA-XX	R_1	34.08	40.84	0.2382	34.97	40.98	0.1291	32.71	46.73	0.1101
	R_2	36.08	26.94	0.0890	39.13	25.39	0.0338	39.30	27.18	0.0832
	R_3	32.24	33.33	0.1682	32.08	35.85	0.0503	43.24	13.82	0.1049
	R_4	33.56	33.98	0.1269	32.23	29.90	0.0644	39.12	16.19	0.0348
	R_5	32.10	28.24	0.1322	31.65	29.12	0.0900	43.61	5.44	0.0767
	R_6	36.83	27.05	0.0818	39.77	5.22	0.0515	42.00	4.01	0.0649
	R_7	31.80	30.47	0.0929	39.20	6.86	0.0190	43.38	—	—
PF-XX	R_1	47.65	19.18	0.0682	43.97	15.60	0.0025	48.66	13.09	0.0376
	R_2	55.56	32.24	0.0000	49.25	24.98	0.0000	57.25	21.11	0.0000
	R_3	41.13	23.59	0.0736	40.03	13.50	0.0408	45.08	4.94	0.0159
	R_4	40.85	25.67	0.0360	40.28	9.12	0.0229	43.18	0.87	0.0209
	R_5	35.32	9.43	0.0152	36.04	8.87	0.0150	39.42	3.91	0.0204
	R_6	48.69	17.80	0.0000	42.99	7.37	0.0000	46.83	37.25	0.0021
	R_7	47.66	7.14	0.0000	40.90	17.15	0.0010	45.45	12.67	0.0010

In Table 3.1, it is observed that changing the dynamic bond induces small changes in the BDE, while the most relevant characteristic is the nature

of the backbone. This variation of the BDE may be ascribed to two main features [69]: the delocalization into the aromatic ring of the unpaired electron of the chalcogenyl radical generated in the dissociation (characterized by the spin density on the chalcogen atom, ρ_X, see Table SI) and the increase of the electron density in the antibonding σ^* orbital (see Appendix for Chapter 3). Lower values of ρ_X denote larger radical stability, and thus, lower BDEs. Similarly, higher values of the electron density in the antibonding σ^* orbital stand for lower bond orders (BO), and thus, lower BDEs. These two effects are additive in the PA-XX derivatives and are responsible of the observed reduction of the BDEs. Thus, the presence of the amino group between the phenyl ring and the X-X bond enhances the delocalization of the chalcogenyl radical (lower ρ_X) and increases the electron density in the σ^* orbital (lower BO). In PD-XX and PF-XX, however, these two effects are compensated and similar BDEs are calculated, in such a way that the bond order is generally higher for PD-XX, as the absence of the amino group directly linked to the dichalcogenide bond leads to lower electron density in the σ^* orbital. Meanwhile, the spin density is generally larger for PF-XX, as the absence of the phenyl group makes the radical to be less delocalized.

3.3.1.1 Effect of Hydrogen Bonding in BDE

In order to analyze the effect of hydrogen bonding (HB) in the cleavage of the X-X bond, the interaction of two dichalcogenide molecules has been considered (see Figure 3.3, left panel). The interaction energy due to HB (ΔH^{HB}) is collected in Table 3.1, and the representation of ΔH^{HB} versus the probability to generate radicals (ρ) is depicted in Figure 3.3, right panel, where a certain trend can be observed.

These results suggest that larger intermolecular interactions may enhance the probability to generate radicals. This feature may be ascribed to longer X-X bonds as a consequence of stronger interactions via hydrogen bonds, which are observed in the radial distribution function of the X-X bond lengths obtained from the QMD simulations. Thus, in order to clarify this feature, different distribution functions are compared in Figure 3.4.

Comparing the radial distribution of two non-interacting (monomeric) systems, such as PD-SeSe substituted with urea and urethane (Figure 3.4, top left), it is observed that the absence of hydrogen bonds produces very similar distributions in the bond lenghts. In top right panel, the distribution function of a monomer (the PD-SeSe urea derivative) is now compared to its corresponding dimer, and it is clearly observed how the presence of hydrogen bonds in the dimer shifts the distribution to larger Se-Se distances, suggesting that the intermolecular interactions favour the elongation of the dichalcogenide bond, and thus, weakening it. Since the number and the

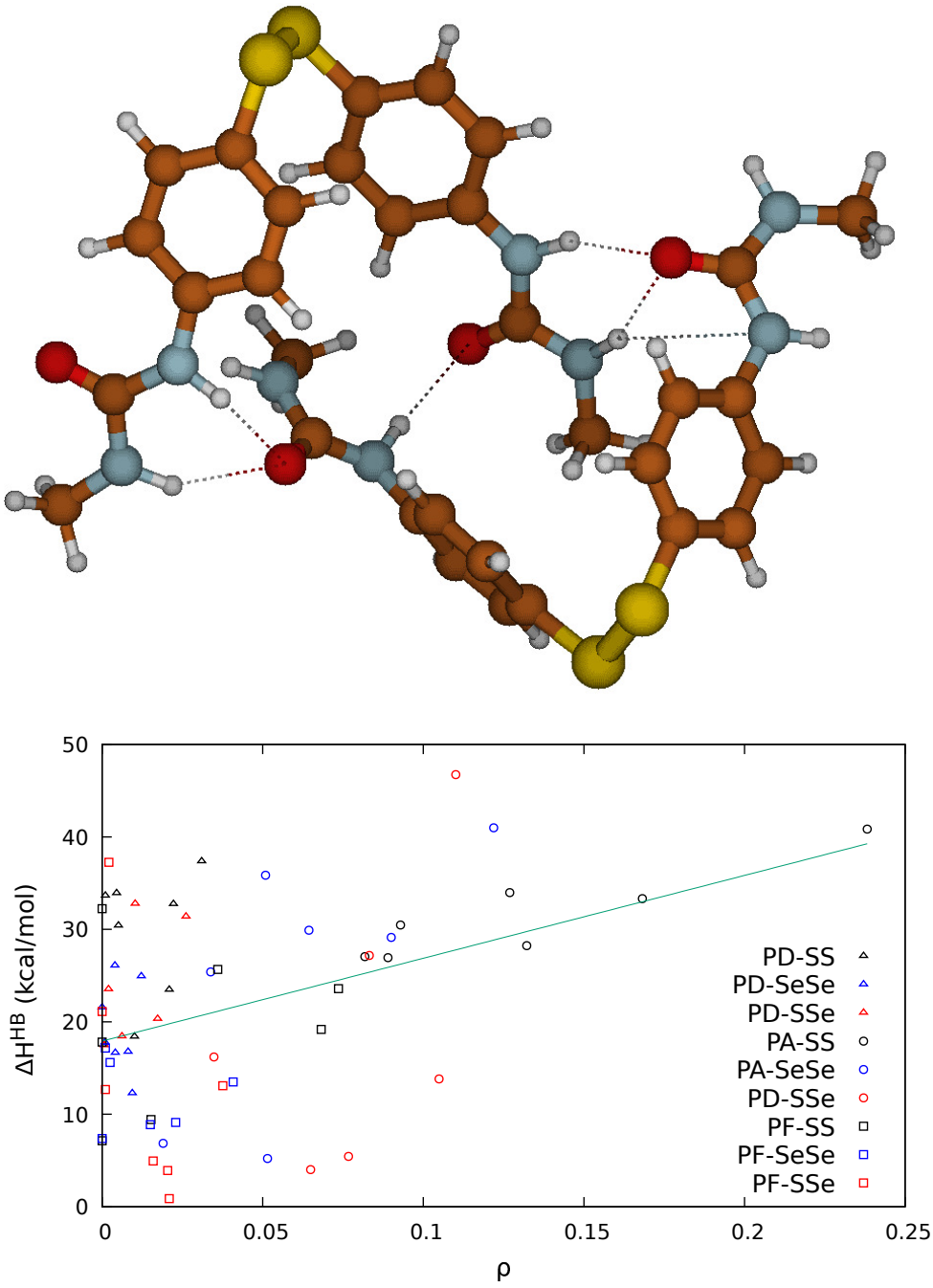

Figure 3.3: Left: Model compound formed by two dichalcogenide units interacting via hydrogen bonds. Right: Interaction energy of different dichalcogenide units (ΔH^{HB}, in kcal/mol), calculated at the ωB97XD/6-311++G(2df,2p)//ωB97XD/6-31+G(d,p) level of theory vs the probability of radicals to be formed (ρ), calculated at the PBE/def-SV(P) level of theory.

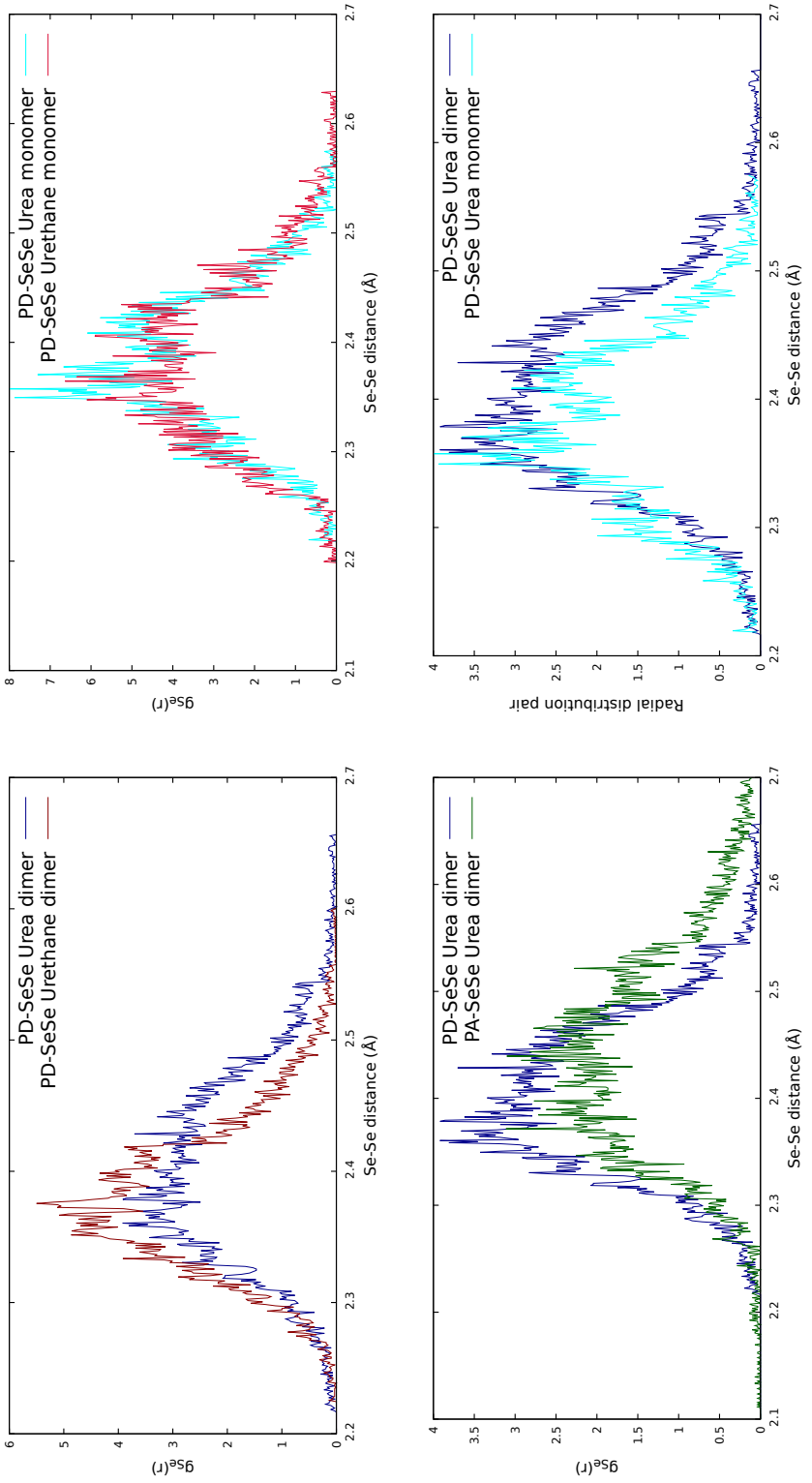

Figure 3.4: Radial distribution functions of the X-X bond by QMD simulations. Top left, comparison of two monomers (absence of HB). Top right, comparison of a monomer and a dimer. Bottom left, comparison of two derivatives (urea and urethane). Bottom right, comparison of two backbones (PD and PA).

strength of the HB depends on the molecular structure, in bottom left panel two different derivatives, urea and urethane dimers, are compared, as urea is more likely to establish hydrogen bonds than urethane. Indeed, the distribution of the urea dimer is also shifted towards larger Se-Se bond lengths, suggesting again that higher number of hydrogen bonds leads to elongation of the X-X bond. Finally, in bottom right panel, two different backbones are compared, PD and PA, and it is observed that the extra HB due to the insertion of the amino group between the X-X bond and the phenyl rings also induces the same effect, as the distribution function of the PA-SeSe urea derivative is shifted towards larger bond distances. This shift can be also noticed regarding the data collected in Table 3.2, where the average distancies of the Se-Se bond obtained in the QMD simulations, in $\mathring{A}$, and their corresponding variancies, in $\mathring{A}^2$, are shown. It can be seen that the mentioned shift in the radial distribution functions comes at once with the bigger average distancies obtained for the dimers. Moreover, larger values of average distancies such that of PA-SeSe-R_1, denote a larger right-shift on the radial distribution functions (Figure 3.4). Nevertheless, although a trend is observed, it is difficult to generalize to all the systems studied in this work.

Table 3.2: Average chalcogen-chalcogen distancies of the monomers and dimers of the PD-SeSe-R_1, PD-SeSe-R_2 and PA-SeSe-R_1 species, in $\mathring{A}$, and their corresponding variance, in $\mathring{A}^2$, calculated at PBE/def-SV(P) level of theory.

	Monomer		Dimer	
	r_{ave}	σ^2	r_{ave}	σ^2
PD-SeSe-R_1	2.384	0.0039	2.407	0.0043
PD-SeSe-R_2	2.386	0.0043	2.383	0.0031
PA-SeSe-R_1	2.444	0.0093	2.456	0.0215

3.3.2 Photodissociation

The photodissociation process has been characterized by the absorption wavelenght (λ) of the $S_0 \rightarrow S_1$ vertical transition and the corresponding oscillator strength (f), which are gathered in Table 2 of the appendix for this chapter, along with the nature of the transition for each molecular system. It is found that, in all the systems studied, the excited electron is located in the σ^* antibonding molecular orbital, which may considerably reduce the BDE of the excited state and, therefore, lead to dissociation [131].

The first striking feature is that the nature of the backbone has a remarkable effect on the absorption wavelength. Thus, PF-XX derivatives show the lowest values of λ, under 300 nm, in the UV region of the spectrum, corresponding to a $\sigma \rightarrow \sigma^*$ transition in the X-X bond, while the inclusion of phenyl groups induces a redshift owed to the participation of the π

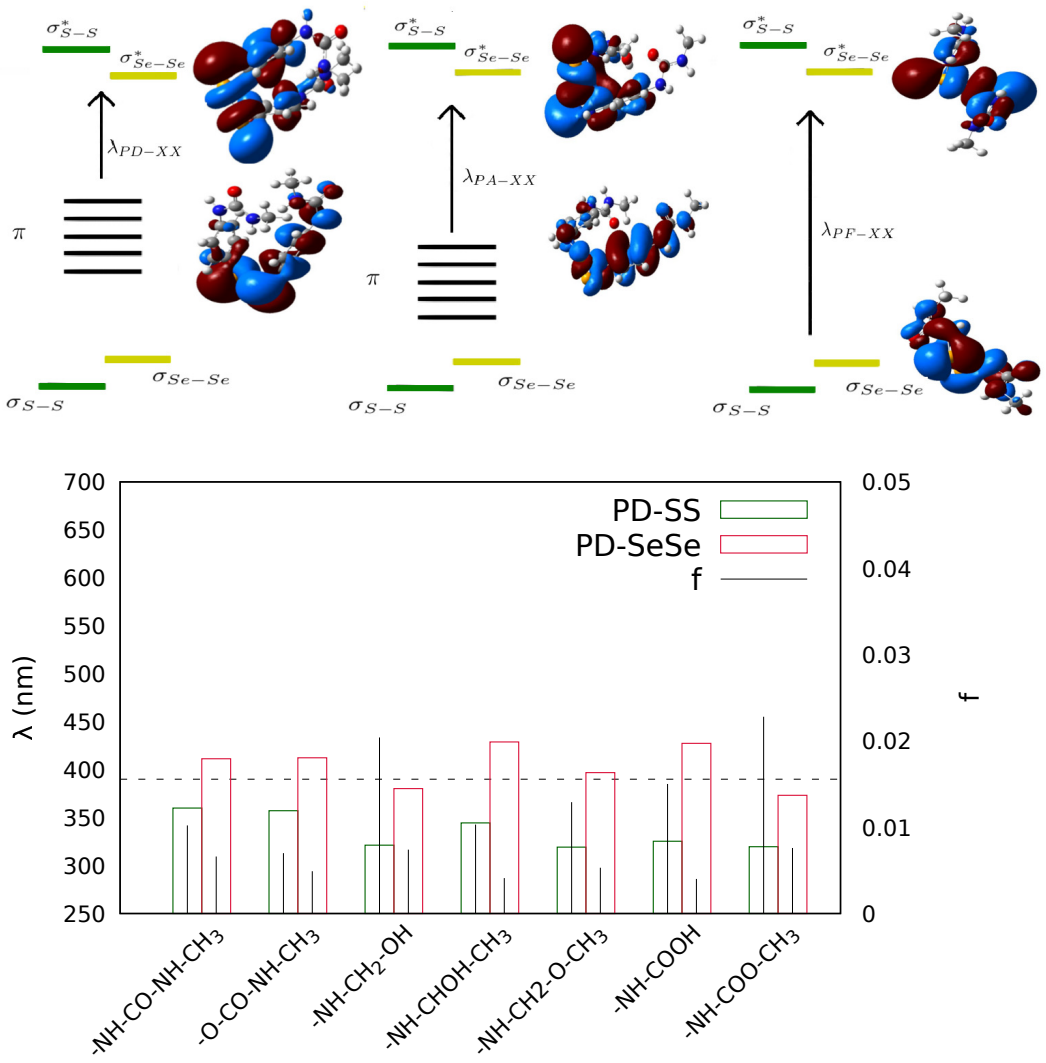

Figure 3.5: Top: Schematic representation of the molecular orbitals involved in the excitation process. Bottom: Graphical representation of the absorption wavelengths, in nm, of the PD-SS and PD-SeSe derivatives, and their corresponding oscillator strengths. Both calculated at the ωB97XD/6-311++G(2df,2p)//ωB97XD/6-31+G(d,p) level of theory.

molecular orbitals of the ring and, therefore, the $S_0 \rightarrow S_1$ transition is now a $\pi \rightarrow \sigma^*$ transition (see Figure 3.5, top panel). Among the systems including phenyl rings, the PD-XX derivatives present a larger redshift than the PA-XX ones, since in the latter the π molecular orbitals are stabilized by the extra π-conjugation with the amino group.

The substitution of sulfur by selenium has also a significant effect on the vertical absorption energy, that may be explained by a larger overlap between the $3p$ orbitals of sulfur in the S-S bond compared to that of the more diffuse $4p$ orbitals of selenium at equilibrium distance. This leads to a decrease of the excitation energies, as the σ_{Se-Se} molecular orbital will be more destabilized than that of the S-S bond, while the σ^*_{Se-Se} antibonding orbital will be more stabilized than the σ^*_{S-S}. The comparison of the absorption wavelength between PD-SS and PD-SeSe can be observed in Figure 3.5, bottom panel.

The combination of these two features allows some PD-SeSe derivatives to absorb in the visible region of the spectrum, with $\lambda > 390$ nm, as it is the case of PD-SeSe combined with substituents R_1, R_2 and R_4 - R_6, see Table 2 of the appendix for this chapter 1, and with λ close to 390 nm for R_3 (380.3 nm) and R_7 (373.2 nm). This means that the self-healing mechanism can be triggered by visible light, in agreement with recent experiments performed by Otsuka and collaborators, where they found that the self-healing process was achieved efficiently by irradiation of visible light in crosslinked polyurethanes containing aromatic diselenide bonds, while in the aliphatic ones the process was much less effective [**?**].

3.3.3 Reaction Mechanism

As it was mentioned in the Introduction, the reaction mechanism of the self-healing process is a [2+1] radical-mediated mechanism, where the generated chalcogenyl radical attacks a neighboring dichalcogenide bond through a three-membered transition state (see Figure 3.6, top panel) [65, 69, 70]. Thus, the characterization of the transition state is essential in order to analyze the reaction barrier. In this section, we have calculated the ΔG of the barrier of the exchange process for each system, that will allow us to estimate the reaction rate constants, k, according to the Wigner, Eyring, Polanyi and Evans formulation of the Transition State Theory [80, 145]:

$$k = \frac{k_B T}{h} e^{-\Delta G/RT} \tag{3.3}$$

Considering the nature of the dynamic bond, the breaking and reforming of homonuclear bonds will produce new homonuclear bonds (k_S, for disulfides,

k_{Se} for diselenides), however, when an heteronuclear bond is broken (S-Se), two different type of radicals are formed, namely, sulfenyl and selenyl radicals, which may attack either a selenium or a sulfur atom of a neighboring heteronuclear bond (see Figure 3.6, bottom panel). In this way, the following products can be generated: i) a disulfide bond, providing that a sulfenyl radical attacks the sulfur atom (k_1); ii) a diselenide bond, in the case that a selenyl radical attacks a selenium atom (k_4); and iii) a sulfur-selenium bond, if the sulfenyl radical attacks a selenium atom (k_2) or the selenyl radical attacks a sulfur atom (k_3).

The average ΔG values of the different systems (PD-XX, PA-XX and PF-XX with all the substituents) for every possible reaction (homonuclear: k_S, k_{Se} and heteronuclear k_1 - k_4) is represented in Figure 3.7, top panel. Regarding the different backbones, it is noticed that the PD-XX derivatives (red line) are the ones presenting lower barriers, between 8 and 14 kcal/mol, while both PA-XX and PF-XX derivatives show average values of ΔG over 14 kcal/mol, except for the homonuclear reaction of PA-SeSe (k_{Se}), which shows a notably lower mean value, around 12 kcal/mol. This behavior can be explained by inspecting the geometry of transition states. Thus, in the transition state of the PD-XX systems, a non-negligible $\pi - \pi$ stacking interaction between the phenyl rings exists, which not only stabilizes the transition state, but also keeps the chalcogenyl radicals close and maintains the optimal geometry to undergo the exchange reaction. The insertion of the amino group between the phenyl ring and the dynamic bond in the PA-XX derivatives causes a slight conformational change in the transition states, hindering an effective $\pi - \pi$ stacking interaction, as in the PD-XX. On the other hand, the PF-XX derivatives lacks the extra stabilization exerted by the phenyl rings and the conformational changes needed to reach the transition state increase the reaction barriers.

Regarding the dynamic bond, the attack of a selenyl radical to a diselenide bond (k_{Se}) shows a remarkably lower reaction barrier (in average) than the attack of a sulfenyl radical to a disulfide bond (k_S). Besides, this barrier is the lowest for PD-XX and PA-XX derivatives. This may be explained by a more effective spatial overlap between the Se $4p$ orbitals, which are bigger than the S $3p$ orbitals. To gain more insight into this, Natural Bonding Orbital (NBO) calculations have been performed on the transition state geometries of the R_1-substituted PD-SS and PD-SeSe systems, see Table 3.3.

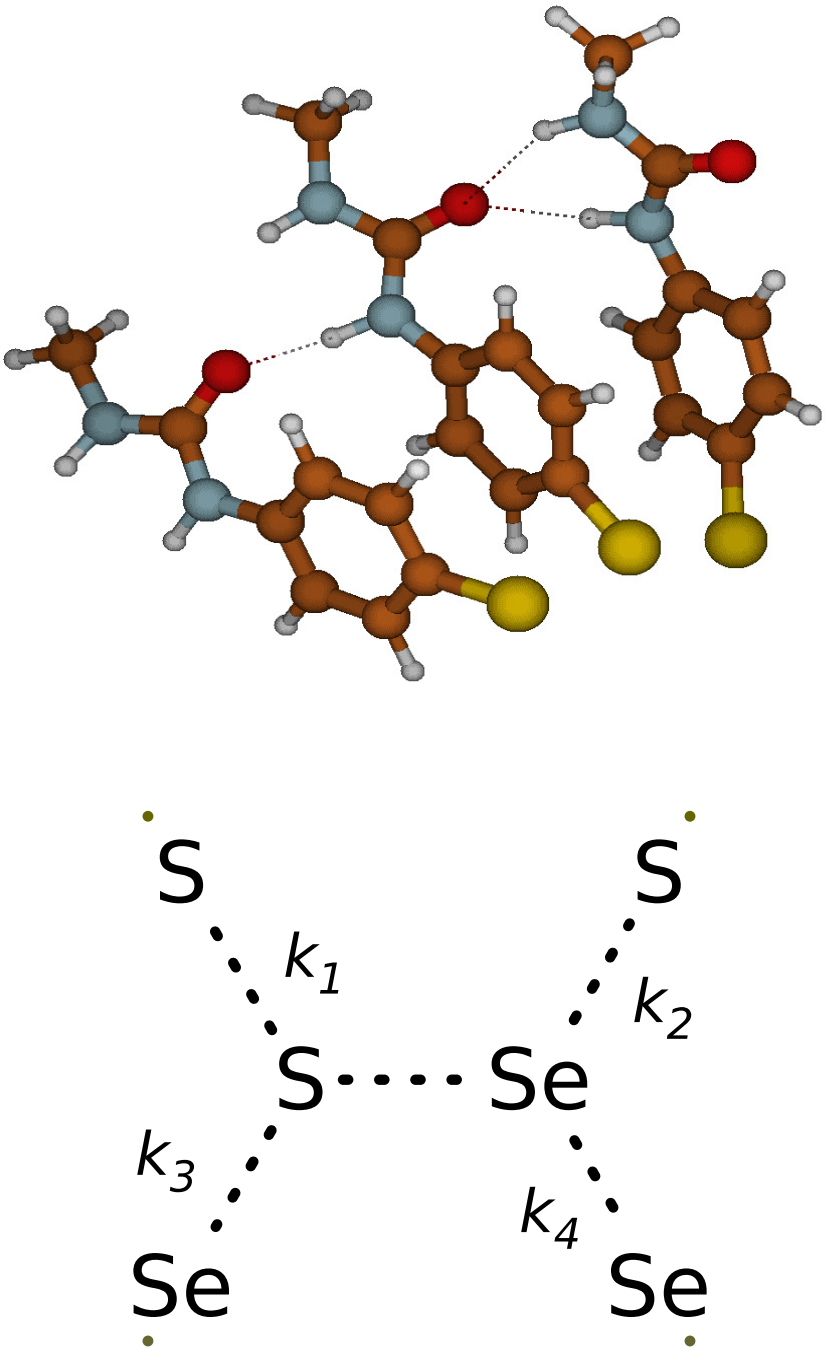

Figure 3.6: Top: Molecular structure of a three-membered transition state, calculated at the ωB97XD/6-311++G(2df,2p)//ωB97XD/6-31+G(d,p) level of theory. Bottom: Schematic representation of the possible reactions when a sulfide-selenide bond is broken.

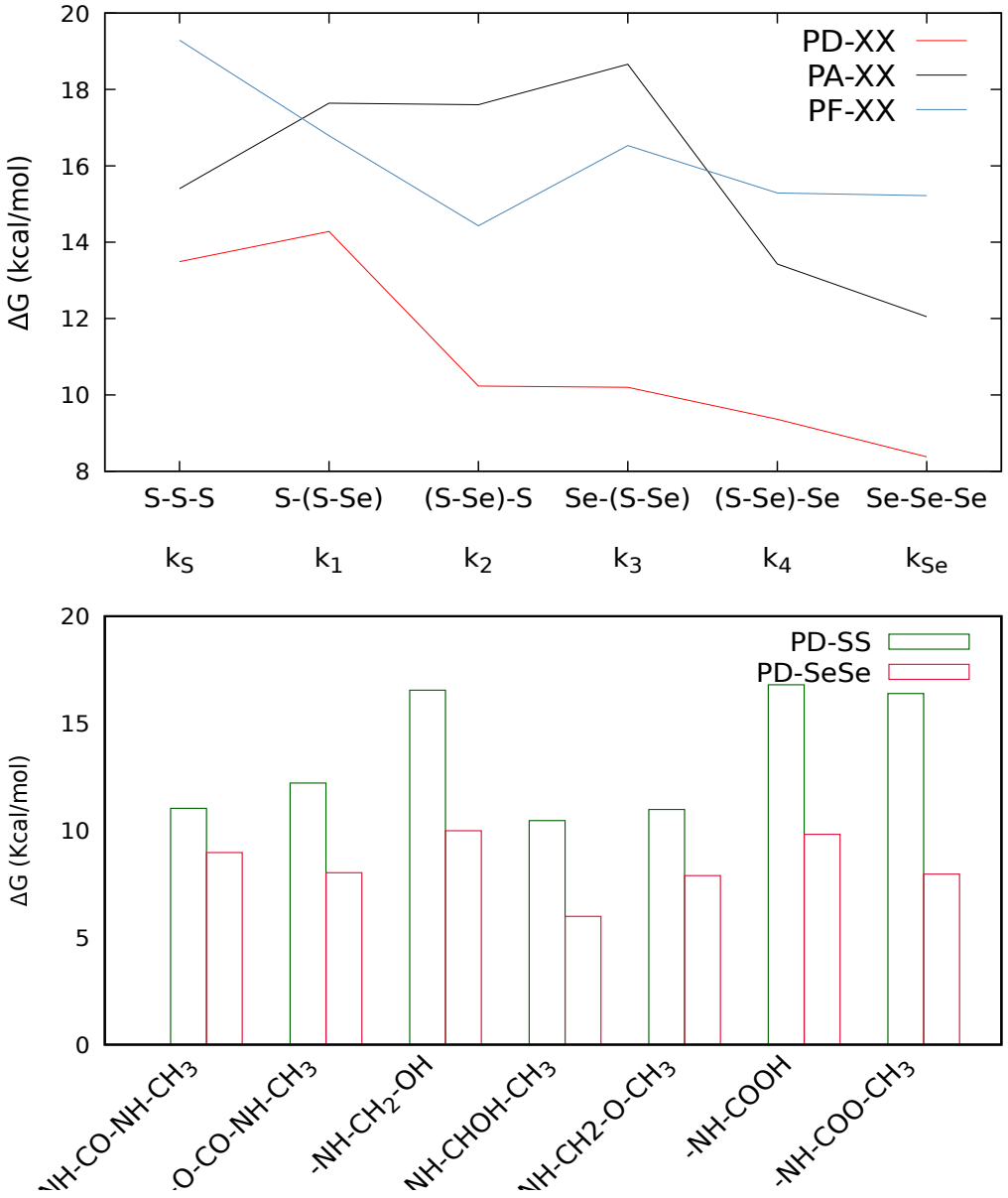

Figure 3.7: Top: Average reaction barriers, in kcal/mol, for PD-XX (red line), PA-XX (black line) and PF-XX (blue line). Bottom: Reaction barrier for PD-SS and PD-SeSe, in kcal/mol, calculated at the ωB97XD/6-311++G(2df,2p)//ωB97XD/6-31+G(d,p) level of theory.

In the case of selenium, two natural Se-Se bonding orbitals (BD), both with occupancy of 0.97, are obtained. In the case of the sulfur, however, only one S-S bond is formed, with lower occupancy (0.89) than that of selenium, while the orbital corresponding to the third sulfur atom appears to be a lone pair (LP) with occupancy of 0.99. These results confirm that the Se $4p$ orbitals are more capable than the S $3p$ orbitals to establish

a bonding interaction, stabilizing the transition states and, thus, yielding lower reaction barriers.

In Figure 3.7, bottom panel, the reaction barriers of the PD-XX derivatives including a homonuclear bond (k_S and k_{Se}) are represented. The decrease of the barriers in the Se-containing systems is clearly observed, with almost all of them showing barriers of less than 10 kcal/mol. Besides, regardless the dynamic bond, the barriers change accordingly with the selected substituent. This could be related to the amount of hydrogen bonds that can be formed, as more hydrogen bonds may stabilize the transition state. The most noteworthy case corresponds to R_4, which, for sulfur, presents a barrier of only 10.46 kcal/mol and for selenium it drops to 5.99 kcal/mol, the lowest value overall (see Table 3.4).

Table 3.3: Orbital occupancies from the NBO calculation in the geometry of the transition state calculated at the ωB97XD/6-311++G(2df,2p)//ωB97XD/6-31+G(d,p) level of theory. BD states for bonding and LP states for lone pair.

PD-SeSe		PD-SS	
Orbital	Occupancy	Orbital	Occupancy
BD Se_1-Se_2	0.97	BD S_1-S_2	0.89
BD Se_2-Se_3	0.97	LP(1) S_3	0.99
		LP(2) S_3	0.97

Finally, among the reactions that arise from the breaking of a heteronuclear bond, general trends may also be devised. Thus, those reactions involving an attack to a Se atom (k_2 and k_4) are faster (lower reaction barriers) that those involving an attack to a S atom (k_1 and k_3). Besides, the reactions leading to a diselenide bond (k_4) are faster than the ones leading to a disulfide bond (k_1).

3.4 Conclusions

In this chapter, a set of organic compounds including selenium-containing homonuclear (Se-Se) and heteronuclear (Se-S) dynamic covalent bonds have been computationally characterized in order to predict their self-healing capacity with the final aim of designing new materials that could improve the self-healing performance of the well-known disulfide-based (S-S) materials. In order to do so, three main compound families have been analyzed, namely, R-PD-XX (diphenyl dichalcogenides), R-PA-XX (diphenyl amine chalcogenides) and R-PF-XX (phenyl-free chalcogenides), being R different substituents such as urea, urethane, ethylenglycol, alcohols or esters. For all these species, we have focused on two main features: i) the sulfenyl and selenyl radical formation probability and ii) the energetic barriers of the exchange reaction that takes place in the healing process.

Table 3.4: Gibbs free energies of the transition state (ΔG^{TS}), in kcal/mol, and rate constants (k), in s^{-1}, calculated at the ωB97XD/6-311++G(2df,2p)//ωB97XD/6-31+G(d,p) level of theory.

		S-S		Se-Se		S-(S-Se)		Se-(S-Se)		(S-Se)-S		(S-Se)-Se	
Model	R	ΔG^{TS}	k	ΔG^{TS}	k	ΔG^{TS}	k	ΔG^{TS}	k	ΔG^{TS}	k	ΔG^{TS}	k
PD-XX	R_1	11.03	$4.97{\cdot}10^{4}$	8.97	$1.62{\cdot}10^{6}$	-	-	8.06	$7.51{\cdot}10^{6}$	5.78	$3.59{\cdot}10^{8}$	-	-
	R_2	12.21	$6.78{\cdot}10^{3}$	8.03	$7.95{\cdot}10^{6}$	-	-	10.45	$1.33{\cdot}10^{5}$	7.96	$8.90{\cdot}10^{6}$	7.75	$1.27{\cdot}10^{7}$
	R_3	16.55	$0.46{\cdot}10^{1}$	9.99	$2.90{\cdot}10^{5}$	18.25	$2.52{\cdot}10^{-1}$	8.14	$6.54{\cdot}10^{6}$	10.72	$8.42{\cdot}10^{4}$	8.20	$5.92{\cdot}10^{6}$
	R_4	10.46	$1.32{\cdot}10^{5}$	5.99	$2.52{\cdot}10^{8}$	13.32	$2.56{\cdot}10^{5}$	9.94	$3.13{\cdot}10^{5}$	14.95	$6.63{\cdot}10^{1}$	12.14	$7.68{\cdot}10^{3}$
	R_5	10.98	$5.40{\cdot}10^{4}$	7.89	$1.01{\cdot}10^{7}$	12.77	$2.66{\cdot}10^{3}$	12.93	$2.00{\cdot}10^{3}$	7.52	$1.87{\cdot}10^{7}$	8.05	$7.63{\cdot}10^{6}$
	R_6	16.80	$0.29{\cdot}10^{1}$	9.82	$3.86{\cdot}10^{5}$	13.69	$5.60{\cdot}10^{2}$	11.65	$1.76{\cdot}10^{4}$	12.58	$3.66{\cdot}10^{3}$	8.82	$2.09{\cdot}10^{6}$
	R_7	16.39	$0.58{\cdot}10^{1}$	7.96	$8.98{\cdot}10^{6}$	13.36	$9.67{\cdot}10^{3}$	10.21	$2.00{\cdot}10^{5}$	12.12	$7.87{\cdot}10^{3}$	9.60	$5.62{\cdot}10^{5}$
PA-XX	R_1	18.26	$2.46{\cdot}10^{-1}$	11.53	$2.15{\cdot}10^{4}$	15.56	$2.39{\cdot}10^{1}$	25.16	$2.12{\cdot}10^{-6}$	26.95	$1.04{\cdot}10^{-7}$	11.57	$2.00{\cdot}10^{6}$
	R_2	16.01	$1.12{\cdot}10^{1}$	11.27	$3.33{\cdot}10^{4}$	14.54	$1.32{\cdot}10^{2}$	25.53	$1.14{\cdot}10^{-6}$	24.41	$7.57{\cdot}10^{-6}$	11.46	$2.42{\cdot}10^{6}$
	R_3	7.87	$1.04{\cdot}10^{7}$	13.36	$9.82{\cdot}10^{2}$	17.30	$0.13{\cdot}10^{1}$	18.76	$1.06{\cdot}10^{-1}$	16.35	$0.63{\cdot}10^{1}$	15.68	$1.94{\cdot}10^{1}$
	R_4	15.30	$3.68{\cdot}10^{1}$	10.33	$1.63{\cdot}10^{5}$	17.46	$9.56{\cdot}10^{-1}$	16.38	$0.59{\cdot}10^{1}$	12.04	$9.07{\cdot}10^{3}$	12.01	$9.52{\cdot}10^{3}$
	R_5	15.85	$1.46{\cdot}10^{1}$	13.20	$1.29{\cdot}10^{3}$	18.42	$1.88{\cdot}10^{-1}$	9.94	$3.13{\cdot}10^{5}$	14.95	$6.63{\cdot}10^{1}$	12.14	$7.68{\cdot}10^{3}$
	R_6	17.02	$0.20{\cdot}10^{1}$	13.73	$5.22{\cdot}10^{2}$	18.40	$1.95{\cdot}10^{-1}$	14.38	$1.75{\cdot}10^{2}$	14.35	$1.82{\cdot}10^{2}$	12.53	$3.95{\cdot}10^{3}$
	R_7	17.47	$9.42{\cdot}10^{-1}$	10.93	$5.91{\cdot}10^{4}$	16.60	$0.41{\cdot}10^{1}$	15.16	$4.68{\cdot}10^{1}$	14.17	$2.47{\cdot}10^{2}$	14.77	$8.92{\cdot}10^{1}$
PF-XX	R_1	18.49	$1.66{\cdot}10^{-1}$	19.57	$2.70{\cdot}10^{-2}$	16.88	$0.25{\cdot}10^{1}$	15.95	$1.22{\cdot}10^{1}$	15.33	$3.48{\cdot}10^{1}$	9.88	$3.50{\cdot}10^{5}$
	R_2	17.47	$9.42{\cdot}10^{-1}$	18.49	$1.67{\cdot}10^{-1}$	14.07	$2.93{\cdot}10^{3}$	16.30	$0.68{\cdot}10^{1}$	17.40	$0.11{\cdot}10^{1}$	15.78	$1.63{\cdot}10^{1}$
	R_3	21.99	$4.56{\cdot}10^{-4}$	12.12	$5.18{\cdot}10^{1}$	15.03	$5.78{\cdot}10^{1}$	15.88	$1.38{\cdot}10^{1}$	12.42	$4.76{\cdot}10^{3}$	16.24	$0.75{\cdot}10^{1}$
	R_4	20.77	$3.52{\cdot}10^{-3}$	11.72	$1.56{\cdot}10^{4}$	17.46	$9.62{\cdot}10^{-1}$	13.16	$1.37{\cdot}10^{3}$	13.87	$4.09{\cdot}10^{2}$	12.04	$9.04{\cdot}10^{3}$
	R_5	21.90	$5.24{\cdot}10^{-4}$	-	-	13.82	$4.46{\cdot}10^{2}$	13.34	$1.01{\cdot}10^{3}$	13.32	$1.04{\cdot}10^{3}$	14.97	$6.45{\cdot}10^{1}$
	R_6	19.51	$2.97{\cdot}10^{-2}$	14.19	$2.40{\cdot}10^{2}$	21.06	$2.16{\cdot}10^{-3}$	21.76	$6.71{\cdot}10^{-4}$	12.09	$8.29{\cdot}10^{3}$	16.37	$0.61{\cdot}10^{1}$
	R_7	14.88	$7.54{\cdot}10^{1}$	-	-	16.59	$0.41{\cdot}10^{1}$	19.29	$4.30{\cdot}10^{-2}$	16.59	$0.41{\cdot}10^{1}$	16.81	$0.29{\cdot}10^{1}$

Radical formation may be due to two different processes, namely, thermal dissociation related to the dichalcogenide bond dissociation energy, and the photodissociation process that may take place after light absorption. Radical formation is the first step of the self-healing process and depends on the heat of the environment and light irradiation. Materials that do not require external activation for self-healing may either generate radicals by one of these processes or both of them. In this vein, thermal dissociation is related to low BDE of the dichalcogenide bond and the photodissociation to the absorption of visible light instead of UV. Hence, in order to analyze the thermal dissociation, the BDE and the probability to generate chalcogenyl radicals (ρ) are used for the discussion. The BDE is decreased due to two main features: the delocalization of the unpaired electron of the radical and the population of the antibonding σ^* molecular orbital. It is observed that these two factors are enhanced in the PA-XX derivatives, due to the amino group inserted between the phenyl ring and the dichalcogenide bond, while for PD-XX and PF-XX are compensated and, thus, similar BDEs are calculated. Besides, it is found that the nature of the dynamic bond slightly affects the BDE. Likewise, the presence of hydrogen bonds slightly tends to increase ρ as a result of an elongation of the X-X that is observed in quantum molecular dynamics.

Regarding the photodissociation, both the backbone and the dynamic bond play an essential role in this process. Thus, the excited electron is located in the antibonding σ^* molecular orbital, which effectively weakens the X-X bond, leading to dissociation. The nature of the transition depends on the backbone, in such a way that in PF-XX systems corresponds to a $\sigma \rightarrow \sigma^*$ transition, while in Ph-containing molecules, the excitation takes place from the aromatic π orbitals, redshifting the transition to longer wavelengths. Finally, the presence of selenium also increase the absorption λ, due to a poorer overlap of the Se $4p$ orbitals compared to the sulfur $3p$ orbitals, decreasing the $\sigma \rightarrow \sigma^*$ transition. Thus, in PD-SeSe derivatives, these two characteristics are additive and some molecules show absorption in the visible region, in accordance with previous experimental observations.

Finally, from the analysis of the reaction barriers, it is possible to conclude that the Ph rings are fundamental in order to decrease the barrier, as the existence of $\pi - \pi$ stacking interactions may stabilize the transition state and keep the radical close and the optimal geometry for the reaction to succeed. Therefore, the PD-XX systems show lower barriers. For the PA-XX, the insertion of the amino group distorts the geometry reducing the strength of the $\pi - \pi$ interactions and, therefore, larger barriers are calculated. Concerning the dynamic bond, the presence of Se reduces, in general, the reaction barriers, a feature that may be explained by a better spatial overlap between the $4p$ orbitals, larger than the corresponding sulfur $3p$ orbitals. As a consequence, the lowest barriers are calculated for PD-

SeSe.

In summary, the substitution of sulfur by selenium together with a proper choice of the backbone directly attached to the dynamic bond, may be considered as a good strategy to enhance the self-healing performance of the disulfide-based materials.

Chapter 4

Molecular Dynamics Study of Dichalcogenides as Building Blocks for Efficient Self-Healing Materials

Abstract

Recently, it has been descovered that the chemical mechanism in self-healing diphenyl dichalcogenide-based polymers involves sulfenil and selenyl radical formations. Hence, the chain mobility is crucial for the chemical reactions involving these radicals. In this work, systematic molecular dynamics simulations in a group of dichalcogenides have been carried out. Concretely, the systems under study have the general formula of R_n-YY-XX, where R_n stands for different substituents resembling different polymers, and YY-XX stands for the crosslinkers used in these polymeric chains. YY may denote PD (phenyl dichalcogenide), PA (phenyl-amine dichalcogenide) and PF (phenyl-free dichalcogenides), and XX stands for S-S (disulfides) and Se-Se (diselenides). First of all, a general protocol to study these systems has been established, and compared to previous protocols. An initial random conformation appears to be very important to obtain less biased results. With these results in mind, a new protocol has been proposed including the generation of the initial polymeric structure, simulation time, and other parameters. Then, molecular dynamics simulations have been carried out with this new protocol, in order to compare the behavior of different R_n-YY-XX systems. Considering previous quantum calculations on the systems under study in this work, and the results obtained in this work, a theoretical self-healing capacity of the systems under study have been estimated. In addition, we conclude that,in general, this new protocol behaves better than the previous one, and according to the obtained results.

4.1 Introduction

In previous works, [69, 131, 146] both aliphatic and aromatic disulfide- and diselenide-based materials, including different substituents, have been studied by analyzing the parameters obtained from quantum chemical calculations, namely, the probability of generating radicals and the reaction barrier. Only in the work of Formoso et. al. [72] the effect of the chain mobility (ω) on the self-healing process of some aromatic disulfide-containing urea and urethanes was estimated by means of molecular dynamics. It was observed that hydrogen bonding was the most relevant feature affecting chain mobility and that, both a large and a small number of hydrogen bonds were detrimental for the self-healing process, as chains would be either too rigid, avoiding the contact between disulfide bonds, or too mobile, decreasing the number of disulfides in the reaction region (lower values of ω). In this way, systems with intermediate number of hydrogen bonds showed larger values of ω.

Therefore, in order to have the complete picture of all the key factors determining the self-healing capacity at the microscopic level, in this chapter we perform a study of the chain mobility in the molecular systems for which the ρ and k parameters have been previously analyzed [69, 131, 146]. Concretely, diphenyl dichalcogenides (PD-XX), diphenyl amine-dichalcogenides (PA-XX) and phenyl free dichalcogenides (PF-XX) para- derivatives have been considered (see Figure 4.1), where X stands for S and Se. Five substituents have been considered in the para- position of all the mentioned cases, with the aim of resembling different polymeric chains where these PD-XX, PA-XX and PF-XX crosslinkers may be inserted. With all these considerations in mind, the studied systems are labeled in general as R_n-YY-XX, where n=1-5, YY= PA, PD, PF and XX = S-S, Se-Se. With these building blocks, different models have been tested for each case based on different sized chain separations between crosslinkers, as detailed in Section 4.2. The reliability of these models will be compared to that used by Formoso and coworkers [72]. In this way, we aim to investigate the effect of the molecular structure in the non-covalent interactions and in the mobility of the chains. Hence, a full theoretical self-healing capacity of the studied systems will be provided, combining the previously obtained parameters (ρ and k) with the parameter obtained from molecular dynamics simulations (ω).

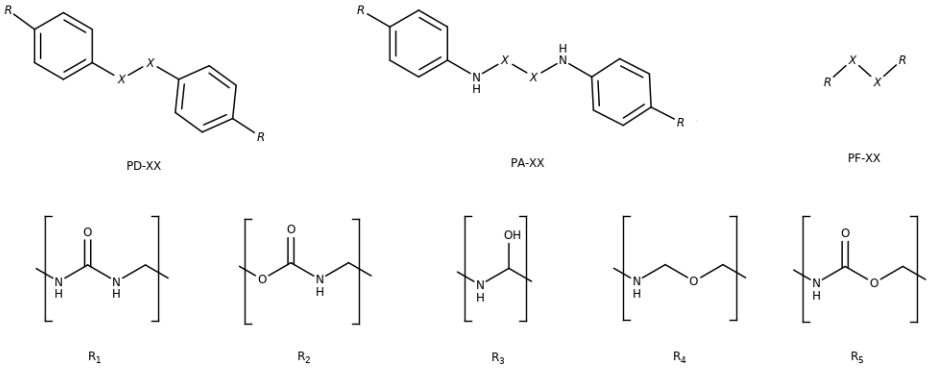

Figure 4.1: Molecular systems studied in this work with X = S, Se. Top: the three backbones, diphenyl (PD), diphenyl amine (PA) and phenyl free (PF). Bottom: the five substituents, urea (R_1), urethane (R_2), secondary alcohol (R_3), ether (R_4) and ester (R_5).

4.2 Computational Details and System Models

4.2.1 Molecular Dynamics Simulations

The Molecular Dynamics (MD) simulations have been performed using ff14SB [147] amber force-field in the AMBER 14 molecular dynamics simulation package [148]. The parameters corresponding to the diphenyl diselenide derivatives have been those obtained by Torsello et. al. [149]. All structures were built via the LEaP module of Ambertools and the charges were computed using the restrained electrostatic potential (RESP) fitting procedure [150]. First the ESP was calculated by means of the Gaussian package [135] using the 6-31G* basis set at Hartree-Fock level of theory and then the RESP charges were obtained. All the simulations were carried out in vacuum in a canonical ensemble (NVT) with a 2 fs timestep. 100000 steps of minimization (50000 steps steep descent minimization plus 50000 steps of conjugate gradient minization) were followed by heating from 80 K to 300 K over 200 ps, an equilibration time of 1800 ps with a Langevin thermostat and a production of 30 ns for the polymeric chains (between 1456 and 1808 atoms). Covalent bond lengths involving hydrogen were constrained using the SHAKE algorithm.

In order to analyze the hydrogen bonds, we consider a threshold for the bond length between the donor and acceptor (X$\cdots$Y) smaller than 3.5 Å and the range of X-H$\cdots$Y angles varies between 140 and 220 degrees. In addition, to see the evolution of the hydrogen bonding along the simulation time, the hydrogen-bond occupancy is defined as $HB_{Occ} = 100\frac{\sum nHB}{t}$,

where nHB denotes the number of formed hydrogen bonds, at a given step, according to the criteria for the bond lengths and angles mentioned above, and t is the number of simulation frames. Thus, HB_{Occ} represents the fraction of time that the hydrogen bond is formed. In addition to this, in order to describe the size of a polymer chain, the radius of gyration (r_{gyr}) is defined as $r_{gyr}^2 = \frac{\left(\sum_{i=1}^{N}(r(i)-\bar{r})^2\right)}{N}$, where $\bar{r}$ is the geometric center of mass of the system. It corresponds to the root-mean-square distance of the atoms from the center of mass.

4.2.2 Validation of the Computational Protocol

In the work by Formoso et. al. [72], molecular dynamics calculations were performed using certain simulation constrains, such as the molecular model or the simulation time. Considering that the interactions among long chains in a complex polymeric system were simulated by short models, these conditions could be too restrictive. In this study, with the aim of obtaining more realistic conditions, different simulation parameters have been evaluated to see how they affect in the analysis of the non-covalent interactions among chains. In particular, we have tested the following: (i) the initial molecular guess, (ii) the length of the chains, (iii) the size of the simulation box and (iv) the simulation time. In order to do such analysis, R_1-PD-SS and R_2-PD-SS compounds were chosen according to the labeling described in the Introduction.

For the validation, we make use of number of hydrogen bonds and their influence in the previously mentioned parameter ω, which is based on the distance between dichalcogenides and is defined as:

$$\omega = \frac{I_i}{I_i + I_{ii}} \tag{4.1}$$

Using the radial distribution function of the chalcogen atoms, three regions may be defined in order to calculate ω: the reacting region (I_i), where dichalcogenides are close enough to undergo the exchange reaction (R $\leq$ 4.5 Å), the neighboring region (I_{ii}), where dichalcogenides are far to react but with a non-negligible probability to approach the reacting region (4.5 $<$ R$<$ 20 Å), and the external region (I_{iii}), where dichalcogenides are neglected (R $>$ 20 Å). The amount of chalcogen atoms located in each region is calculated by integration of the radial distribution function within the limits defined above. These limits may change depending on the system analyzed, as it will be discussed hereafter.

4.2.2.1 Initial Guess and Chain Length

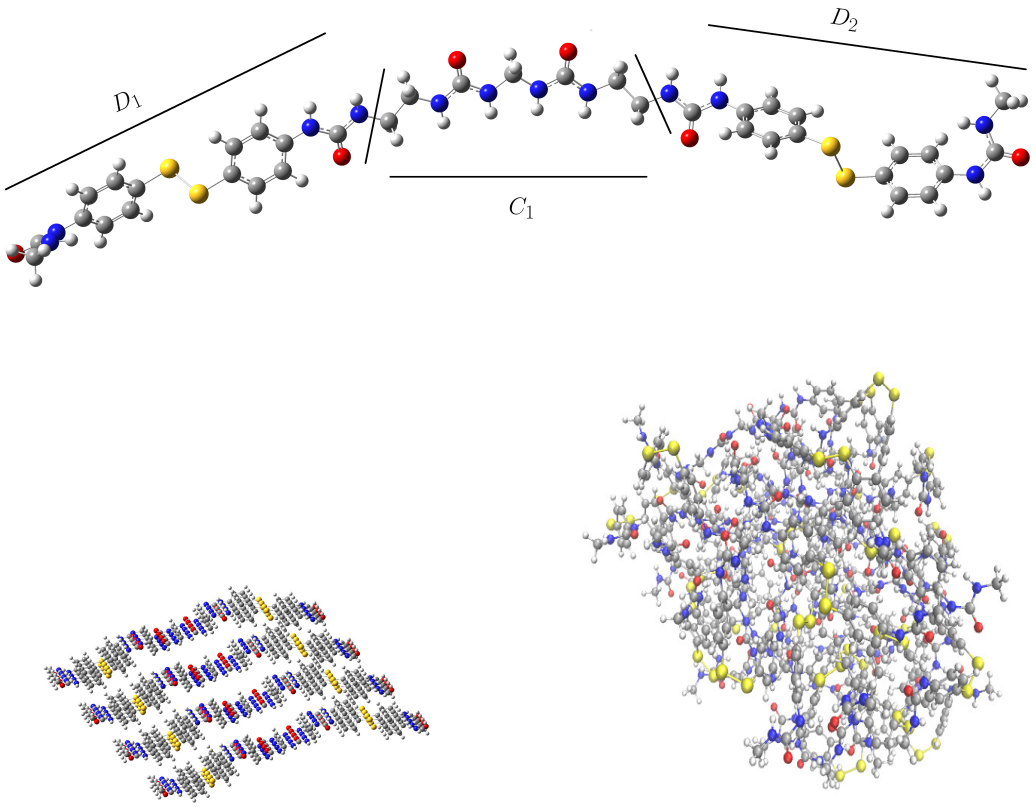

Figure 4.2: Top: Single chain of the molecular model used in the validation step, consisting of two urea-substituted diphenyl disulfides (D_1 and D_2 units) linked by a polyurea-like chain (C_1 unit). Bottom: periodic (left) and random (right) initial conformations before equilibration. Sulfur atoms in yellow, nitrogen in blue and oxygen in red.

In the previous work, Formoso et. al. built the model from a single chain formed by two phenyl disulfide monomers (D_1 and D_2 units in Figure 4.2, top) linked by a urea-methyl-urea or urethane-methyl-urethane unit (C_1 in the same Figure). This chain was then replicated in space in order to generate a 3D structure. For that, four replicas of the chain were placed along two spatial directions using translation vectors. The resulting initial conformation, before the equilibration step, is depicted in Figure 4.2 (bottom left).

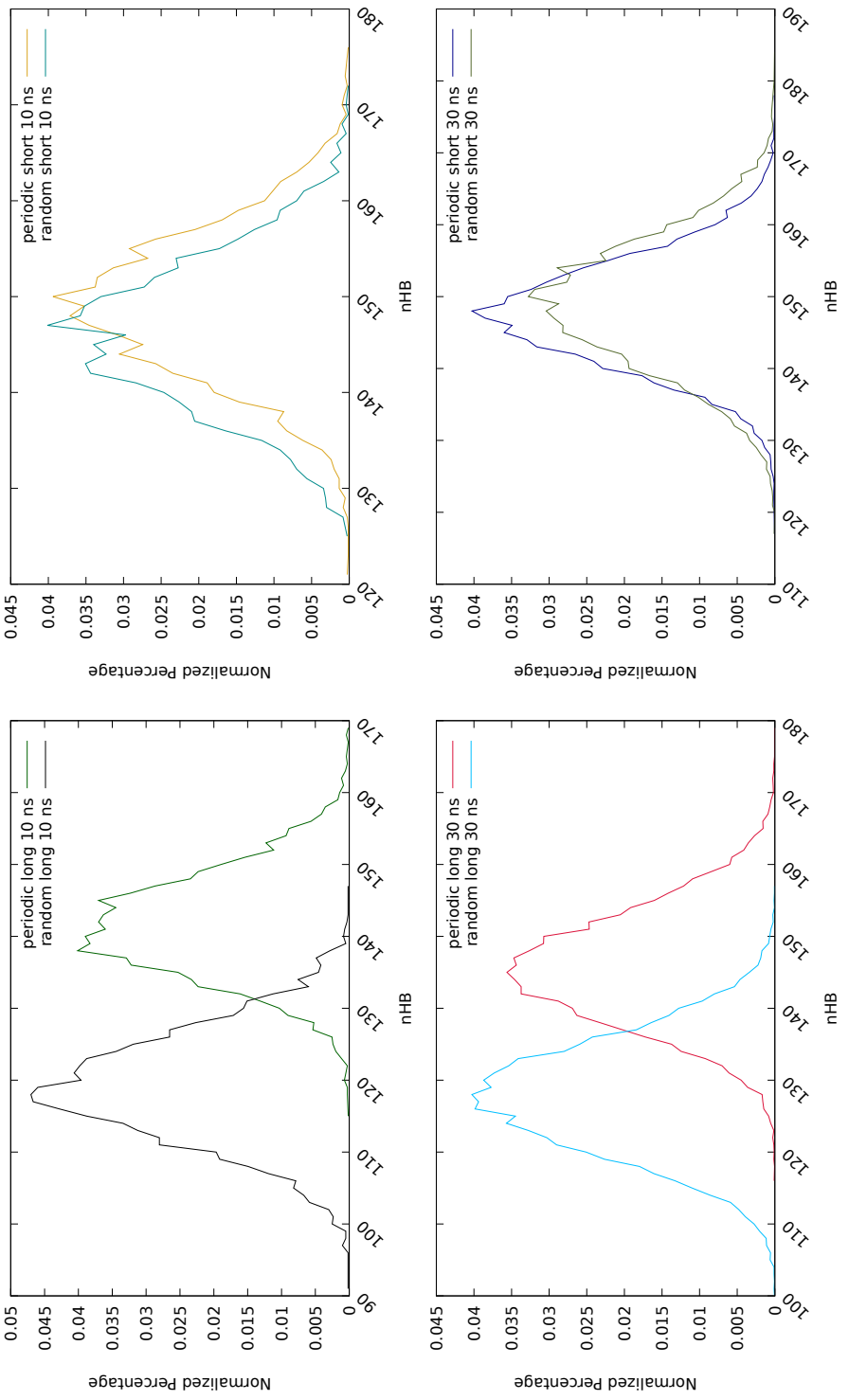

Figure 4.3: Normalized percentage of hydrogen bonds of the periodic and random conformations with short (top) and long (bottom) chains, obtained after 10 (left) and 30 (right) ns of simulation.

It can be observed that the use of translation vectors yields a laminar-like periodic structure that may introduce a structural bias. In this work, we have considered a random initial guess (see Figure 4.2, bottom right) in order to have a more realistic description of a complex polymeric system. Besides, the chain length has also been increased by including one additional -(CH_2)- group between both disulfides and the polyurea chain (C_1 unit).

The results of the simulations for the two initial structures (periodic and random) and the two molecular chains (with and without the additional methyl group, labeled as long and short, respectively) are collected in Table 4.1, where the total number of hydrogen bonds (HB_{tot}) and the maximum (HB_{max}), minimum (HB_{min}) and average (HB_{ave}) number of hydrogen bonds at a given step of the simulation are provided, together with ω. Besides, two simulation times (10 and 30 ns) are considered, that will be discussed later.

Considering the initial guess for the short chain, the total number of hydrogen bonds is similar for both systems, see Table 4.1 and also Figure 4.3 (top), where the normalized percentage of hydrogen bonds is represented. Nevertheless, the distribution is different. In the periodic structure, the hydrogen bonds are mainly formed between the same components of different chains, that is, both the disulfide units and the linking chain tend to form HBs with their counterparts of the surrounding chains (D_1-D_1, D_2-D_2 and C_1-C_1), see Figure 4.2, bottom left. This introduces a bias that will affect the equilibration step and, therefore, the rest of the simulations. On the other hand, in the random conformation, each unit can establish HBs with any other unit of the surrounding chains that is close enough, and may be considered as a more realistic situation. This change in the distribution is responsible of the observed decrease in ω for the random conformation. In the periodic model, disulfide bonds are located periodically along the system, in such a way that every disulfide is close to another neighboring disulfide bond, favoring the D_1-D_1 and D_2-D_2 interactions and maximizing the value of ω. On the other hand, the interactions between disulfides laying on different sides of the chain (D_1-D_2) will be more scarce, contributing to a lowering of this parameter. In the random conformation, however, an opposite situation may take place. Since the disulfides will not necessarily have another disulfide nearby, the probability of the D_i-D_i interaction is lower and, hence, ω will also be smaller. Nevertheless, the probability of the D_i-D_j interaction is higher, contributing to enlarge ω. The net effect, as it is observed in Table 4.1, is that ω is lower for the random conformation. This effect is found to be independent of the length of the chain and the simulation time. This means that the use of a periodic model induces an arbitrary preference in the interaction between adjacent disulfides (D_i-D_i) and ω may be overestimated.

Table 4.1: Total number of hydrogen bonds (HB_{tot}), maximum (HB_{max}), average (HB_{ave}) and minimum (HB_{min}) number of hydrogen bonds at a given step, and ω obtained for the periodic and random starting guess, with and without the extra methyl group in the molecular model (long and short chains, respectively), for 10 and 30 ns of simulation time.

Chain	Guess	HB_{tot}	HB_{max}	HB_{ave}	HB_{min}	ω	HB_{tot}	HB_{max}	HB_{ave}	HB_{min}	ω
				10 ns					30 ns		
Short	Periodic	746461	176	149	121	0.0884	2215568	178	148	117	0.0776
	Random	730119	172	146	118	0.0696	2233776	184	149	117	0.0627
Long	Periodic	707860	169	142	115	0.0931	2184978	179	146	116	0.0970
	Random	595587	147	119	91	0.0393	1917000	157	128	100	0.0188

If a long chain is considered (with an extra -(CH_2)- group), notable differences are found between the periodic and the random systems regarding the hydrogen bonds. In both cases, a decrease of the total number of hydrogen bonds is observed, but it is particularly pronounced for the random system (from 730119 to 595587, after 10 ns). A larger chain unit (C_1) means a separation of the groups that can form HBs, both intermolecular and intramolecular, reducing the possibility of interactions and, therefore, the total (HB_{tot}), maximum (HB_{max}) and average (HB_{ave}) number of HBs is decreased. In the periodic system, this effect is small, since the laminar structure is kept and the starting HBs (from the D_i-D_i and C_1-C_1 interactions) remain. The observed decrease (from 746461 to 707860, after 10 ns) may be ascribed to the changes in the geometry of the chains induced by the new methyl group. In fact, this effect is largely mitigated in the longer (30 ns) simulation of the periodic structure, since a longer simulation time allows the structure to reorganize and recover the lost HBs. The differences between the periodic and random structures are clearly observed in Figure 4.3 (bottom), in the normalized percentage of hydrogen bonds after 10 ns (left) and 30 ns (right) of simulation time is represented.

Comparing the radius of gyration of the short chains (Figure 4.4, top), the periodic system oscillates close to 14 Å, while the one corresponding to the random system appears around 12.5 Å. This suggests that the periodic structure somewhat retains the laminar-like structure after the equilibration, while the random structure acquires a more coiled conformation. When the system is built with long chains, the same feature is observed (Figure 4.4, bottom), but with larger values.

As a summary, we can conclude that the periodic starting structure is less suitable to perform the simulations, since its periodicity introduces a bias that may affect to the estimation of ω.

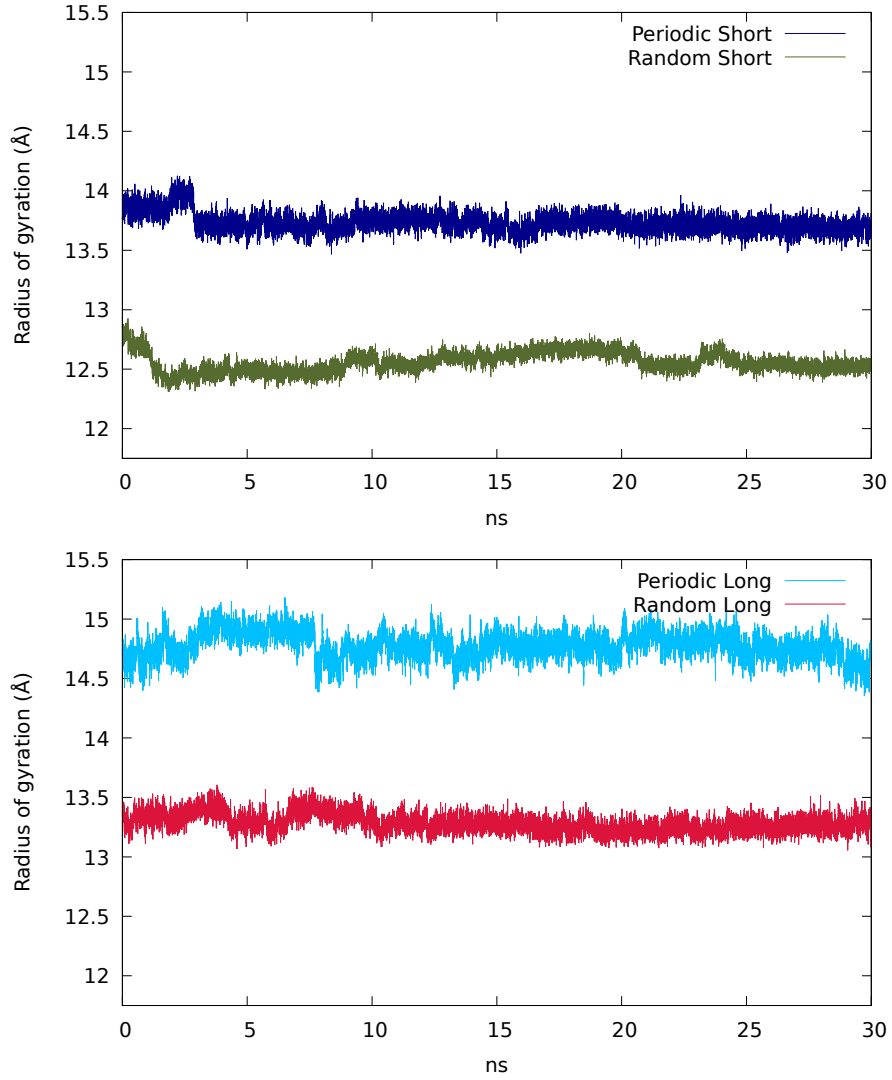

Figure 4.4: Radius of gyration (Å) of the periodic and random systems with the short (top) and long (bottom) chains obtained in 10 and 30 ns simulations.

4.2.2.2 Size of the Simulation Box

Table 4.2: Total number of hydrogen bonds (HB_{tot}), maximum (HB_{max}), average (HB_{ave}) and minimum (HB_{min}) number of hydrogen bonds at a given step, and ω, for three simulation boxes using the random system with long chains after 30 ns of simulation.

Box	HB_{tot}	HB_{max}	HB_{ave}	HB_{min}	ω
40×30×30	1917000	157	128	100	0.0188
40×40×40	1900841	158	127	95	0.0490
50×50×50	1902463	160	127	97	0.1058

Another important parameter is the size and shape of the simulation box, which determines the density of the system along the simulations. In the previous simulations by Formoso et. al. [72], a square prism of 40×30×30 nm was used and now it has been compared to a cubic box of two different sizes: 40×40×40 and 50×50×50 nm. The results are collected in Table 4.2 and in Figure 4.5, where the radial distribution function of each sulfur with respect to the others is represented, excluding their counterparts in the disulfide S-S bond. Despite the number of hydrogen bonds remains basically unchanged, the shape and the size of the box have a big impact on the radial distribution function and, thus, in ω. This suggests that there is a frontier effect that may be avoided using larger and regular boxes.

In conclusion, having all these considerations in mind, a random conformation with long chain have been selected to carry out the molecular dynamics simulations, using a cubic simulation box, with a simulation time of 30 ns for each system, given that longer the simulation time allows the exploration of a bigger number of conformations.

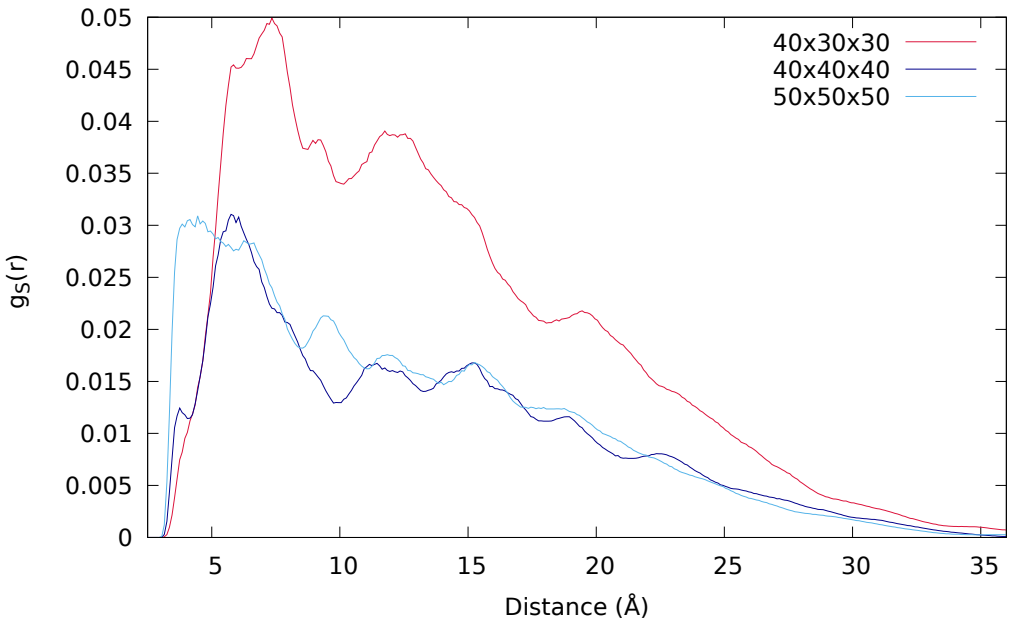

Figure 4.5: Radial distribution functions of the sulfur atoms of the PD-urea derivative including the extra -(CH_2)- obtained in 10 and 30 ns simulations by using simulation boxes of 40×30×30, 40×40×40 and 50×50×50 nm.

4.3 Results

Once the simulation conditions have been optimized, the results obtained for all the R_n-YY-XX molecular systems are presented and analyzed. In

particular, we discuss the influence of the backbone YY (PD, PA, PF), substituents R_n (n = 1-5) and chalcogenide XX (X = S, Se) in: (i) the dimension and flexibility of the chains, (ii) the non-covalent interactions, namely, the hydrogen bonding, and (iii) the radial distribution functions of the sulfur and selenium, from where ω is obtained. Finally, we will estimate the self-healing theoretical capacity for each material.

4.3.1 Influence of the Backbone: PD, PA and PF

In order to analyze the effect of the backbone composition, the PD-, PA- and PF-SS disulfides substituted with the urea moiety (R_1) were chosen. The results are collected in Table 4.3. It is observed that HB_{tot} is similar in PD and PF but is notably increased in the PA derivatives. This result is consistent with the incorporation of an extra amino group that is able to establish hydrogen bonds. This feature is also clearly noticed in Figure 4.6 (right), where the normalized percentage of hydrogen bonds is represented.

Table 4.3: Total number of hydrogen bonds (HB_{tot}), maximum (HB_{max}), average (HB_{ave}) and minimum (HB_{min}) number of hydrogen bonds at a given step, and ω obtained for urea-substituted (R_1) disulfides including the three backbones PD, PA and PF.

R	Backbone	HB_{tot}	HB_{max}	HB_{ave}	HB_{min}	ω
R_1	PD	1902463	160	127	97	0.1058
	PA	2620182	213	175	142	0.0419
	PF	1940357	161	129	102	0.1224

In Figure 4.6 (left), the radial distribution functions of sulfur for the three derivatives are represented. It can be seen that the PF derivative presents higher peaks (larger values of disulfide population) at rather close distances and decay more rapidly than the other two. Taking into account the structure of this derivative, the absence of the phenyl ring may favour the presence of neighbouring disulfides closer. The steric hindering caused by the phenyls is also clearly seen in the radial distribution functions of the PD and PA, as they show lower values than PF of disulfide population at distances where the phenyl rings are expected to be (<10 Å). Moreover, since in PF and PA the disulfide bond is directly attached to a group that can form hydrogen bonds (the amino group), these interactions may contribute to limiting the mobility of the disulfides and, therefore, hindering their approach. This feature is reflected in the radial distribution functions, where PF and PA show the highest peaks shifted to longer distances compared to that of PD, especially for PA, for which both the reduced mobility due

to hydrogen bonding and the steric hindrance of the phenyls contribute to shifting this peak to even longer distances than for PF.

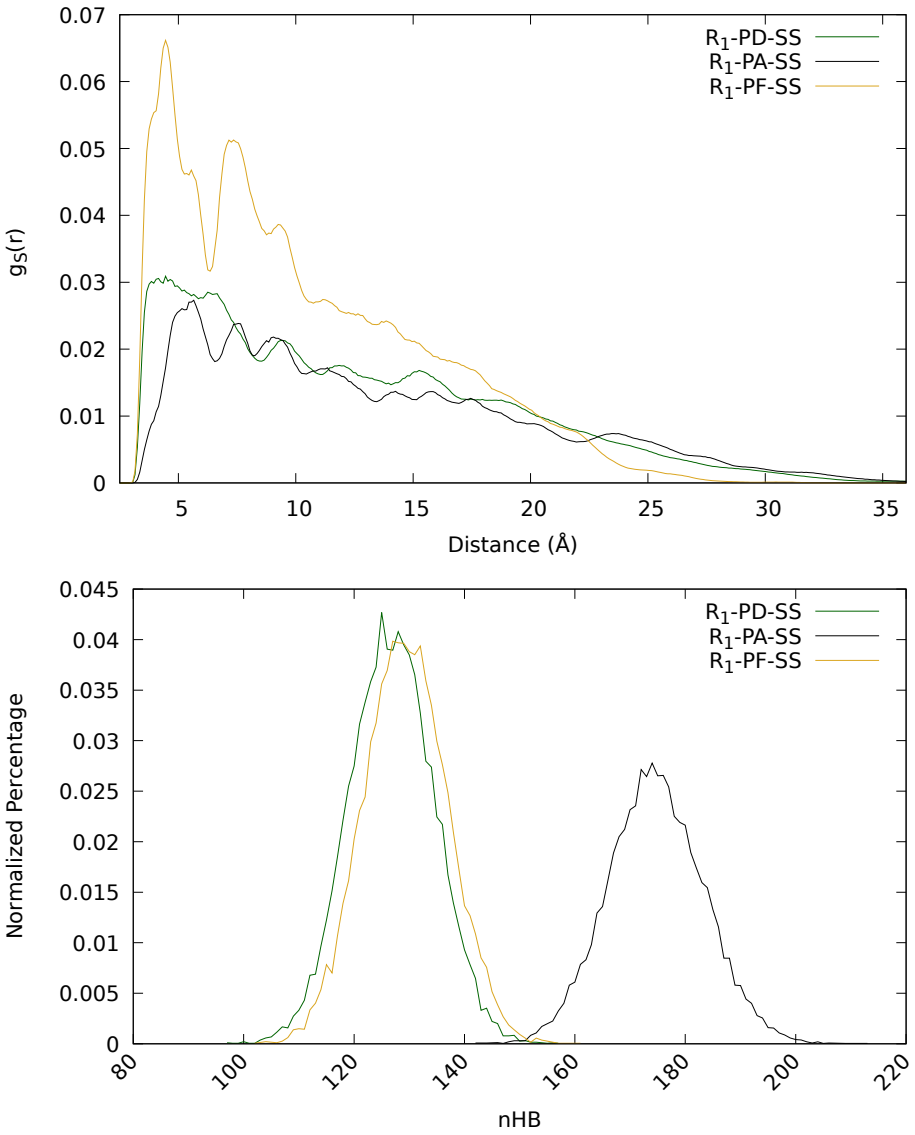

Figure 4.6: Radial distribution functions (left) and normalized percentage of hydrogen bonds (right) of the urea-substituted PD-, PA and PF-disulfide derivatives.

Regarding ω, as it has been previously observed, the main factor is the hydrogen bonding. Formoso et al. showed that both an excessively large or small amount of hydrogen bonds is detrimental for an optimal ω value [72]. Thus, the remarkable increment of hydrogen bonds in the PA derivative with respect to PD and PF (see Table 4.3), leads to a lower value of ω, which can be related to too rigid chains. Both PD and PF show similar

values of ω, which may be explained due to the lack of steric hindrance of the phenyl in PF compensating the less mobility of the sulfurs induced by the hydrogen bonds formed by the extra amino group.

4.3.2 Influence of the Substituents (R_1-R_5) and Chalcogenide Atoms

In this subsection, the effect of the chemical structure of the polymeric chain (R) and dichalcogenide bond (S-S vs Se-Se) are analyzed. Concretely, R_n-PD-XX systems have been chosen to carry out such analysis, being n=1-5 and XX=S-S; Se-Se. All the obtained data are collected in Table 4.4.

First, we focus on the influence of R_n by using the molecular model of Figure 4.2, where the D sections correspond to the PD-SS and the C_1 chain is built with different functional groups, namely, urea (R_1), urethane (R_2), secondary alcohol (R_3), ether (R_4) and ester (R_5). Similar systems were considered for studying the influence of diselenides.

Table 4.4: Total number of hydrogen bonds (HB_{tot}), maximum (HB_{max}), average (HB_{ave}) and minimum (HB_{min}) number of hydrogen bonds at a given step, and ω obtained for the PD-SS and PD-SeSe systems with different polymeric chains built using the following functional groups: urea (R_1), urethane (R_2), secondary alcohol (R_3), ether (R_4) and ester (R_5).

	S-S					Se-Se				
R	HB_{tot}	HB_{max}	HB_{ave}	HB_{min}	ω	HB_{tot}	HB_{max}	HB_{ave}	HB_{min}	ω
R_1	1902463	160	127	97	0.1058	2233772	184	149	115	0.0418
R_2	1078729	100	72	50	0.0471	921219	87	61	37	0.0538
R_3	-	-	-	-	-	1359569	119	91	64	0.0307
R_4	731072	76	49	26	0.0212	592646	66	40	16	0.0332
R_5	927209	83	62	42	0.0348	790616	74	53	34	0.0443

The differences between chains arise from their distinct ability to establish hydrogen bonds, independently of the nature of the X-X bond. This is clearly seen in Figure 4.7 (top left), where the normalized percentage of hydrogen bonds is represented for each system (see the numerical values in Table 4.4). The smallest numbers of HB are provided by the ether- and ester-containing chains (R_4 and R_5, respectively), while urea (R_1) shows the highest number, as expected, due to the presence of the -NH- group. This reduction of HBs induces a decrease in the value of ω, which suggests an excessive mobility of the chains. As it was previously explained, a too small number of hydrogen bonds may be detrimental for the self-healing processes, since too mobile chains may reduce the number of disulfides in the reacting region (I_i of the radial distribution function) and, therefore, decreasing the value of ω. Inspecting the radius of gyration

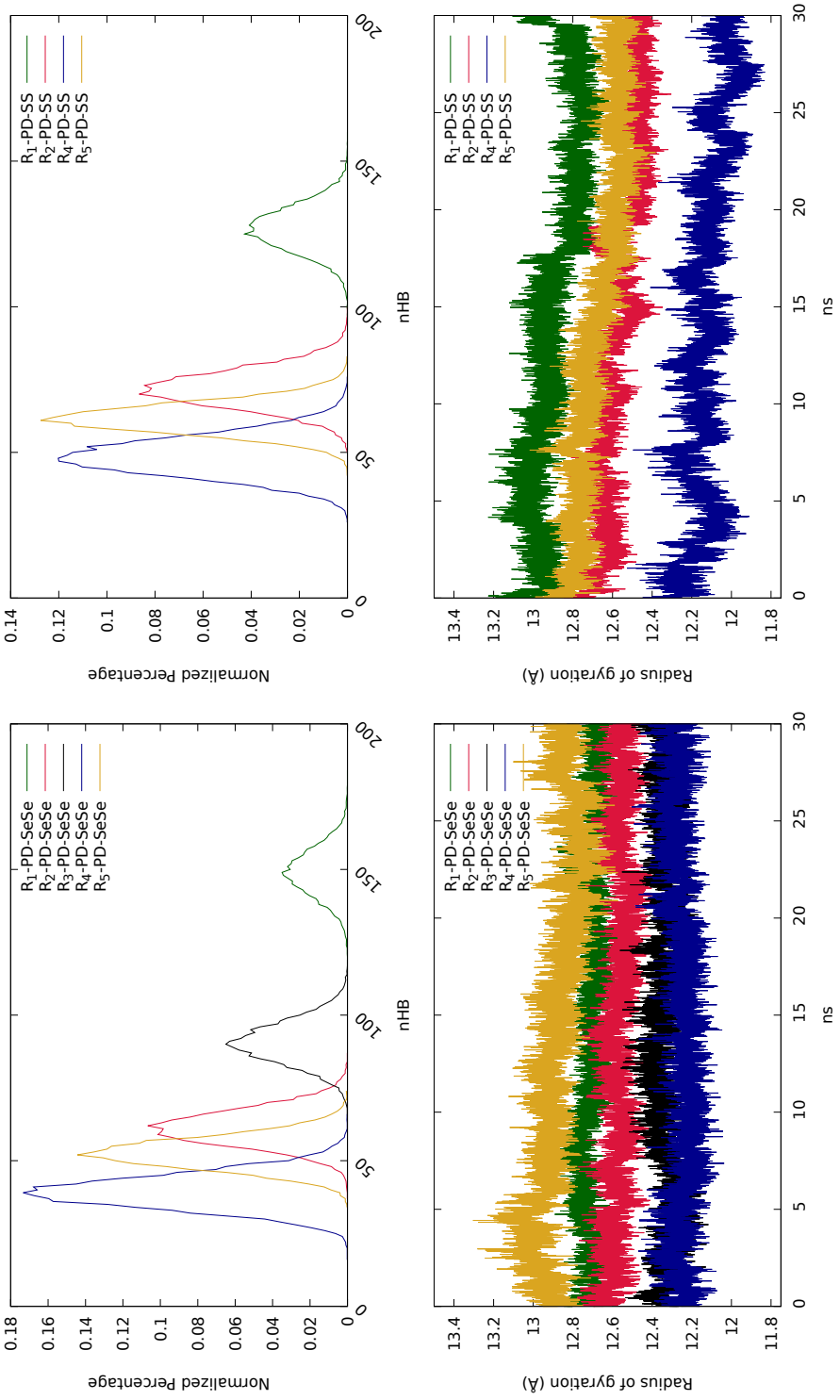

Figure 4.7: Normalized percentage of hydrogen bonds (left) and radius of gyration (right), in Å, of the disulfide (top) and diselenide (bottom) derivatives.

(Figure 4.7, top right), chains with larger number of atoms present larger values of radius of gyration, as expected.

Finally, we have analyzed the effect of changing sulfur by selenium, since it has been recently found that selenium can enhance the self-healing process [63, 64, 65, ?, 146]. Regarding the number of hydrogen bonds, the same trend as for disulfides can be observed, since the ability to establish HBs is, in principle, independent from the dynamic bond. Nevertheless, with the exception of the urea-containing systems (R_1), the diselenide derivatives establish less hydrogen bonds than the disulfides, which pinpoints to different structural reorganizations that may affect to the interaction among functional groups and, therefore, an indirect influence of the dynamic bond might be devised. The substitution of sulfur by selenium has also an impact on the radius of gyration of the systems. Inspecting Figure 4.7 (top-right and bottom-right panels), the radius of gyration of the systems including diselenide bonds show, in general, smaller variations, indicating a more rigid character than their disulfide counterparts. This could be a consequence of Se being heavier and less mobile than S.

This lower mobility of the Se-containing chains may explain the observed variations in the hydrogen bonding and in ω. For those chains with a large number of HBs, such as the urea-based system (R_1), the reduced mobility of Se may enhance the rigidity if the system, keeping the number of hydrogen bonds and even favoring the formation of new bonds. Thus, HB_{max}(R_1-PD-SS) = 160, while for the corresponding diselenide is increased to 184. On the other hand, if the molecular chain contains few groups able to create hydrogen bonds, the presence of Se atoms may further limit the capacity to establish hydrogen bonds, since the probability of the functional groups to approach will be smaller (due to lower mobility). As a consequence, the diselenide derivatives show smaller HB_{max} values. Nevertheless, it is difficult to establish a direct comparison between diselenides and disulfides in terms of ω, since the definition of the regions that characterize this parameter is different. The reacting region (I_i) for disulfides included all sulfurs laying closer than 4.5 Å, as quantum calculations showed that at this distance the exchange reaction may take place [69]. Nevertheless, 4.25 Å was found to be the distance at which the exchange reaction could be triggered in the case of diselenides [146]. Besides, since diselenides are less mobile, the neighboring region (I_{ii}), where diselenides have a non-zero probability to undergo the reaction, has been reduced from 20 to 15 Å. Therefore, the trend observed in Table 4.4 may not be considered as a general trend.

4.3.3 Theoretical Self-Healing Capacity

As it was mentioned in the Introduction, the theoretical self-healing capacity (at the microscopic level) of a dichalcogenide-based polymer can be estimated by three parameters: the probability to generate radicals by cleavage of the dichalcogenide bond (ρ), the exchange reaction constant (k) and the mobility of the chains (ω) [131]. The first two parameters, ρ and k, have been calculated in a recent work for a set of disulfide- and diselenide-containing materials [146]. In Table 4.5, these values have been collected together with those of ω calculated in this work. In addition to k, the Gibbs free energy of the transition states (ΔG^{TS}) are given as well. The calculation of the rate constant, using the Eyring equation, requires two main parameters; the activation Gibbs free energy and the pre-exponential factor:

$$k(T) = Ae^{-\Delta G^{TS}/RT} \tag{4.2}$$

While the activation energy can be calculated with high accuracy, the calculation of the pre-exponential factor (A), which depends on the molecular partition functions, is very challenging [73]. Hence, in order to estimate the theoretical self-healing capacity, ΔG^{TS} will be used instead of k. Since there is no experimental evidence to assess the relative weight of these parameters in the self-healing process, we can only estimate the theoretical self-healing capacity by inspecting the trends of each parameter. Thus, we expect the self-healing capacity to be enhanced for larger values of ρ and ω, and lower values of ΔG^{TS}. Inspecting Table 4.5, it is observed that the diselenide compounds have notably smaller reaction barriers than the disulfides. In addition to this, ω is generally larger, with the exception of R_1-PD-SS. As a consequence, we would expect larger values of self-healing capacity for diselenides, as it may be for R_1-PD-SS, given that it shows the largest value of ω among the PD derivatives. The effect of the backbone can be analyzed comparing the R_1 derivatives for PD, PA and PF. It is observed a remarkably lower reaction barrier for PD due to the stability of the TS produced by the $\pi - \pi$ interactions among phenyl rings. These interactions are less effective when the amino group is inserted between the SS bond and the ring in the PA derivative (see Figure 4.1), so that the barrier is notably increased. The largest ω value is calculated for the PF derivative, but it also shows the highest reaction barrier. Considering that the slight increase of ω after substituting PD by PF may not be enough to compensate the notably larger reaction barrier calculated for PF, the combination of these two factors may suggest that the theoretical self-healing capacity of PF will be lower than that of PD. Moreover, the low values of ω combined with the high reaction barriers shown by the PA derivative

Table 4.5: Probability to generate sulfenyl and selenyl radicals (ρ), Gibbs free energy of the transition state (ΔG^{TS}), in kcal/mol, rate constant (k) at T = 298.15 K, in s^{-1} , and ratio of dichalcogenides in the reaction region (ω) for the PD-SS and PD-SeSe systems with different functional groups, namely, urea (R_1), urethane (R_2), secondary alcohol (R_3), ether (R_4) and ester (R_5).

		S-S				Se-Se			
Backbone	R	ρ	ΔG^{TS}	k	ω	ρ	ΔG^{TS}	k	ω
PD	R_1	0.0051	11.03	$4.97{\cdot}10^{4}$	0.1058	0.0122	8.97	$1.62{\cdot}10^{6}$	0.0418
	R_2	0.0010	12.21	$6.78{\cdot}10^{3}$	0.0471	0.0040	8.03	$7.95{\cdot}10^{6}$	0.0538
	R_3	0.0310	10.46	$1.32{\cdot}10^{5}$	—	0.0094	5.99	$2.52{\cdot}10^{8}$	0.0307
	R_4	0.0101	10.98	$5.40{\cdot}10^{4}$	0.0212	0.0041	7.89	$1.01{\cdot}10^{7}$	0.0332
	R_5	0.0045	16.39	$0.58{\cdot}10^{1}$	0.0348	0.0000	7.96	$8.98{\cdot\cdot}10^{6}$	0.0443
PA	R_1	0.2382	18.26	$2.46{\cdot}10^{-1}$	0.0419				
PF	R_1	0.0682	18.49	$1.66{\cdot}10^{-1}$	0.1224				

suggest that the self-healing capacity of the PA derivative will also be low, in spite of the large value calculated for ρ. As a summary, we may suggest that the largest self-healing capacity corresponds to the PD derivatives.

Finally, comparing the different substituents (R_1), similar reaction barriers are observed, between 10 and 12 kcal/mol (except for R_5), as well as similar values of ρ. This means that the most important effect is the mobility of the chains (ω). We have found that a smaller number of hydrogen bonds has as a consequence lower values of ω due to too mobile chains (see Table 4.4) and, thus, the largest self-healing capacity would be expected for R_1, the urea derivative, which shows both a low reaction barrier and a notable number of hydrogen bonds among chains.

4.4 Conclusions

In this chapter, a set of dichalcogenides (including disulfide and diselenide bonds) with different backbones (PA, PD and PF) combined with five different functional groups as substituents have been studied by means of molecular dynamics simulations. First of all, a theoretical protocol is established for creating an adequate model by assessing the relevance of four different parameters, namely, initial guess, chain length, simulation box and simulation time, and then it has been compared to that from Formoso's work [72]. With this new protocol we have calculated different properties of the systems, such as the hydrogen bonding and the mobility of the chains (ω). It has been shown that the backbone has a direct influence in ω, with PD and PF showing similar values, while for PA derivatives a clear decrease is observed. The number of hydrogen bonds established affects the value of ω, in such a way that those systems with an intermediate number of hydrogen bonds are the ones showing larger ω values. Moreover, it can be

seen that systems including diselenide bonds tend to show bigger values of ω than their disulfide counterparts (excepting R_1-PD-SS). After the calculation of ω, we combine this parameter with ρ (the probability of radicals to be formed) and ΔG^{TS} (the reaction barrier of exchange reaction), that were calculated in previous works, to estimate the theoretical self-healing capacity of the systems studied, that will be directly proportional to ρ and ω, and inversely proportional to ΔG^{TS}. We conclude that, in general, the PD-SeSe derivatives show the best theoretical self-healing capacities.

Chapter 5

Theoretical Protocol To Study The Self-Healing Character Applied to Real PU and PHMA Polymers

Abstract

In this chapter we have tested and applied the theoretical protocol developed by Matxain, Ruipérez et. al. to real PU designed by Kim et. al. and Takahashi et. al. For this purpose, realistic system models are used, where accurate description of both the disulfide bond and the polymeric chains are considered, along with the hardener part when necessary. The combination of both quantum calculations and molecular dynamics simulations lead to a qualitatively correct description of the experimental evidence, predicting in which cases self-healing process is likely to happen. However, the quantum part of the theoretical protocol is not able to predict the observed different behaviours of each system when temperature is increased. This is due to the impossibility of considering all the relevant conformations in the quantum calculations. The temperature influence may be taken into account in the molecular dynamic simulations, but the lack of quantum effects make impossible the accurate prediction of the self-healing properties. A combination of both simulations, on the other hand, has been shown to explain the experimental evidence. Hence, the proposed protocol is a very useful tool to study real systems and predict their self-healing properties.

5.1 Introduction

It is known that, in the case of polyurethanes (PUs), the mechanical properties are greatly affected by supramolecular interactions, as hydrogen bonds, as well as by the packaging of the hard segments [31, 51, 52, 53], so tuning these features could provide the materials with a reasonable level of mechanical strenght for their further application. In this vein, Kim et. al. [54] and Takahashi et. al. [55] studied a set of disulfide materials with different crosslinkers and hardeners, in order to check for the self-healing properties at different temperatures.

Concretely, Kim et. al. focused on aromatic disulfide-based PUs with three different hard segments (or hardeners, see Figure 5.2) with varying rigidity, namely, IP (asymmetric alicyclic structure); 4,4´-methylenebis(cyclohexyl isocyanate), HM; (symmetric alicyclic structure); 4,4´-methylenebis(phenyl isocyanate) and M; (aromatic structure). In their work, Kim et. al. obtained a self-healing PU at room temperature (IP) with mechanical properties such as robustness, stretchability, and durability, surpassing those of room-temperature self-healable materials to date. The other two systems (HM and M) improved their self-healing capacity with the increase of the temperature, but at room temperature no healing capacity was observed.

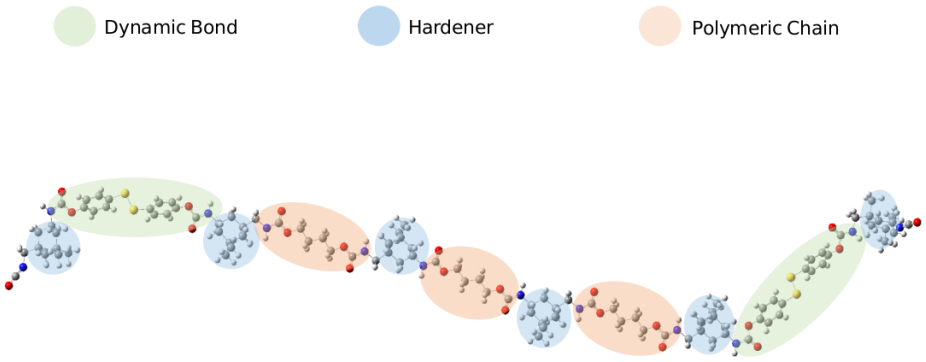

Figure 5.2: Schematic representation of the different components of the IP polymer, with the dynamic bond in green, the polymeric chain in red and the hardener in blue.

Takahashi et. al. [55], on the other hand, focused on materials consisting on polymethacrylate networks, with thermally exchangeable bis(2,2,6,6-tetramethylpiperidin-1-yl)disulfide (BiTEMPS) crosslinkers, in order to study the effect of different packings. Concretely, two different crosslinkers were used, containing aliphatic disulfides and -N-S-S-N- disulfides leading to ADSA and BTA structures, respectively. They observed that their BTA material (with N atoms linked to disulfides) presented healing capacity at room temperature and at high temperature, while ADSA, with aliphatic

Kim et. al. [54]

IP

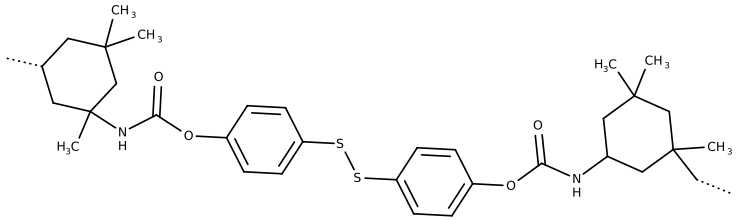

HM

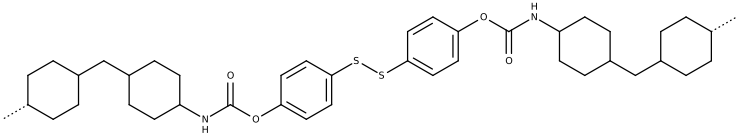

M

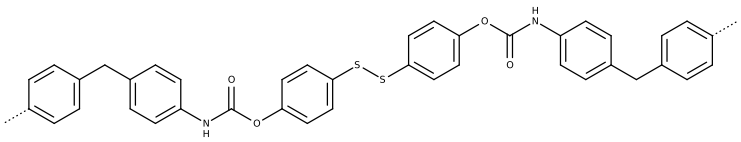

Takahashi et. al. [55]

BTA

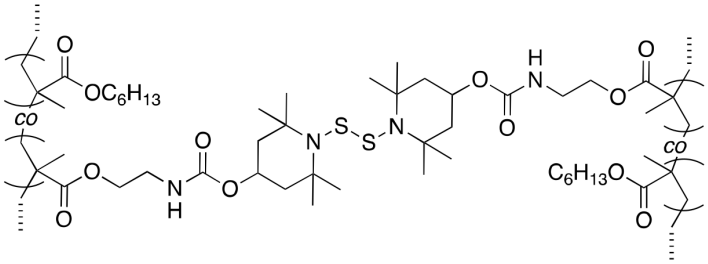

ADSA

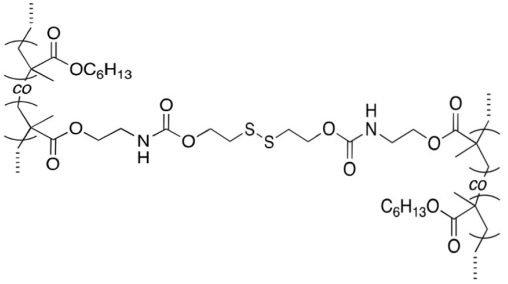

Figure 5.1: Molecular structure of the systems studied.

chains linked to disulfides, did not show healing capacity even at high temperature, regardless the hardener structure was the same.

With these previous works in mind, the main goal of our work will be the simulation of real systems, concretely, those designed by Kim et. al. and Takahashi et. al., by using the theoretical protocol developed previously by Formoso et. al. [72] and Irigoyen et. al. [151], in order to validate the protocol and update it if necessary. In addition to that, the simultaneous effect of the crosslinker and the hardener will be analyzed, in order to provide physical and chemical processes that explain the experimental observation.

5.2 Computational Details and System Models

5.2.1 Computational Details

All geometry optimizations were carried out in gas phase within density functional theory (DFT) [94, 95], by using the long-range corrected ωB97XD functional [132] combined with the 6-31+G(d,p) basis set [133]. Harmonic vibrational frequencies were obtained by analytical differentiation of gradients, in order to determine whether the structures found were minima or transition states. The frequencies were then used to evaluate the zero-point vibrational energy (ZPVE) and the thermal (T = 298 K) vibrational corrections to the enthalpy (H) and Gibbs free energy (G) in the harmonic oscillator approximation. Single point calculations using the 6-311++G(2df,2p) basis set [134] were performed on the optimized structures to refine the electronic energy. In order to understand the photodissociation process, Time-Dependent Density Functional Theory (TDDFT) [100] was used together with the 6-31+G(d,p) basis set. All DFT calculations were carried out using the GAUSSIAN16 package [135].

Ab initio Born–Oppenheimer Molecular Dynamics (BOMD) calculations were further carried out for the optimized species in order to determine their thermal stability, using the PBE functional [136, 137] combined with a DZP quality basis set and the RI formalism with the corresponding auxiliary basis sets [138, 139, 140]. The calculations were carried out at 298 K by means of the Nose–Hoover thermostat. All these simulations were as long as 40.000 a.u. (9.651 ps), with a time step of 40 a.u. (1.93 ps), and were performed using the TURBOMOLE package [141].

The Molecular Dynamics (MD) simulations have been performed using ff14SB [147] amber force-field in the AMBER 14 molecular dynamics simulation package [148]. The parameters corresponding to the diphenyl diselenide derivatives have been those obtained by Torsello et. al. [149]. All

structures were built via the LEaP module of Ambertools and the charges were computed using the restrained electrostatic potential (RESP) fitting procedure [150]. First the ESP was calculated by means of the Gaussian package[135] using the 6-31G* basis set at Hartree-Fock level of theory and then the RESP charges were obtained. All the simulations were carried out in vacuum in a canonical ensemble (NVT) with a 2 fs timestep. 100000 steps of minimization (50000 steps steep descent minimization plus 50000 steps of conjugate gradient minization) were followed by heating from 80 K to 300 K over 200 ps, an equilibration time of 1800 ps with a Langevin thermostat and a production of 30 ns for the polymeric chains (between 1456 and 1808 atoms). Covalent bond lengths involving hydrogen were constrained using the SHAKE algorithm.

In order to analyze the hydrogen bonds, we consider a threshold for the bond length between the donor and acceptor (X$\cdots$Y) smaller than 3.5 Å and the range of X-H$\cdots$Y angles varies between 140 and 220 degrees. In addition, to see the evolution of the hydrogen bonding along the simulation time, the hydrogen-bond occupancy is defined as $HB_{Occ} = 100\frac{\sum nHB}{t}$, where nHB denotes the number of formed hydrogen bonds, at a given step, according to the criteria for the bond lengths and angles mentioned above, and t is the number of simulation frames. Thus, HB_{Occ} represents the fraction of time that the hydrogen bond is formed. In addition to this, in order to describe the size of a polymer chain, the radius of gyration (r_{gyr}) is defined as $r_{gyr}^2 = \frac{\left(\sum_{i=1}^{N}(r(i)-\bar{r})^2\right)}{N}$, where $\bar{r}$ is the geometric center of mass of the system. It corresponds to the root-mean-square distance of the atoms from the center of mass.

5.2.2 System Models

Different sized model structures were used to carry out both quantum simulations and molecular dynamics simulations. In quantum simulations, small chain models were used, including the disulfide unit and the sorrounding chemical structure of the studied experimental materials. Concretely, one and two model chains were used for quantum calculations. In the top of Figure 5.3 these models for IP system are depicted. The model chains (see Figure 5.3, bottom left) for the molecular dynamics simulations are built following the experimental synthesis from references [54] and [55], and then 16 chain units are put randomly in a simulation box, following the procedure concluded previously in our group [151], reproducing the experimental density of PUs and polymetachrylates after equilibration (see Figure 5.3, bottom right). The system models used for the other studied PU systems are given in the APPENDIX VI.

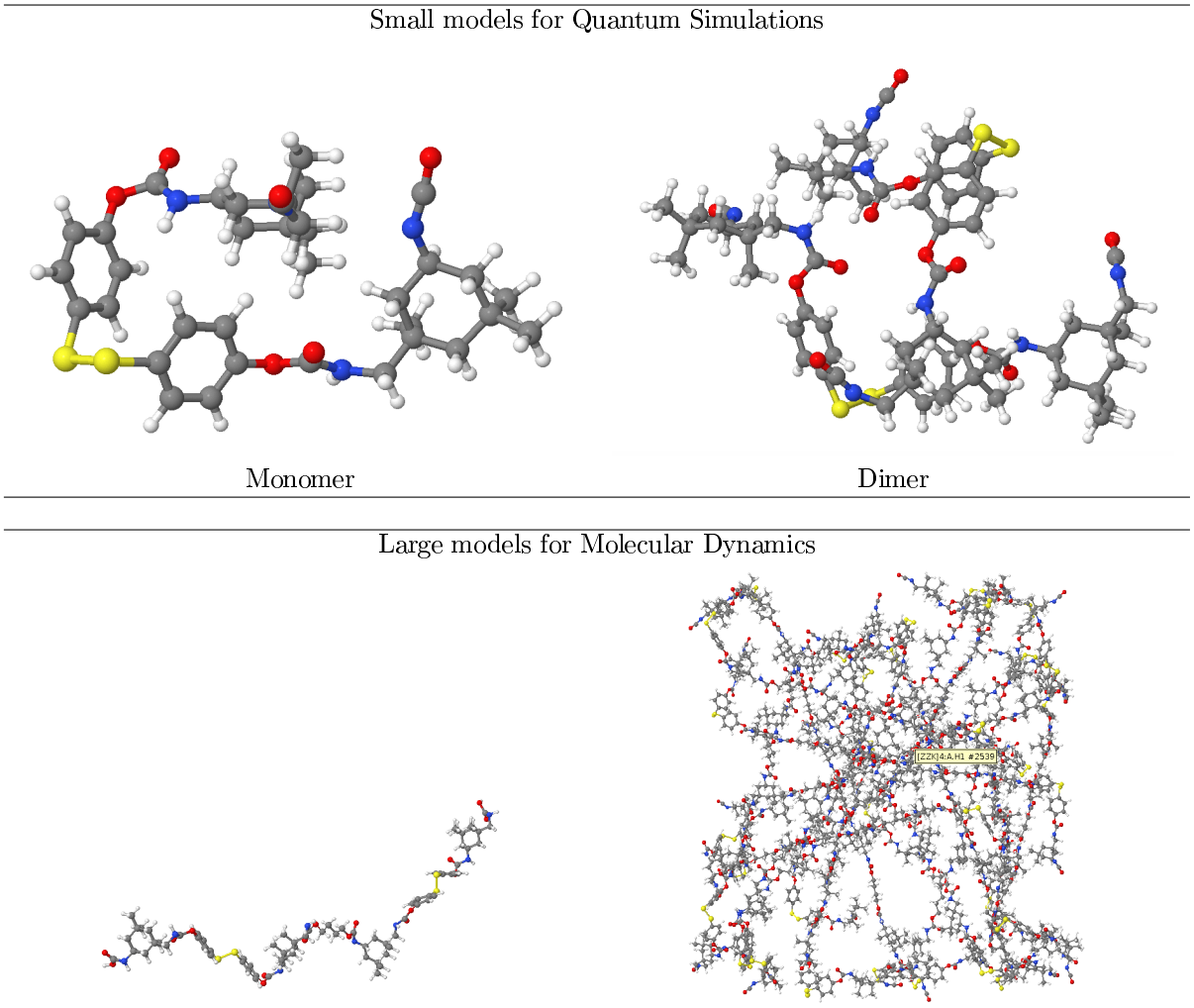

Figure 5.3: Model structures used for IP system for quantum simulations and molecular dynamics simulations. Above, the monomers and dimers used for quantum calculations. Below, in the left, the polymer chain model used in the MD simulations, and in the right, the total system with 16 chains used in the MD simulations.

5.3 Results and Discussion

In this section, the obtained results will be presented and discussed, in order to rationalise the experimental data obtained by Kim et. al. [54] and Takahasi et. al. [55] by using the theoretical protocol designed in our group. Concretely, this section will be divided into two different subsections. First, the formation of disulfide radicals will be analyzed by studying the the bond dissociation energy (BDE), the probability of radicals to be formed (ρ), and the reaction barriers (ΔG), of all considered systems by means of *ab initio* calculations. Afterwards, the probability of disulfide bonds to find a neighbour disulfide bond will be analyzed, in order to trigger the exchange reaction (ω), and the effect of the hydrogen bonds (HB) in the mobility of the chains. Molecular dynamics will be carried out for this purpose.

5.3.1 Radical Formation and Disulfide Exchange

Several energetic and structural parameters have been studied in order to consider the S radical formation and their influence in the disulfide exchange in the systems under study. Concretely, the disulfide bond strength has been analyzed by calculating the BDE in a system model chain, considering two different chain conformations, open and closed. In addition to this, the interaction between two chain models have been calculated, considering the possible hydrogen bonding, $\pi - \pi$ stacking or other weak interactions. Finally, the reaction energy barriers have been calculated for the attack of the sulfur radical to the neighbour disulfide bond. All the energetic and geometrical data for the mentioned features are collected in Table 5.1.

Let us begin by the analysis of the conformation of one-chain model and the calculated BDE corresponding to the S-S bond. Table 5.1 contains both the geometrical and energetical data obtained for the two considered conformations, namely, open and closed. In the first one, the X-S-S-X dihedral angle are large, of more than 160 degrees, so both chains linked to the disulfides are away from each other, hindering the intra-chain interaction. In the closed one, on the other hand, the X-S-S-X dihedral angle is small, of around 60 degrees, which allows the intra-chain interactions. In principle, a combination of different conformations would be prensent in the polymeric material due to the presence of multiple chains. However, in the single-chain system calculations, only the closed conformation was obtained in most cases. This conformation is, indeed, the most favored one in materials including diphenyl disulfides, where the interaction between the phenyl rings adjacent to the sulfur atoms helps reducing the steric repulsion with the rest of the chain. In BTA and ADSA, the absence of phenyl groups leads to an increment of the steric repulsion between the two chains, and more open conformations are found in single-chain calculations.

Table 5.1: Bond dissociation energy (BDE), in kcal/mol $\frac{kcal}{mol}$, S-S bond lenghts, in Å, XSSX dihedral angles, in º, of the studied systems.

	Open Conformation			Closed Conformation		
	BDE ($\frac{kcal}{mol}$)	R (S-S)	XSSX	BDE ($\frac{kcal}{mol}$)	R (S-S)	XSSX
IP	-	-	-	59.31	2.096	-65.9
HM	-	-	-	47.34	2.112	-57.8
M	51.20	2.050	122.1	65.65	2.062	-60.5
BTA	33.77	2.200	164.1	-	-	-
ADSA	58.19	2.059	179.1 (179.1)*	63.13	2.061	46.8 (90.4)

	Chain interactions				
	ΔH	R (S-S)	XSSX	R (S-S)	XSSX
IP		2.094	81.8	2.100	70.4
HM		2.067	97.0	2.122	-50.5
M	OPT	2.092	97.6	2.088	-92.0
BTA	31.71	2.114	145.1	2.126	116.7
ADSA	31.41	2.066	-42.8 (131.6)*	2.067	-46.5 (115.4)*

In previous works, the BDE of different kinds of disulfides was calculated to be around 48 kcal/mol for diphenyl disulfides, around 33 kcal/mol for sulfenamides and around 60 kcal/mol for aliphatic disulfides, and the calculated values for BTA (sulfenamide) and ADSA (aliphatic disulfide) in this work are in agreement with these values. Regarding the diphenyl disulfides, the BDE value of HM agrees with previous works, but those calculated for IP and M are much larger. Nevertheless, notice that unlike HM, both IP and M are allowed to have attractive hydrogen bonding and $\pi - \pi$ stacking, while in HM there is no attractive intra-chain interaction. This lack of intra-chain interaction make that the calculated BDE corresponds entirely to the breaking of the S-S bond, while in IP and M the BDE also includes the breaking of intra-chain interactions. In addition to this, notice that the S-S bond-length is the largest one in HM. Hence, intra-chain interactions could affect the S-S bond distance.

Interchain interactions have been found to be important in the self-healing capacity of materials. Therefore, chain interactions have been also analyzed by means of DFT, including two chain models in our system, as explained above in the System Model subsection. A deeper analysis will be carried out later by means of Molecular Dynamics simulations, including larger and more chains. Having a look to the calculated interaction enthalpies (ΔH), we observe that in all cases inter-chains interactions are strong enough so that disulfides may reach the neighborhood of other disulfides, in order to lead to the disulfide exchange. On the other hand, the intra-chain conformation may be open or closed, as may be deduced from the XSSX dihedral angles and image of IP dimer in Figure 5.1. It is not clear how this may affect to the probability of radical formation, ρ. In previous works ρ is related to lower values of BDE and larger S-S bond lengths, but these might be affected by the chain conformation of the models used.

Clearly, since both BDE and S-S bond lengths are affected by chain conformation, the ρ parameter could be somehow affected by this. Recall that ρ would be directly proportional to the formation of sulfur radicals, which are the necessary first step for the self-healing process. Hence, the calculated theoretical values of ρ should be related to the experimental observation. In order to introduce this dynamic character, ρ is calculated by means of *ab initio* molecular dynamics.

$$\rho = \frac{N_{S-S}}{N_{Tot}} \tag{5.1}$$

In this work, ρ has been calculated for all the systems in different temperatures to match the experimental results, and to see the influence of rising the temperature in the formation of radicals. So that, 4 different temperatures (25, 40, 60, and 80 ^{o}C) have been calculated for the systems of J. Kim

et. al [54] namely, IP, HM and M, and two for the pair of sytems (ADSA and BTA) of Takahashi et. al [55]. In Table 5.2 the calculated values of ρ and the average values of the SS bond lenght in the QMD are given, and are depicted in Figure 5.4

Starting with Kim's trio, it can be seen that, at room temperature, IP is the only one presenting a value of ρ different from 0, which means that, theoretically, this would be the only material that could trigger the exchange reaction at that temperature, as would be the only one in which radicals could be formed. At 40 ºC, IP still gives a value of ρ different from 0, meaning that the self-healing process would continue to happen, meanwhile the value for M is still 0, implying the lack of radicals and thus, the lack of self-healing. More interestingly, HM now presents a value of ρ bigger than 0, but still considerably low. This means that, theoretically, the presence of a little amount of radicals could lead to a self-healing character to a certain extent at that temperature. At 60 ºC all of the systems studied present positive values of ρ, with HM's value rising considerably, meaning that in principle, its self-healing capability has been improved. The value for M is still very low, but a value different from zero would mean that the presence of a small amount of radicals could trigger the exchange reaction to a certain extent if other conditions favour it. At 80 ºC, all of the systems present values higher than zero, but the value for M is still relatively low.

Table 5.2: Avergae S-S bond distancies, R_{av}, in Å, obtained in QMD simulations, and ρ as a function of temperature of all the studied systems. The calculated temperatures are those in which experiments were performed, 25 40 60 and 80 ºC for IP, HM and M, and 25 and 120 ºC for BTA and ADSA.

	25		40		60		80		120	
	R_{av}	ρ	R_{av}	ρ	R_{av}	ρ	R_{av}	ρ	R_{av}	ρ
IP	2.122	0.0117	2.119	0.0063	2.123	0.0050	2.115	0.0012	-	-
HM	2.103	0.0000	2.111	0.0003	2.123	0.0089	2.113	0.0047	-	-
M	2.084	0.0000	2.107	0.0000	2.109	0.0002	2.101	0.0005	-	-
BTA	2.303	0.4750	-	-	-	-	-	-	2.293	0.2165
ADSA	2.092	0.0000	-	-	-	-	-	-	2.091	0.0000

On the other hand, regarding the systems of Takahashi and coworkers, it can be seen that the ADSA polymer would not present self healing character at the studied temperatures as the value of ρ at 25 and 120 ºC is zero, meanwhile the BTA polymer presents high values of ρ at both temperatures, meaning that the exchange reaction, and thus, the self healing process would happen both at room temperature and at 120 ºC.

However, it can be seen that the trend for ρ does not come at once with the expected one, as one could think that the increment of temperature should lead to a bigger dissociation ratio, provided that the S-S bond distancies

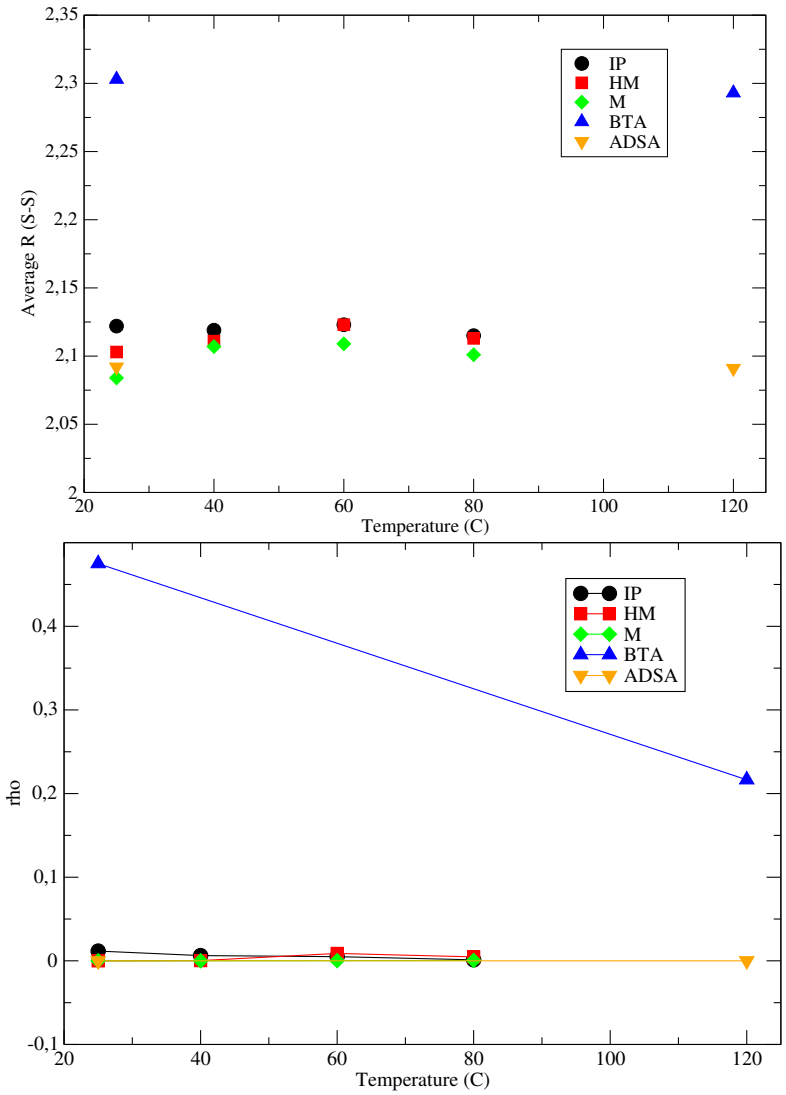

Figure 5.4: Top: Graphical representation of the avergae S-S bond distancies from QMD simulations, in Å, at different temperatures. Bottom: probability of radical formation (ρ) at different temperaures for the five systems considered, and only for those of Kim's zoomed.

will be larger, and thus, weaker. Instead, in some cases, the opposite trend is observed, that is, ρ descends with temperature, as occurs for IP. In Figure 5.5, the disulfide bond distancies used for the calculation of ρ are depicted, with the black line corresponding to the monomer, and red and green to the dimer's disulfides. It is clearly seen that one of dimer's disulfides (in green) provides a very similar bond distance distribution than that of the monomer, meanwhile the red one presents a far higher variation along the simulation, meaning that the two disulfides of the dimer are not completely equivalent, and thus, there must be a difference between them. Looking closely at Figure 5.3, it can be seen that the dihedrals formed between each disulfide bond and the phenyl groups sorrounding them are quite different. In this sense, one of the disulfides leads to a closed conformation (green) and the other to an open conformation (red). The main difference among these two conformations is that, in the closed one, the phenyl groups adjacent to the disulfide unit are able to interact via a $\pi-\pi$ stacking interaction, keeping the sulfur atoms closer along the simulation, while in the open one (red), this interaction does not exist, providing the sulfur atoms with more mobility, as it is seen in Figure 5.3. Thus, it is clear that we are introducing a conformational bias in the dynamics. Not only that, the interaction between the chains (see Figure 5.1) also depends ond the used conformation, as strongly interacting chains favour the conformational stability of the dimer. However, the increment of the temperature disrupts this conformation stability, as now the system is able to explore a bigger number of conformations. This could be the reason of the decrease seen in ρ for the IP case. But still, knowing that the used conformation has a big influence in the calculation of ρ, in order to calculate it accurately, a bunch of possible conformations should be explored, which seems rather impossible by means of *ab initio* molecular dynamics.

The last parameter calculated by means of quantum chemistry methods is the exchange reaction barrier, ΔG, which is related to the kinetics of the named reaction. In previous works [146], it was seen that the key feature affecting this parameter was the chemical structure around the dynamic bond, and that systems with similar chemical structure around the dynamic bond provide similar values of ΔG. Given that the systems studied in this work are bigger than those studied in [146], the computational effort needed to compute the reaction barrier is, by far, bigger than those previously calculated. So that, the reaction barrier was computed for the IP system only, obtaining a value of 12.02 kcal/mol. This value is similar (12.21 kcal/mol [146]) to the ones previously calculated with a similar chemical structure around the disulfide bond, that is, with an aromatic ring directly attatched to it, and an urethane unit attatched to the ring in para position. So that, we can assume that the reaction barrier for all of IP, M and HM, will be similar since all of them have the same chemical structure around the dynamic bond, and thus, no differencies are expected regarding this parameter for this three systems.

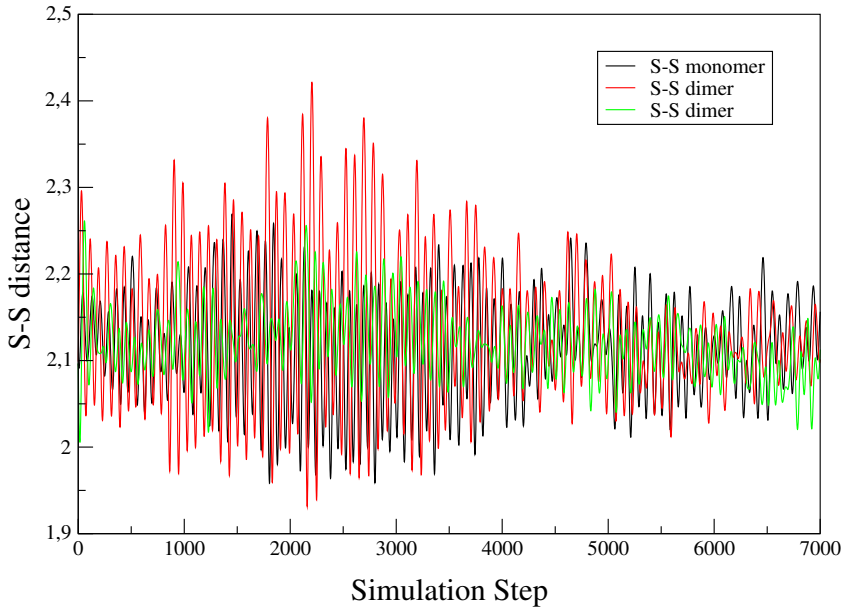

Figure 5.5: Variations of the S-S bond lenght (in) in the QMD simulations for the isolated monomer (in black) and for each monomer in the dimer (red and green lines).

5.3.2 Influence of the Hard Segment and the Crosslink Structure in the Chain Mobility.

In this section, the results obtained in the molecular dynamics simulations will be analyzed. As stated in the introduction, the mobility of the chains is a key factor in the self-healing process, as it determines the ability of chains, and sulfur atoms in particular, to move and rearrange, which is essential for sulfur radicals to attack disulfide bonds and trigger the exchange reaction, and thus, the self healing process. Moreover, as it was discussed previously, a bunch of conformations is needed in order to accurately measure ρ, and meanwhile it is very difficult to obtain that in *ab initio* methods, it is relatively easy to obtain in a molecular dynamics simulation, where not only there are more than two disulfide units, but also the effect of the environment is now included, and thanks to the random character of the build up, lots of different disulfide conformations can be obtained too. So that, we will focus on the ω parameter (see Eq. 5.3), and in the hydrogen bonds formed between the chains, and we will also try to use the disulfide conformation variety to obtain a value for ρ from molecular dynamics.

If we look at the radial distribution functions obtained from the molecular dynamics simulations, two clearly defined different regions can be observed: the one corresponding to the sulfur atoms of each disulfide bond, with a high, narrow peak at around the S-S bond equilibrium distance (2.10 Å) and a more diffuse region, ranging from 4 to 25 Å, (see 5.6 Figure top,

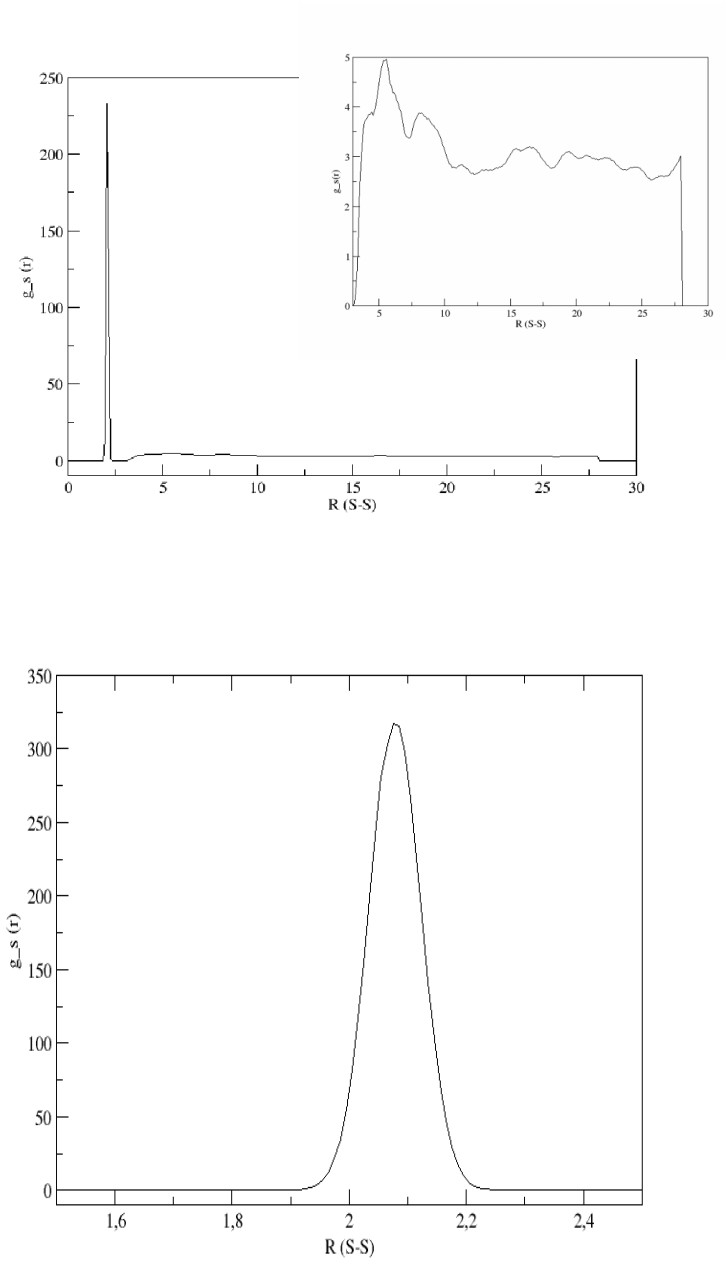

Figure 5.6: Radial distribution function and the regions of interest for the calculation of ω and ρ_{MD}

where this region is zoomed) which corresponds to the distancies between different disulfide bonds. As it has been stated, ω is obtained by integration of different regions of the radial distribution functions to estimate the distancies between disulfide units. In the same manner, a value for ρ can be defined by integrating the radial distribution function in the region of the S-S bond equilibrium distance (see Figure 5.7), with the aim of obtaining a ratio of the sulfur atoms laying away from the equilibrium distance, which, as in the same way as on the previously defined ρ (see Eq. 5.1), could be considered as dissociated.

First, we will focus on the region of the radial distribution function corresponding to the sulfur atoms of each disulfide bond. In Figure 5.7, top left, the radial distribution functions of all the studied systems at 25 ^{o}C are represented, with the regions of interest, that is, the regions used for the integration, zoomed being represented on the right. In the zoomed picture, it can be seen that both M and BTA systems show the highest population of sulfur atoms at larger distancies, while ADSA shows the lowest one, with IP and HM laying in between with a very similar profile. BTA and ADSA being the highest and lowest can be explained due to the chemical structure around the disulfide bond; BTA is a sulfenamide, and as it is known [131], these kind of systems provide weaker bonds, leading to higher bond distancies, and thus, to an easier dissociation, while the structure in the ADSA system consists on an aliphatic disulfide, producing a stronger bond, and thus, shortest bonds. On the other hand, IP, HM and M have the same structure, that is, an aromatic ring attached to each sulfur atom of the disulfide bond, producing intermediate bond strengths, and similar profiles, except for M, which is a bit higher.

In Figure 5.7, bottom, the radial distribution functions for the IP systems are represented at the calculated temperatures. It is seen that, as expected, the higher the temperature the lower the peak height, as the increment of the temperature, and thus, the increment of the energy, leads to a more mobile bonds. The same can be seen in the zoomed part, where the highest temperatures show a larger amount of sulfur atoms at larger distancies, and thus, higher probabilities for disulfide bonds to be dissociated.

Now, this region of the radial distribution function will be integrated in order to estimate the proportion of the sulfur atoms laying at larger distancies, and thus, with a higher probability to be dissociated. For that, a similar approach to that followed for obtaining ω has been carried out, leading to the so called parameter ρ_{MD} (see Eq. 5.2). The regions selected for the integration are the following: I_I ranges from 2.20 Å to 3.00 Å and it takes into account those sulfur atoms with higher proability to be dissociated, and I_{II} ranges from 1.80 to 3.00 Å, with the aim of taking into account the whole disulfide bond. In this way, we obtain a proportion of

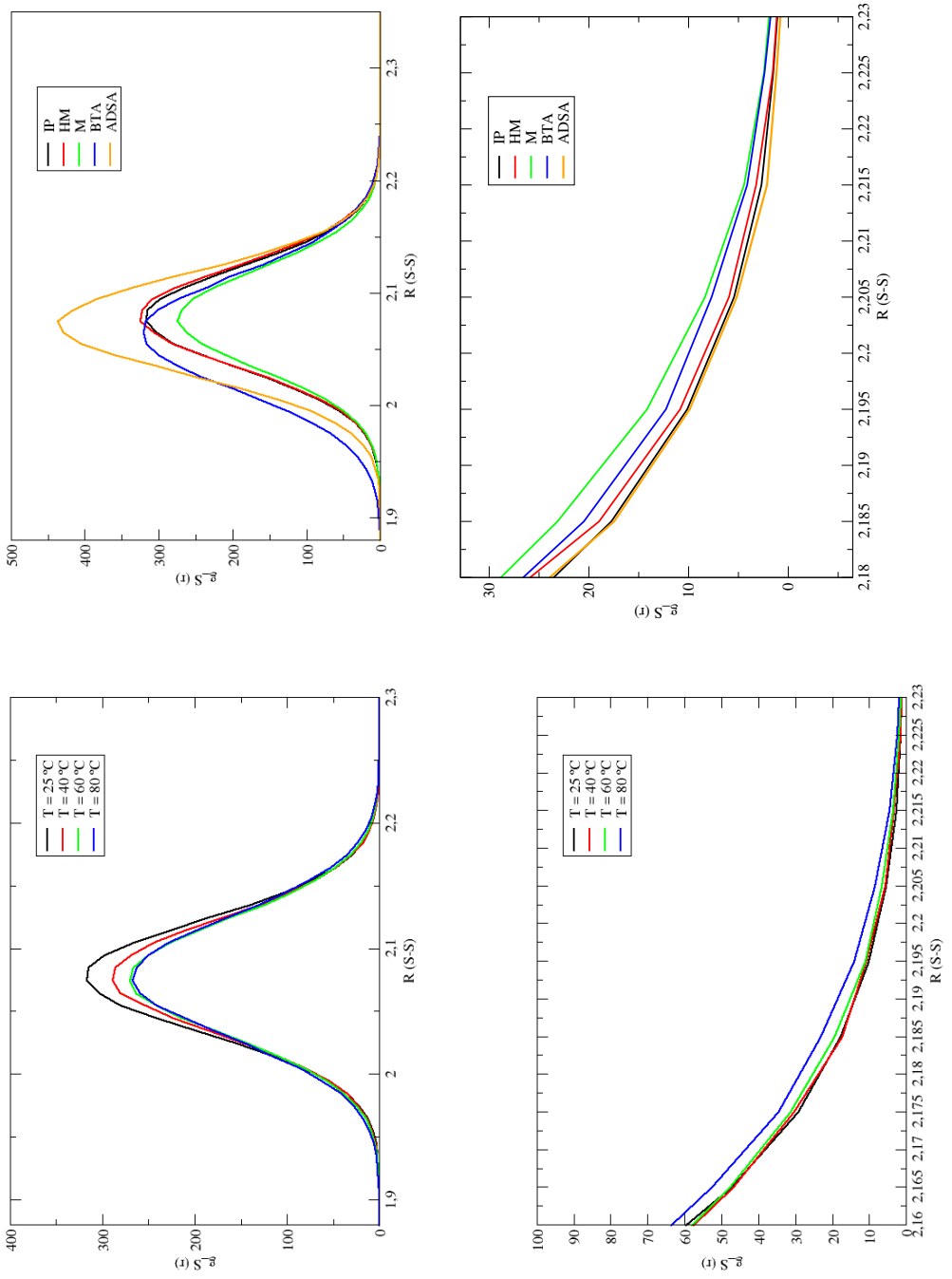

Figure 5.7: Regions of the radial distribution functions corresponding to the sulfur atoms of the disulfide bonds.

Table 5.3: Calculated values of ρ_{MD} for all the studied systems at different temperatures.

ρ_{MD}	25 ºC	40 ºC	60 ºC	80 ºC	120 ºC
IP	.0030	.0036	.0042	.0055	-
HM	.0034	.0040	.0050	.0032	-
M	.0028	.0037	.0045	.0056	-
BTA	.0039	-	-	-	
ADSA	.0019	-	-	-	.0056

the sulfur atoms that could be dissociated, similar to what was obtained by using *ab initio* molecular dynamics. The values are collected in Table 5.3. It can be seen that BTA presents the higher proportion and ADSA the lowest, as it was expected, meanwhile the rest of them present very similar values. The increment of the value with the temperature is also consistent with what was expected.

$$\rho_{MD} = \frac{I_I}{I_I + I_{II}} \tag{5.2}$$

Now the focus will be shifted to the region of the radial distribution function corresponding to the distancies between different disulfide units. Now the region to be integrated is that zoomed in Figure 5.6, which corresponds to the distance between the different disulfide units. The regions selected to carry on the integration are now the following: I_I, the reacting region, where units laying there are considered being enough to react, ranging from 3 Å to 4.5 Å, and I_{II}, the neighboring region, where units laying there are given a non-zero probability to enter the reacting region, ranging from 4.5 Å to 20 Å, as they where defined in previous works [72].

$$\omega = \frac{I_I}{I_I + I_{II}} \tag{5.3}$$

As it can be seen in figure 5.8, different values of ω are obtained for the different hardeners, but it can also be seen that ω also varies with respect to the temperature. Nevertheless, when changing temperature, the values of ω fluctuate around a certain value. The reason of these fluctuations is that the systems we are studying are solids, and thus, the variations in the molecular structure caused by the increment of the temperature are rather small in this range of temperatures (see Table 5.4), as the temperatures studied are well below the T_g of polyurethanes, which lays at 120-130 ºC. So that, it makes sense to define an average value for ω (ω_{ave}), which should be characteristic of each material when studying it below its T_g.

Table 5.4: ω as a function of temperature of all the studied systems, including ω_{ave}.

T (ºC)	ω_{IP}	ω_{HM}	ω_{M}	ω_{ADSA}	ω_{BTA}
25	0.0698	0.0903	0.0324		0.0004
40	0.0517	0.1169	0.0481	-	-
60	0.0659	0.0422	0.0227	-	-
80	0.0579	0.0728	0.0412	-	-
120	-	-	-		
ω_{ave}	0.0613	0.0806	0.0361		

In this manner, the average values of ω obtained for each of the sytems are the following: 0.0613 for IP, 0.0806 for HM and 0.0361 for M. The differencies can be explained by looking at the chemical structure of each of the hardeners, as it directly affects the mobility of the disulfide bonds. The highest average value of omega is obtained for the HM hardener, which consists on two cyclohexanes, while the lowest one is obtained for M, which consists on two phenyl groups. It is obvious that the phenyl groups are more rigid than the cyclohexanes due to their planar, and thus, more rigid structure, while the cyclohexanes have more degrees of freedom, providing them with higher mobility. On the other hand, we obtain an intermediate value for the IP system, consisting on a substituted ciclohexane, which is more mobile than the phenyl groups, but not as mobile as the two cyclohexanes.

Regarding the hydrogen bonds, no big differencies are seen, as the three systems share the same polymeric chain (polyurethane) and this is the component with a bigger influence in the capacity of forming hydrogen bonds. It can be seen that IP and HM provide very similar number of hydrogen bonds (see Figure 5.8), meanwhile M provides a higher value. In the case of M, the hardener being two phenyl groups reduces the mobility of the chains, giving them a more rigid character overall, whic results in a bigger amount of hydrogen bonds than their counterparts.

The last parameter of our theoretical protocol, ω, is obtained from molecular dynamics simulations, and it is a measure of the mobility of the disulfinde bonds along the bulk material. Large values of ω imply that the formed radicals have the ability to find another disulfide bonds at larger distancies than systems where ω is low, and it is closely related to the mobility of the chains. In this study we have observed that the increment of the temperature does not really have an impact in ω, as the properties of the bulky materials are not affected that much when working at temperatures well below their T_g, as their solid structure is rather kept. Nonetheless,

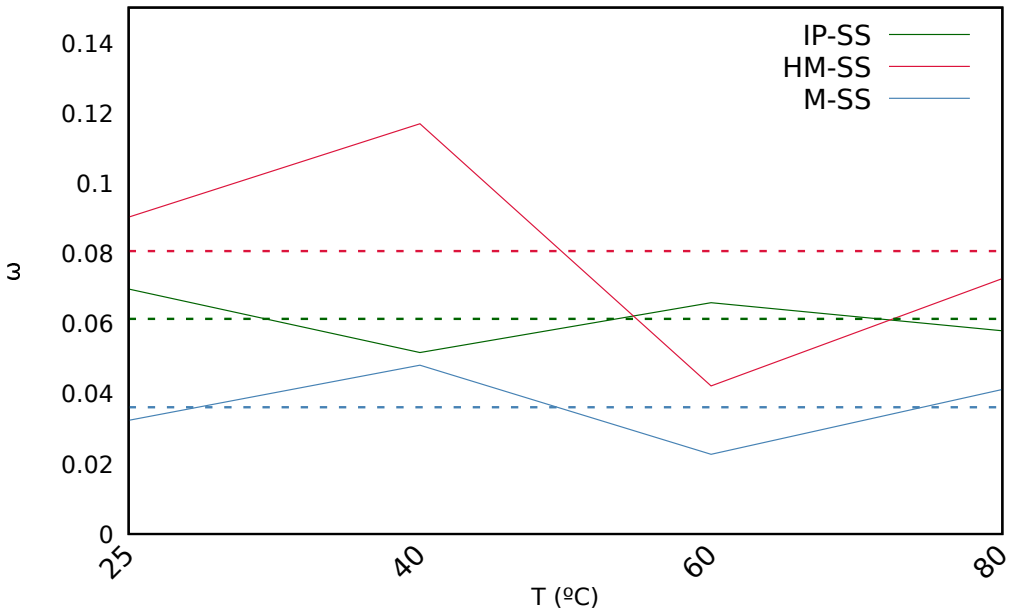

Figure 5.8: ω as a function of temperature for Kim's trio, including ω_{ave}.

the different chemical structures of the different hardeners provide each of the materials studied a characteristic mobility, hence we obtained different values of ω for the studied materials, which ordering from largest to lowest we see that $\omega_{HM} > \omega_{IP} > \omega_{M}$. This suggests that, once the radicals are formed, HM would provide the radicals with the highest mobility inside the bulk to find another disulfide bonds, leading to an appropiate environement for the self-healing process, while for M, the formed radicals would be more stucked, making the self-healing process very difficult. Besides, it has to be taken into account that, in molecular dynamics, the electronic interaction of the phenyl rings $(\pi - \pi)$ is not calculated, and that this interaction would hinder even more the mobility of the sulfur radicals. Lastly, the value obtained for the IP hardener, despite not being as high as the one obtained for HM, is still high enough for the radicals to find adjacent disulfide bonds and trigger the exchange reaction, and thus, the self healing process.

5.4 Conclusions

In this work, we have analyzed the theoretical self-healing capacity of some real systems, and compared it to the experimental results obtained in that regard by using the protocol developed by our group. In general, the protocol qualitatively agrees with the experimental results, since it is able to explain qualitatively the different experimental self-healing capacities of

the studied experimental systems. Concretely, it explains the great performance of the IP and BTA systems, also explaining the lack of self-healing capacity of M and ADSA systems. More interestingly, it can also describe the improvement in the self-healing capacity of HM with the rise of temperature.

However, correctly taking into account the effect of the temperature is complicated with the current protocol, especially in the *ab initio* molecular dynamics, where the initial conformation used may induce a conformational bias along the simulations. So that, for correctly evaluating ρ, a bunch of conformations should be taken into accound, that is, more and larger QMD simulations, which seems rather unfeasible. Nonetheless, ρ is still a clear indicator of the self-healing capacity, in the sense that it acts as a switch; when different from zero, self-healing is possible, but when equal to zero, no self-healing will take place. From the quantum calculations we also may conclude that the kinetic barriers for the attack of the formed sulfur radicals to other disulfides lie lower than 20 kcal/mol, which indicate that this is not a key factor in the differences observed experimentally.

On the other hand, it has been observed that the variety of conformations needed to calculate ρ is already available in the molecular dynamics simulations, with the main drawback being that quantum effects, such as $\pi - \pi$ stacking interactions leading to open and closed conformations of the chains and the S-S bond dissociation, are not included. In spite of this, a variation of the quantum ρ parameter has been introduced in order to obtain a probability of forming radicals through molecular dynamics too: ρ_{MD}. This parameter is not appropriate to describe the formation of radicals, as the quantum ρ parameter, but is valid to predict the influence of the temperature in a given system. In addition to this, we have observed that the increment of the temperature does not really have an impact in ω, as the properties of the bulky materials are not affected that much when working at temperatures well below their T_g, as their solid structure is rather kept.

Chapter 6

Final Conclusions

In this thesis, the self-healing properties of a great variety of dichalcogenide-based materials including homonuclear S-S and Se-Se, and heteronuclear S-Se bonds, have been studied. In order to do so, both *ab initio* calculations and molecular dynamics simulations have been combined, following a theoretical protocol established previously in our research group. According to this protocol, the theoretical self healing capacity can be related to three computational parameters. Two of these parameters, ρ and ΔG^{TS}, are calculated from the quantum calculations, and the third one, ω, from the molecular dynamics simulations. Focusing on the parameters derived from quantum calculations, ρ is related to the capacity of the system to generate chalcogenyl radicals by thermal dissociation, and is calculated from *ab initio* quantum dynamics, while ΔG^{TS} is the energy barrier that should be gained in the attack of a chalcogenide radical to a dichalcogenide bond. Note that with the absence of light irradiation, this thermal process is the only one that may lead to the formation of chalcogenyl radicals. Non-zero ρ values and small ΔG^{TS} are related to self-healing processes. In addition to this, dichalcogenide bonds need to be sufficiently closed to each other, if the mentioned radical attack may occur. Molecular dynamics simulations allow us to calculate the probability of having dichalcogenide bonds closed to each other, which is related to the ω value. Along this thesis we have carried out several studies to characterize which of these factors is the most important one, and to refine the theoretical protocol to be able to use it in realistic models.

First of all, we studied by means of quantum methods, a set of organic compounds including selenium-containing homonuclear (Se-Se) and heteronuclear (Se-S) dynamic covalent bonds, in order to compare the calculated ρ and ΔG^{TS} with related materials based on disulfide bonds (S-S). In this vein, we would be able to compare and predict partly their self-healing capacity with the final aim of designing new materials that could improve the

self-healing performance of the well-known disulfide-based (S-S) materials. Three main compound families were analyzed, namely, R-PD-XX (diphenyl dichalcogenides), R-PA-XX (diphenyl amine dichalcogenides) and R-PF-XX (phenyl-free dichalcogenides), being R different substituents such as urea, urethane, ethylenglycol, alcohols or esters. As mentioned above, for all these species, we have focused on two main features: i) the sulfenyl and selenyl radical formation probability (related to ρ) and ii) the energetic barriers of the exchange reaction that takes place in the healing process (related to ΔG^{TS}). The main radical formation process without external factors is the thermal dissociation, which is related to low BDE of the dichalcogenide bond. Hence, in order to analyze the thermal dissociation, the BDE and the probability to generate chalcogenyl radicals (ρ) are used for the discussion. The BDE is decreased due to two main features: the delocalization of the unpaired electron of the radical and the increment of the population of the antibonding σ^* molecular orbital. It is observed that these two factors are enhanced in the PA-XX derivatives, due to the amino group inserted between the phenyl ring and the dichalcogenide bond, while for PD-XX and PF-XX are compensated and, thus, similar BDEs are calculated. Besides, it is found that the nature of the dynamic bond slightly affects the BDE. Likewise, the presence of hydrogen bonds slightly tends to increase ρ as a result of an elongation of the X-X that is observed in quantum molecular dynamics. Finally, from the analysis of the reaction barriers, we concluded that the phenyl rings are fundamental in order to decrease the barrier, as the existence of $\pi - \pi$ stacking interactions may stabilize the transition state and keep the radical close and the optimal geometry for the reaction to succeed. Therefore, the PD-XX systems show lower barriers than others. For the PA-XX, the insertion of the amino group distorts the geometry reducing the strength of the $\pi - \pi$ interactions and, therefore, larger barriers are calculated. Concerning the dynamic bond, the presence of Se reduces, in general, the reaction barriers, a feature that may be explained by a better spatial overlap between the $4p$ orbitals, larger than the corresponding sulfur $3p$ orbitals. As a consequence, the lowest barriers are calculated for PD-SeSe. Moreover, in these systems the wavelength necessary for photodissociation is located in the visible region of the electromagnetic spectrum, which in addition to thermal dissociation may help to the radical formation and hence increase the self-healing capacity. All these results are in agreement with the experimental evidence, and hence, based on all these results, we may conclude that the substitution of sulfur by selenium together with a proper choice of the backbone directly attached to the dynamic bond, may be considered as a good strategy to enhance the self-healing performance of the disulfide-based materials.

Once ρ and ΔG^{TS} were analyzed and compared for S-S, S-Se and Se-Se containing materials, we extended the theoretical calculation of ω to these materials, in order to improve the protocol designed in our group [72].

In order to do so, a set of dichalcogenides (including disulfide and diselenide bonds) with different backbones (PA, PD and PF) combined with five different functional groups as substituents were studied. Compared to Formoso's protocol, the relevance of four different structural parameters, namely, the initial guess, chain length, simulation box and simulation time, were considered and compared to that from Formoso's work [72], in order to generate meaningful simulation models. According to our calculations, these parameters are very important to generate good starting conformations. With this new protocol we calculated different properties of the systems, such as the hydrogen bonding and the mobility of the chains (ω). We observed that the backbone had a direct influence in ω, with PD and PF showing similar values, while for PA derivatives a clear decrease was observed. The number of hydrogen bonds established affected the value of ω, in such a way that those systems with an intermediate number of hydrogen bonds are the ones showing larger ω values. Moreover, it can be seen that systems including diselenide bonds tend to show bigger values of ω than their disulfide counterparts (excepting R_1-PD-SS). After the calculation of ω, we combined this parameter with ρ and ΔG^{TS}, calculated previously, to estimate the theoretical self-healing capacity of the systems studied, that will be directly proportional to ρ and ω, and inversely proportional to ΔG^{TS}. We conclude that, in general, the PD-SeSe derivatives show the best theoretical self-healing capacities.

After the refinement of this protocol in model systems, we applied it to real systems. Concretely, we focused on several PUs developed by Kim et. al. and some polymetachrylates developed by Takahashi et. al. The main feature of those developed by Kim et. al. is that these materials are based on diphenyl disulfides, with different hardeners, while those by Takahashi et. al. contain the same polymeric chain combined with aliphatic disulfides (CH_2-S-S-CH_2) and tertiary amine disulfides (N-S-S-N). One of the Kim's PU (named IP) and of Takahashi´s polymetachrylates (the tertiary amine one) showed self-healing properties at low temperatures, while others did not have self-healing properties even at high temperatures. With all this, the theoretical protocol defined previously was tested in these real systems to check wether it was able to explain the different self-healing capabilities of them. In general, the protocol qualitatively agrees with the experimental results, as it is able to explain, in a general way, the different experimental-self-healing capacities of the studied systems. However, correctly taking into account the effect of the temperature is complicated with the current protocol, especially in the *ab initio* molecular dynamics, where we have realized that the initial conformation used induces a conformational bias along the simulations. Nonetheless, ρ is still a clear indicator of the self-healing capacity, in the sense that it acts as a switch; when different from zero, self-healing is possible, but when equal to zero, no self-healing will take place. Moreover, it was seen that the increment of the temperature

does not really have an impact in ω, as the properties of the bulky materials are not affected that much when working at temperatures well below their T_g, as their solid structure is rather kept.

Based on all these results, we have shown which are the main theoretical factors that govern the self-healing process in dichalcogenide materials, and we have refined a theoretical protocol that is able to explain the observed experimental self-healing capacities. Nevertheless, the main drawback of our protocol lies in the fact that very few chain conformations may be considered in the *ab initio* calculations, while no quantum effects are taken into account in the molecular dynamics simulations, which in contrast contains different conformations. It would be desirable to combine both quantum dynamics accuracy and molecular dynamics conformation number in order to provide a more quantitative protocol with larger predictive power. Fortunately, the protocol set up in this thesis is accurate enough for the prediction of new dichalcogenide based self-healing materials.

Part II

Dikalkogenuroetan Oinarritutako Material Autokonpongarri Eraginkorren Azterketa Teorikoa

Chapter 7

Sarrera

Gaur egungo kimikaren oinarriak Antoine Lavoisier kimikari frantziarrak XVIII. mendean finkatu zituen, zeinek kimika erreaktibo kuantitate finito eta neurgarrien baitan ulertuta izan zezakeen erakutsi zuen, eta analisi zehatzak egiteko oinarri kontzeptualak garatzen lagundu zuen. Horren ondoren, konposatu kimiko ezberdinen konposizioa finkatzea posible izan zen, erabilitako erreaktiboak eta kimikoki lotutakoan sorturiko produktuak kontu askoz pixatuz; erreakzio izenezko prozesu kimikoaren bidez emandako loturan. Orduz geroztik, kimikariak gai izan dira jada ezagunak diren konposatuak eta konposatu kimiko berriak sintetizatzeko.

7.1 Kimika Itzulkorra

Historikoki, konposatu organikoen sintesia zinetikoki kontrolatutako erreakzioetan oinarritu da [1], lotura kobalente itzulezinak eratuz. Kimika sintetiko mota honetan, erreaktiboen (edo katalizatzaileen) aukera arreta askoz egiten da, ahalik eta puruen den produktu bakarra lortzeko asmoz. Funtsean, produktu jakin baten erakuntza faboratzen duen erreakzio-bide energetikoa hobestea da helburua, adibidez, A-k C ematen du B ordez 7.1 Irudian. Erreakzioaren izaera itzulezinak behin produktua formatzean, hasierako erreaktiboetara ez itzultzea ziurtatzen du, ez emandako erreakzio baldintzetan gutxienez.

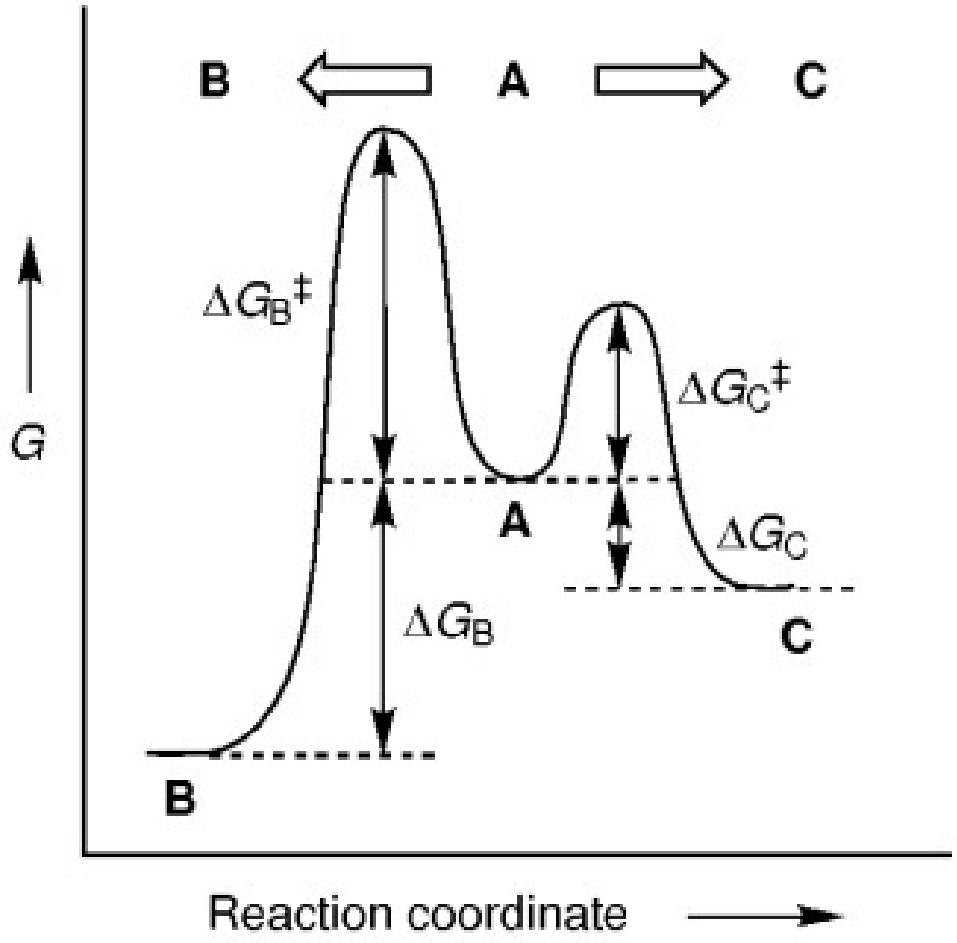

Figure 7.1: Energia askearen profila produktuen distribuzioa kontrol zinetikoaren (A→C) eta termodinamikoaren (A→B) menpean irudikatuz. Kimika kobalentearen gehiengoa itzulezina da, beraz, kontrol zinetikoaren menpean gauzatzen da, kimika dinamiko kobalentea, ordea, itzulkorra da, eta hortaz, kontrol termodinamikoaren menpean ematen da.

Berriki, ordea, kimikaren adar batean interesa berpiztu egin da, non oreka baldintzen menpe, lotura kobalenteak eratzeko eta apurtzeko, eta hain zuzen ere, bereratzeko gaitasuna duen [2]. Ekilibrazio prozesua nahiko azkarra izanez gero, orduan, kimika dinamiko kobalentea deituriko honek, produktu termodinamikoen erakera eraginkorra gauzatu dezake, adibidez, 7.1 Irudian, A-k B emango du C ordez. Mota honetako erreakzioetan, bukaerako produktuen arteko egonkortasun erlatiboa (ΔG^0_B etaΔG^0_C alderatuz 7.1 Irudian) da produktuen arteko proportzioa kontrolatzen duena, eta ez B eta C produktuen bitarteko trantsizio egoeren arteko magnitude

erlatiboak (ΔG_B versus $\Delta G_C^{\neq}$). Honezkero, apurtu eta bereratzeko gaitasuna (izenez, lotura itzulkorrak) duten lotura kobalenteen bilaketa kimika itzulkorraren arloko oinarri bat bilakatu da.

Lotura itzulkor bat oreka baldintzetan apurtu eta bereratu daitekeen lotura kimiko bat bezala definitu daiteke. Honek lotura hauetaz osatutako materialak moldagarriak izatea ahalbidetzen du, kanpo estimulu baten bidez termodinamikoki egonkorrago den estatu bat hobetsiz haien egitura aldatuz, [3, 4, 5]. Lotura kobalente dinamiko ugari daude, baina, oro har, erreakzio itzulgarri oro hurrengo bi kategoriatako bati eslei dakioke: lotura itzulkorraren eraketa/apurketa beste lotura mota bat eratuz (ikus 7.2 Irudia a), eta b), elkartrukatze zuzeneko errekazioak, non sortzen eta apurtzen diren loturak mota berdinekoak diren (ikus 7.2 Irudia b). Funtzionaliate hau erakusten duten loturak [2] azetalak, disulfuroak edo iminak izan daitezke. Lortzen eta apurtzen diren loturak funtsean lotura berdinak izateak produktuen eta erreaktiboen arteko desberdintasun energetikoak oso txikiak izatea eragiten du, haien arteko diferentzia deuseztagarria ez denean.

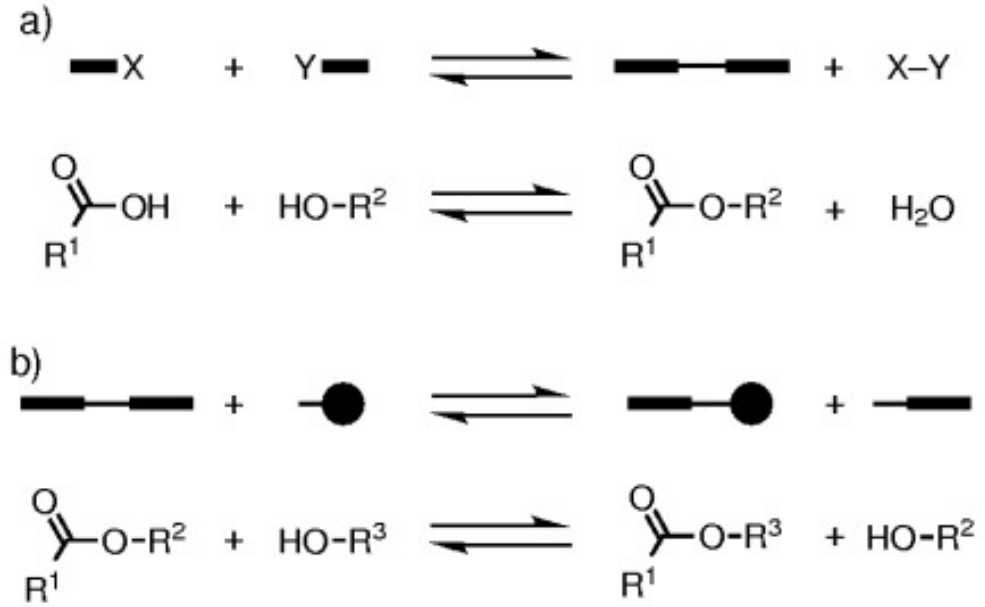

Figure 7.2: Erreakzio itzulkorren bi eredu: a) lotura mota berri baten eraketa/apurketa (adibidez esterren formazioa/apurketa) eta b) elkartrukaketa zuzena (adibidez, transesterifikazioa).

Kimika itzulgarritik sortzen den aplikaziorik erakargarrienetako bat ma-

terial batzuek autokonpontzeko, eta honela, jasandako kaltea sendatzeko duten gaitasuna da, eta, hala, jatorrizko propietateak berreskuratzeko gai izateak [6, 7, 8, ?, 9]. Horrela, lotura kimikoen berrantolakuntza dela eta, kaltetutako zatiek berriz konektatzeko gaitasuna daukate, eta materiala partzialki edo osorik berreskuratuko da. Hau da material autokonpongarrien kontzeptuaren jatorria.

7.2 Material Autokonpongarriak

Material biologikoak eboluzioaren bidez optimizatutako sistema funtzionalak dira, eta, haien funtzionalitate-sorta zabalaren artean, azpimarragarrienetako bat bere burua autokonpontzeko gaitasuna da [10]. Ezaugarri horren adibide batzuk 7.3 Irudian ageri dira, non organismo bizi batzuek (fauna eta flora barne) metodo ugarien bidez, daukaten autokonpontzeko gaitasuna ikus daitekeen. Hala, naturan, argi dago autokonponketa-prozesua maila molekularrean (DNA-ren konponketa,) zein maila makroskopikoan (hezur hautsien urtzea edo azalean ebaki txikien sendaketa), gerta daitekeela.

Ezaugarri garrantzitsu honetan oinarrituta, ahalegin handia egin da material-autokonpongarriak garatzeko; besteak beste, polimero autokonpongarriak garatzeko, hauek funtzionaltasun- eta aplikazio-eremu zabala baitute [6, 11, 12, 13]. Material autokonpongarriak hasierako propietateak, era autonomoan edo kanpo estimulu baten bidez, berreskuratzeko gaitasunean erabilitako agente sendagarriaren hautaketak garrantzi handia dauka.

Sistema biologikoetan inspiratuta, metodo intrintsekoak, sendatze-kapsuletan edo metodo baskularretan oinarritutako metodo estrintsekoak (azken bi hauek kanpo estimuluak behar baitituzte) izan dira materialak autokonpontze funtzionalitatetaz hornitzeko erabili diren bide nagusiak.

Horretarako, hainbat kimika-mota erabili dira (7.4 Irudian deskribatzen den bezala), Diels-Alderren erreakzioa [14, 15, ?], siloxanoen trukaketa [16, 17], trans esterifikazioa [18, 19] edo disulfuroak [20, 21] barne, hala nola efektu esterikoen [22, 23, 24, 25] edo elektronikoen [26, 27, 28, 29, 30, 31] erabilera,

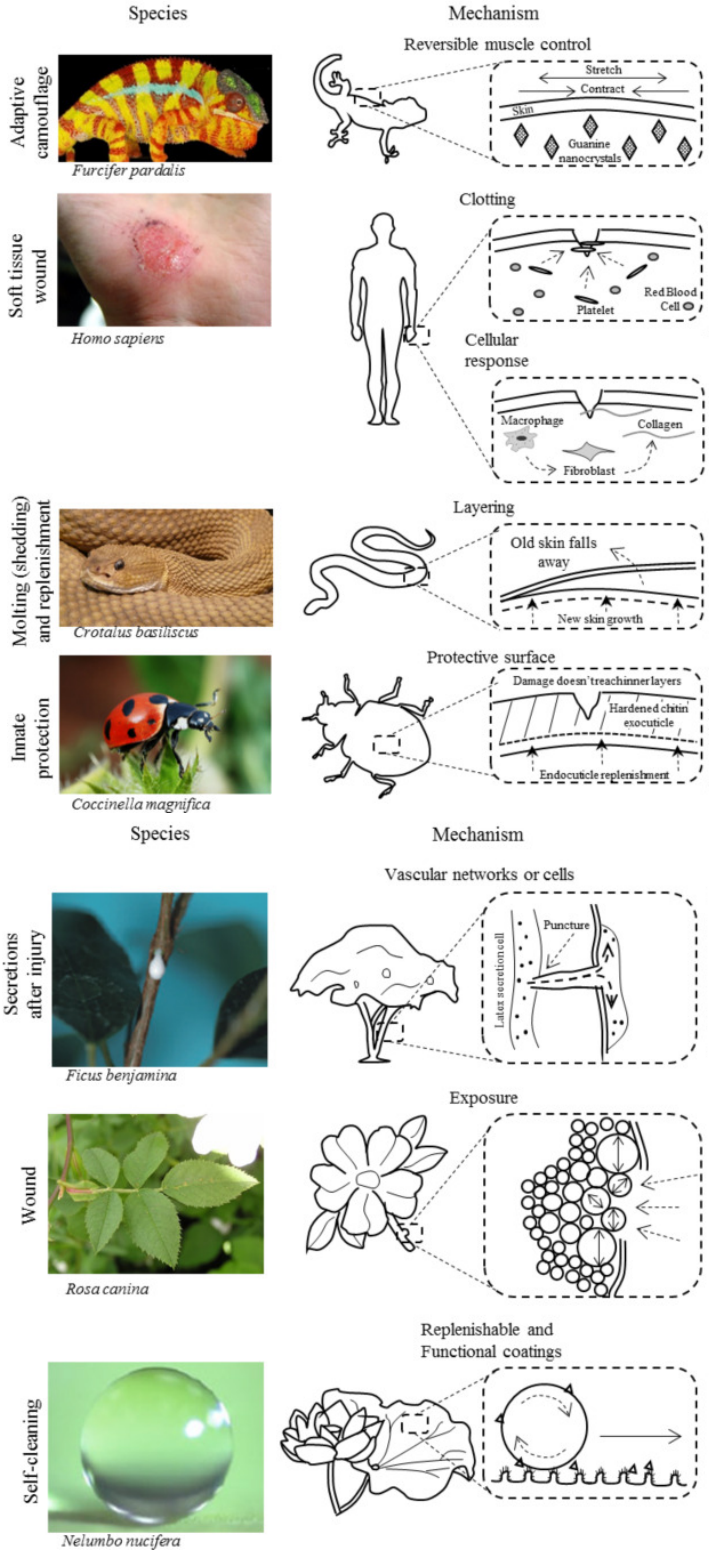

Figure 7.3: Naturan ematen diren hainbat autokonpontze prozesuren ereduak, goian fauna, behean flora. [10] erreferentziatik hartutako irudia.

adibidez. Itzulgarritasun-prozesuan oinarrituta, material-autokonpongarri intrintsekoen artean, bi talde nagusi bereiz daitezke elkarrekintzaren izaeraren arabera: lehenengoak elkarrekintza ahul eta ez-kobalenteetan oinarrituak, hidrogeno-loturak [?], $\pi - \pi$ "stacking" [32] edo metal-ioi elkarrekintzak [33] bezala, eta bigarrenak, lotura kobalenteetan oinarritatukoak [34, 35, 36], bi talde horien arteko desberdintasun nagusia sare kobalenteen erabilerak indar mekaniko eta egonkortasun handiagoko materialak eman ditzakeela izanez.

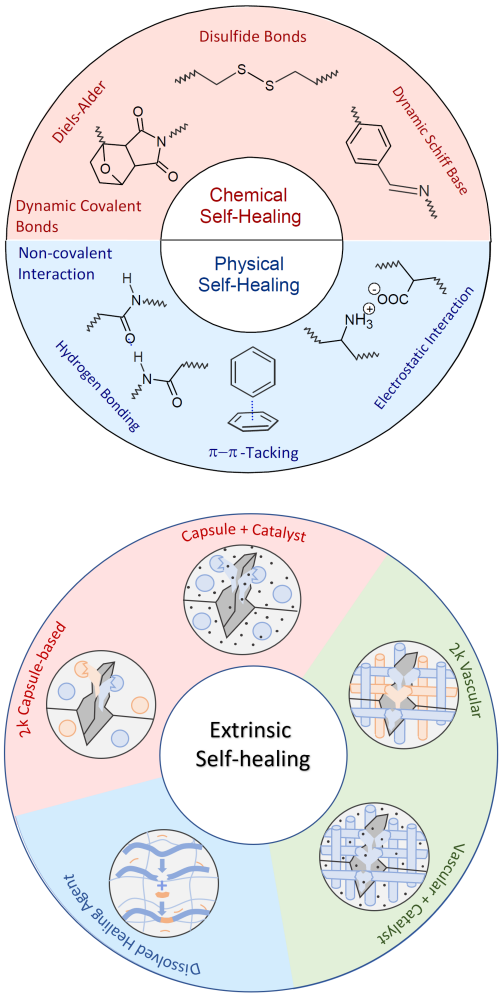

Figure 7.4: Autokonpontze agente ezberdinen errepresentazio eskematikoa. Ezkerrean: intrintsekoak, agente kimikoak eta fisikoak barne. Eskuinean: estrintsekoak.

Berriki, polimeroen zientzia polimero "argiak" sintetiza daitezkeen puntura iritsi da, haien artean hasierako propietateak erabat berreskuratzeko gaitasun bio-inspiratua duten, idealki, kanpo estimulurik gabeko polimeroak.

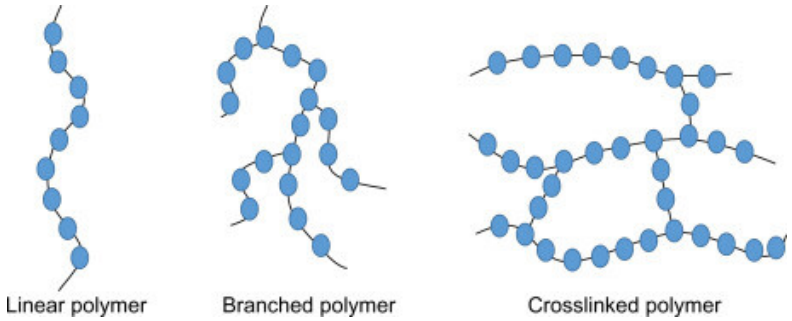

Figure 7.5: Polimero egitura ezberdinen irudikapen eskematikoa haien lotura-egituraren araberakoa.

Polimero horiek material autokonpongarrien kategoria garrantzitsuenetariko bat osatzen dute, polimero autokonpongarri intrintsikoena. Kasu honetan, matrize-fasea osatzen duten loturen itzulgarritasunaren bidez lortzen da konponketa; hots, fase hori agente sendagarri gisa aritzen da.

Material autokonpongarri ideal bat gai da osagai polimerikoen bizitza osoan zehar kalteak atzeman eta haiei etengabe erantzuteko, horrela, materialaren errendimendua lehengoratzen, hasierako materialaren propietateei kalte egin gabe. Materialak seguruagoak, fidagarriagoak eta iraunkorragoak izatea espero da, kostuak eta mantentze-lanak murrizten dituzten bitartean. Material polimeriko autokonpongarrien garapen arrakastatsuak aukera handiak eskaintzen ditu material arin horiek egitura-osagaien eta osagai kritikoen fabrikazioan dituzten aplikazioak zabaltzeko.

Hala ere, polimeroen matrize-fasea agente sendatzaileak soilik osatzen badu, gerta daiteke materialaren prozesagarritasunak, propietate mekanikoak eta etorkizuneko aplikazioak kaltetuak izatea, beraz, material-autokonpongarriak garatzeko bide ezberdinak bilatzea komenigarria dela dirudi. Polimeroen propietate mekanikoetan masiboki eragin gabe izaera autokonpongarria sartzeko, agente kuratibo bat, lotura kobalente dinamiko bat adibidez, kate polimeriko nagusien arteko “crosslinker” gisa (ikus 7.5 Irudia) sartzea irtenbide egokia izan liteke, bi efektu kontrastatzaile horien arteko balantza bat aurkitzeko [37].

Hala eta guztiz ere, lotura kobalente itzulgarriak dituzten polimero askok berezko erreaktibotasun txikiak dituzte, hortaz, kanpoko estimulazioa behar dute itzulgarritasun prozesua gauzatzeko, hala nola beroa edo UV ir-

radiazioa. Hala, autonomoa den edo estimulu ahulak behar dituen autokonpontze kobalente itzulgarria lortzeko, erabilitako lotura kobalentearen hautaketa egokia funtsezkoa da [23, 38, ?]. Alde horretatik, disulfuro loturak tenperatura baxuagoetan (giro tenperatura ingurukoetan) sendatzeko funtzionaltasuna sartzeko hautagai onak dira, zentzuzko lotura-indarrak mantentzen diren bitartean.

7.3 Dikalkogenuroetan Oinarritutako Material Autokonpongarriak

Disulfuroen kimika oso moldakorra da. S-S loturen apurketaren izaera dinamikoa eta itzulgarritasuna dela eta (sulfenilo erradikalak sortzeko), disulfuro-konposatuak funtsezkoak dira zenbait arlotan, hala nola kimika fisiologikoan, non disulfuro-zubiak proteinen jarduera biologikoan eta haien egonkortasun konformazionalean funtsezkoan diren [39, 40, 41], edo kimika sintetikoan [42]. Horrez gain, aipagarria da materialen zientzian duten erabilera, nanokristal koloidalen sintesirako oso aldakorrak diren aitzindari gisa [43] edo kautxuaren bulkanizazioaren ondorioz sortzen diren "crosslinker" talde gisa, disulfuroek proteinetan duten zereginaren analogiaz, materialaren erreologian eragin handia izanik [44].

Disulfuro-konposatu batzuetan elkartrukatze erreakzioa eman egiten da katalizatzaileak erabiliz [45, 46] edo UV [47] irradiazioaren mepean ere, baina, errendimendua hobetzeko, komeni da elkartrukatze hori giro-tenperaturan eta kanpoko estimulurik gabe ematea. Beraz, lotura disoziazio-energi baxuak dituzten disulfuroak beharrezkoak dira material autokonpongarriak baldintza leunetan prestatzeko. Hau da, hain zuzen ere, disulfuro aromatikoaren kasua, non jakin egin den metatesia giro-tenperaturan gertatzen dela, bai soluzioan [48], bai egoera solidoan [49].

Ikuspegi horretatik, lan arrakastatsu bat agertu da berriki literaturan, non bis(4-aminofenil) disulfuroa "crosslinker" dinamiko gisa erabiltzen den autokonpongarriak diren poliuretano elastomeroak diseinatzeko, zeinek eraginkortasun kuantitatiboa erakusten duten giro-tenperaturan, katalizatzailerik edo kanpo-estimulurik gabe [50]] (ikus 7.6 Irudia). Sendatzeko eraginkortasun handia giro-tenperaturan ematen den disulfuro aromatikoen

truke konstanteari esker azal daiteke, urea unitateen arteko hidrogeno loturen erakuntzaz hobeturikoa, %50eko sendatze-eraginkortasuna lortuz.

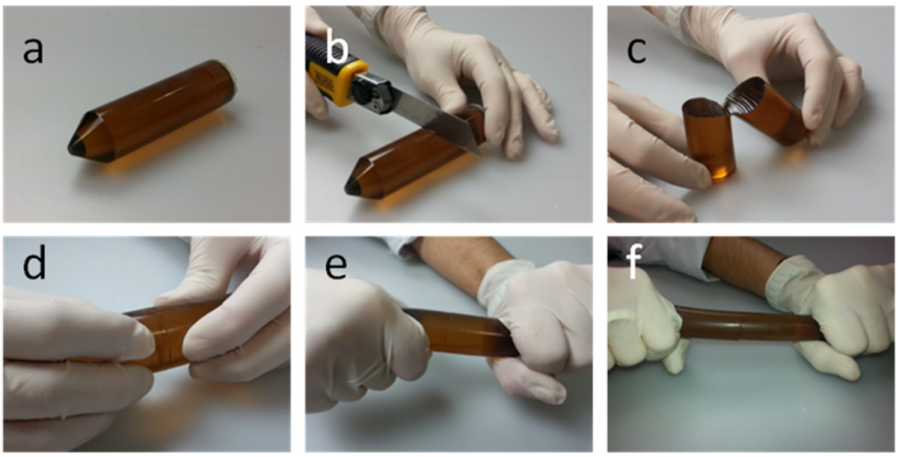

Figure 7.6: Dikalkogenuroan oinarritutako poliuretano baten ("Terminator" izenekoa) autokonpontze prozesuaren irudukiapen grafikoa ([?] erreferentziatik hartutako irudia.).

Ezaguna da, poliuretanoen (PU) kasuan, elkarrekintza supramolekularrek haien propietate mekanikoetan garrantzi haundia daukatela, bai hidrogeno loturek eta bai segmentu gogorren paketatzeak ere [31, 51, 52, 53], beraz, bi elementu hauen eraginak optimizatuz gero, materialak haien etorkizuneko aplikaziorako propietate mekaniko aproposaz hornitu daitezke. Zentzu honetan Kim et. al.-ek [54] eta Takahashi et. al.-ek [55] disulfuroetan oinarritatutako bi material sorta diseinatu zituzten, crosslinker eta hardener ezberdinak erabiliz, haien autokonpontze gaitasuna aztertzeko tenperatura ezberdinetan.

Alde batetik, Kim et. al.-ek disulfuro aromatikoetan oinarritutako hiru PU sintetizatu zituzten, bakoitzak zurruntasun ezberdineko segmentu gogor (edo hardener, ikus 7.7 Irudia) ezberdin batekin, izenez; IP (egitura alizikliko asimetrikoa); 4,4´-metilenobis(ziklohexil isozianatoa), HM; (egitura alizikliko simetrikoa); 4,4´-metilenobis(fenil isozianatoa), eta M; (egitura aromatikoa). Haietako batek, IP-k zehazki, giro tenperaturan autokonpontzeko gaitasuna aurkezten zuen, hala nola, aurretik ezagunak ziren giro tenperaturako material autokonpongarrien propietate mekanikoak (sendotasuna, luzagarritasuna eta iraungarritasuna) hobetuz. Beste bi sistemek

haien autokonpontze gaitasunak tenperaturaren igoerarekin hobetzen zituzten, giro tenperaturan autokonpontzerik aurkezten ez zuten bitartean.

Bestetik, Takahashi et. al.-ek polimetakrilato sareetan oinarritutako eta bi "crosslinker" ezberdinen arteko konbinazioaz eratutako materialak sintetizatu zituzten, batak disulfuro alifatikoz osatuta eta besteak sulfenaminaz (-N-S-S-N-), ADSA eta BTA izeneko egiturak lortuz, hurrenez hurren, paketzearen eragina autokonpontze prozesuan aztertzeko nahian. Ikusi zuten BTA egiturak autonkonponketa aurkezten zuela bai giro tenperaturan bai tenperatura altueta, ADSA egiturak, berriz, ez zuen autonkoponketarik azaldu ez giro tenperaturan ez tenperatura altuetan, harderner berdina erabili izan arren.

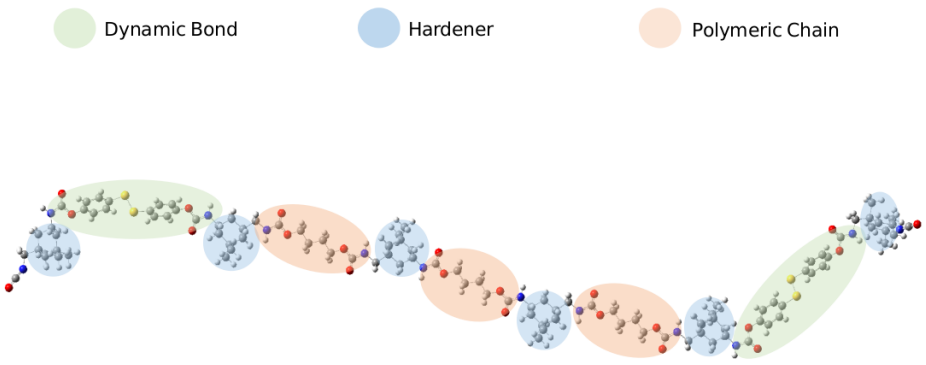

Figure 7.7: IP polimeroaren atal ezberdinen irudikapen grafikoa; berdez: lotura dinamikoa, gorriz: kate polimerikoa eta urdinez: "hardener"-ra.

Sufreaz gain, selenioaren azterketa ere garrantzitsua da, sufrea proteinetan eta beste sistema biologiko batzuetan ordezka baitezake. Hala ere, berezko desberdintasun atomikoak, hala nola tamaina edo elektronegatibotasuna, selenioan oinarritutako konposatuetan hautemandako portaeren erantzule dira, hala nola S_N2 erreakzioen erreaktibotasun kimikoaren hobekuntza [58] edo selenil erradikalen egonkortasun hobetuan [59]. Interesgarriagoa da selenioak konposatu biologiko batzuk oxidazio bidezko inaktibazioari erresistentziaz hornitu dezakeela ohartu izana [60].

Diseleniuroen kimika material autokonpongarri berriak diseinatzeko ere erabil daiteke. Halakoxeak dira selenioaren eta sufrearen edo nitrogenoaren konbinazioak [61, 62]; haien loturen disoziazio-energiek iradokitzen baitute

kimika itzulgarrian ere erabil daitezkeela, baita baldintza leunagoetan ere. Adibidez, Ji et. al. [63] gai izan ziren konposatu diseleniuro alifatikoak sintetizatzeko, zeinak argi ikusgarriak eta UV irradiazioak eragindako prozesu batean autokonpontzeko gai zirenak; iluntasunean, ordea, erreakziorik ez zen gertatu. Era berean, Pan et. al. [64] UV irradiazioaren ondorioz diseleniuro alifatikoz osatutako polimero-sareeen sendatzeko eta berprozesatzeko gaitasuna kanpo eraginik gabe frogatu zuten [65].

7.4 Erreakzio Mekanismoa eta Lan Teorikoak

Beraz, argi dago oso garrantzitsua eta aplikagarria den prozesu baten mekanismoa aztertzea oso garrantzitsua dela, elkartrukatze erreakzioa maila molekularrean hobeto ulertzeko. Honek, materialen autokonpontze-gaitasuna hobetu dezake, katalizatzailerik edo UV irradiaziorik gabe elkartrukaketa esperimentatuko duten lotura berriak aurreikusiz. Disulfuro-loturaren disoziazioarekin lotutako zenbait lan teorikotaz gain [66, 67, 68], disulfuroetan oinarritutako material konpongarrien elkartrukatze erreakzioaren mekanismoa aztertu zuen lehen lan teorikoa Matxainek eta Ruipérez-ek burutu zuten [69].

Uste ez bezala, [2+1] erradikal bidezko mekanismo bat (ikus 7.8 Irudia) autokonpontze-erreakzioaren erantzulea da, eta ez espero zen [2+2] metatesi-mekanismoaren erantzulea. [2+1] mekanismoan, lehenengo urratsa sulfenil erradikalen sorketa da, S-S lotura apurtuz. Ondoren, sortutako erradikal horiek inguruan dauden beste disulfuro-lotura batzuei eraso diezaiekete, hiru kideko trantsizio-egoera baten bidez. Bukaeran, disulfuro lotura berri bat eta sulfenil erradikal bat eratzen dira, desplazamendu erreakzioaren ondorioz, prozesuan sufre atomoak elkartrukatuz.

Sulfenilo erradikalen eraketa esperimentalki berretsi da [70], aurkikuntza teorikoak ziurtatuz. Beste baieztapen esperimental bat ere aurki daiteke Odriozola et. al.-en lanean, non disulfuroak zituen beira-zuntz bat mailu batekin jo zuten, materialaren kolorea aldatuz, eta giro-tenperaturan 24 ordu igaro ondoren bere jatorrizko kolorea berreskuratu zuen. Kalkulu

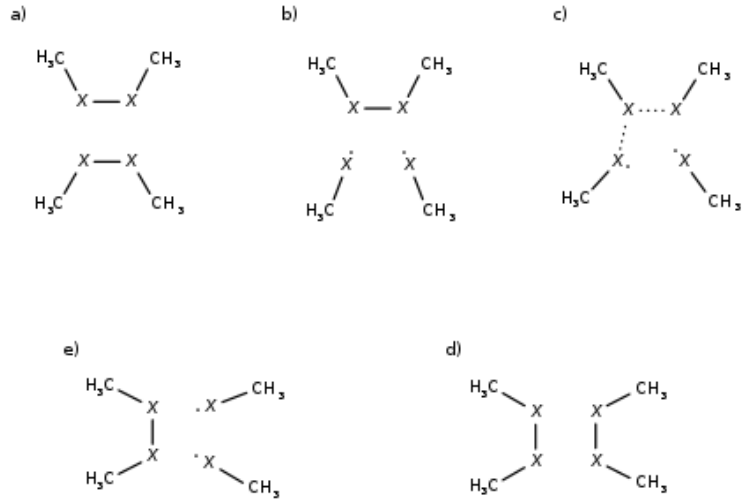

Figure 7.8: [2+1] erradikal bidezko erreakzio mekanismoaren irudikapen eskematioa, a) Erreakzioa baino lehenagoko egoera b) disulfuro lotura baten apurketa, hots, erradikalen eraketa c) 3 kideko trantsizio egoeraren eraketa d) disulfuro lotura berriaren eraketa e) disulfuro loturen arteko elkartrukaketa.

teorikoek kolorearen arduradunak sulfenilo erradikalak zirela ziurtatu zuten [71].

Matxain eta Ruipérezen lanean [69], disulfuroaren egitura kimikoak autokonpontze-prozesuan duen garrantzia nabarmentzen da, eta eragina izan dezaketen hiru ezaugarri aztertzen dira. Lehenik, S-S loturaren haustura aztertzen da, horixe baita erreakzioaren lehen urratsa. Prozesua giro-tenperaturan gertatu behar denez, disoziazio termikoa gauzatzeko, loturen disoziazio-energiak baxuak behar dira izan, baita fotodisoziazio prozesua argi ikuskorraren bidez gauzatu ere. Bigarrenik, energia gutxiko erreakzio-langak nahitaezkoak dira erreakzioa modu itzulgarrian gauzatzea errazteko. Azkenik, hidrogeno-loturak eginkizun estrukturala dutela prozesuan ikusi zuten, disulfuroak erreakzioa gauzatzeko bezain gertu mantendu baititzake. Hala ere, erabilitako eredu txikiek ez zuten ezaugarri horren azterketa sakonagorik baliatu.

Ondorengo lan batean, [72] autore berdinek eredu handiagoak erabili zituzten sistema horietan elkarrekintza ez-kobalenteen eragina aztertzeko, hidrogeno-loturena barne, dinamika molekularren bidez. Lan horretan ikusi zuten sortutako hidrogeno-lotura kopurua ere faktore giltzarria dela, zuze-

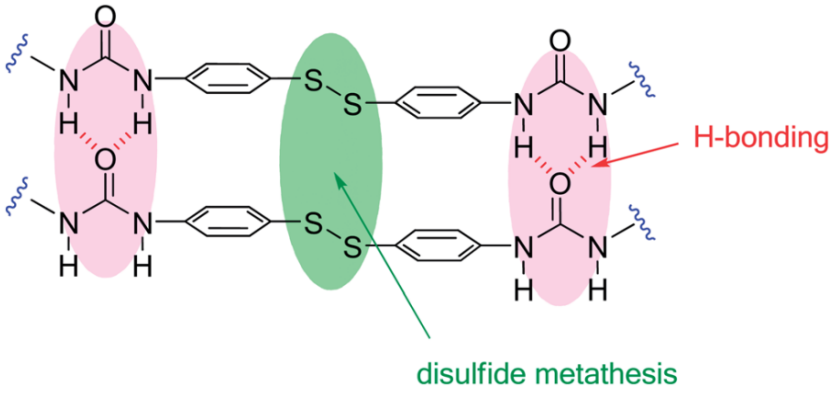

Figure 7.9: Disulfuro aromatikoetan oinarritutako materialen autokonpontze prozesuan eragin handia daukaten faktoreak goraipatzen dituen irudi eskematikoa; berdez: lotura dinamikoa eta gorriz hidrogeno loturak. [?] erreferentziatik hartutako irudia.

nean eragiten baitio kateen mugikortasunari. Hala, hidrogeno-loturen kopuru handiegiak eta txikiegiak kaltegarriak dira autokonpontze-prozesurako; izan ere, kateak zurrunegiak izan daitezke, disulfuroen arteko kontaktua saihestuz (haien mugimendua mugatuz), edo sobera mugikorrak, disulfuruoak bata-bestetik urruntzen eta, ondorioz, erreakzionatzeko bezain hurbil dauden disulfuroen proportzioa txikiagoa eginez.

7.5 Tesiaren Motibazioa eta Helburu Nagusiak

Puntu honetan, argi dago propietate mekaniko aproposekin konbinatutako sare dinamikoen diseinu simultaneoa materia autokonpagarrien zelaiaren mugarri bihurtu dela eta eta kimika teorikoa oso tresna ahaltsua izan liteke helburu hori lortzeko, emaitza esperimentalak ulertzen eta arrazionalizatzen laguntzen baitu, bai eta material polimeriko berriak diseinatzen ere [73]. Orain arte, kimika teorikoak dikalkogenuroen trukaketa erreakzioa ren erreakzio-mekanismoa ulertzen lagundu du, bai eta elkartrukatze prozesuan lotura dinamikoaren inguruan egitura kimikoak duen garrantzia nabarmentzen ere. Gainera, kimika konputazionala gai da atomo gutxiko sistemak ez ezik, milaka atomoko sistemak ere aztertzeko. Hori dela eta, oso tresna erabilgarria da bolumen handiko materialen dinamika aztertzeko. Beraz, tesi honen helburu nagusia dikalkogenuroetan oinarritutako material autokonpongarrien eskala anitzeko azterketa izango da.

Tesi honen helburu espezifikoak hauek dira:

- Lotura dinamikoaren izaera eta haren inguru kimikoak daukan garrantzia aztertzea kimika kuantikoaren bidez, batez ere termo- eta fotodisoziazioan oinarrituta, hala nola, elkartrukatze erreakzioaren zinetikan.
- Materialen portaera dinamikoa aztertzea. Horretarako, eredu atomistikoak eraikitzeko protokoloa ebaluatuko da, eta, ondoren, dinamika molekularraren bidez dikalkogenuro ezberdinak aztertuko dira.
- Gure taldean garatutako protokolo teorikoa erabiliz, sitema esperimental batzuk aztertuko dira [54, 55], bi asmo nagusirekin: i) protokolo teorikoaren baliogarritasuna frogatzea, eta ii) behatutako joera eta ezaugarri esperimentalak arrazionalizatzea.

Bukatzeko, ondorio orokorrak aipatuko dira.

Chapter 8

Oinarri Teorikoak

Dentsitate Funtzionalaren Teoriak, N elektroiren uhin funtzioa eta dagokion Schrödinger-en ekuazioaren ordez, $\rho(r)$ elektroi dentsitatea darabil. $\rho(r)$ hiru koordenatu espazialen funtzioa besterik ez da eta beraz uhin funtzioa baino sinpleago da. Egoera elektronikoa, energia eta edozein sistemaren propietate elektronikoak, $\rho(r)$ honen funtzioan deskribatzen dira.

Hohenberg eta Kohn-ek [94] degeneratua ez den oinarrizko egoera duen sistema baten propietate elektronikoak $\rho(r)$ elektroi dentsitateak determinatzen dituela demostratu zuten. Beraz, E_0 oinarrizko egoeraren energia $\rho(r)$-ren funtzionala da. Orokortuz, oinarrizko egoeraren elektroi-dentsitatea jakinez gero, oinarrizko egoeraren propietate elektroniko guztiak kalkulatzea posible da, funtzional dependentziak finkatu ostean. Energi funtzionala aurkitzeko energiaren bariazio- printzipio bat finkatu zuten. Horrela, $E[\rho]$ funtzionalaren forma zehatza jakinik oinarrizko egoeraren dentsitatea bilatu genezake. Zoritxarrez, funtzionalaren forma zehatza ezezaguna dugu.

Kohn eta Sham-ek [95] funtzional honen hurbilketa ez-zuzen bat garatu zuten. Ondorioz, DFT kalkulu zehatzak egiteko tresna erabilgarria bihurtu zen. Haiek N elektroiz osaturiko eta ρ oinarrizko egoeraren elektroi dentsitatea duen molekula baten E_0 oinarrizko egoeraren energia elektronikoa ondorengoa dela erakutsi zuten:

$$E_0 = -\frac{1}{2}\sum_{i=1}^{N} < \psi_i(1)|\nabla_i^2|\psi_i(1) > + \int v(r)\rho(1)d\vec{r}_1 + \\ + \frac{1}{2}\int\int \frac{\rho(1)\rho(2)}{r_{12}} d\vec{r}_1 d\vec{r}_2 + E_{xc}[\rho] \tag{8.1}$$

$v(r) = -\sum_\alpha \frac{Z_\alpha}{r_{1\alpha}}$ nukleoen eraginez dagoen kanpo potentziala da, ψ_i Kohn-Sham orbitalak eta $E_{xc}[\rho]$ truke-korrelazio energia. Kohn-Sham prozeduran oinarrizko egoeraren ρ zehatza, Kohn-Sham orbitaletatik lor daiteke,

$$\rho = \sum_{i=1}^{N} |\psi_i|^2 \tag{8.2}$$

eta Kohn-Sham orbitalak:

$$\hat{F}_{KS}(1)\psi_i(1) = \epsilon_i\psi_i(1) \tag{8.3}$$

elektroi bakarreko ekuazioak ebatziz lortzen dira, $\hat{F}_{KS}$ Kohn-Sham operadorea:

$$\hat{F}_{KS} = -\frac{1}{2}\nabla_1^2 - v(1) + \sum_{j=1}^{n} \hat{J}_j(1) + V_{xc}(1) \tag{8.4}$$

$\hat{J}$ Coulomb operadorea da, eta V_{xc} truke-korrelazio potentziala (2.15):

$$V_{xc} = \frac{\delta E_{XC}[\rho]}{\delta\rho} \tag{8.5}$$

Hartree-Fock ekuazioetanV_{xc}, $\hat{F}_{KS}$ agertzen den Fock operadorea bezalakoa da, gauza batean izan ezik. Truke operadorearen ordez, truke eta korrelazioa kontuan hartzen dituen V_{xc} jartzen da.

Ekuazio hauek iteratiboki ebazten dira. Hasierako dentsitate batetik hasita $\hat{F}_{KS}$ eraikitzen da, eta 8.3 ekuazioa ebazten da. Emaitza $\hat{F}_{KS}$ berri bat eratzeko erabiltzen da. Prozedura hau konbergentzia lortu arte errepikatzen da.

Kohn-Sham orbitalen esanahi fisikoa eztabaidan dago oraindik. Autore batzuen iritziz ez dute inolako zentzurik, eta ρ zehatzaren kalkuluan dira erabilgarri soilik. Era berean, Kohn-Sham orbitalen energiak molekulen orbitalen energiekin ez lirateke nahastu behar. Beste batzuek ordea, HOMOaren Kohn-Sham energia ionizazio potentzialaren negatiboa dela kontuan harturik, eta honetaz gain Kohn-Sham ekuazioak, HF kasuaren antzera partikula askeen eredua gogora ekartzen duela kontutan harturik, Kohn-Sham orbitalei HF orbital kanonikoek duten antzeko esanahi fisikoa egokitzen diete.

Dena den, $E_{xc}[\rho]$ truke-korrelazio funtzionala eta beraz, V_{xc} truke-korrelazio potentziala elektroi gas uniformearen kasurako baino ez da ezagutzen. Zorionez, funtzional hurbilduak garatu dira. Horietako bat, dentsitate lokalaren hurbilketa (DLH) da. Honen ideia, $\rho(\vec{r})$ dentsitate lokala duen bolumen elementu bakoitza elektroi gas homogeneoa bezala kontsideratzea da. Ikuspuntu honetatik hurbilketa hau dentsitatea espazioan zehar mantso aldatzekotan zehatza da. $E_{xc}[\rho]$ ondorengo espresioak emana dator:

$$E_{xc}^{DLH}[\rho] = \int \rho(\vec{r})\varepsilon_{xc}(\rho)d\vec{r} \tag{8.6}$$

$\varepsilon_{xc}(\rho)$, ρ elektroi dentsitatea duen elektroi gas homogeneoaren truke-korrelazio energia da, elektroi bakoitzeko. Espresio hau aplikatuta dentsitate lokalaren hurbilketa (DLH) edo spin dentsi- tate lokalaren hurbilketa (SDLH) lortzen dira. Azken honen kasuan spin ezberdina duten elektroientzat orbital eta ra eta rb dentsitate ezberdinak erabiltzen dira. Noski, molekulen kasuan hauek funtzional zehatzaren hurbilketa dira, ρ homogeneoa ez delako. Hurbilketa, dentsitate gradientearen espansio bat eginez hobetu liteke, aurretikoa Taylor seriearen lehen terminotzat hartuz. Metodo hauek generalizaturiko gradientearen hurbilketa (GGA) dira, eta molekulen azterke-

tan garrantzi handia dute, elektroi dentsitatea homogeneoa dela ezin baita kontsideratu.

Hohenberg-Kohn-en teorematik, jakina da E_{xc} zehatza existitzen dela. Hala ere, ezezaguna da eta beraz zehazki mintzatuz, esan liteke DFT kalkuluak ez direla *ab initio* kalkuluak. Dena den, datu esperimentalak doitzeko parametrorik erabiltzen ez dutenez, abinitio direla esan liteke. Metodo honen abantaila handienetakoa HF metodoaren koste konputazional antzekoa izanik elektroi korrelazioa kontuan hartzen dutela da. Dena den, korrelazio efektu hauek ezin dira zehazki sailkatu, hastapenetik ez korrelaturiko emaitzarekin nahasturik daudelako. Honetaz gain, sofistikazio gehiago aplikatuz, kalkuluak hobetzeko bide sistematikorik ez dago, eta honen ondorioz emaitzak diren bezala onartu behar dira.

Arazo hauek izan arren, DFT-k sistema kimiko batzuen oinarrizko ego- eraren propietateentzat emaitza onak eman ditu. Koste konputazional baxua dela eta, sistema handien kasurako DFT aukeratzen den metodoa da, elektroi korrelazioa MP edo CI metodoen bidez kontsideratzea oso garestia delako. Funtzional asko daude gaur egun merkatuan eta dugun problema kimiko zehatzerako balioko duen funtzionala erabili beharko da.

Chapter 9

Kimika Kuantikoaren Bidezko Dikalkogenuroetan Oinarritutako Material Autokonpongarri Eraginkorren Azterketa Teorikoa

9.1 Sarrera

Disulfuroen jarduera on honen arrazoiak konputazionalki azaldu egin dira berriki. Lehen aldiz, Matxain and Ruipérez-ek [69] disulfuro aromatikoetan oinarritutako material autokonpongarrien, Odriozolak et al. [**?**] lortutako modukoak, erreakzio mekanismoa ikertu zuten. Uste ez bezala [2+1] erradikal bidezko mekanismoa (ikus 9.1 irudia) nagusi zela ikusi zuten, eta ez esperotako [2+2] metatesis mekanismoa.

[2+1] erradikal bidezko mekanismoaren lehenengo urratsa sulfenil erradikalen eraketa da, disulfuro lotura (S-S) apurtuz, ondoren, erradikal hauek, behin sortutakoan, haien inguruan dauden beste disulfuro loturak eraso ditzakete. Eraso honek 3 sulfuro unitatez osatutako trantsizio egoera baten bitartez ematen da, azkenean disulfuro lotura berri bat eta sulfenil erradikal bat produzituz, horrela, sufre atomoen elkartrukaketa burutzen.

Duela gutxi, erradikalen eraketa esperimentalki ziurtaratu egin da [70], aurkikuntza teorikoak egiaztatuz.

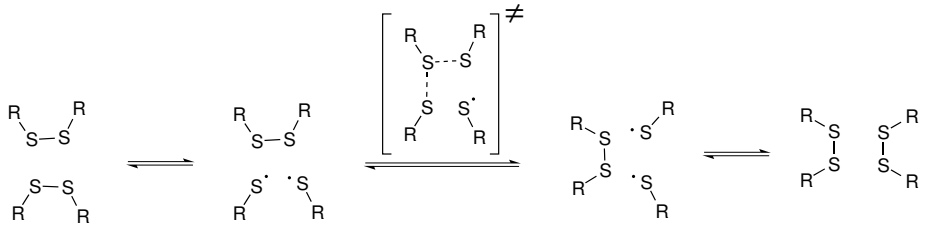

Figure 9.1: [2+1] erradikal bidezko erreakzio mekanismoaren irudikapen eskematikoa.

Erradikalen eraketa S-S loturaren ahulketaren ondorioz faboratua ikusten da, adibidez, amino taldeak difenil disulfuroei gehituz, eta honezkero, zenbait kasutan material batzuek autokonponketa prozesua giro tenperaturan azaltzeko gaitasuna azaldu daiteke, zeren eta, giro tenperaturan ere, erradikal kopuru txiki bat sortu daitezkeen, autonkonpoketa prozesua gauzatuz.

Hau dela eta, autore berdinek, disulfuro lotura ahultzeko bide ezberdinak aztertu zituzten, adibidez amino taldeak disulfuro loturaren eta eraztun aromatikoen tartean sartuz [131]. Autoreek amino talde hauek disulfuro lotura ahultzen zutela baieztatu zuten, hala ere, amino taldearen inklusioak difenil disulfuroak baino erreakzio langa handiagoak sortzen zituela ikusi zuten.

Gainera, disulfuro loturaren apurketa argiaren bitartez, hau da, fotodisoziazoa, ere aztertu zuten, non argi ultramorearen (UM) absortzio bitartez erradikalak sortzen diren, baina aztertutako kasu guztiaek ultramore eremuan absorbitu egiten zuten, beraz, eremu ikusgarrian absorbatzen duten materialen bilaketa nahitaezkoa izango litzateke materialek metodo honen bitartez autokonponketa prozesua autonomoki, hau da, kanpo faktorerik gabekoa, azaltzeko.

Aipatutako lanetan, eredu txikiak erabili ziren espezie ezberdinen erreaktibitatea ikertzeko. Hala ere, eredu hauek txikiegiak ziren material hauetan garrantzi handia daukan beste ezaugarri estruktural batzuk ikertzeko, adibidez, kateen artean sorturiko hidrogeno loturak. Hauek kontuan hartzeko, Formosok et al. [72] eredu haundiagoak erabili zituzten material hauetan ematen diren elkarrekintza ez-kobalenteen eraginak ikertzeko asmoarekin, hidrogeno loturak barne, dinamika molekularrez baliatuz. Autoreek eraz-

tun aromatikoen arteko $\pi - \pi$ elkarrekintzaen eragina mespresagarria zela ikusi zuten hidrogeno loturen eraginarekin konparatuz.

Gainera, sortutako hidrogeno loturen kopurua funtsezkoa zela ikusi zuten; izan ere, kateen mugikortasunean garrantzi haundia dauka, bai hidrogeno lotura kopuru handiek, bai txikiek, eragin negatiboa baitute autokonponketa prozesuan, zeren eta hidrogeno lotura asko sortzekotan, materialaren kateen mugikortasuna txikitu egiten den, disulfuroen arteko elkarrekintza mugatuz materialaren izaera zurruna dela eta, eta bestalde, kopuru txikiegiek disulfuroak gehiegi mugitzea ahaltzen dute, disulfuro loturak bata bestearengandik urrunduz.

Lan hauetan oinarrituz, autoreek protokolo teoriko berri bat proposatu zuten disulfuroan oinarritutako materialen autokonponketa ahalmena estimatzeko, hiru parametro ezberdinez osatutakoa, bakoitza aurretik aipatutako ezaugarri batean oinarrituta: i) erradikalak sortzeko probabilitatea (ρ); ii) erreakzio konstantea (k) eta iii) erreakziona daitezen sobera hurbil dauden bi disulfuro lotura aurkitzeko probabilitea (ω).

Hala ere, oraindik erantzunik gabeko galdera asko daude. Adibidez, zergatik diseleniuroek disulfuroen autokonponketa ahalmena hobetzen dute? Posible al da eremu ikusgarriak absorbatzen duten disulfuro edo diseleniuro loturak aurkitzea? Posiblea izango litzateke urea unitateak dikalkogenuro loturari atxikituta ez daukaten materialek autokonponketarako gaitasuna erakustea?

Galdera hauek erantzuteko asmoarekin, atal honetan disulfuro (S-S), diseleniuro (Se-Se) eta sufre-selenio lotura mistoetan (S-Se) oinarritutako hainbat material ezberdin ikertuko dira. Zehazki, difenil dikalkogenuroen eta eraztun aromatiko gabezko dikalkogenuroen azterketa teorikoa burutu da kimika kuantikoaren metodo terikoetaz baliatuz, hauek disulfuroen alternatiba izateko gaitasuna duten ala ez ikertzeko. Dikalkogenuro loturaren (X-X, non X=S, Se) disoziazio energia (ingelesez, BDE), fotodisozioazioa, erreakzio langak, eta hidrogeno loturek daukaten eragina ikertuko dira lan honetan, material hauen autokonpontze gaitasuna determinatzeko, hobetutako propietateak dituzten material berriak aurresateko asmoarekin.

9.2 Zehaztasun Konputazionalak

Geometria optimizazio guztiak gas fasean burutu dira, dentsitate funtzionalaren teoriaren (ingelesez, DFT) [94, 95] esparruan, helmen-luzeko ωB97XD funtzionalarekin [?] eta 6-31+G(d,p) oinarri funztioak erabiliz [?]. Bibrazio frekuentzia armonikoak gradienteen diferentziazio analitikoaz lortuak izan dira, lortutako egiturak minimoei edo trantsizio egoerei dagozkien ikusteko. Ondoren, frekuentziak zero-puntuko energia bibrazionala (ingelesez, ZPVE) ebaluatzeko erabili dira, hala nola entalpiren (H) eta Gibbs-en energia askearen (G) zuzenketak osziladore armonikoaren hurbilketan egiteko. Puntu bakarreko kalkuluak 6-311++G(2df,2p) oinarri funztioak [?] erabiliz burutu dira optimizitatuako egituretan, energia elektronikoa hobetzeko. Fotodisoziazio prozesua aztertzeko, denboraren menpeko dentsitate funtzionalaren teoria (ingelesez, TDDFT) [?] erabili da, 6-31+G(d,p) oinarri funtzioekin. DFT kalkulu guztiak Gaussian16 programarekin burutu dira [135].

Ab initio Born–Oppenheimer Dinamika Molekularrak (QMD) burutu dira ondoren, optimizitatutako egituren egonkortasun termikoa determinatzeko, PBE funtzionala [136, 137], DZP oinarri funtzioak eta RI formalismoa erabiliz, dagokion oinarri funtzio lagungarriekin [?, ?, ?]. Simulazioak 298 K-tan burutu dira, Nose–Hoover termostatoa erabiliz. Simulazio hauen luzeera 40.000 a.u. (9.651 ps)-koa izan da, 40 a.u. (1.93 ps)-ko simulazio urratsak eta TURBOMOLE programa erabiliz [?].

Orbital naturalen populazio aztertzeko orbital natural lotzailearen metodoa (ingelesez, NBO) erabili da [152, ?, ?].

9.3 Emaitzak

Atal honetan, selenioz osatutako lotura dinamiko kobalente homonuklear (Se-Se) eta heteronuklearretaz (Se-S) osatutako konposatu multzo bat konputazionalki aztertuak izan dira, eta ezagunak diren disulfuro (S-S) loturekin konparatuta, orain arte ezagunak diren dikalkogenuroetan oinarritutako material autokonpongarrien gaitasuna hobetzen dituzten material berriak aurkitzeko asmoarekin. Hortarako, lotura dinamiko hauen

disozioazio termikoa, fotodisoziazioa eta lotura hauek sortutako erreakzio langak ikertu egin dira, kimikoa kuantikoaren metodoetaz baliatuz. Erabilitako eredu kimikoak hiru lotura dinamiko ezberdinen (Se-Se, S-Se eta S-S) eta hauek inguratzen duten egitura kimiko ezberdinen (PD-XX (difenil), PA-XX (difenil amino) and PF-XX (eraztun gabekoa, ingelesez, PF, "phenyl-free")) arteko konbinazioan oinarritzen dira. Gainera, zazpi talde funtzional ezberdin ere (R_1 - R_7) erabili dira, guztira 63 sistema molekular ezberdin osatuz (ikus 9.2 irudia).

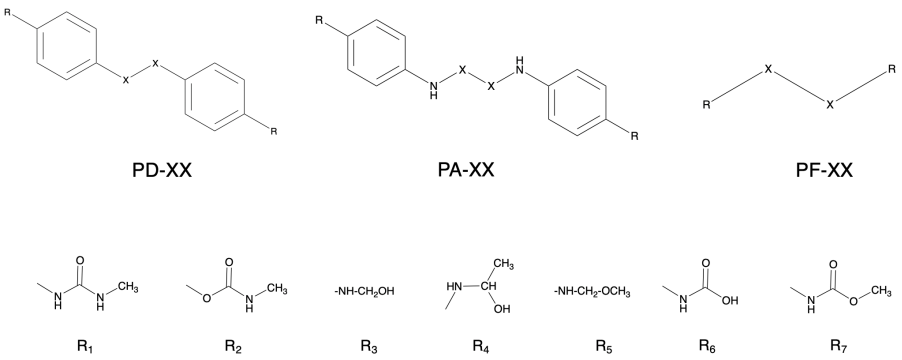

Figure 9.2: Atal honetan erabilitako ereduak, non X = S, Se. *Para* posizioan kokatutako ordezkatzaileak: urea (R_1), uretanoa (R_2), alkohol primarioa (R_3), alkohol sekundarioa (R_4), eterra (R_5), azidoa (R_6) eta esterra (R_7).

Emaitzei dagokien ordena honakoa da: i) sulfenil eta/edo selenil erradikalen eraketa aztertuko da, dikalkogeno loturaren BDE erabiliz, eta prozesu honetan hidrogeno loturek daukaten eragina ere aztertuta izanen da; ii) lotura berdinaren fotodisoziazio prozesua eta iii) elkartrukatze erreakzioaren erreakzio langa, zeinek erreakzio konstantearen estimazio bat eman dezakeen.

9.3.1 Disoziazio Termikoa

Atal honetan erabilitako ereduen disoziazioa analizatuko da, haien BDE-an oinarrituz, zeinak elkartrukatze prozesuan ematen den entalpia aldaketa bezala kalkulatu daitekeen (ikus 9.1 ekuazioa).

Table 9.1: X-X loturen disoziazio energia (BDE) eta bi dikalkogenuro unitate ezberdinen arteko hidrogeno loturei dagokien elkarrekintza energia (RX-XR), ΔH^{HB}, kcal/mol-etan ωB97XD/6-311++G(2df,2p)//ωB97XD/6-31+G(d,p) teoria mailan kalkulatuta. ρ QMD bidez lortutako X-X loturek sulfenil eta selenil erradikalak sortzeko probabilitatea da.

		S-S			Se-Se			Se-S		
Model	R	BDE	ΔH^{HB}	ρ	BDE	ΔH^{HB}	ρ	BDE	ΔH^{HB}	ρ
PD-XX	R_1	48.55	30.40	0.0051	47.78	24.92	0.0122	44.03	32.21	0.0058
	R_2	51.99	33.64	0.0010	49.90	26.08	0.0040	47.05	17.45	0.0007
	R_3	45.36	23.46	0.0209	41.73	16.74	0.0081	41.12	31.38	0.0261
	R_4	37.66	37.35	0.0310	43.01	12.27	0.0094	40.79	32.76	0.0103
	R_5	47.86	18.38	0.0101	41.75	16.64	0.0041	41.41	18.42	0.0062
	R_6	45.27	32.73	0.0222	46.18	17.76	0.0009	44.18	23.52	0.0020
	R_7	41.57	33.91	0.0045	43.37	21.55	0.0000	43.53	20.31	0.0173
PA-XX	R_1	34.08	40.84	0.2382	34.97	40.98	0.1291	32.71	46.73	0.1101
	R_2	36.08	26.94	0.0890	39.13	25.39	0.0338	39.30	27.18	0.0832
	R_3	32.24	33.33	0.1682	32.08	35.85	0.0503	43.24	13.82	0.1049
	R_4	33.56	33.98	0.1269	32.23	29.90	0.0644	39.12	16.19	0.0348
	R_5	32.10	28.24	0.1322	31.65	29.12	0.0900	43.61	5.44	0.0767
	R_6	36.83	27.05	0.0818	39.77	5.22	0.0515	42.00	4.01	0.0649
	R_7	31.80	30.47	0.0929	39.20	6.86	0.0190	43.38	—	—
PF-XX	R_1	47.65	19.18	0.0682	43.97	15.60	0.0025	48.66	13.09	0.0376
	R_2	55.56	32.24	0.0000	49.25	24.98	0.0000	57.25	21.11	0.0000
	R_3	41.13	23.59	0.0736	40.03	13.50	0.0408	45.08	4.94	0.0159
	R_4	40.85	25.67	0.0360	40.28	9.12	0.0229	43.18	0.87	0.0209
	R_5	35.32	9.43	0.0152	36.04	8.87	0.0150	39.42	3.91	0.0204
	R_6	48.69	17.80	0.0000	42.99	7.37	0.0000	46.83	37.25	0.0021
	R_7	47.66	7.14	0.0000	40.90	17.15	0.0010	45.45	12.67	0.0010

$$RX - XR \xrightarrow[heat]{h\nu} 2RX^{\cdot} \tag{9.1}$$

Dinamika molekular kuantikoak (ingelesez, Quantum molecular dynamics, QMD) burutu dira erabilitako ereduek erradikalak sortzeko duten probabilitatea (ρ) estimatzeko, hurrengo parametroa erabiliz (Ek. 9.2):

$$\rho = \frac{N_{X-X}}{N_{tot}} \tag{9.2}$$

zeinek burututako simulazioetan, X-X lotura distantzia muga jakin baten gainetik dauden simulazio urrats kopurua (N_{X-X}), non X-X lotura disoziatuta dagoela kontsidera daitekeen, kontuan hartzen dituen, eta balio hori simulazio urrats kopuru totalaz zatitzen, N_{tot}, duenak. Muga horren determinazioa trantsitzio egoeren azterketaren ondorioz finkatzen da, eta 2.30, 2.56 eta 2.45 Å-tan kokatzen da S-S, Se-Se eta S-Se loturentzat, hurrenez hurren.

Datuak aztertuz, 9.1 taulan ikus daiteke lotura dinamikoaren aldaketak eragin txikia duela BDE-n, bizkarrezurra (dikalkogenuro loturaren inguruan dagoen egitura kimikoa) ordea garrantzi handiko faktorea dela kontsidera daiteke. BDE-n aldaketa hauek bi faktore nagusiekin lotuta daude [69]: elektroi desparekatuaren delokalizazioa eraztun aromatikoan eta elektroi dentsitatearen igoera σ^* orbital antilotzailean (ikus S1 taula). ρ_X-en balio txikiagoek erradikalaren egonkortasun handiagoa adierazten dute, hortaz, BDE txikiagoak.

Era berean, elektroi dentsitate handiagoek σ^* orbital antilotzailean lotura ordena txikiagoak produziten dituzte, hortaz, BDE txikiagoak. Bi efektu hauek aditiboak dira PA-XX deribatuetan, eta BDE-n ikusten den jaitsieraren arrazoia dira. Bestalde, PD-XX eta PF-XX-n efektu bakoitzak besteak konpensatzen du, antzeko BDE-ak lortuz konposatu mota hauentzako.

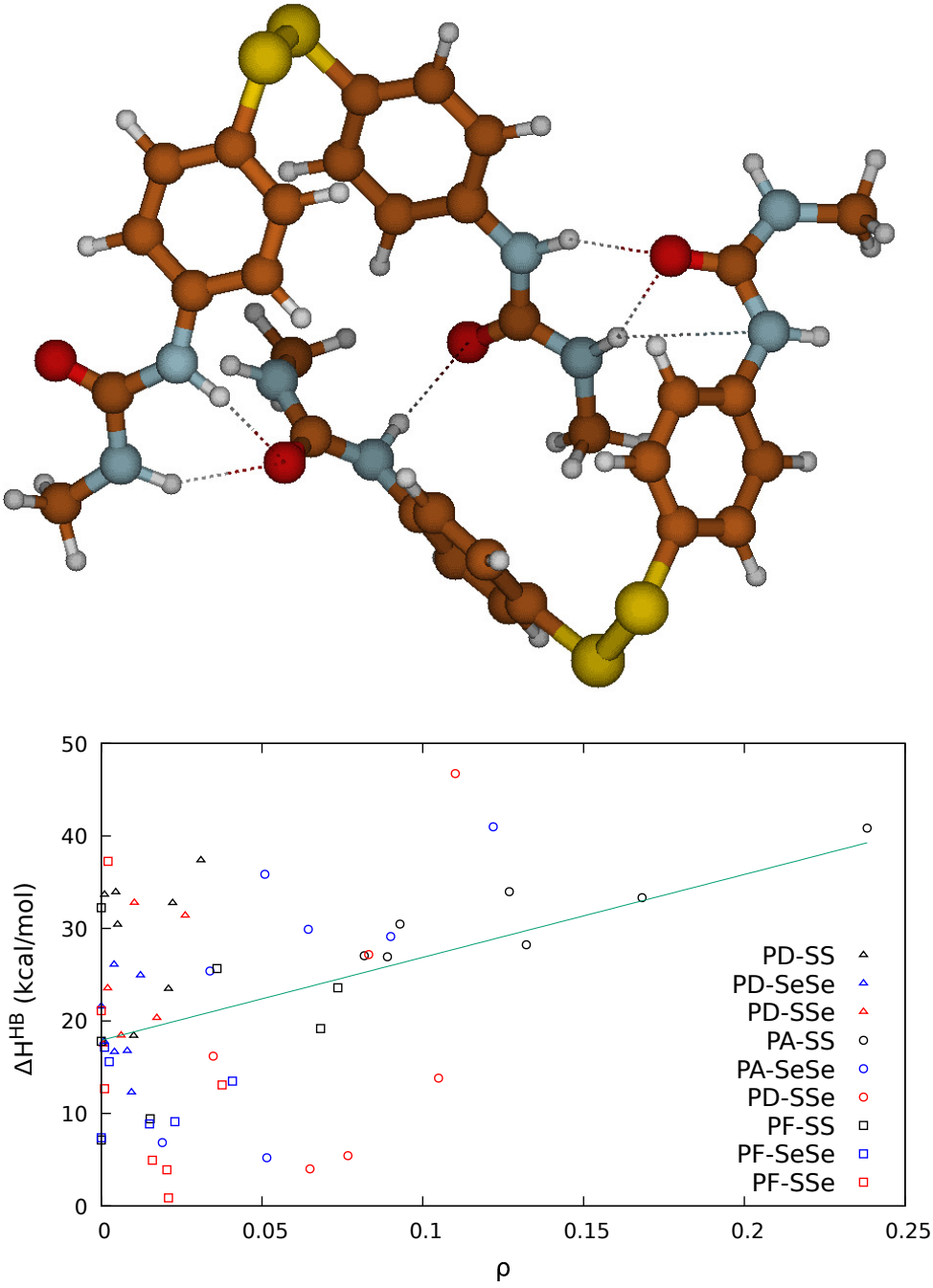

Figure 9.3: Ezkerrean: Bi dikalkogenuro unitateen arteko elkarrekintza neurtzeko erabilitako eredua. Eskuinean: Bi dikalkogenuro unitateen arteko elkarrekintza energia (ΔH^{HB}, kcal/mol-etan), ωB97XD/6-311++G(2df,2p)//ωB97XD/6-31+G(d,p) teoria mailan kalkulatua vs erradikalak sortzeko probabilitatea (ρ), PBE/def-SV(P) teoria mailan kalkulatuta.

9.3.2 Hidrogeno Loturen Eragina BDE-n

X-X loturaren disoziazioan hidrogeno loturek (ingelesez, hydrogen bonding, HB) daukaten eragina bi dikalkogenuro unitateen arteko elkarrekintza energiaren (ΔH^{HB}) bidez aztertuko da (ikus 9.3 irudia, ezkerrean). Datuak 9.1 taulan jaso dira, eta 9.3 irudian, eskuinean, ΔH^{HB} erradikalak generatzeko probabilitatearen (ρ) aurka irudikatu da.

Emaitzek elkarrekintza intermolekular handiek erradikalak sortzeko probabilitatea handitzen dutela dirudi. elkarrekintza intermolekular handiak direla eta X-X loturak luzapen handiagoak jazan ditzakeela diote, baina, argiago ikusteko, eredu hauen distribuzio funtzio erradialak (ingelesez, radial distribution function, rdf) irudikatu dira 9.4 irudian.

Ikus daitekeen moduan, hidrogeno loturen ausentziak (9.4 irudia, goian ezkerrean) X-X loturen distribuzio antzekoak sortzen ditu. Goian eskuinean ikus daiteke nola hidrogeno loturen presentziak dimeroan X-X loturaren distribuzioa eskuinera desplazatzen duen, lotura distantzia handiagotara, hain zuzen ere. Behean ezkerrean, urea eta uretanoren arteko ezberdintasuna ikusi daiteke, biek daukaten gaitasuna hidrogeno loturak eratzeko ezberdina da, eta ikus daitekeenez ureak HB-ak eratzeko gaitasuna handiagoa daukanez, X-X lotura distantzien distribuzioa eskuinera desplazatu egiten du ere. Azkenik, behean eskuinean, PA eta PD-ren arteko diferentzia ikus daiteke, non PA-k, HB-ak eratu daitekeen amino talde extra bat daukanez, X-X loturen distribuzioa ere eskuinerantz desplazatzen duen.

9.3.3 Fotodisoziazioa

Fotodisoziazio prozesua $S_0 \rightarrow S_1$ trantsizio bertikalaren absortzio uhinluzera (λ) eta dagokion osziladorearen indarra (f) erabiliz karakterizatu egin da (ikus **??** taula, non aipatutako parametroak jasota dauden, hala nola dagokien trantsizioen natura, eredu molekular bakoitzerako). Eredu guztietan, eszitatutako elektroiak σ^*antilotzaile orbitalean kokatzen da, egoera eszitatuaren BDE-a nabarmenki gutxitzen duelarik, hortaz, disoziazioa gauzatuz [131].

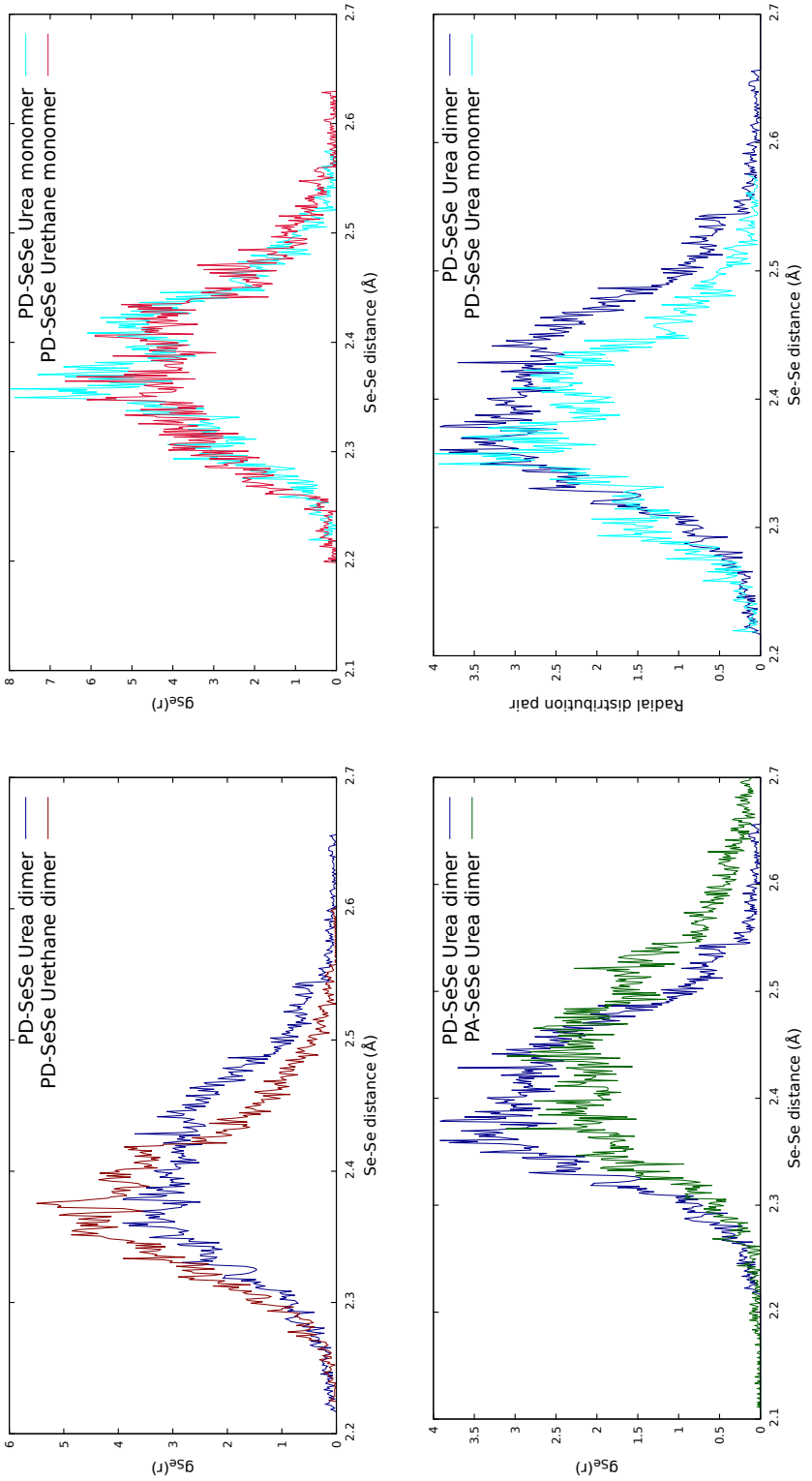

Figure 9.4: Hainbat X-X loturaren distribuzio funtzio erradialak, QMD-ren bidez kalkulatutak. Goian ezkerrean, bi monomero (HB-rik ez). Goian eskuinean, monomero bat eta dimero bat. Behean ezkerrean, urea eta uretanoa. Behean eskuinean, PD eta PA.

Ikus daitekeenez, bizkarrezurrak garrantzi nabaria dauka absortzio uhin-luzeran. PF-XX deribatuek X-X loturari dagozkion $\sigma \rightarrow \sigma^*$ transitzioak aurkezten dute, eta, ondorioz, λ baxuenak, 300 nm-tik behera, hau da, espektro elektromagnetikoaren eremu ultramorean.

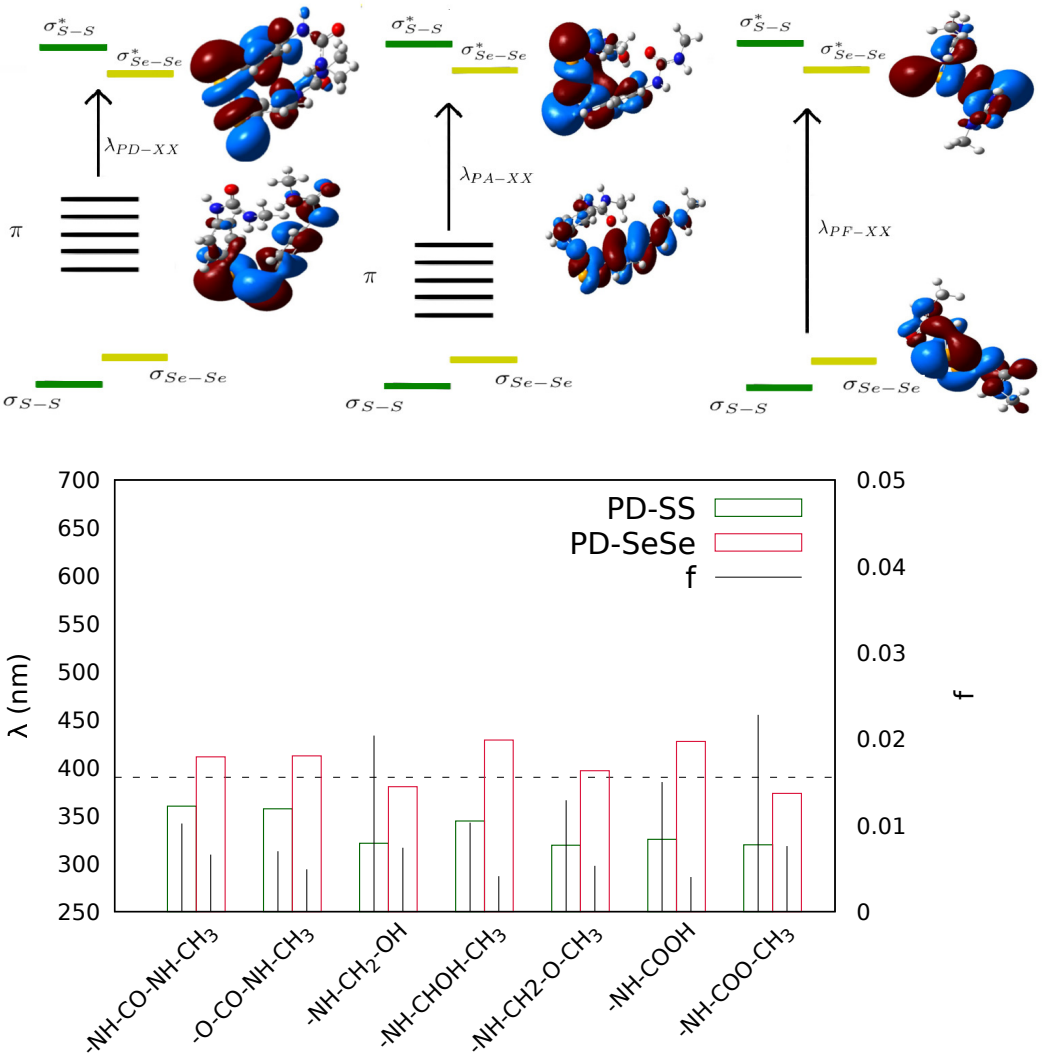

Figure 9.5: Goian: Exzitazio prozesuan parte hartzen duten orbital molekularren eredu eskematikoa. Behean: PD-SS eta PD-SeSe deribatiuen absortzio uhin-luzera, λ, nm-tan eta dagokien osziladorearen indarrarren, f, irudikapen grafikoa. Biak ωB97XD/6-311++G(2df,2p)//ωB97XD/6-31+G(d,p) teoria mailan kalkulatutak.

Bestalde, fenilo taldeen inklusioak trantsizio energiak txikitu egiten ditu, eraztunen π orbital molekularren inklusioa dela eta. Transtizio hauek orain $\pi \rightarrow \sigma^*$ izaera dute (ikus 9.5 irudia, goian). PA-XX deribatuek PD-XX de-

ribatuek baino absortzio uhin-luzera txikiagoak aurkezten dituzte, zeren eta eraztun aromatikoen π orbital molekularrak egonkorragoak diren, amino taldearekin jazaten duten konjugazio estragatik.

Sufrea selenioz ordezkatuz gero, aldaketa nabariak ere ikus daitezke absortzio uhin-luzeran. Aldaketa hau X-X lotura osatzen duten sufre eta selenioren orbitalen arteko diferentziari dagokio. Oreka distantzian, sufrearen $3p$ orbitalek gainezartze eraginkorragoa sortzen dute selenioren $4p$ orbitalek baino; izan ere, azken hauek izaera difusoagoa daukate. Honek selenioaren σ_{Se-Se} orbital molekularretik σ^*_{Se-Se} orbital molekular antilotzailerako eszitazio energia txikitu egiten du (ikus 9.5 irudia, behean).

Bi faktore hauen konbinazioak PD-SeSe deribatu batzuek espektro elektromagnetikoaren eremu ikusgarrian absorbatzea eragiten du, haien λ 390 nm baino handiagoa delarik. Honek esan nahi du, teorikoki, autokonponketa prozesua argi ikusgarriarekin aktibatu daitekeela eta emaitza teoriko hauek bat datozela Otsukak et. al. lortutako emaitza esperimentalekin [**?**].

9.3.4 Erreakzio Mekanismoa

[2+1] erradikal bidezko mekanismoan trantsizio egoeraren (ikus 9.6 irudia, ezkerrean) karakterizazio aproposa ezinbestekoa da erreakzio langak, ΔG, aztertzeko [65, 69, 70], eta, ondorioz, erreakzio konstanteak, k, estimatu ahal izateko, Wigner, Eyring, Polanyi eta Evans-en Trantsizio Egoeraren Teorian oinarrituz: [145, 80]

$$k = \frac{k_B T}{h} e^{-\Delta G/RT} \tag{9.3}$$

Lotura dinamikoen izaera kontuan hartuz, lotura homonuklearren hausturak eta berrantolaketak lotura homonuklearrak ere sortuko dituzte (k_S, disulfuroentzat, k_{Se} diseleniuroentzat). Bestalde, lotura heteronuklear bat apurtuz gero, haren berrantolaketak lotura homonuklearrak edo heteronuklearrak sor ditzake, sortutako sulfenil edo selenil erradikalek zein lotura

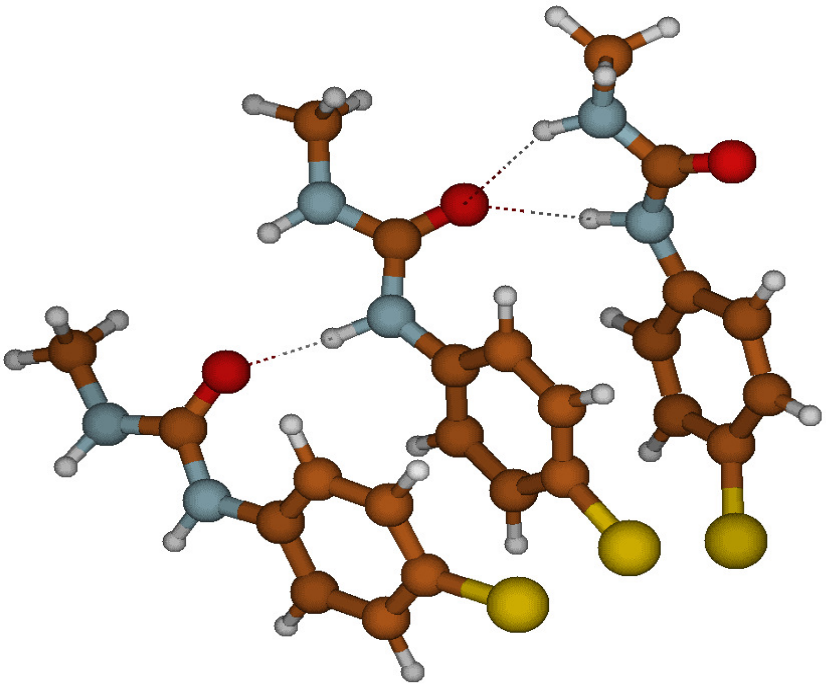

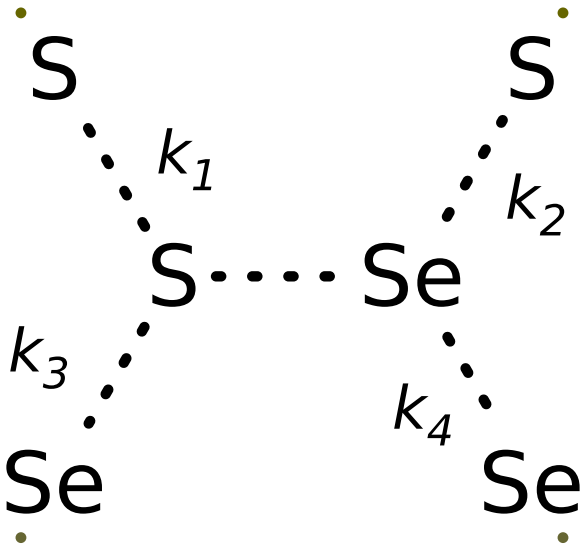

Figure 9.6: Ezkerrean: Trantsizio egoeraren eredu molekularra, ωB97XD/6-311++G(2df,2p)//ωB97XD/6-31+G(d,p) teoria mailan kalkulatua. Eskuinean: Lotura heteronuklear baten apurketak gauzatu ditzakeen erreakzio posible guztien eredu eskematikoa.

mota erasotzen duten baitan (ikus 9.6 irudia, eskuinean). Honela, horrelako produktuak sor daitezke: i) disulfuro lotura bat, sulfenil erradikalak sulfuro atomo bat erasotuz gero (k_1); ii) diseleniuro lotura bat, selenil erradikalak selenio atomo bat erasotuz gero (k_4); eta iii) sufre-selenio lotura bat, sulfenil erradikalak selenio atomo bat erasotuz gero (k_2) edo selenil erradikalak sufre atomo bat erasotzean (k_3).

9.7 irudian, ezkerrean, eman daitezkeen erreakzio posible guztien bataz besteko ΔG-ren balioak (PD-XX, PA-XX eta PF-XX ordezkatzaile guztiekin konbinaturik) jasota daude. Bizkarrezur ezberdineei dagokienez, erreakzio langa txikienak aurkezten duten deribatuak PD-XX-ak (gorriz) dira, 8 eta 14 kcal/mol bitarteko balioak aurkeztuz, PA-XX and PF-XX deribatuen batazbesteko ΔG balioak, ordea, 14 kcal/mol baino handiagoak dira. Datu hauek trantsizio egoeren geometria aztertuz arrazionalizatu daitezke.

PD-XX deribatuek sortutako trantsitzio egoeretan, ez-deuseztagarria den eraztun aromatikoen arteko $\pi-\pi$ elkarrekintza existitzen da, zeinek ez duen soilik trantsitzio egoera bera egonkortu, baizik eta kalkogenuro atomoen arteko elkartrukatze erreakzioa gauzatzeko geometria aproposa mantzen duen ere. Amino talde estraren inklusioak PA-XX deribatuetan geometria hori apur bat distortsionatu egiten du, eraztun aromatikoen arteko $\pi - \pi$ elkarrekintza erginkorra trabatzen. Bestalde, PF-XX deribatuek eraztun aromatikoek ematen duten egonkortasun horren eza aurkezten dute, hauek ez baitute eraztun aromatikorik haien baitan, eta, ondorioz, erreakzio langek gora egiten dute.

Lotura dinamikoari dagokionez, selenil erradikal baten erasoak diseleniuro lotura bati (k_{Se}), bataz-beste, sulfenil erradikalaren erasoak disulfuro lotura bati (k_S) baino erreakzio langa txikiagoak ematen ditu. Honen arrazoia selenioaren $4p$ orbitalek sulfuroaren $3p$ orbitalek baino gainezartze espazial eraginkorragoa sortarazten dutelako da.

9.7 irudian, eskuinean, lotura dinamiko homonuklear batez osatutako PD-XX deribatuen erreakzio langak (k_S eta k_{Se}) irudikatzen dira. Selenioz osatutako loturek produzitzen duten erreakzio langen jaitsiera nabarmenki ikusten da, denek 10 kcal/mol baino gutxiagoko balioak aurkezten baitituzte. Gainera, erreakzio langak deribatuekiko aldatu ere egiten dira, de-

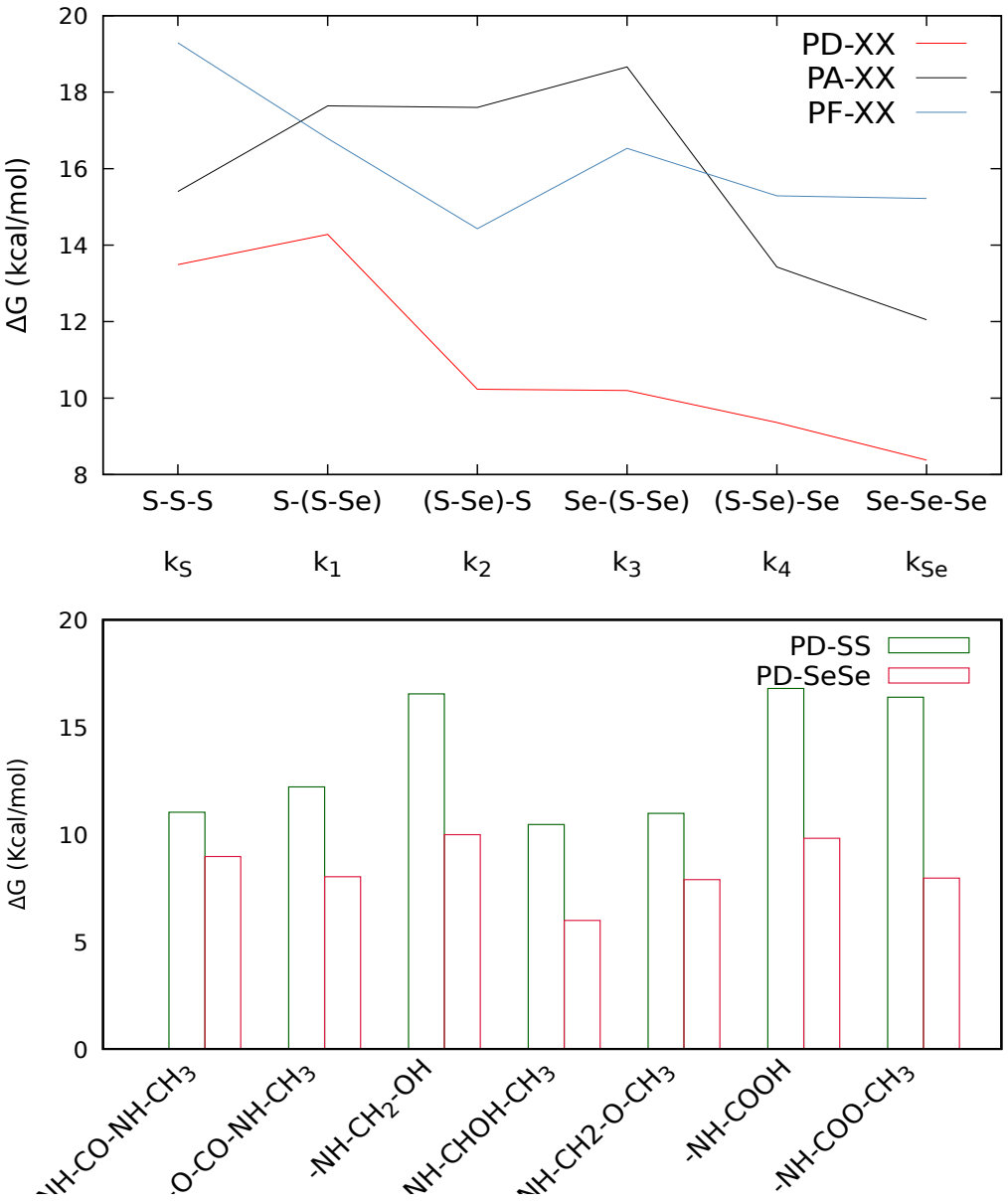

Figure 9.7: Ezkerrean: Bataz-besteko erreakzio langak, kcal/mol-etan, PD-XX (linea gorria), PA-XX (linea beltza) eta PF-XX (linea urdina) deribatuentzat. Eskuinean: PD-SS eta PD-SeSe deribatuen erreakzio langak, kcal/mol-etan, ωB97XD/6-311++G(2df,2p)//ωB97XD/6-31+G(d,p) teoria mailan kalkulatutak.

ribatu ezberdinek erreakzio langak handitu egiten duten hidrogeno loturak osatzeko gaitasuna, hots, transtizio egoera egonkortzeko gaitasuna, ezberdina baitute. Beraz, PD-SeSe deribatuek, oro har, errakzio langa txikienak ematen dituzte.

Table 9.2: Trantsizio egoerei dagozkien Gibbs-en energia askea (ΔG^{TS}), kcal/mol-etan, eta errakzio konstanteak (k), in s^{-1}, ωB97XD/6-311++G(2df,2p)//ωB97XD/6-31+G(d,p) level teoria mailan kalkulatuak.

		S-S		Se-Se		S-(S-Se)		Se-(S-Se)		(S-Se)-S		(S-Se)-Se	
Model	R	ΔG^{TS}	k	ΔG^{TS}	k	ΔG^{TS}	k	ΔG^{TS}	k	ΔG^{TS}	k	ΔG^{TS}	k
PD-XX	R_1	11.03	$4.97{\cdot}10^{4}$	8.97	$1.62{\cdot}10^{6}$	-	-	8.06	$7.51{\cdot}10^{6}$	5.78	$3.59{\cdot}10^{8}$	-	-
	R_2	12.21	$6.78{\cdot}10^{3}$	8.03	$7.95{\cdot}10^{6}$	-	-	10.45	$1.33{\cdot}10^{5}$	7.96	$8.90{\cdot}10^{6}$	7.75	$1.27{\cdot}10^{7}$
	R_3	16.55	$0.46{\cdot}10^{1}$	9.99	$2.90{\cdot}10^{5}$	18.25	$2.52{\cdot}10^{-1}$	8.14	$6.54{\cdot}10^{6}$	10.72	$8.42{\cdot}10^{4}$	8.20	$5.92{\cdot}10^{6}$
	R_4	10.46	$1.32{\cdot}10^{5}$	5.99	$2.52{\cdot}10^{8}$	13.32	$2.56{\cdot}10^{5}$	9.94	$3.13{\cdot}10^{5}$	14.95	$6.63{\cdot}10^{1}$	12.14	$7.68{\cdot}10^{3}$
	R_5	10.98	$5.40{\cdot}10^{4}$	7.89	$1.01{\cdot}10^{7}$	12.77	$2.66{\cdot}10^{3}$	12.93	$2.00{\cdot}10^{3}$	7.52	$1.87{\cdot}10^{7}$	8.05	$7.63{\cdot}10^{6}$
	R_6	16.80	$0.29{\cdot}10^{1}$	9.82	$3.86{\cdot}10^{5}$	13.69	$5.60{\cdot}10^{2}$	11.65	$1.76{\cdot}10^{4}$	12.58	$3.66{\cdot}10^{3}$	8.82	$2.09{\cdot}10^{6}$
	R_7	16.39	$0.58{\cdot}10^{1}$	7.96	$8.98{\cdot}10^{6}$	13.36	$9.67{\cdot}10^{3}$	10.21	$2.00{\cdot}10^{5}$	12.12	$7.87{\cdot}10^{3}$	9.60	$5.62{\cdot}10^{5}$
PA-XX	R_1	18.26	$2.46{\cdot}10^{-1}$	11.53	$2.15{\cdot}10^{4}$	15.56	$2.39{\cdot}10^{1}$	25.16	$2.12{\cdot}10^{-6}$	26.95	$1.04{\cdot}10^{-7}$	11.57	$2.00{\cdot}10^{6}$
	R_2	16.01	$1.12{\cdot}10^{1}$	11.27	$3.33{\cdot}10^{4}$	14.54	$1.32{\cdot}10^{2}$	25.53	$1.14{\cdot}10^{-6}$	24.41	$7.57{\cdot}10^{-6}$	11.46	$2.42{\cdot}10^{6}$
	R_3	7.87	$1.04{\cdot}10^{7}$	13.36	$9.82{\cdot}10^{2}$	17.30	$0.13{\cdot}10^{1}$	18.76	$1.06{\cdot}10^{-1}$	16.35	$0.63{\cdot}10^{1}$	15.68	$1.94{\cdot}10^{1}$
	R_4	15.30	$3.68{\cdot}10^{1}$	10.33	$1.63{\cdot}10^{5}$	17.46	$9.56{\cdot}10^{-1}$	16.38	$0.59{\cdot}10^{1}$	12.04	$9.07{\cdot}10^{3}$	12.01	$9.52{\cdot}10^{3}$
	R_5	15.85	$1.46{\cdot}10^{1}$	13.20	$1.29{\cdot}10^{3}$	18.42	$1.88{\cdot}10^{-1}$	9.94	$3.13{\cdot}10^{5}$	14.95	$6.63{\cdot}10^{1}$	12.14	$7.68{\cdot}10^{3}$
	R_6	17.02	$0.20{\cdot}10^{1}$	13.73	$5.22{\cdot}10^{2}$	18.40	$1.95{\cdot}10^{-1}$	14.38	$1.75{\cdot}10^{2}$	14.35	$1.82{\cdot}10^{2}$	12.53	$3.95{\cdot}10^{3}$
	R_7	17.47	$9.42{\cdot}10^{-1}$	10.93	$5.91{\cdot}10^{4}$	16.60	$0.41{\cdot}10^{1}$	15.16	$4.68{\cdot}10^{1}$	14.17	$2.47{\cdot}10^{2}$	14.77	$8.92{\cdot}10^{1}$
PF-XX	R_1	18.49	$1.66{\cdot}10^{-1}$	19.57	$2.70{\cdot}10^{-2}$	16.88	$0.25{\cdot}10^{1}$	15.95	$1.22{\cdot}10^{1}$	15.33	$3.48{\cdot}10^{1}$	9.88	$3.50{\cdot}10^{5}$
	R_2	17.47	$9.42{\cdot}10^{-1}$	18.49	$1.67{\cdot}10^{-1}$	14.07	$2.93{\cdot}10^{3}$	16.30	$0.68{\cdot}10^{1}$	17.40	$0.11{\cdot}10^{1}$	15.78	$1.63{\cdot}10^{1}$
	R_3	21.99	$4.56{\cdot}10^{-4}$	12.12	$5.18{\cdot}10^{1}$	15.03	$5.78{\cdot}10^{1}$	15.88	$1.38{\cdot}10^{1}$	12.42	$4.76{\cdot}10^{3}$	16.24	$0.75{\cdot}10^{1}$
	R_4	20.77	$3.52{\cdot}10^{-3}$	11.72	$1.56{\cdot}10^{4}$	17.46	$9.62{\cdot}10^{-1}$	13.16	$1.37{\cdot}10^{3}$	13.87	$4.09{\cdot}10^{2}$	12.04	$9.04{\cdot}10^{3}$
	R_5	21.90	$5.24{\cdot}10^{-4}$	-	-	13.82	$4.46{\cdot}10^{2}$	13.34	$1.01{\cdot}10^{3}$	13.32	$1.04{\cdot}10^{3}$	14.97	$6.45{\cdot}10^{1}$
	R_6	19.51	$2.97{\cdot}10^{-2}$	14.19	$2.40{\cdot}10^{2}$	21.06	$2.16{\cdot}10^{-3}$	21.76	$6.71{\cdot}10^{-4}$	12.09	$8.29{\cdot}10^{3}$	16.37	$0.61{\cdot}10^{1}$
	R_7	14.88	$7.54{\cdot}10^{1}$	-	-	16.59	$0.41{\cdot}10^{1}$	19.29	$4.30{\cdot}10^{-2}$	16.59	$0.41{\cdot}10^{1}$	16.81	$0.29{\cdot}10^{1}$

Chapter 10

Dinamika Molekularren Bidezko Dikalkogenuroetan Oinarritutako Material Autokonpongarri Eraginkorren Azterketa Teorikoa

10.1 Sarrera

Aurreko lanetan, [69, 131, 146], disulfuro eta diseleniuro aromatiko zein alifatikoetan oinarritutako material autokonpongarriak aztertuak izan dira, kimika kuantikoaren bidez lortutako parametroak erabiliz, zehazki, erradikalak sortzeko probabilitatea eta erreakzio langak. Soilik Formoso et. al.-en lanean [72] kate polimerikoen mugikortasunaren (ω) eragina autokonponketa prozesuan hainbat disulfuro aromatikoetan oinarritutako urea eta uretanoetan aztertua izan zen dinamika molekularrak erabiliz.

Lan horretan ikusi zen hidrogeno loturak zirela kateen mugimenduan garrantzi handiagoa daukan faktorea, eta bai hidrogeno lotura kopuru handiak zein txikiak kaltegarriak zirela autokonpontze prozesurako, zeren eta disulfuroen mugikortasun ezak, hala nola, haien gehiengo mugimenduak erreakzio eremuan aurkitzen diren disulfuro unitate kopurua mugatzen duten (ω balio txikiagoak). Hortaz, tarteko hidrogeno lotura kopuruak aurkezten zituzten ereduak ziren ω balio optimoak aurkezten zituztenak.

Hortaz, autokonpontze prozesuaren ikuspegi orokor bat izateko, atal honetan ω-ren kalkulua burutuko da aurrez aztertutako eredu sortan, non ρ eta k parametroak jadanik kalkulatutak dauden [69, 131, 146]. Zehazki, difenil dikalkogenuroak (PD-XX), difenildiamino-dikalkogenuroak (PA-XX) eta fenilorik gabeko (ingelesez, phenyl-free, PF-XX) deribatuak erabili dira (ikus 10.1 irudia, non X=S,Se den). Ereduak osatzeko para posizioan bost ordezkatzaile erabili dira, hainbat kate polimeriko ezberdin simulatzeko nahian. Horrela, ereduen nomenklatura orokorra horrelakoa izanen da: R_n-YY-XX, non n=1-5, YY= PA, PD, PF eta XX = S-S, Se-Se.

Eredu ezberdinak eraiki dira lehen aipatutako oinarrien konbinazioaz baliatuz, eta eredu hauek aurretik eraikitako ereduekin [72] konparatuko dira, ahalik eta sistema errealak hobekien islatzen dituzten eredu molekularrak eraikitzeko asmoz. Era honetan, egitura molekularrak elkarrekintza ez-kobalenteetan, hots, kateen mugikortasunean eta ondorioz, autokonpontze prozesuan daukan eragina aztertu nahi da. Azkenean, autokonpontze gaitasun teorikoaren ikuspegi orokor bat emango da, orain dinamika molekularren bidez lortzen diren datuak (ω) eta lehenago lortutakoak (ρ eta k) konbinatuz.

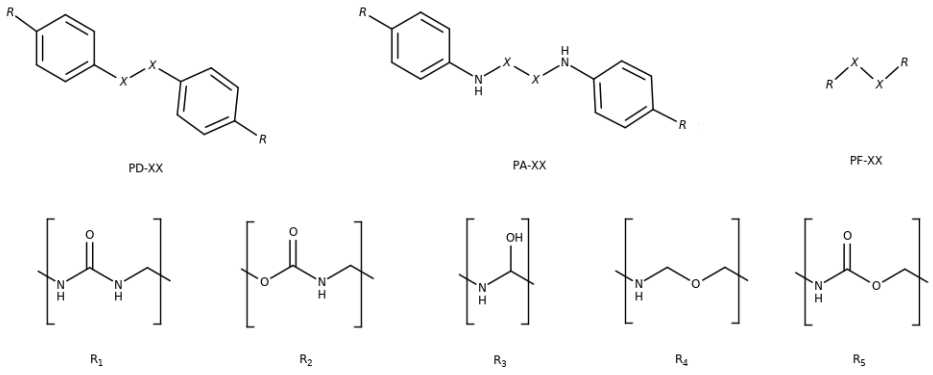

Figure 10.1: Aztertutako eredu molekularrak non X = S, Se. Goian: erabilitako hiru bizkarezurrak, difenil (PD), difenil-amino (PA) eta "phenyl free" (PF). Behean: erabilitako bost ordezkatzaileak, urea (R_1), uretanoa (R_2), alkohol sekundarioa (R_3), eterra (R_4) eta esterra (R_5).

10.2 Protokolo Konputazionalaren Balidazioa

Formoso et. al.-en lanean [72], dinamika molekularrak burutu egin ziren, baina dinamika horiek muga jakin batzuk zeuzkaten, adibidez, eredu molekular berak eta simulazio denbora. Jakinda lan horretan kate polimeriko luzeen arteko elkarrekintzak neurtu zirela eredu motzak erabiliz, muga hauek neurketen zehaztasuna muga dezaketela kontsidera daiteke. Lan honetan, muga horiek aztertuko dira, errealitatean aurkitzen diren sistemak era zehatzago batean irudikatu nahiean, hortaz, hainbat simulazio parametro ebaluatuak izan dira haien eragina ikustearren kateen arteko elkarrekintza ez-kobalenteetan. Zehazki, hurrengo parametroak aztertu dira: (i) hasierako ustezko egitura molekularra, (ii) kate polimerikoen luzeera, (iii) simulazio kaxaren tamaina eta (iv) simulazio denbora. Analisi hau R_1-PD-SS eta R_2-PD-SS deribatuak erabiliz burutu da.

Balidazioarako, hidrogeno lotura kopurua erabiliko da, eta hauek daukaten eragina aurrez aipatutako ω parametroan, zein dikalkogenuro unitateen arteko distantzian oinarrituta dagoen, eta horrela definituta dago:

$$\omega = \frac{I_i}{I_i + I_{ii}} \tag{10.1}$$

Distribuzio funtzio erradiala erabiliz ω kalkulatzeko hiru eremu ezberdin definitu daitezke: erreakzio eremua (I_i), non dikalkogenuroek erreakzioa gauzatzeko sobera hurbil dauden (R $\leq$ 4.5 Å), aldameneko eremua (I_{ii}), non dikalkogenuroek erreakzionatzeko urrun dauden, baina erreakzio eremuan sartzeko probabilitate ez-mesprezagarria daukaten (4.5 $<$ R$<$ 20 Å), eta kanpo eremua (I_{iii}), hemen dauden dikalkogenuroak ω kalkulutik kanpo uzten dira haien urruntasunagatik. Eremu bakoitzean kokatutako dikalkogenuroen kopurua finkatutako mugetan, distribuzio funtzio erradialaren integrazioz kalkulatu egiten da. Eremu hauen mugak sistemaren menpekoak izan litezke, ondoren ikusiko den moduan.

10.2.1 Metodologia Espezifikoa

Dinamika molekularrak ff14SB [147] amber indar-eremua erabiliz burutu dira, AMBER 14 programa erabiliz [148]. Difenil diseleniuro loturari dagozkion parametroak Torsello et. al. [149] garatutakoak izan dira. Egitura guztiak Ambertools-en LEaP modulua erabiliz eraiki dira, eta kargak RESP metodologia erabiliz [150]. Lehenik eta behin ESP kalkulatzen da Gaussian [135] erabiliz 6-31G* oinarri funtzioak eta Hartree-Fock teoria maila erabiliz eta ondoren RESP kargak. Simulazio guztiak NVT bidezko minimizatuak izan dira, beroketa prozesu batetaz jarraituak, eta NPT bidez ekilibratuak. Hidrogenoa barne daukaten lotura kobalenteak SHAKE algoritmoa erabiliz mugatuak izan dira.

10.2.2 Hasierako Ustezko Egitura eta Kateen Luzera

Aurreko laneko ereduak eraikitzeko, Formosok et. al. bi difenil disulfuro monomeroz (D_1 eta D_2 unitateak, 10.2 irudian, goian) eta kate polimeriko batez (C_1 unitatea irudi berdinean) osatutako kate bakarretik abiatu zen. Kate hau espazioan erreplikatzen zen hiru dimentsioko egitura osatuz. Horretarako, lau erreplika kokatu ziren bi norabide espazialetan translazio bektoreak erabiliz. Lortutako hasierako konformazioa, ekilibratu baino lehen, 10.2 irudian ikus daiteke (behean ezkerrean). Nabaritzen da translazio bektoreen erabilerak egitura periodiko laminar baten antzeko konformazio batera eramaten duela, egitura edo konformazio jakin bat hobetsiz, eta hori sahiesteko, lan honetan ustezko egitura sortzeko era aleatorioa (ikus 10.2 irudia, behean eskuinean) proposatu da, polimeroen egitura ez-hain-ordenatua erreplikatu nahian. Gainera, kate polimerikoa luzatu egin da, difenil dikalkogenuro unitateen artean -(CH_2)- talde adizional bat txertatuz.

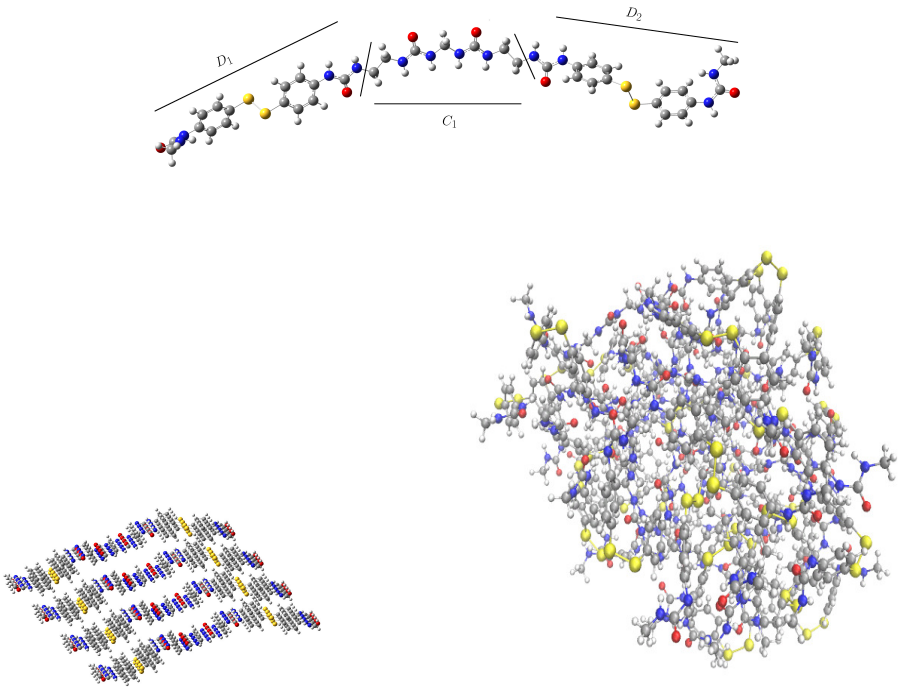

Figure 10.2: Goian: Balidazioan erabilitako eredu molekularraren kate bakarra, urea ordezkatzaile gisa duten bi difenil disulfuro unitatez osaturikoa (D_1 eta D_2 unitateak) poliurea kate polimeriko batetaz elkarturikoak (C_1 unitatea). Behean: Ekilibratu baino lehenagoko hasierako ustezko egitura periodikoa (ezkerrean) eta aleatorioa, edo randoma, (eskuinean). Sufre atomoak horiz, nitrogenoak urdinez eta oxigenoak gorriz.

Burututako simulazioen emaitzak hasierako bi egiturekin (periodikoa eta random) eta bi kate polimeriko ezberdinekin (luzea, metilo talde estra barne daukana, eta motza, metilo talde estrarik gabekoa) 10.1 irudian bilduta daude, non hidrogeno lotura kopuru totala (HB_{tot}) hala nola maximoa (HB_{max}), minimoa (HB_{min}) eta bataz-bestekoa (HB_{ave}) simulazio urrats jakin batean azaltzen diren, ω-rekin batera. Gainera, bi simulazio denbora ezberdin kontsideratu dira (10 eta 30 ns).

Kate motzarako hasierako ustezko egiturak kontsideratuz, hidrogeno lotura kopuru totala antzekoa dela kasu bietan ikus daiteke (ikus 10.1 taula eta 10.3 irudia, goian, non hidrogeno lotura kupuruaren ehuneko normalizatua ageri den), hala ere, haien distribuzioa ezberdina da. Egitura periodikoan hidrogeno loturak batez ere kate ezberdinen osagai berdinen tartean eratzen dira (D_1-D_1, D_2-D_2 eta C_1-C_1), eta honek hasierako egituraren mantenzea hobestuko du ekilibrazioaren orduan eta, ondorioz, simulazio osoan zehar.

Bestalde, random egituran unitate bakoitzak sobera hurbil dauden inguruko edozein beste unitateekin eratu ditzake hidrogeno loturak. Distribuzio hau aurrekoa baino errealistagoa dela kontsidera daiteke, eta polimeroetan eman ohi den egituraren antza gehiago dauka egitura periodikoak baino.

Egitura periodikoak, D_1-D_1 eta D_2-D_2 unitateen arteko elkarrekintzak hobestean, ω-ren balio maximizatzen du, hidrogeno loturek ez baitituzte disulfuro loturak bata bestetik aldentzen, bestalde egitura honek D_1-D_2 arteko disulfuroen arteko elkarrekintzak mugatu egiten ditu. Random egiturak, ordea, ez du ziurtatzen D_i-D_i unitateen arteko elkarrekintzarik egongo denik, haien distribuzioa espazioan orain hain finkatuta ez dagoelako. Distribuzio honek, ordea, D_i-D_j unitateen arteko elkarrekintza probabilitatea handitzen du. Azkenean, random distribuzioa distribuzio periodikoaren eszenario idealetik urruntzen da, eszenario errealago batera hurbilduz, eta honek, ω parametroaren jaitsiera dakar (ikus 10.1 taula).

Table 10.1: Hidrogeno lotura kopuru totala (HB_{tot}) hala nola maximoa (HB_{max}), minimoa (HB_{min}) eta bataz-bestekoa (HB_{ave}) simulazio urrats jakin batean, eta ω hasierako ustezko egitura periodikoa eta random egiturarako kalkulatua, metil talde estrarekin eta hura gabe (kate luzeak eta kate motzak, hurrenez hurren), 10 eta 30 ns-tzat .

Chain	Guess	HB_{tot}	HB_{max}	HB_{ave}	HB_{min}	ω
				10 ns		
Short	Periodic	746461	176	149	121	0.0884
	Random	730119	172	146	118	0.0696
Long	Periodic	707860	169	142	115	0.0931
	Random	595587	147	119	91	0.0393
		30 ns				
Short	Periodic	2215568	178	148	117	0.0776
	Random	2233776	184	149	117	0.0627
Long	Periodic	2184978	179	146	116	0.0970
	Random	1917000	157	128	100	0.0188

Kate luzea kontsideratuz gero (estra -(CH_2)- talde batekin), ezberdintasun nabariak ikusten dira egitura periodikoaren eta random egituraren artean hidrogeno loturei dagokienez. Kasu bietan, hidrogeno lotura kopuru totalaren jaitsiera ikusten da, baina random kasuan jaitsiera hau bereziki nabaritzen da (730119-tik 595587-ra, 10 ns ondoren). Kate luzeago batek hidrogeno loturek, bai intermolekularrak bai intramolekularrak, eratu dezaketen taldeen arteko

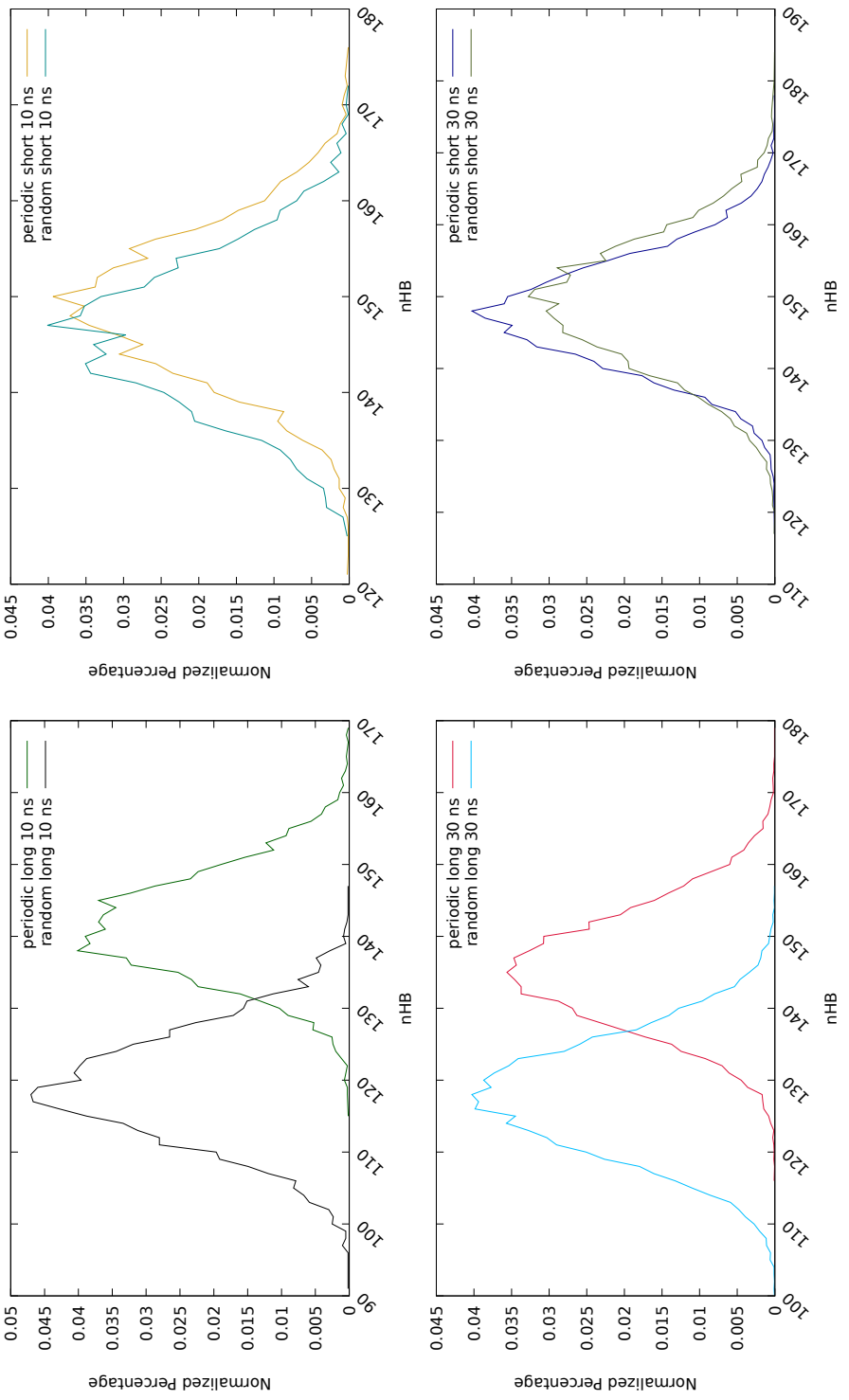

Figure 10.3: Hidrogeno lotura kupuruaren ehuneko normalizatua egitura periodikoa eta random egiturentzako kate luzeak erabiliz (goian) eta motzak (behean) 10 ns (ezkerrean) eta 30 ns-ko simulazio ondoren (eskuinean) lortutakoak.

banaketa handiagoa suposatzen du, taldeen arteko elkarrekintza probabilitatea gutxituz, eta, ondorioz, hidrogeno lotura kopuru totala (HB_{tot}) hala nola maximoa (HB_{max}), minimoa (HB_{min}) eta bataz-bestekoa (HB_{ave}) jaitsi egiten dira.

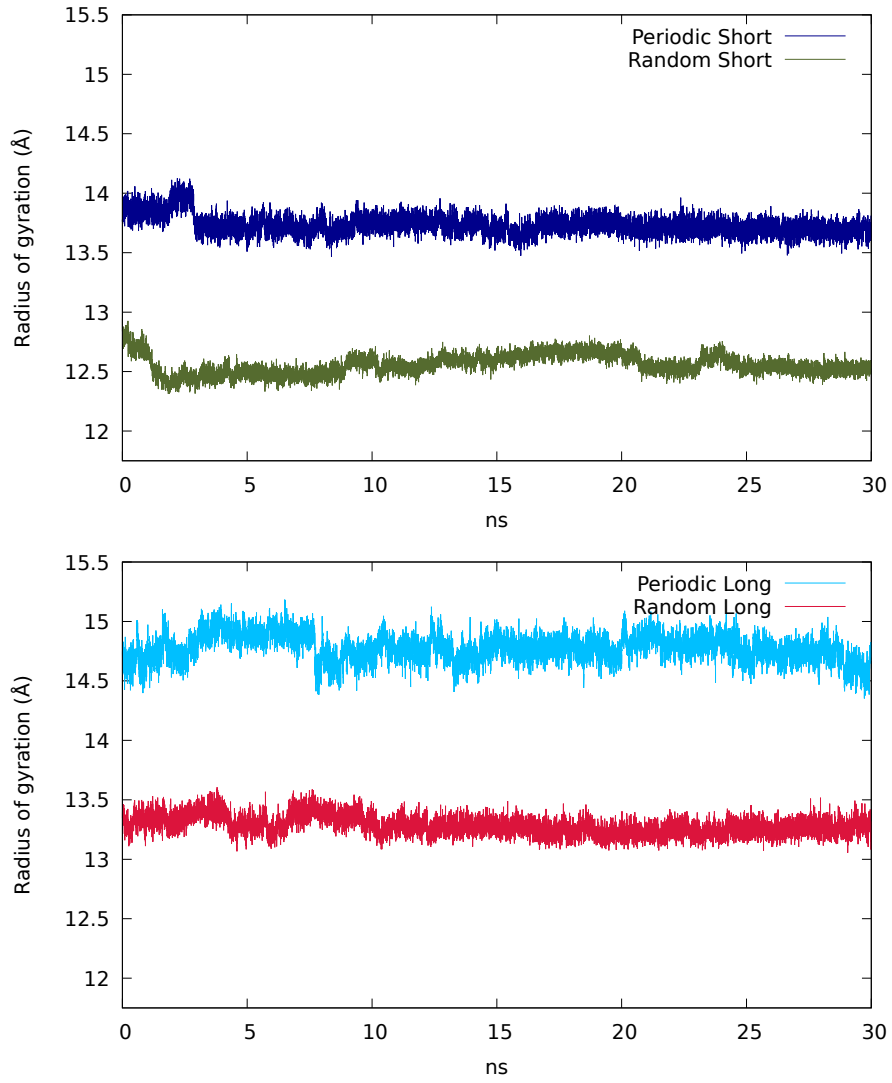

Figure 10.4: Egitura periodikoa eta random egituren biraketa erradioa (Å-etan) kate motzak erabiliz (goian) eta kate luzeak erabiliz (behean) 10 ns eta 30 ns-ko simulazio ondoren lortutakoak..

Egitura periodikoan, ordea, jaitsiera hau ez da hainbeste nabaritzen, zeren eta nahiz eta katea luzatu, egitura laminarra mantentzen den, eta honen ondorioz, D_i-D_i eta C_1-C_1 unitateen arteko elkarrekintzak ematen jarraitzen dira. Ikusitako jaitsiera (746461-tik 707860-ra, 10 ns ondoren) metil talde

estraren inklusioak kateen geometrian sortutako aldaketari dagokio. Egitura periodikoren eta randon egituraren arteko diferentziak argi ikusten dira 10.3 irudian, non hidrogeno lotura kupuruaren ehuneko normalizatua 10 ns ondoren (ezkerrean) eta 30 ns ondoren (eskuinean) ikus daitezkeen.

Kate motzen biraketa erradioa (ingelesez, radius of gyration) konparatuz gero (10.4 irudia, goian), egitura periodikoan 14 Å-etik gertu oszilatu egiten du, random egituran, berriz, 12.5 Å-etan oszilatzen duen bitartean. Honek egitura periodikoa ekilibrazio prozesua eta gero mantentzen dela adierazten du. Guzti hau kontuan izanda, egitura periodikoa material hauen simulazio teorikoak egiteko desaproposa dela ondoriozta dezakegu, zeren eta egitura laminarrak eta periodikotasunaren mantentzea hobesten duen, polimero errealetan ez bezala.

10.2.3 Simulazio Kaxaren Tamaina

Dinamika molekularrak burutzean garrantzia handia daukan beste parametro bat simulazio kaxaren tamaina da, sistemaren dentsitatea determinatzen baitu simulazioan zehar. Aurreko simulazioetan [72], 40×30×30 nm-ko prisma karratua erabili zen kaxa gisa, eta orain, bi tamaina ezberdinetako (40×40×40 eta 50×50×50 nm) kaxa kubikoekin alderatua izan da. Emaitzak 10.2 taulan eta 10.5 irudian ikus daitezke, non sufre atomoen distribuzio funtzio erradialak ikus daitezkeen. Hidrogeno loturen kopurua aldaketa askorik jasaten ez duen bitartean, distribuzio funtzio radialek aldaketa nabariak aurkezten dituzte, ω-ren balioan eragin handia izanez.

Table 10.2: Hidrogeno lotura kopuru totala (HB_{tot}) hala nola maximoa (HB_{max}), minimoa (HB_{min}) eta bataz-bestekoa (HB_{ave}) simulazio urrats jakin batean, eta ω, random egitura erabiliz 30 ns-ko simulazioetan lortuta simulazio kaxa ezberdinentzako.

Box	HB_{tot}	HB_{max}	HB_{ave}	HB_{min}	ω
40×30×30	1917000	157	128	100	0.0188
40×40×40	1900841	158	127	95	0.0490
50×50×50	1902463	160	127	97	0.1058

Ondorioz, aipatutako guztia kontuan hartuz, random egitura erabiltzea erabaki da, kate polimeriko luzearekin, kaxa kubikoetan eta 30 ns-ko simulazioak burutuz, denbora luzeagoak simulazioan zehar konformazio gehiago aztertzea baimentzen duelako.

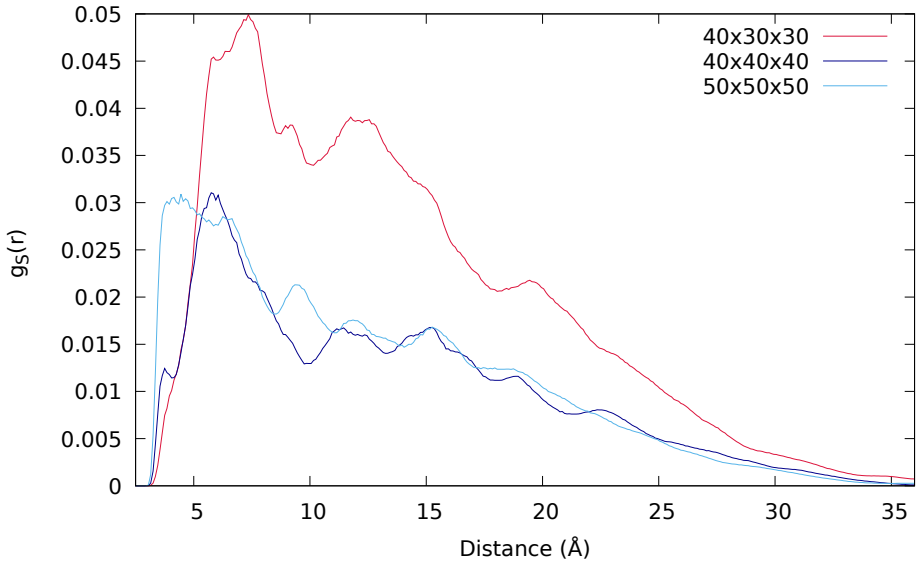

Figure 10.5: PD-urea deribatuaren distribuzio funtzio erradialak -(CH_2)- talde estra barne, 10 eta 30 ns-ko simulazioetan lortutak, 40×30×30, 40×40×40 eta 50×50×50 nm-ko simulazio kaxak erabiliz.

10.3 Emaitzak

Behin simulazio baldintzak optimizatutak daudela, R_n-YY-XX eredu molekularrekin burututako simulazioen emaitzen aurkezpena eta analisia burutuko dira. Zehazki, bizkarrezurren YY (PD, PA, PF), ordezkatzaileen R_n(n = 1-5) eta dikalkogenuro loturaren XX (X = S, Se) eragina eztabaidatuko da: (i) kateen dimentsioan eta mugikortasunean, (ii) elkarrekintza ez kobalenteetan, hots, hidrogeno loturetan, eta (iii) sufre eta selenioaren distribuzio funtzio radialetan, nondik ω lortzen den. Azkenean, ikertutako material bakoitzaren autokonpontze gaitasun teorikoa eztabaidatuta izanen da.

10.3.1 Bizkarrezurraren Garrantzia: PD, PA eta PF

Bizkarezurraren garrantzia aztertzeko, urea (R_1) ordezkatzaile bezala daukaten PD-, PA- and PF-SS disulfuru deribatuak hautatu ziren. Emaitzak 10.3 taulan azaltzen dira. Ikus daiteke HB_{tot}-k antzeko balioak dituela PD

eta PF deribatuentzat, baina PA deribatuentzak bereziki handitzen da. Emaitza hauek amino talde estrak hidrogeno lotura kopuru handiago eratzeko daukan gaitasunari dagokio, 10.6 irudian, eskuinean, argi ikus daiteke, non hidrogeno loturen ehuneko normalizatua irudikatzen den.

Table 10.3: Hidrogeno lotura kopuru totala (HB_{tot}) hala nola maximoa (HB_{max}), minimoa (HB_{min}) eta bataz-bestekoa (HB_{ave}) simulazio urrats jakin batean, eta ω, ureaz ordezkatutako (R_1) disulfuroentzat hiru bizkarezurrak barne, izenez, PD, PA eta PF.

R	Backbone	HB_{tot}	HB_{max}	HB_{ave}	HB_{min}	ω
R_1	PD	1902463	160	127	97	0.1058
	PA	2620182	213	175	142	0.0419
	PF	1940357	161	129	102	0.1224

10.6 irudian, ezkerrean, sufre atomoen distribuzio funtzio erradialak aukeratutako hiru ereduentzat irudikatuta daude. Ikus daiteke PF deribatuak gailur altuagoak, hots, sufre populazio handiagoak, aurkezten dituela distantzia motzetan, eta beste bi deribatuekin konparatuz azkarrago egiten du behera. Deribatu honen egitura molekularra kontuan hartuz, eraztun aromatikoen ezak disulfuroen arteko kontaktua erraz dezakeela esan daiteke. Eraztun aromatikoen oztopo esterikoa argi ikus daiteke PD eta PA deribatuetan, non disulfuro populazio txikiagoak ikusten diren eraztun aromatikoak kokatuta dauden distantzietan (<10 Å). Gainera, PF eta PA deribatuetan, disulfuro lotura hidrogeno loturak eraiki dezakeen amino talde batera lotuta egonez gero, haien mugikortasuna txikitua ikusten da, beste disulfuroekin kontaktua oztopatuz.

ω-ren kasuan, lehen aipatu den bezala, hidrogeno loturak dira faktore garrantzitsuena. Jakina da [72] bai kupuru handiek bai kopuru txikiek kaltegarriak direla ω-ren balio optimoak lortzeko. Hortaz, PA deribatuek aurkezten duten igoerak hidrogeno lotura kopuruan PD eta PF-rekin aldenduz (ikus 10.3 taula), ω-ren balio txikietara eramaten du, kateen mugikortasun murriztua dela eta.

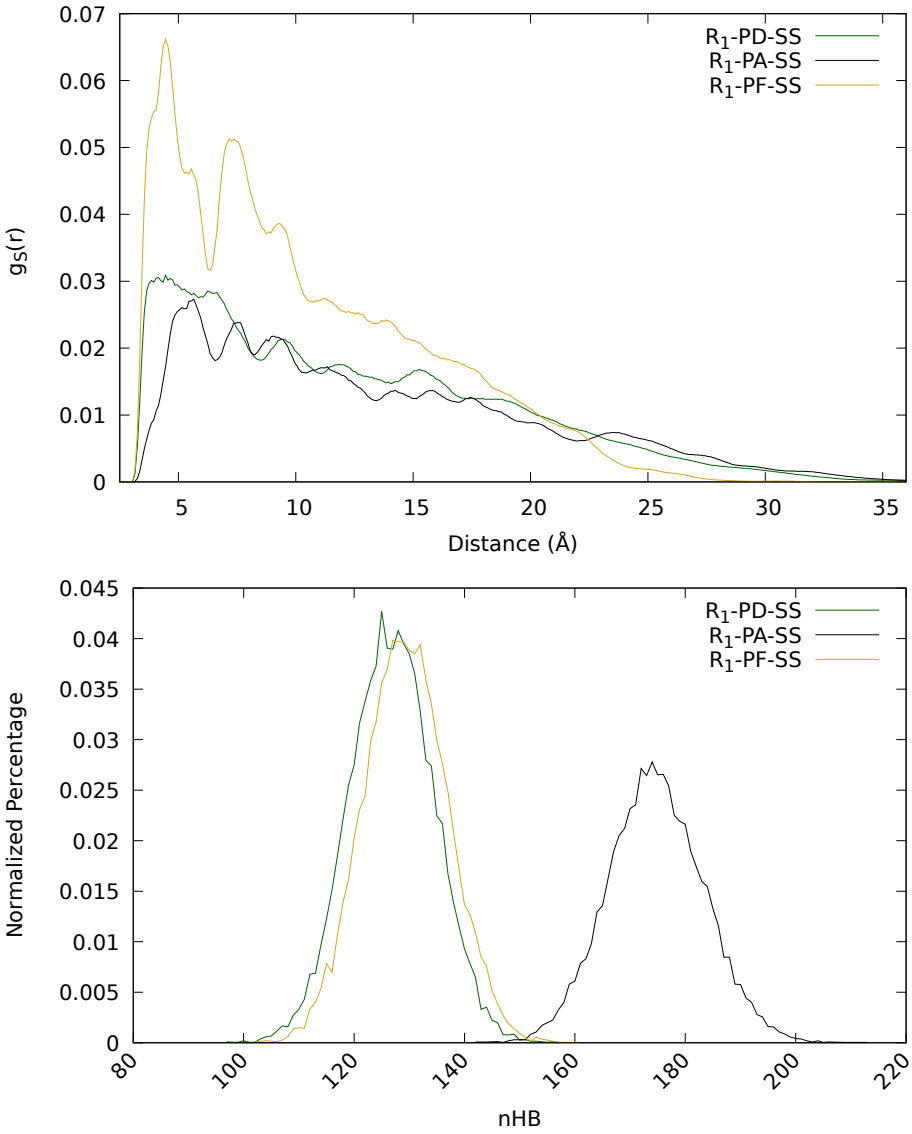

Figure 10.6: Radial distribution functions (top) and normalized percentage of hydrogen bonds (bottom) of the urea-substituted PD-, PA and PF-disulfide derivatives.

10.3.2 Ordezkatzaileen (R_1-R_5) eta Dikalkogenuro Loturaren Eragina

In this subsection, the effect of the chemical structure of the polymeric chain (R) and dichalcogenide bond (S-S vs Se-Se) are analyzed. Concretely, R_n-PD-XX systems have been chosen to carry out such analysis, being n=1-5 and XX=S-S; Se-Se. All the obtained data are collected in Table 10.4.

Table 10.4: Hidrogeno lotura kopuru totala (HB_{tot}) hala nola maximoa (HB_{max}), minimoa (HB_{min}) eta bataz-bestekoa (HB_{ave}) simulazio urrats jakin batean, eta ω, PD-SS eta PD-SeSe deribatuentzat, hurrengo talde funtzionalez osaturiko kateak erabiliz: urea (R_1), uretanoa (R_2), alkohol sekundarioa (R_3), eterra (R_4) eta esterra (R_5).

				S-S		
Backbone	R	HB_{tot}	HB_{max}	HB_{ave}	HB_{min}	ω
PD	R_1	1902463	160	127	97	0.1058
	R_2	1078729	100	72	50	0.0471
	R_3	-	-	-	-	-
	R_4	731072	76	49	26	0.0212
	R_5	927209	83	62	42	0.0348
		Se-Se				
PD	R_1	2233772	184	149	115	0.0418
	R_2	921219	87	61	37	0.0538
	R_3	1359569	119	91	64	0.0307
	R_4	592646	66	40	16	0.0332
	R_5	790616	74	53	34	0.0443

First, we focus on the influence of R_n by using the molecular model of Figure 10.2, where the D sections correspond to the PD-SS and the C_1 chain is built with different functional groups, namely, urea (R_1), urethane (R_2), secondary alcohol (R_3), ether (R_4) and ester (R_5). Similar systems were considered for studying the influence of diselenides.

Hasteko R_n-ren influentzia aztertuko da. Kateen arteko ezberdintasunak hidrogeno loturak eratzeko daukaten gaitasun ezberdinetatik datozte, X-X loturaren natura kontuan izan gabe. Hau argi ikus daiteke 10.7 irudian (goian, ezkerrean), non sistema bakoitzarentzat normalizatutako hidrogeno lotura kopourua irudikatzen den, ω-rekin batera (balio numerikoak 10.4 taulan ikus daitezke). Balio txikienak eter eta esterrez osatutako kateek (R_4 eta R_5, hurrenez hurren) azaltzen dituzte, ureaz osatutako kateak (R_1) balio altuenak azaltzen dituen bitartean, espero bezala. Jeitsiera honek ω-ren balioetan ere jaitsiera dakar, kate hauen gehiegizko mugikortasuna dela eta. Lehen esan bezala, hidrogeno louta kopuru txikiegiek autokonponketa prozesurako kaltegarriak dira, kateen gehiezko mugikortasunak disulfuroak bata bestearengandik urruntzea dakarrelako, eremu erreaktiboan, hots, I_i-n dagoen disulfuro populazioa murriztuz.

Bukatzeko, lotura dinamikoan sufre selenioz ordezkatzearen efektua neurtu da, zeren eta jakina da selenioak sufreak baino autokonponketa prozesu

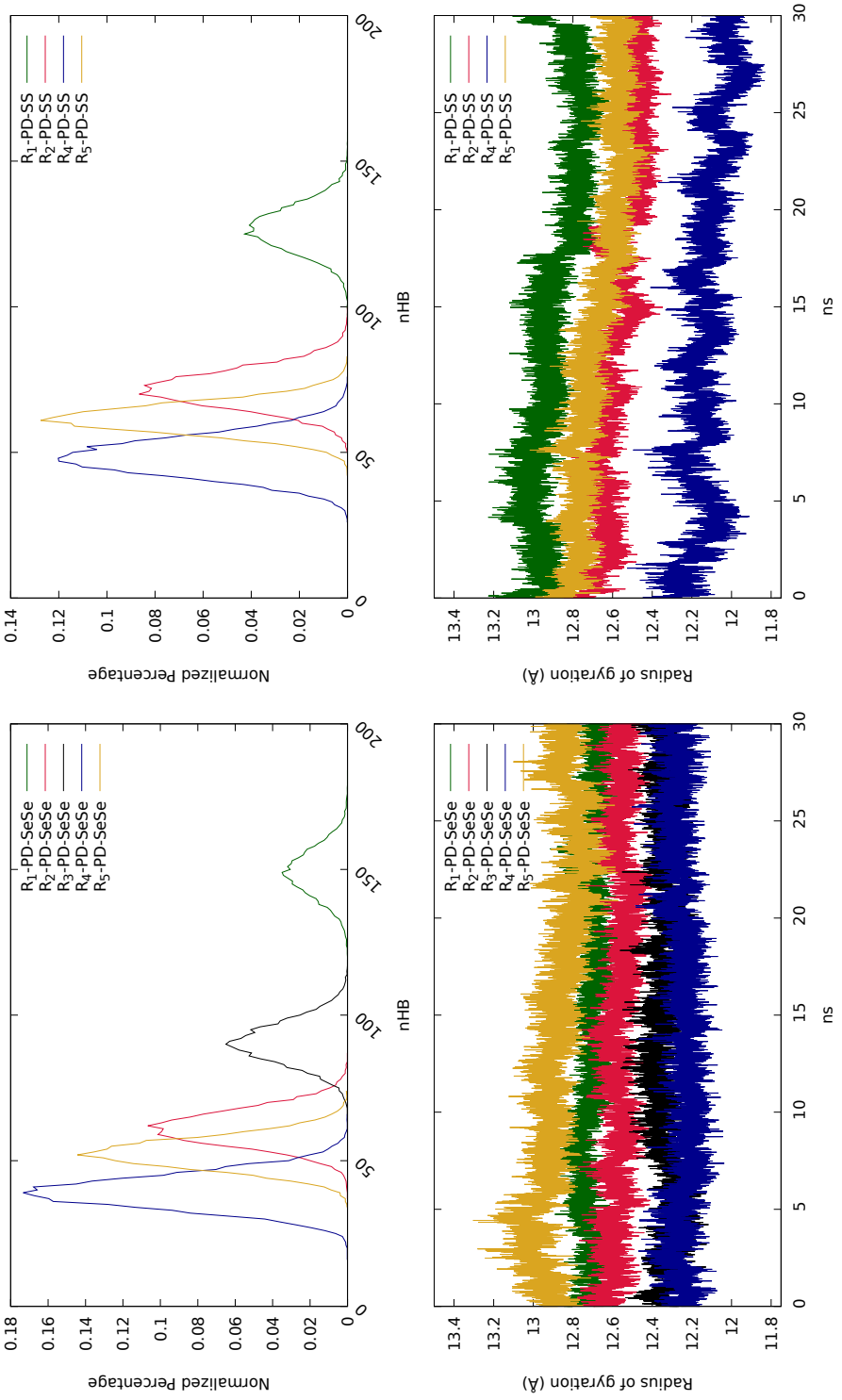

Figure 10.7: Normalizatutako hidrogeno lotura kopourua (ezkerrean) eta biraketa radioa (eskuinean), Å-etan, disulfuro (goian) eta diseleniuro (behean) deribatuentzat.

hobeagoa eman dezakeela [63, 64, 65, **?**, 146]. Printzipioz hidrogeno loturak eratzeko gaitasuna ez da lotura dinamikoaren menpeko ezaugarria, baina ikus daiteke diseleniuroek disulfuroek baina hidrogeno lotura gutxiago eratzen dituztela, beraz eragin ez-zuzena dagoela badirudi. Bestalde, biraketa erradioa aztertuz (10.7 irudia, eskuinean) ikus daiteke diseleniuroak bariazio txikiagoak azaltzen dituztela, beraz, disulfuroak baino izaera trinkoago bat daukatela esan daiteke, ziurrenik selenioaren masa sufrea baino handiagoa delako, haren mugikortasuna mugatuz.

Selenioz osatutako kateen mugikortasun txikiagoak hidrogeno lotura kopuruan eta ω-n ikusitako bariazioak azal ditzake. Hidrogeno lotura kopuru handiak dituzteen kateetan, urea adibidez (R_1), selenioren mugikortasun mugatuak sistema osoaren trinkotasuna handitu dezake, hidrogeno lotura kopurua mantentzen, hortaz HB_{max} (R_1-PD-SS) = 160, diseleniuroari dagokion balioa 184 den bitartean. Bestalde, loturak eratzeko gaitasun txikia daukaten kateetan selenioaren presentziak kateen mugikortasuna mugatuta ikus daiteke, hidrogeno loturak eratu dezaketeen taldeen hurbilpena eragozten.

10.3.3 Autokonpontze Gaitasun Teorikoa

Lehen aipatu den bezala, dikalogenuroetan oinarritutako polimero baten autokonpontze gaitasun teorikoa (maila mikroskopikoan) hiru parametroren bidez kalkula daiteke: erradikalak sortzeko probabilitatea (ρ) , truke-erreakzioaren erreakzio konstantea (k) eta kateen mugikortasuna (ω) [131]. Lehenengo bi parametroak aurreko atalean kalkulatuak izan dira [146]. 10.5 Taulan, balio guzti hauek bilduta daude.

Datuak aztertuz, ikus daiteke diselniuroek disulfuroek baino erreakzio langa baxuagoak aurkezten dituztela. Gainera, ω oro har handiagoa aurkezten dute ere. Hortaz, diselniuroen autokonpontze gaitasuna disulfuroena baino haundiagoa izatea espero daiteke. PD deribatuek trantsizio egoera egonkortzen dute, erreakzio langa txikiagoak emanez. Bestalde, PF deribatuek ω balio haundienak ematen dituzte, hain egitura kimikoa dela eta. Hala ere, PD deribatuekin alderatuz, diferentzia ez da nahikoa erreakzio lange-

Table 10.5: Erradikalak sortzeko propabilitatea (ρ), trantsizio egoeren Gibbs-en energia askea (ΔG^{TS}), kcal/mol-etan, erreakzio konstantea (k) T = 298.15 K-etan, s^{-1}-etan, erreakzionatzeko sobera hurbil dauden dikalkogenruen ratioa (ω) PD-SS eta PD-SeSe sistementzat talde funtzional desberdinekin, izenez, urea (R_1), uretanoa (R_2), alkohol sekundarioa (R_3), eterra (R_4) eta esterra (R_5).

		S-S				Se-Se			
Backbone	R	ρ	ΔG^{TS}	k	ω	ρ	ΔG^{TS}	k	ω
PD	R_1	0.0051	11.03	$4.97{\cdot}10^{4}$	0.1058	0.0122	8.97	$1.62{\cdot}10^{6}$	0.0418
	R_2	0.0010	12.21	$6.78{\cdot}10^{3}$	0.0471	0.0040	8.03	$7.95{\cdot}10^{6}$	0.0538
	R_3	0.0310	10.46	$1.32{\cdot}10^{5}$	—	0.0094	5.99	$2.52{\cdot}10^{8}$	0.0307
	R_4	0.0101	10.98	$5.40{\cdot}10^{4}$	0.0212	0.0041	7.89	$1.01{\cdot}10^{7}$	0.0332
	R_5	0.0045	16.39	$0.58{\cdot}10^{1}$	0.0348	0.0000	7.96	$8.98{\cdot\cdot}10^{6}$	0.0443
PA	R_1	0.2382	18.26	$2.46{\cdot}10^{-1}$	0.0419				
PF	R_1	0.0682	18.49	$1.66{\cdot}10^{-1}$	0.1224				

tan ikusten den diferentzia gainditzeko, hortaz PD deribatu aproposenak dirudite autokonpontze prozesu eraginkorrak izateko.

Hortaz, PD deribatuak sintetitazea diseleniuro loturekin, aztertutako sistema guztien artean dira autokonpontze eraginkorrena azaltzen dituztenak.

Chapter 11

Protokolo Teorikoaren Erabilera Disulfuroetan Oinarritutako Material Errealen Autokonpontze Gaitasuna Aztertzeko

11.1 Sarrera

Ezaguna da, poliuretanoen (PU) kasuan, elkarrekintza supramolekularrek haien propietate mekanikoetan garrantzi haundia daukatela, bai hidrogeno loturek eta bai segmentu gogorren paketatzeak ere [31, 51, 52, 53], beraz, bi elementu hauen eraginak optimizatuz gero, materialak haien etorkizuneko aplikaziorako propietate mekaniko aproposaz hornitu daitezke. Zentzu honetan Kim et. al.-ek [54] eta Takahashi et. al.-ek [55] disulfuroetan oinarritatutako bi material sorta diseinatu zituzten, crosslinker eta hardener ezberdinak erabiliz, haien autokonpontze gaitasuna aztertzeko tenperatura ezberdinetan.

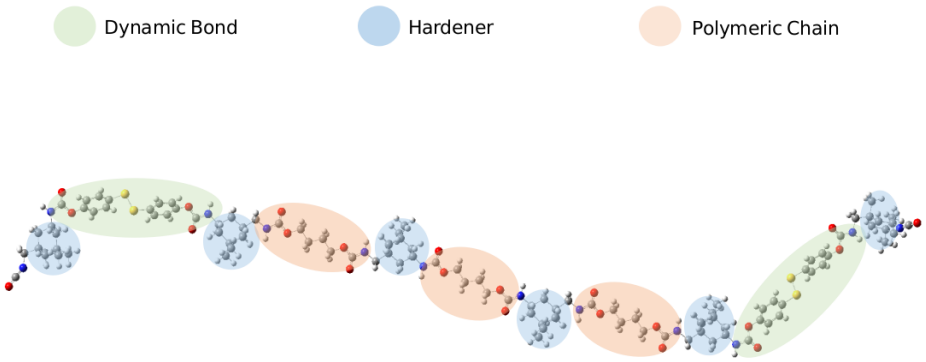

Figure 11.1: IP polimeroaren atal ezberdinen irudikapen grafikoa; berdez: lotura dinamikoa, gorriz: kate polimerikoa eta urdinez: "hardener"-ra.

Alde batetik, Kim et. al.-ek disulfuro aromatikoetan oinarritutako hiru PU sintetizatu zituzten, bakoitzak zurruntasun ezberdineko segmentu gogor (edo hardener, ikus 11.1 Irudia) ezberdin batekin, izenez; IP (egitura alizikliko asimetrikoa); 4,4´-metilenobis(ziklohexil isozianatoa), HM; (egitura alizikliko simetrikoa); 4,4´-metilenobis(fenil isozianatoa), eta M; (egitura aromatikoa). Haietako batek, IP-k zehazki, giro tenperaturan autokonpontzeko gaitasuna aurkezten zuen, hala nola, aurretik ezagunak ziren giro tenperaturako material autokonpongarrien propietate mekanikoak (sendotasuna, luzagarritasuna eta iraungarritasuna) hobetuz. Beste bi sistemek haien autokonpontze gaitasunak tenperaturaren igoerarekin hobetzen zituzten, giro tenperaturan autokonpontzerik aurkezten ez zuten bitartean.

Bestetik, Takahashi et. al.-ek polimetakrilato sareetan oinarritutako eta bi "crosslinker" ezberdinen arteko konbinazioaz eratutako materialak sintetizatu zituzten, batak disulfuro alifatikoz osatuta eta besteak sulfenaminaz (-N-S-S-N-), ADSA eta BTA izeneko egiturak lortuz, hurrenez hurren (ikus 11.2 Irudia), paketzearen eragina autokonpontze prozesuan aztertzeko nahian. Ikusi zuten BTA egiturak autonkonponketa aurkezten zuela bai giro tenperaturan bai tenperatura altueta, ADSA egiturak, berriz, ez zuen autonkoponketarik azaldu ez giro tenperaturan ez tenperatura altuetan, harderner berdina erabili izan arren.

Aurreko lan hauetan oinarrituta, atal honen helburu nagusia sistema errealen simulazioa izango da, zehazki, Kim et. al. eta Takahashi, et. al.

Kim et. al. [54]

IP

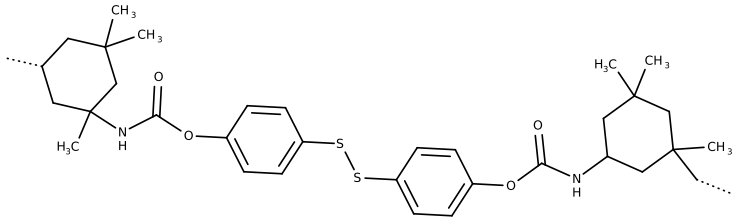

HM

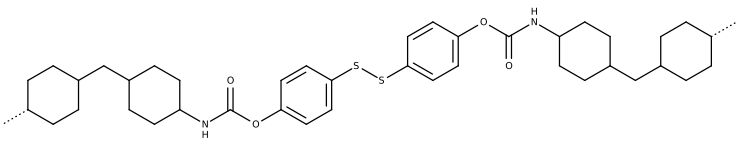

M

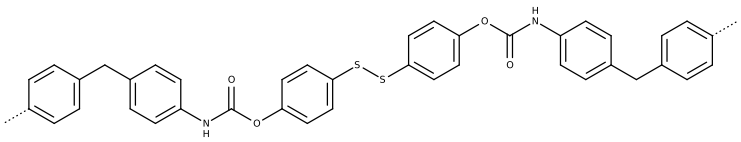

Takahashi et. al. [55]

BTA

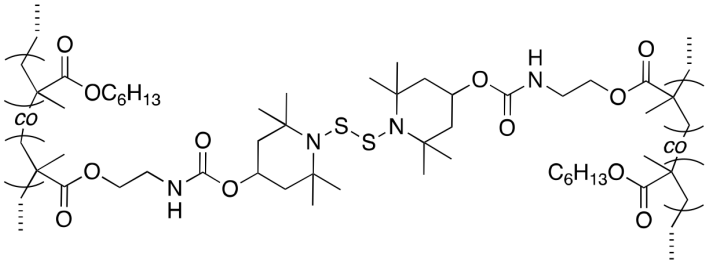

ADSA

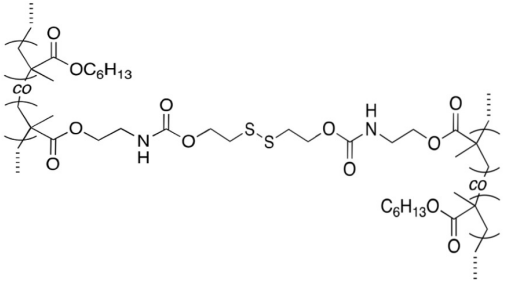

Figure 11.2: Erabilitako ereduen egitura molekularren errepresentazioa.

aztertutakoak. Horretarako, Formoso et. al.-ek [72] eta Irigoyen et. al.-ek [151] aldez aurretik garatutako protokolo teorikoa erabiliko da, protokoloa baliozkotzeko eta, beharrezkoa bada, eguneratzeko. Gainera, crosslinkerrek eta segmentu gogorrek duten eragina aztertuko da, behaketa esperimentala azalduko duten prozesu fisiko eta kimikoak eskaintzeko.

11.2 Ereduak

Tamaina ezberdineko eredu-egiturak erabili ziren simulazio kuantikoak eta dinamika molekularrak burutzeko. Simulazio kuantikoetan eredu txikiak erabili ziren, zeinek esperimentalki aztertutako disulfuro unitatea eta haren inguruko egitura kimikoa kontuan hartzen zituzten. Zehazki, kate bakarreko eta bi kateetako ereduak erabili ziren simulazio kuantikoetan. 11.3 Irudian, goian, IP sistemarentzak aipatutako eredu hauek ikus daitezke. 11.3 Irudian, behean, dinamika molekularrak burutzeko erabilitako kate eredua, prozedura espirimentala jarraituz eraikita dagoena [54] eta [55]. Simulazio kaxa eraikitzeko, horrelako 16 kate erabili ziren aurretik gure taldean ezartutako protokoloa jarraitauz [151], poliuretanoen eta polimetakrilatoen dentsitate esperimentala erreproduzituz.

11.3 Zehaztasun Konputazionalak

Geometria optimizazio guztiak gas fasean burutu dira, dentsitate funtzionalaren teoriaren (ingelesez, DFT) [94, 95] esparruan, helmen-luzeko ωB97XD funtzionalarekin [**?**] eta 6-31+G(d,p) oinarri funztioak erabiliz [**?**]. Bibrazio frekuentzia armonikoak gradienteen diferentziazio analitikoaz lortuak izan dira, lortutako egiturak minimoei edo trantsizio egoerei dagozkien ikusteko. Ondoren, frekuentziak zero-puntuko energia bibrazionala (ingelesez, ZPVE) ebaluatzeko erabili dira, hala nola entalpiren (H) eta Gibbs-en energia askearen (G) zuzenketak osziladore armonikoaren hurbilketan egiteko. Puntu bakarreko kalkuluak 6-311++G(2df,2p) oinarri funztioak [**?**] erabiliz burutu dira optimizitatuako egituretan, energia elektronikoa hobetzeko. Fotodisoziazio prozesua aztertzeko, denboraren menpeko dentsitate funtzionalaren

Small models for Quantum Simulations

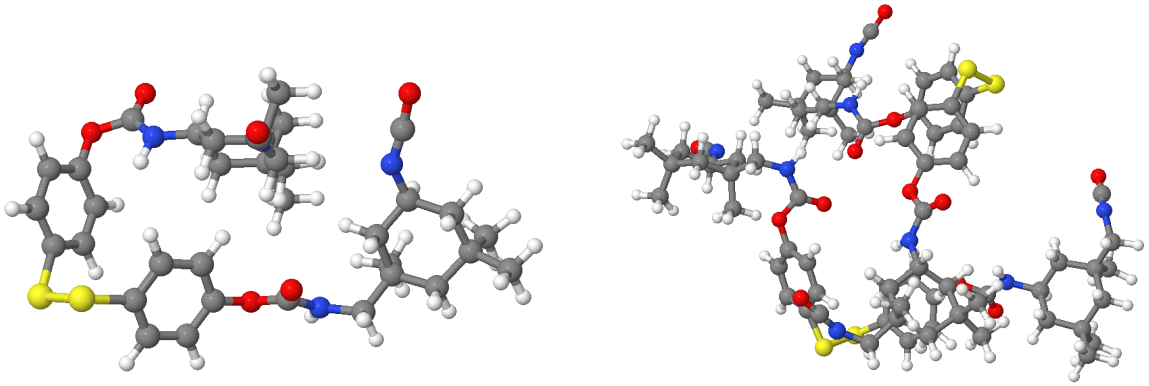

Monomer

Dimer

Large models for Molecular Dynamics

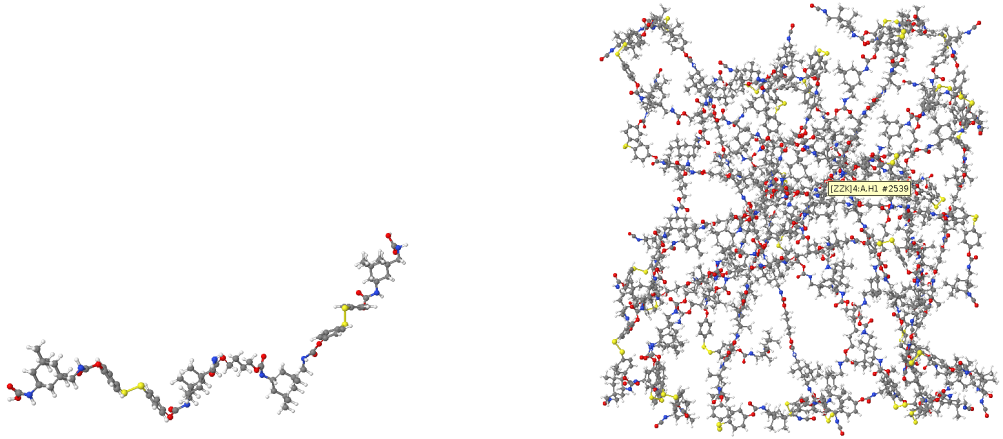

Figure 11.3: Goian: IP sistemarentzat kalkulu kuantikoetan erabilitako ereduak. Behean: IP sistemarentzat dinamika klasikoetan erabilitako ereduak.

teoria (ingelesez, TDDFT) [?] erabili da, 6-31+G(d,p) oinarri funtzioekin. DFT kalkulu guztiak Gaussian16 programarekin burutu dira [135].

Ab initio Born–Oppenheimer Dinamika Molekularrak (QMD) burutu dira ondoren, optimizitatutako egituren egonkortasun termikoa determinatzeko, PBE funtzionala [136, 137], DZP oinarri funtzioak eta RI formalismoa erabiliz, dagokion oinarri funtzio lagungarriekin [?, ?, ?]. Simulazioak 298 K-tan burutu dira, Nose–Hoover termostatoa erabiliz. Simulazio hauen luzeera 40.000 a.u. (9.651 ps)-koa izan da, 40 a.u. (1.93 ps)-ko simulazio urratsak eta TURBOMOLE programa erabiliz [?].

Dinamika molekularrak ff14SB [147] amber indar-eremua erabiliz burutu dira, AMBER 14 programa erabiliz [148]. Egitura guztiak Ambertools-en LEaP modulua erabiliz eraiki dira, eta kargak RESP metodologia erabiliz [150]. Lehenik eta behin ESP kalkulatzen da Gaussian [135] erabiliz 6-31G* oinarri funtzioak eta Hartree-Fock teoria maila erabiliz eta ondoren RESP kargak. Simulazio guztiak NVT bidezko minimizatuak izan dira, beroketa prozesu batetaz jarraituak, eta NPT bidez ekilibratuak. Hidrogenoa barne daukaten lotura kobalenteak SHAKE algoritmoa erabiliz mugatuak izan dira.

11.4 Emaitzak

Atal honetan, lortutako emaitzen eztabaida egingo da, Kim et al [54] eta Takahasi et. al-ek [55] lortutako emaitza esperimentalak gure taldean garatutako protokolo teorikoaren bidez azaltzeko. Zehazki, atal hau bi azpiataletan banatuko da. Lehenik eta behin, sulfenil erradikalen eraketa aztertuko da, honako hauek aztertuz: sulfenil erradikalen eraketa *ab initio* metodoen bidez, BDE, ρ eta ΔG parametroak erabiliz. Ondoren, disulfuro loturek alboko disulfuro loturak aurkitzeko probabilitatea (ω) neurtuko da, hala nola, hidrogeno loturen eragina kateen mugikortasunean, honetarako dinamika molekularrak erabiliz.

11.4.1 Erradikalen Eraketa eta Disulfuroen Elkartrukaketa

Sulfenil erradikalen sorketa aztertzeko, hainbat parametro energetiko eta geometrikotaz baliatu egin gara. Zehazki, disulfuro loturaren BDE-a neurtu da, bi konformazio ezberdin kontsideratuz, bata itxia eta bestea irekia. Honetaz gain, bi eredu-kateen elkarrekintzak ere aztertu dira, hidrogeno loturak, $\pi - \pi$ elkarrekintzak edota bestelako elkarrekintza ahulak kontuan hartuz. Bukatzeko, elkartrukatze erreakzioaren energia-langa ere aztertu egin da. Aipatutako parametro energetiko eta geometriko guztiak 11.1 Taulan ikus daitezke.

Table 11.1: Aztertutako sistemen BDE, kcal/mol-etan, S-S lotura distantziak, Å-etan eta XSSX angelu dihedroak, º-tan.

	Open Conformation			Closed Conformation		
	BDE ($\frac{kcal}{mol}$)	R (S-S)	XSSX	BDE ($\frac{kcal}{mol}$)	R (S-S)	XSSX
IP	-	-	-	59.31	2.096	-65.9
HM	-	-	-	47.34	2.112	-57.8
M	51.20	2.050	122.1	65.65	2.062	-60.5
BTA	33.77	2.200	164.1	-	-	-
ADSA	58.19	2.059	179.1 (179.1)*	63.13	2.061	46.8 (90.4)
	Chain interactions					
	ΔH	R (S-S)	XSSX	R (S-S)	XSSX	
IP		2.094	81.8	2.100	70.4	
HM		2.067	97.0	2.122	-50.5	
M		2.092	97.6	2.088	-92.0	
BTA	31.71	2.114	145.1	2.126	116.7	
ADSA	31.41	2.066	-42.8 (131.6)*	2.067	-46.5 (115.4)*	

Has gaitezen kate bakarreko ereduaren konformazioaren analisiarekin eta S-S loturari dagokion BDE-rekin. 11.1 taulak kontuan hartutako bi konformazioetarako (itxia eta irekia) lortutako datu geometrikoak eta energetikoak biltzen ditu. Lehenengoan, X-S-S-X angelu dihedroa handia da, 160 gradutik gorakoa; beraz, disulfuroei lotutako bi kateak elkarrengandik urrun daude, haien arteko elkarrekintzak mugatuz. Konformazio itxian, X-S-S-X angelu dihedroa txikia da, 60 gradu ingurukoa, eta horrek kateen arteko elkarrekintzak ahalbidetzen ditu. Printzipioz, material polimerikoetan, bi konformazioen arteko nahasketa emango dela pentsa daiteke, hala nola tarteko konformazioak ere, kate kopuru haundia dela eta. Hala ere, kate bakarreko sistemen kalkuluetan, konformazio itxia baino ez zen lortu kasu

gehienetan. Konformazio hau da, hain zuzen ere, disulfuro aromatikoetan lortzen den konformazioa, non sufre atomoen ondoko fenilo eraztunen arteko elkarrekintzak katearen gainerako atalen arteko aldarapen esterikoa murrizten laguntzen duen. BTA eta ADSAn, fenilo talderik ez dagoenez, bi kateen arteko aldarapen esterikoa handitu egiten da, eta kate bakarreko kalkuluetan konformazio irekiagoak lortzen dira.

Aurreko lanetan kalkulatu zen disulfuro mota desberdinen BDE-a 48 kcal/mol ingurukoa zela disulfuro aromatikoentzat, 33 kcal/mol ingurukoa sulfenamidentzat eta 60 kcal/mol ingurukoa disulfuro alifatikoentzat, eta BTA-rentzat (sulfenamida) eta ADSA-rentzat (disulfuro alifatikoa) lan honetan kalkulatutako balioak bat datozte balio hoiekin. Disulfuro aromatikoen kasuan, ordea, HM-ren BDE-a bat dator balio hoiekin, baina IP eta HM-rentzat kalkulatutakoak balio hori baino haundiagoak dira. Hala ere, kontuan izan HM-k ez bezala, bai IP-k bai M-k hidrogeno loturak sortu ditzaketela haien kateen artean, hala nola, eraztun aromatikoen arteko $\pi-\pi$ elkarrekintza erakargarria ere. Elkarrekintza eza honen ondorioz, HM-rentzat kalkulatutako balioa guztiz S-S loturaren apurketari dagokio, IP-rentzat eta Hm-rentzat kalkulatutakoak, ordea, lehen aipatutako elkarrekintza hoien apurketari ere dagokio. Gainera, HM-ren kasuan S-S lotura luzera haundienak ere lortzen dira.

Kateen arteko elkarrekintzek materialen autokonpontze gaitasunean garrantzia daukatela jakina da. Hortaz, elkarrekintza hauen analisia ere burutu da DFT-ren bidez, bi kate eredu erabiliz. Analisi sakonagoa burutuko da aurrerago, dinamika molekularretaz baliatuz, non kate gehiago, eta luzeagoak, erabili diren. Elkarrekintza entalpiak (ΔH) aztertuz, ikus daiteke kateen arteko elkarrekintzek nahiko indartsuak direla disulfuro unitate ezberdinak erreakziona dezaten distantzia aproposetara mantentzeko. Bestalde, kateek konformazio desberdinak eduki ditzakete (itxiak edo irekiak), baina honen eragina ρ-n ez dago guztiz argi.

Argi dago, kateen konformazioak eragina daukala bai BDE-n bai S-S loturaluzereetan, eta, beraz, baliteke horrek nolabait errdikalak sortzeko probabilitatean (ρ) eragitea. Gogoan izan ρ sulfenil erradikalen eraketarekiko zuzenki proportzionala izango litzatekeela, autokonpontze prozesuarentzat ezinbestekoak direnak. Beraz, ρ-rentzat lortutako balio teorikoek behaketa

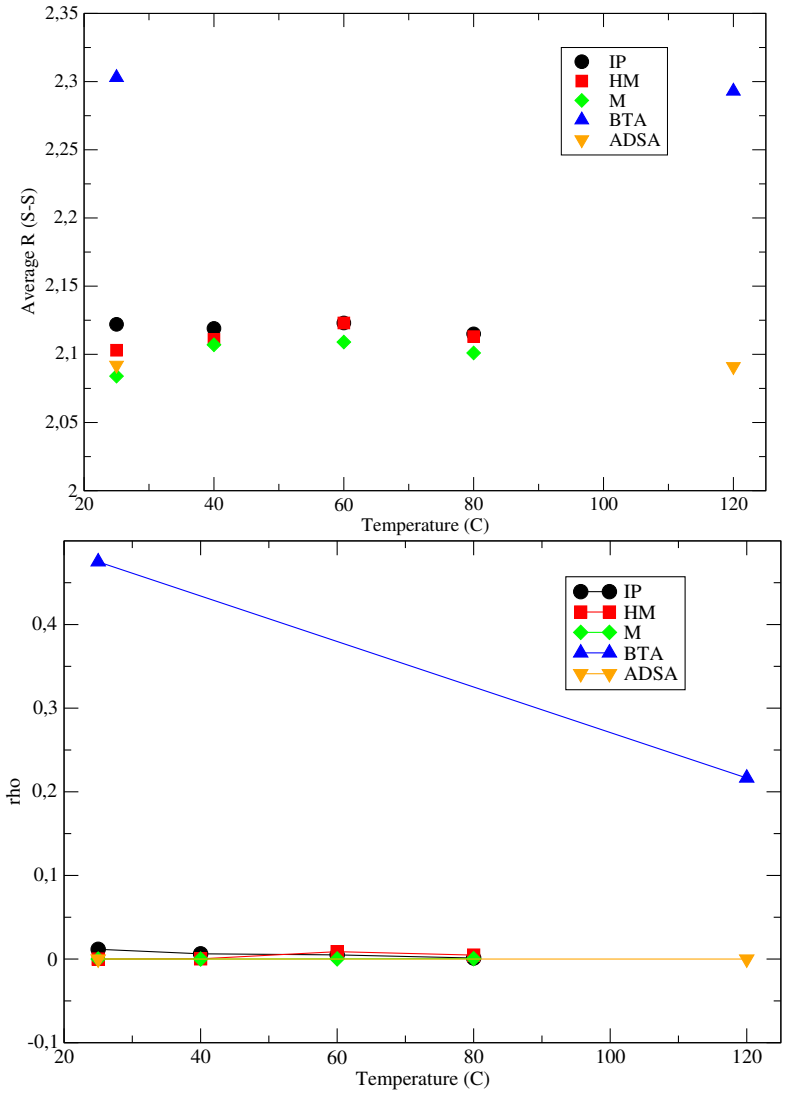

Figure 11.4: Top: S-S loturaren bataz-besteko distantzien irudikapen grafikoa, Å-etan, QMD simulazioetan lortutak tenperatura desberdinetan. Bottom: erradikalak eratzeko probabilitatea (ρ) tenperatura desberdinetan.

esperimentalarekin lotuta egon beharko lukete. BDE parametro estatiko bat denez, S-S loturaren disoziazioaren izaera dela eta, *ab initio* dinamika molekularren bidez kalkulatzen den ρ parametroa erabiltzen da, horrela kalkulatzen dena:

$$\rho = \frac{N_{S-S}}{N_{Tot}} \tag{11.1}$$

Lan honetan, ρ sistema guztietarako kalkulatu da tenperatura desberdinetan, baldintza esperimentalak erreplikatu nahian, eta tenperaturaren eragina erradikalen eraketan aztertzeko. Beraz, 4 tenperatura desberdin erabili dira (25, 40, 60 eta 80 ^{o}C) J. Kim et. al-en [54] sistemetan, izenez, IP, HM eta M, eta bi (25 eta 120 ^{o}C) H. Otsuka et. al-en [55] sistemetan. Lortutako balioak ρ-rentzat 11.2 taulan bilduta daude, hala nola S-S loturaren distantziak simulazioan zehar. 11.4 irudian datu hauen irudikapena ikus daiteke.

Table 11.2: S-S loturaren bataz-besteko distantziak, Å-etan, QMD simulazioetan lortutak tenperatura desberdinetan eta ρ aztertutako sistema guztientzat. Erabilitako temperaturak esperimentuetan erabilitakoak dira, 25 40 60 eta 80 ^{o}C IP, HM eta M-rentzat, eta 25 eta 120 ^{o}C BTA eta ADSA-rentzat.

	25		40		60		80		120	
	R_{av}	ρ	R_{av}	ρ	R_{av}	ρ	R_{av}	ρ	R_{av}	ρ
IP	2.122	0.0117	2.119	0.0063	2.123	0.0050	2.115	0.0012	-	-
HM	2.103	0.0000	2.111	0.0003	2.123	0.0089	2.113	0.0047	-	-
M	2.084	0.0000	2.107	0.0000	2.109	0.0002	2.101	0.0005	-	-
BTA	2.303	0.4750	-	-	-	-	-	-	2.293	0.2165
ADSA	2.092	0.0000	-	-	-	-	-	-	2.091	0.0000

Kim-en hirukotearekin hasiz, giro tenperaturan IP da 0 ematen ez duen sistema bakarra. Honek esan nahi du, teorikoki, IP izango dela giro tenperaturan erradikalak sortzeko gaitasuna izango duen sistema bakarra. Ondorioz, IP izango da giro tenperaturan autokonponketa prozesua gauzatu dezakeen sistema bakarra ere. 40 ^{o}C-tan IP-k oraindik, 0 ez den balio bat ematen du, eta horrek esan nahi du autokonpontze prozesua tenperatura honetan ere emango dela. M-ren balioak, berriz, 0 izaten jarraitzen du, eta horrek erradikalen falta eta, beraz, autokonpontze eza dakar. Bestalde, interesgarria da nola orain HM-k 0 ez den balio bat ematen duen, oso txikia izan arren, autokonpontze prozesua orain posiblea izatea gauzatu zezakeena. 60 °C-tan, HM-ren balioa nabarmen handitu dela ikus daiteke, eta, beraz, berez autokonpontzeko gaitasuna hobetu egin da. M-ren kasuan lortutako balioa oso txikia da oraindik, baina zero ez den beste balio batek esan nahi du erradikal kopuru txiki bat sortzen ahal dela, eta hau truke-erreakzioa eragin lezakeela neurri batean, beste baldintza batzuek laguntzen badute. 80 ^{o}C-tan, sistema guztiek zero baino balio handiagoak dituzte, baina M-ren balioa nahiko txikia da oraindik.

Bestalde, Otsuka et. al.-en sistemei dagokienez, ikus daiteke ADSA polimeroak ez lukeela autokonpontze izaerarik izango aztertutako tenperaturetan; izan ere, ρ-k 0 ematen du, hau da, elkartrukatze erreakziorako beharrezkoak diren erradikalak ez dira sortuko giro tenperaturan, ez eta 120 ^{o}C-tan ere. BTA polimeroak, berriz, ρ-ren balio handiak aurkezten ditu bi tenperaturetan; horrek esan nahi du truke-erreakzioa, eta, ondorioz, autokonpontze prozesua bi tenperaturetan eman daitekeela.

Hala ere, ikus daiteke ρ-ren joera ez datorrela bat espero denarekin; izan ere, pentsa liteke tenperatura igotzeak disoziazio probabilitate handiagoak eragin beharko behar dituela, energia gehiagok S-S lotura gehiago luzatuko baitu, ahulago egiten. Aldiz, kasu batzuetan, kontrako joera ikusten da, hau da, ρ-k behera egiten du tenperaturaren igoerarekin, IP-ren kasuan gertatzen den bezala. 11.5 irudian, ρ kalkulatzeko erabili diren S-S lotura distantziak irudikatutak daude, monomeroari dagokiona lerro beltzarekin eta dimeroari dagozkion S-S loturenak berdez eta gorriz. Argi ikusten da dimeroari dagokion disulfuro batek (berdea) monomeroaren antzeko distribuzioa ematen duela, besteak bariazio handiak ematen dituen bitartean (gorria). Hortaz, ondoriozta daiteke dimeroaren bi disulfuroak ez direla ekibalenteak, eta nahitaez ezberdintasunen bat egon behar dela haien artean. 11.3 irudia arretaz begiratuz, ikus daiteke sufre atomoak eta fenilo taldeen artean eratutako diedroak oso desberdinak direla.

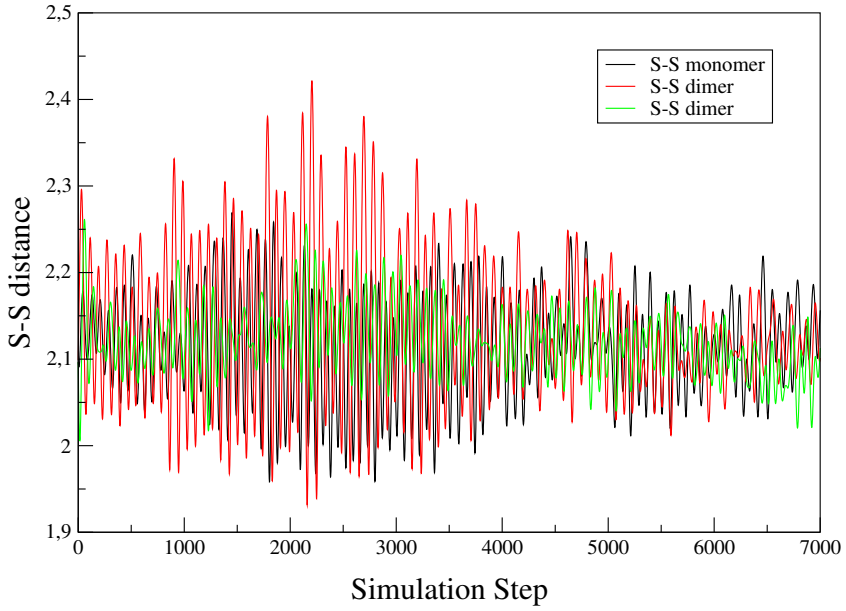

Figure 11.5: S-S loturaren bariazioak QMD simulazioetan zehar, kate bakarreko kalkuluan (beltzez) eta dimeroaren bi disulfuro unitateenak (gorria eta berdea).

Zentzu honetan, disulfuro lotura batek konformazio irekia erakusten du (berdea), bestea konformazio irekia erakusten deun bitartean (gorria). Bi konformazio hauen arteko ezberdintasun nagusia sufre atomoen ondoan dauden fenilo taldeen arteko elkarrekintza da, zeinak $\pi - \pi$ elkarrekintza erakargarrian datzan. Elkarrekintza honek sufre atomoak elkarrekin mantentzen ditu simulazioan zehar (berdea), baina interkazio honen ezean, sufre atomoek mugikortasun haundiagoa daukate (gorria). Beraz, argi dago zeihartasun bat sartzen ari garela dinamiketan. Hori ez ezik, kateen arteko elkarrekintza ere (ikus 11.1 irudia) erabilitako konformazioaren araberakoa da, zeren eta, elkarrekintza haundia den kasuetan, dimeroaren konformazio jakin baten egonkortasuna bermatzen dute. Hala ere, tenperatura igotzeak eten egiten du konformazio-egonkortasun hori, energia gehiagorekin, sistemak konformazio gehiago esplora dezakelako, eta hori izan daiteke ρ-ren jaitsieraren arrazoia. Baina, hala ere, kontuan izanik erabilitako konformazioak eragin handia duela ρ-ren kalkuluan, azken hau zehaztasunez kalkulatzeko, konformazio posible asko aztertu behar dira simulazian zehar, eta hori bereziki zaila izan daiteke *ab initio* dinamika molekularren bidez.

Kimika kuantikoko metodoen bidez kalkulatutako azken parametroa elkartrukatze erreakzioaren erreakzio langa, ΔG, izan da. Aurreko lanetan [146], ikusi zen parametro horretan eragiten zuen ezaugarri nagusia lotura dinamikoaren inguruko egitura kimikoa zela, eta antzeko egiturek antzeko erreakzio langak ere ematen zutela. Jakinda orain ikertatuko sistemek lehen ikertutako sistemen egitura kimiko antzekoa daukatela, suposatu daiteke oraingoan ere erreakzio langak antzekoak izanen direla, giro tenperaturan gainditzeko modukoak.

11.4.2 Segmentu Gogorraren Eragina Kateen Mugikortasunean

Atal honetan, dinamika molekularren bidez lortutako emaitzak aztertuko dira. Lehen aipatu bezala, kateen mugikortasuna faktore garrantzitsua da autokonpontze prozesuan. Honek disulfuro loturen, eta ondorioz, sortutako sulfenil erradikalen mugikortasuna determinatzen du eta aldameneko loturei eraso egiteko gaitasunaren muga izan daiteke. Gainera, aurreko atalean aipatu den moduan, konformazio asko behar dira ρ zehaztasunez

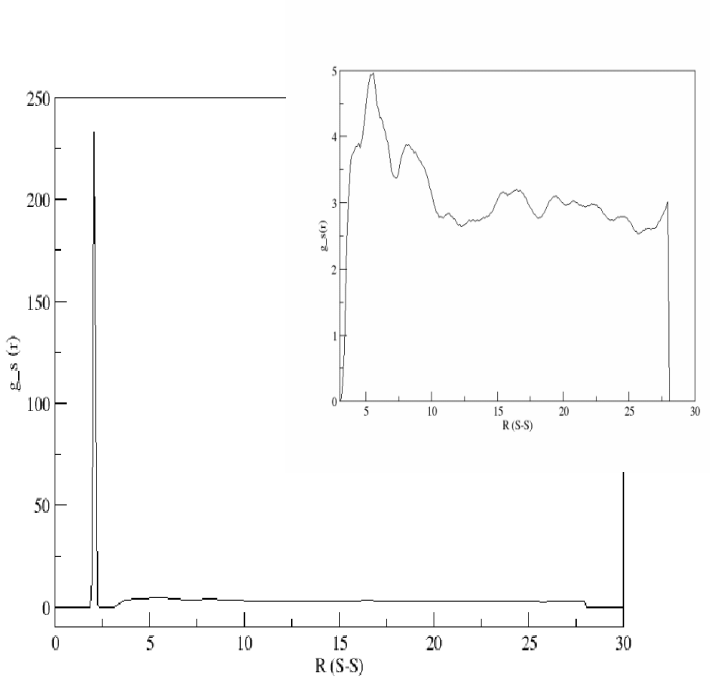

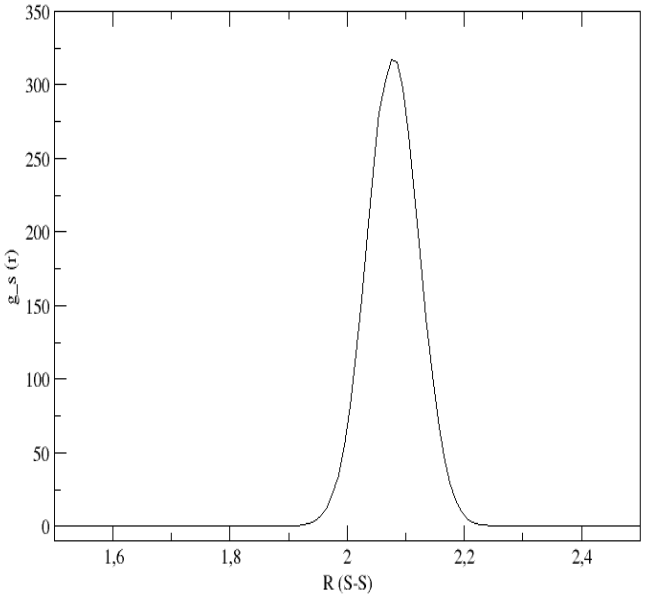

Figure 11.6: Radial distribution function and the regions of interest for the calculation of ω and ρ_{MD}

neurtzeko, eta *ab initio* metodoetan zaila den bitartean, dinamika molekularretan berez lortzen dira, simulazio baldintzak direla eta, atomo kopurua, simulazio denbora eta tenperaturaren eragina direla eta, adibidez. Beraz, ω parametroa (ikus 11.3 ekuazioa) aztertuko dugu, eta konformazio aniztasuna erabiliz dinamika molekularretatik ρ kalkulatzea posiblea den ala ez aztertuko dugu ere.

Dinamika klasikoetan lortutako distribuzio funtzio erradiala aztertuz, argi definitutako bi eskualde ikus daitezke: disulfuro loturaren sufre atomoei dagokiona, 2.10 Å inguruan, eta beste bat disulfuro ezberdinen arteko sufre atomoei dagokiona 4 Å-tik 25 Å-ra (ikus 11.6 Irudia, goian, non eremu hau handituta dagoen). Esan den bezala, ω distribuzio funtzio erradialaren eremu ezberdinen integrazioz kalkulatzen da. Era beran, ρ-ren balio bat ere definitu daiteke, rdf-ren disulfuro loturaren sufre atomoei dagokion eremua integratuz (ikus 11.7 irudia), oreka-distantziatik urrun dauden sufre-atomoen (aurrez definitutako ρ-n bezala, ikus 11.7 ekuazioa, disoziatutzat har daiteke) eta hurbil daudenen arteko erlazioa lortzeko.

Hasteko, disulfuro loturaren sufre atomoei dagokion rdf-aren eremua aztertuko dugu. 11.7 Irudian, goian, ikertutako distribuzio funtzio erradialak 25 ^{o}C-tan irudikatuta daude, integrazioan erabilitako eremua eskuinean dagoelarik. Handitutako irudian ikus daitekeenez, bai M eta bai BTA sistemek distantzia handiagoetan sufre atomoen populazio handiena erakusten dute; ADSA-k, berriz, baxuena, IP eta HM tartekoak aurkezten duten bitartean, haien profilak oso antzekoak direla. BTA eta ADSA-ren kasuak disulfuro loturaren inguruko egiturarekin azaldu daitezke; izan ere, BTA sulfenamida bat da, eta jakina den bezala [131], sistema mota hauek lotura ahulagoak izaten dituzte, disozioazio ratio haundiagoak produzituz. ADSA, ordea, disulfuro alifatikoetan oinarrituta dago, zeinek lotura sendoagoak eratzen dituzten. Bestalde IP, HM eta M-k egitura berdina daukate disulfuro loturaren inguruan (hirurak disulfuro aromatikoetan oinarrituta daude), beraz tarteko lotura indarrak, ematen dute.

11.7 irudian, behean, IP sistemarako tenperatura ezberdinetan lortutako distribuzio funtzio erradialak irudikatuta daude. Ikus daiteke nola, espero bezala, tenperatura handiagoetan tamaina txikiago tontorrak ikusten diren, lotura distantzien distribuzio zabalagoak direla eta.

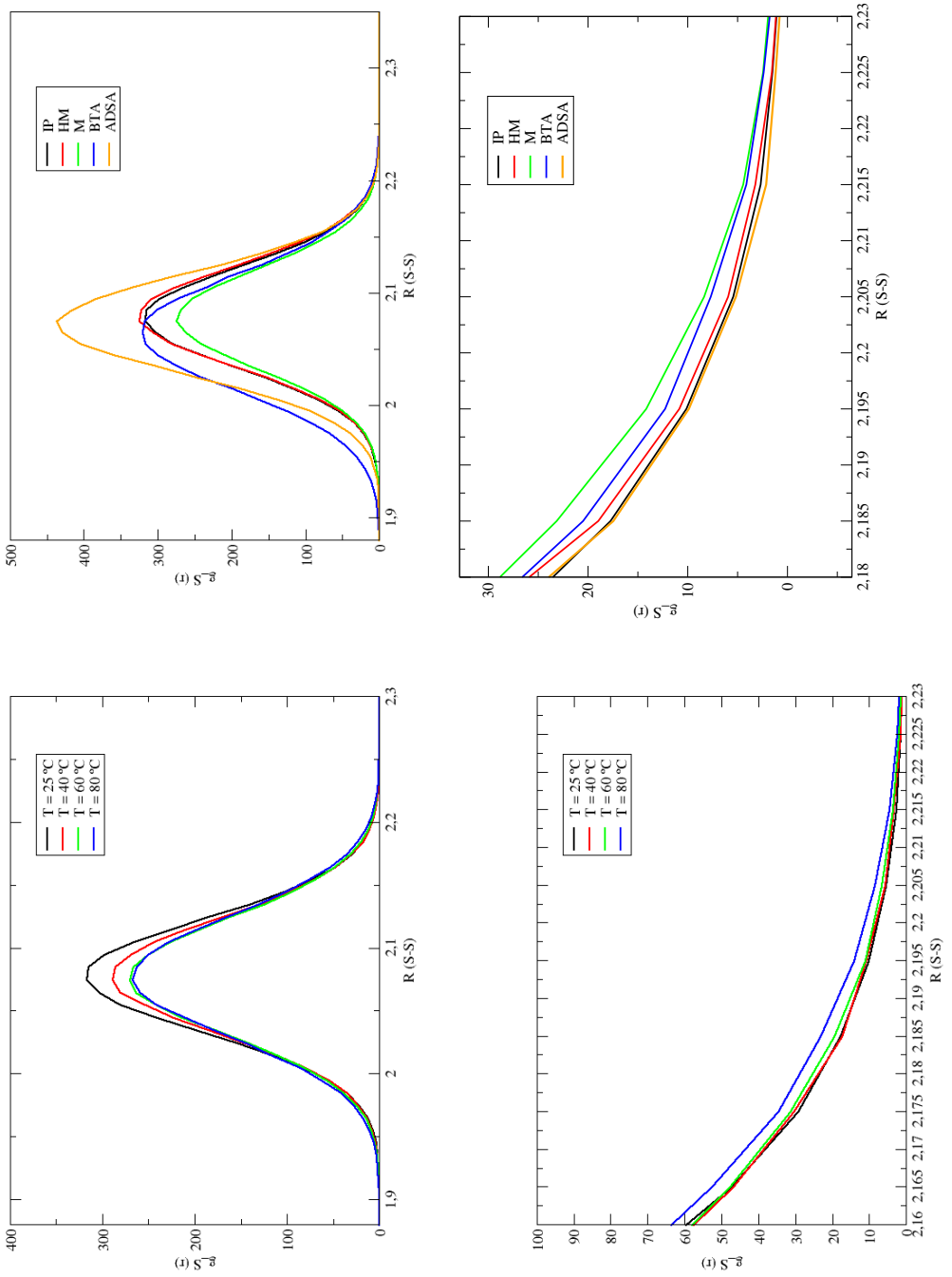

Figure 11.7: S-S loturen sufre atomoei dagozkion rdf-aren eremua. Goian: sistema guztiak 25 ºC-tan. Behean: IP sistemarentzat lortutako rdf-ak tenperatura desberdinetan. Integrazioarako erabili den eremua handituta dago bi kasuetan.

Table 11.3: ρ_{MD}-ren balioak sistema guztientzat tenperatura ezberdinetan.

ρ_{MD}	25 ^{o}C	40 ^{o}C	60 ^{o}C	80 ^{o}C	120 ^{o}C
IP	.0030	.0036	.0042	.0055	-
HM	.0034	.0040	.0050	.0032	-
M	.0028	.0037	.0045	.0056	-
BTA	.0039	-	-	-	
ADSA	.0019	-	-	-	.0056

Lotura distantzien zabaltze honek, handitutako irudian ikusten den bezala, distantzia haundietan dauden sufre atomoen kopuruaren igoera dakar, zeinek disoziatuta kontsideratzen ahal dira.

Orain, rdf-aren eremu hau integratuta izan da, distantzia luzeetan dauden sufre atomoen proportzioa lortzeko asmoarekin, disoziazio prozesuarekin lotuta baitago. Horretarako, ω kalkulatzen den era berean, ρ_{MD} (ikus 11.2 ekuazioa) parametroa definitu da, rdf-a bi eremu ezberdinetan integratuz. Eremu hauek hurrengoak dira: I_I, 2.20 Å-tik 3.00 Å-ra dijoana, eta disoziatuta kontsidera daitekeen sufre atomoak kontuan hartzen dituen, eta I_{II}, 1.80 Å-tik 3.00 Å-ra dijoana, eta disulfuro lotura osoa hartzen duena. Horrela, disoziatuta kontsidera daiteken sufre atomoen proportzio bat lortu dezakegu, *ab initio* dinamika molekularretan bezala. Lortutako balioak 11.3 taulan bilduta daude. Ikus daitekeenez, BTAk du proportziorik handiena, eta ADSAk, berriz, baxuena, espero zen bezala; gainerakoek, berriz, oso antzeko balioak dituzte. Balioa tenperaturarekin handitzen da, espero denarekin orain bat etorriz.

$$\rho_{MD} = \frac{I_I}{I_I + I_{II}} \tag{11.2}$$

Orain, disulfuro ezberdinen arteko sufre atomoei dagokien rdf-aren eremura mugituko gara. Oraingoan integratuta izango den eremua 11.6 irudian handituta dagoena da, eta integrazio mugak hurrengoak dira: I_I, eremu erreaktiboa, 3 Å-tik 4.5 Å-ra, non bertako sufreak erreakzionatzeko sobera hurbil dauden, eta I_{II}, 4.5 Å-tik 20 Å-ra, non bertako atomoek erreakzio eremuan sartzeko probabilitate ez deuseztagarria daukaten. Eremu hauek aurreko lanetan definitutak izan ziren [72].

$$\omega = \frac{I_I}{I_I + I_{II}} \tag{11.3}$$

Ikus daitekeen bezala 11.8 irudian, segmentu gogor ezberdinentzak ω-ren balio ezberdinak lortzen dira, baina ω tenperaturarekin ere aldatzen dela ikusten da. Hala eta guztiz ere, ω-k balio zehatz baten inguruan fluktuatzen du tenperatura gora egin ahala. Honen arrazoia honakoa da; ikertutako sistemak polimeroak dira, hau da, material solidoak, eta ikertutako baldintzak polimero hauen T_g-a baino txikiagoak dira (poliuretanoentzat: 120-130 ^{o}C). Hortaz, ondoriozta daiteke haien egitura ez duela aldaketa askorik jasoko tenperatura gora egin ahala. Horrela, bataz-besteko ω_{ave} definitzea zentzua dauka, material bakoitzaren ezaugarri izango dena.

Table 11.4: ω tenperaturaren funtzioan sistema guztientzat, ω_{ave} barne.

T (^{o}C)	ω_{IP}	ω_{HM}	ω_{M}	ω_{ADSA}	ω_{BTA}
25	0.0698	0.0903	0.0324		0.0004
40	0.0517	0.1169	0.0481	-	-
60	0.0659	0.0422	0.0227	-	-
80	0.0579	0.0728	0.0412	-	-
120	-	-	-		
ω_{ave}	0.0613	0.0806	0.0361		

Modu hontan, lortutako bataz besteko ω balioak hurrengoak dira: 0.0613 IP-rentzat, 0.0806 HM-rentzat eta 0.0361 M-rentzat. Desberdintasun hauek, segmentu gogorraren egitura kimiko ezberdina dela eta ematen dira, disulfuro unitateen mugikortasunean eragin zuzena baitu. Baliorik haundiena HM-rako lortzen da, bi ziklohexanotan oinarrituta, txikiena, ordea, M-rentzat. M-ren fenilo taldeak egitura zurrunagoak sortzen dituzte, haien planartasuna eta eraztunen arteko elkarrekintza dela eta. IP, ordea, tarteko balioa ematen du. Hidrogeno loturetan erreparatuz, ordea, ez dira desberdintasun nabariak ikusten.

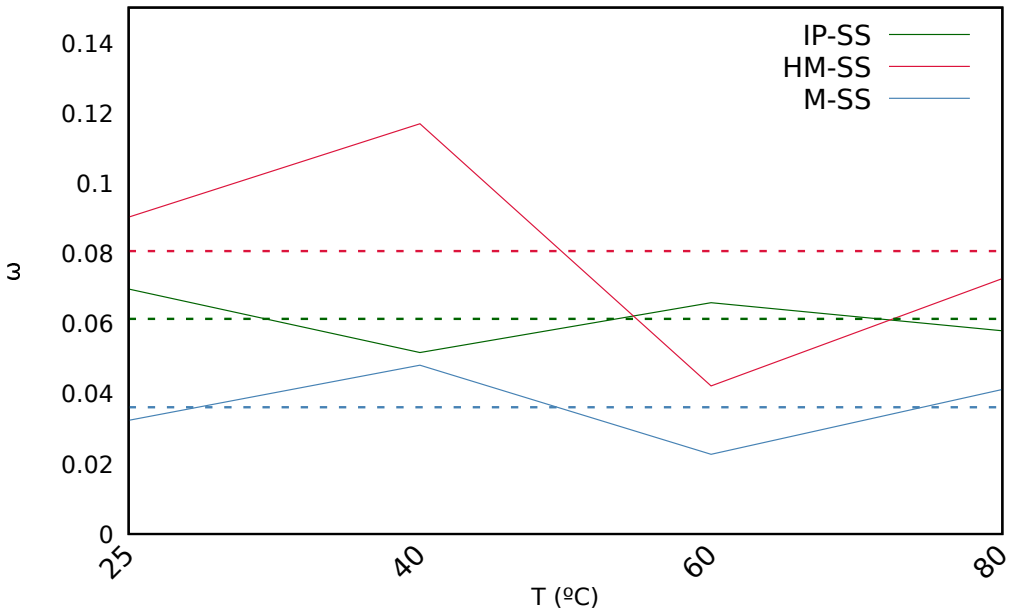

Figure 11.8: ω as a function of temperature for Kim's trio, including ω_{ave}.

11.5 Ondorioak

Atal honetan, sistema erreal batzuen autokonpontze gaitasun teorikoa aztertu dugu, gure taldeak garatutako protokoloaren bidez. Lortutako emaitza teorikoak esperimentalekin alderatu ditugu.

Oro har, protokoloa bat dator, kualitatiboki, emaitza esperimentalekin; izan ere, gai da, oro har, aztertutako sistemen autokonpontze ahalmen esperimentalak azaltzeko, IP eta BTA sistemen errendimendu handia azaltzen baitu, eta, aldi berean, M eta ADSA sistemen autokonpontze ahalmenik eza ere azaltzen du. Interesgarriagoa da, halaber, tenperatura igota HM-ak bere kabuz konpontzeko duen gaitasuna nola hobetu den deskribatu ahal izatea.

Hala ere, tenperaturaren eragina behar bezala kontuan hartzea zaila da egungo protokoloarekin, batez ere *ab initio* dinamika molekularretan, non ohartu baikara hasierako konformazioak konformazio-joera bat eragiten duela simulazioetan zehar. Hortaz, ρ zehazki neurtzeko QMD simulazio luzeegiak behar dira, bidezkoak ez direnak. Hala ere, ρ-k autokonpontzeko gaitasunaren adierazle argia izaten jarraitzen du, etengailu gisa jarduten baitu;

zero ez denean, autokonpontzea posible da, baina zero denean, ez da autokonpontzea gertatuko.

Beste alde batetik, ohartu gara dagoeneko eskuragarri daukagula ρ kalkulatzeko behar den konformazio aniztasuna dinamika molekularreko simulazioetan, bertan efektu kuantikoak kontuan hartzen ez direla eragozpen nagusia izanez ($\pi - \pi$ elkarrekintzak, zeinek konformazio itxiak edo irekiak sor dezaketeen). Beraz, dagoeneko existitzen den parametroaren hedapen bat definitu dugu, ρ_{MD}, dinamika molekularraren bidez ere erradikalak eratzeko probabilitatea lortzeko.

Lan honetan ikusi dugunez, tenperatura igotzeak ez du eraginik izango ω-n; izan ere, bolumen handiko materialen propietateek ez dute hainbesteko eraginik jasango T_g-tik oso beherako tenperaturetan lan egiten denean, egitura solidoari eusten baitiote.

Chapter 12

Ondorio Nagusiak

Tesi honetan, dikalkogenuroetan oinarrituako material polimeriko askotarikoen autokonpontze gaitasuna ikertu egin da, S-S eta Se-Se lotura homonuklearrez, hala nola, S–Se lotura heteronuklearrez osaturikoak. Hau egiteko bai *ab initio* kalkuluak, bai dinamika molekularrak burutu dira, gure ikerketa taldean garaturiko protokolo teorikoa jarraituz. Protokolo honen arabera autokonpontze gaitasun teorikoa hiru parametro komputazionalen arabera neurtu daiteke. Hoietako bi, ρ eta ΔG^{TS}, kalkulu kuantikoetatik lortzen dira, eta hirugarren bat, ω, dinamika molekularretatik. Kalkulu kuantikoetatik lortutako parametroei erreparatuz, ρ sistema jakin batek kalkogenil erradikalak sortzeko dituen gaitasunarekin lotuta dago, disozioazio termikoaren bidez, eta *ab initio* dinamika kuantikoetaz baliatuz kalkulatzen da, ΔG^{TS}, ordea, kalkogenil erradikal batek dikalkogenuro lotura bat erasotzeko gainditu behar duen erreakzio langa da. Aipatzekoa da argi-irradiazioarik ez dagoenean, kalkogenil erradikalak soilik prozesu termikoen eraginez sor daitezkeela. Zero ez diren ρ-ren balioak eta ΔG^{TS}-ren balio baxuak autokonpontze prozesuarekin lotuta daude. Honetaz gain, dikalkogenuro loturak bata bestearengandik sobera hurbil egon behar dira haien arteko erreakzioa gerta dezan. Dinamika molekularrek gertutasun maila hori neurtzea ahalbidetzen dute, hain zuzen ere, eta horrela, ω parametroa definitu daiteke. Tesi honetan zehar, hainbat lan burutu ditugu faktore hauen garrantzia autokonpontze prozesuan aztertzeko, bai eta protokolo teorikoa findu nahiean, sistema errealetan aplikatzeko asmoarekin.

Lehenik eta behin, metodo kuantikoak erabiliz, selenioan oinarritutako (Se-

Se lotura dinamiko kobalente homonuklearretan eta Se-S lotura dinamiko kobalente heteronuklearretan) konposatu organiko sorta bat aztertu genituen, kalkulatutako ρ eta ΔG^{TS}parametroak disulfuro loturan oinarritutako materialekin alderatzeko asmoz. Horrela, haien autokonpontze gaitasuna alderatu eta aurresateko gai izango gara, autokonpontze prozesu eraginkorragoa erakusten duten material berrien diseinua helburu dugula. Hiru konposatu familia nagusi aztertu ziren, izenez, R-PD-XX (difenil dikalkogenuroak), R-PA-XX (difenil amino dikalkogenuroak) and R-PF-XX (fenilorik gabeko "phenyl-free" dikalkogenuroak), R ordezkaitzaile ezberdinak izanez, urea, uretanoa, etilenglikol, alkoholak edo esterrak bezalakoak. Goian aipatu den bezala, espezie guztietan bi ezaugarri nagusietan zentratu gara: i) sulfenil eta selenil erradikalak eratzeko propabilitatean (ρ) eta ii) elkartrukatze erreakzioa gauzatzeko gainditu behar den erreakzio langa (ΔG^{TS}). Erradikalak kanpo-eraginik gabe eratzeko modu nagusia X-X loturaren disoziazio termikoa da, dikalkogenuro loturaren disoziazio energiarekin (BDE) loturik dagoena. Beraz, disoziazio termikoa aztertzeko BDE eta ρ erabili dira. BDE-a bi faktore nagusien bitartez jaitsi egiten da: erradikalaren elektroi desaparekatuaren delokalizazioaren bitartzez eta σ^* orbital molekular antilotzailearen populazioaren igoeraren bitartez. Ikusi da bi faktore hauen eragina aditiboa dela PA-XX deribatuetan, dikalkogenuro loturaren eta fenilo taldeen artean dagoen amino taldearen eraginez, PD-XX eta PF-XX deribatuetan bata besteak konpesatzen duen bitartean. Hortaz, bi azken hauek antzeko BDE-ak aurkezten dituzte, PA-XX deribatuek balio txikagoak aurkezten dituzten bitartean. gainera, lotura dinamikoaren naturak bde-an eragina daukala ikusi zen ere. halaber, hidrogeno loturen presentziak ρ-ren igoera txiki bat dakar, x-x loturaren elongazioa dela eta, dinamika kuantiketan ikus daitekeen bezala. erreakzio langen analisitik ondoriozta dezakegu eraztun aromatikoak ezinbestekoak direla haien balioak jeisteko, zeren eta eraztunek sortutako $\pi - \pi$ elkarrekintzak erreakzio-geometria aproposa bermatzen du, sulfenil erradikalak elkarrekin mantenduz. hortaz, pd-xx deribatuentzat erreakzio langa txikiagoak lortzen dira. lotura dinamikoari erreparatuz, ikus daiteke selenioaeren presentziak erreakzio langak ere txikitu egiten dituela. honen arrazoia selenioren $4p$ orbitalen izaera da, zeinek haien izaera difusoa dela eta, gainezartze eraginkorragoa sortzen dute distantzia haundiaetan

sufreren $3p$ orbitalak baino, erreakzioa erraztuz. ondorioz, erreakzio langa txikienak pd-sese deribatuentzat lortzen dira. gainera, deribatu hauen fotodisoziazioa gauzatzeko beharrezkoa den uhin-luzera espektru elektromagnetikoaren eremu ikuskorrean aurkitzen da. honek, disoziazio termikoarekin batera, autokonpontze gaitasuna haunditu dezake. Emaitza guzti hauek bat datozte ebidentzia esperimentalekin, eta hortaz, emaitz hauetan oinarrituz, sufrea selenioz ordezkatzea eta bizkarrezur apropos bat lotura dinamikoari lotuta izatea, material autokonpongarri eraginkorrak sintetizatzeko bide aproposa dela ondoriozta dezakegu.

Behin ρ eta ΔG^{TS}aztertutak eta alderatutak izan zirela S-S, S-Se eta Se-Se lotura dinamikoetan oinarritutako materialetan, kalkulu teorikoak luzatu genituen material hauen ωkalkulatuz, gure ikerketa taldean garatutako protokolo teorikoa hobetzeko asmoz [72]. Hau egiteko, dikalkogenuro loturetan (S-S, Se-Se) oinarritutako ereduak, hiru bizkarrezur ezberdinekin (PA, PD eta PF) eta hainbat talde funtzionalekin ordezkatzaile bezala konbinatuta aztertutak izan ziren. Formosoren lanarekin alderatuz, hainbat egitura parametroen garrantzia aztertuta izan zen, adibidez, hasierazko ustezko egitura, kateen luzera, simulazio kaxa eta simulazio denbora, eta aurreko lanarekin [72] alderatua, simulazio eredu esanguratsuak eraikitzeko asmoarekin. Gure emaitzen arabera, parametro hauek garrantzi haundia daukate hasierako konformazio aproposak eraikitzeko. Baldintza berriak erabiliz, eredu sistemen hainbat propietate aztertutak izan ziren, hidrogeno loturak eta kateen mugikortasuna (ω) bezalakoak. Bizkarrezurra ω-n influentzia haundia zeukala ikusi zen, PD eta PF deribatuek antzeko balioak emanez, PA derinatuek balio txikiagoak ematen zituen bitartean. Hidrogeno lotura kopurua garrantzi haundia dauka kateen mugikortasunean, eta hortaz, ω-n. Hala, tarteko hidrogeno lotura kopuruak dira ω balio altuenak sortzen dituztenak. Gainera, ikusi zen selenioan oinarritutako sistemek ω balio altuagoak ere sortzen zituztela. ω kalkulatu ondoren, parametro hau lehenago lortutako bi parametroekin, ρ eta ΔG^{TS}, konbinatu genuen, ikertutako sistemen autokonpontze gaitasun teorikoa estimatzeko, zeinak ρ eta ω-rekiko, zuzenki proportzionala izango den eta ω-rekiko alderantziz. PD-SeSe deribatuek autokonpontze gaitasun teoriko haundiena daukatela ondorioztatzen dugu.

Eredu sistemetan protokoloa findu ondoren, hurrengo urratsa sistema errealetan aplikatzea izan zen. Zehazki, Kim et. al.-ek garatutako hainbat poliuretanotan eta Takahashi et. al.-ek garatutako hainbat polimetakrilatoetan. Kim et. al. garatutako materialak disulfuro aromatikoetan oinarritutako poliuretanoak ziren, segmentu gogor ezberdinekin konbitatutak. Takahashi et. al.-enak, ordea, kate alifatikoak (CH_2-S-S-CH_2) eta amina tertziario eta disulfuroak (N-S-S-N) crosslinker gisa zeukaten polimetakrilatoak ziren. Kim-en sistema bat (IP izenakoa) eta Takahashi-ren bat (BTA izenekoa) autokonpontze gaitasuna azaltzen zuten giro tenperaturan eta tenperatura handitan baita, besteek, ordea, ez (soilik Kim-en HM sistema, tenperatura altuagoetan). Oro har, protokoloa bat dator, kualitatiboki, emaitza esperimentalekin; izan ere, gai da, oro har, aztertutako sistemen autokonpontze ahalmen esperimentalak azaltzeko, IP eta BTA sistemen errendimendu handia azaltzen baitu, eta, aldi berean, M eta ADSA sistemen autokonpontze ahalmenik eza ere azaltzen du. Interesgarriagoa da, halaber, tenperatura igota HM-ak bere kabuz konpontzeko duen gaitasuna nola hobetu den deskribatu ahal izatea. Hala ere, tenperaturaren eragina behar bezala kontuan hartzea zaila da egungo protokoloarekin, batez ere *ab initio* dinamika molekularretan, non ohartu baikara hasierako konformazioak konformazio-joera bat eragiten duela simulazioetan zehar. Hortaz, ρ zehazki neurtzeko QMD simulazio luzeegiak behar dira, bidezkoak ez direnak. Hala ere, ρ-k autokonpontzeko gaitasunaren adierazle argia izaten jarraitzen du, etengailu gisa jarduten baitu; zero ez denean, autokonpontzea posible da, baina zero denean, ez da autokonpontzea gertatuko. Gainera, tenperatura igotzeak ez du eraginik izango ω-n; izan ere, bolumen handiko materialen propietateek ez dute hainbesteko eraginik jasango T_g-tik oso beherako tenperaturetan lan egiten denean, egitura solidoari eusten baitiote.

Emaitza guzti hauetan oinarrituta, disulfuroetan oinarritutako materialen autokonpontze prozesua gidatzen duten faktore nagusiak zeintzuk diren azaldu dugu, eta haiek neurtzeko eta azaltzeko den protokoloa findu ere, zeinek esperimentalki behatutako emaitzak azaltzeko gai den. Hala eta guztiz ere, gure protokoloaren muga nagusia *ab initio* kalkuluetan kontuan hartzen ditugun konformazio kopuru mugatua da, dinamika molekularretan, ordea, konformazio kopuru aproposa izan arren, efektu kuantikoak ez dira kontuan hartzen. Komenigarria litzateke bai dinamika kuantikoek

prezisioa eta dinamika molekularren konformazio aniztasuna, protokoloa izaera kuantitatibo hobeagoa izatearren eta baita gaitasun prediktibo handiagoa ere. Zorionez, tesi honetan ezarritako protokoloa dikalkogenuroetan oinarritutako materialen autokonpontze gaitasuna aurresateko gai da.

Bibliography

[1] Seebach, D. *Angew. Chemie Int. Ed. English* **1990**.

[2] Lehn, J.-M. *Chem. - A Eur. J.* **1999**.

[3] Rowan, S. J.; Cantrill, S. J.; Cousins, G. R. L.; Sanders, J. K. M.; Stoddart, J. F. *Angew. Chemie Int. Ed.* **2002**, *41*(6), 898–952.

[4] Zou, Z.; Li, S.; He, D.; He, X.; Wang, K.; Li, L.; Yang, X.; Li, H. *J. Mater. Chem. B* **2017**, *5*(11), 2126–2132.

[5] Roy, N.; Bruchmann, B.; Lehn, J.-M. *Chem. Soc. Rev.* **2015**, *44*(11), 3786–3807.

[6] Wu, D. Y.; Meure, S.; Solomon, D. *Prog. Polym. Sci.* **2008**, *33*(5), 479–522.

[7] Bergman, S. D.; Wudl, F. *J. Mater. Chem.* **2008**, *18*(1), 41–62.

[8] Mauldin, T. C.; Kessler, M. R. **2013**, *6608*(2010).

[9] Burattini, S.; Greenland, B. W.; Chappell, D.; Colquhoun, H. M.; Hayes, W. *Chem. Soc. Rev.* **2010**, *39*(6), 1973.

[10] Bioinspired self-healing materials: Lessons from nature. Cremaldi, J. C.; Bhushan, B. **2018**.

[11] Hager, M. D.; Greil, P.; Leyens, C.; van der Zwaag, S.; Schubert, U. S. *Adv. Mater.* **2010**, *22*(47), 5424–5430.

[12] Billiet, S.; Hillewaere, X. K. D.; Teixeira, R. F. A.; Du Prez, F. E. *Macromol. Rapid Commun.* **2013**, *34*(4), 290–309.

[13] Kuhl, N.; Geitner, R.; Bose, R. K.; Bode, S.; Dietzek, B.; Schmitt, M.; Popp, J.; Garcia, S. J.; van der Zwaag, S.; Schubert, U. S.; Hager, M. D. *Macromol. Chem. Phys.* **2016**, *217*(22), 2541–2550.

[14] Chen, X.; Wudl, F.; Mal, A. K.; Shen, H.; Nutt, S. R. *Macromolecules* **2003**, *36*(6), 1802–1807.

[15] *Macromol. Chem. Phys.* **2007**, *208*(2), 224–232.

[16] Cho, S.; Andersson, H.; White, S.; Sottos, N.; Braun, P. *Adv. Mater.* **2006**, *18*(8), 997–1000.

[17] Schmolke, W.; Perner, N.; Seiffert, S. *Macromolecules* **2015**, *48*(24), 8781–8788.

[18] Montarnal, D.; Capelot, M.; Tournilhac, F.; Leibler, L. *Science* **2011**, *334*(6058), 965–8.

[19] Cromwell, O. R.; Chung, J.; Guan, Z. *J. Am. Chem. Soc.* **2015**, *137*(20), 6492–6495.

[20] Azcune, I.; Odriozola, I. *Eur. Polym. J.* **2016**, *84*, 147–160.

[21] Takahashi, A.; Ohishi, T.; Goseki, R.; Otsuka, H. *Polymer* **2016**, *82*, 319–326.

[22] Frenette, M.; Aliaga, C.; Font-Sanchis, E.; Scaiano, J. C. *Org. Lett.* **2004**.

[23] Imato, K.; Nishihara, M.; Kanehara, T.; Amamoto, Y.; Takahara, A.; Otsuka, H. *Angew. Chemie - Int. Ed.* **2012**, *51*(5), 1138–1142.

[24] Ying, H.; Zhang, Y.; Cheng, J. *Nat. Commun.* **2014**, *5*(1), 3218.

[25] Hutchby, M.; Houlden, C. E.; Haddow, M. F.; Tyler, S. N.; Lloyd-Jones, G. C.; Booker-Milburn, K. I. *Angew. Chemie - Int. Ed.* **2012**.

[26] McElhanon, J. R.; Wheeler, D. R. *Org. Lett.* **2001**.

[27] Gandini, A. *Macromolecules* **2008**.

[28] Biomedical applications of boronic acid polymers. Cambre, J. N.; Sumerlin, B. S. **2011**.

[29] Xin, Y.; Yuan, J. **2012**.

[30] Zhang, Z. P.; Rong, M. Z.; Zhang, M. Q.; Yuan, C. *Polym. Chem.* **2013**.

[31] Zhang, C.; Hu, J.; Li, X.; Wu, Y.; Han, J. *J. Phys. Chem. A* **2014**, *118*(51), 12241–12255.

[32] Burattini, S.; Colquhoun, H. M.; Fox, J. D.; Friedmann, D.; Greenland, B. W.; Harris, P. J. F.; Hayes, W.; Mackay, M. E.; Rowan, S. J. *Chem. Commun.* **2009**, *44*.

[33] Burnworth, M.; Tang, L.; Kumpfer, J. R.; Duncan, A. J.; Beyer, F. L.; Fiore, G. L.; Rowan, S. J.; Weder, C. *Nature* **2011**, *472*(7343), 334–337.

[34] Kamplain, J. W.; Bielawski, C. W. *Chem. Commun.* **2006**, (16), 1727.

[35] Ruff, Y.; Lehn, J. M. *Biopolymers* **2008**, *89*(5), 486–496.

[36] Otsuka, H.; Muta, T.; Sakada, M.; Maeda, T.; Takahara, A. *Chem. Commun. (Camb).* **2009**, (9), 1073–1075.

[37] Nevejans, S.; Ballard, N.; Fernández, M.; Reck, B.; García, S. J.; Asua, J. M. *Polymer (Guildf).* **2019**, *179*, 121670.

[38] Zheng, P.; McCarthy, T. J. *J. Am. Chem. Soc.* **2012**, *134*(4), 2024–2027.

[39] Ritz, D.; Beckwith, J. *Roles of thiol-redox pathways in bacteria;* 2001.

[40] Kim, Y. H. *Organic Sulfur Chemistry: Biochemical Aspects;* CRC Press: Boca Raton, 1992.

[41] Wedemeyer, W. J.; Welker, E.; Narayan, M.; Scheraga, H. A. *Biochemistry* **2000**.

[42] Oae, S.; CRC Press: Boca Raton, 1992; chapter 4.

[43] Guo, Y.; Alvarado, S. R.; Barclay, J. D.; Vela, J. *ACS Nano* **2013**, *7*(4), 3616–3626.

[44] Hoffmann, W. *Vulcanization and Vulcanizing agents;* 1967.

[45] Tsarevsky, N. V.; Matyjaszewski, K. *Macromolecules* **2002**, *35*(24), 9009–9014.

[46] Oh, J. K.; Tang, C.; Gao, H.; Tsarevsky, N. V.; Matyjaszewski, K. *J. Am. Chem. Soc.* **2006**, *128*(16), 5578–5584.

[47] Otsuka, H.; Nagano, S.; Kobashi, Y.; Maeda, T.; Takahara, A. *Chem. Commun.* **2010**, *46*(7), 1150–2.

[48] Sarma, R. J.; Otto, S.; Nitschke, J. R. *Chem. - A Eur. J.* **2007**.

[49] Belenguer, A. M.; Frisic, T.; Day, G. M.; Sanders, J. K. M. *Chem. Sci.* **2011**, *2*(4), 696.

[50] Martin, R.; Rekondo, A.; Ruiz de Luzuriaga, A.; Cabañero, G.; Grande, H. J.; Odriozola, I. *J. Mater. Chem. A* **2014**, *2*(16), 5710.

[51] Brunette, C. M.; Hsu, S. L.; MacKnight, W. J. *Macromolecules* **1982**, *15*(1), 71–77.

[52] Mattia, J.; Painter, P. *Macromolecules* **2007**, *40*, 1546–1554.

[53] Erice, A.; Azcune, I.; Ruiz de Luzuriaga, A.; Ruipérez, F.; Irigoyen, M.; Matxain, J. M.; Asua, J. M.; Grande, H.-J.; Rekondo, A. *ACS Appl. Polym. Mater.* **2019**, *1*(9), 2472–2481.

[54] Kim, S.-M.; Jeon, H.; Shin, S.-H.; Park, S.-A.; Jegal, J.; Hwang, S. Y.; Oh, D. X.; Park, J. *Adv. Mater.* **2017**, *1705145*, 1705145.

[55] Takahashi, A.; Goseki, R.; Ito, K.; Otsuka, H. *ACS Macro Lett.* **2017**, pages 1280–1284.

[56] Bock, A.; Forchhammer, K.; Heider, J.; Leinfelder, W.; Sawers, G.; Veprek, B.; Zinoni, F. *Mol. Microbiol.* **1991**, *5*(3), 515–520.

[57] Atkins, J. F.; Gesteland, R. F. *Nature* **2000**, *407*(6803), 463–464.

[58] Bachrach, S. M.; Demoin, D. W.; Luk, M.; Miller, J. V. *J. Phys. Chem. A* **2004**, *108*(18), 4040–4046.

[59] Nauser, T.; Steinmann, D.; Grassi, G.; Koppenol, W. H. *Biochemistry* **2014**, *53*(30), 5017–5022.

[60] Snider, G. W.; Ruggles, E.; Khan, N.; Hondal, R. J. *Biochemistry* **2013**, *52*(32), 5472–5481.

[61] Ji, S.; Xia, J.; Xu, H. *ACS Macro Lett.* **2016**, *5*(1), 78–82.

[62] Ji, S.; El Mard, H.; Smet, M.; Dehaen, W.; Xu, H. *Sci. China Chem.* **2017**, *60*(9).

[63] Ji, S.; Cao, W.; Yu, Y.; Xu, H. *Angew. Chemie - Int. Ed.* **2014**, *53*(26), 6781–6785.

[64] *ACS Macro Lett.* **2017**, *6*(2), 89–92.

[65] An, X.; Aguirresarobe, R. H.; Irusta, L.; Ruipérez, F.; Matxain, J. M.; Pan, X.; Aramburu, N.; Mecerreyes, D.; Sardon, H.; Zhu, J. *Polym. Chem.* **2017**, *8*(23), 3641–3646.

[66] Benassi, R.; Fiandri, G. L.; Taddei, F. *Tetrahedron* **1994**, *50*, 12469.

[67] Zou, L.-f.; Fu, Y.; Shen, K.; Guo, Q.-x. **2007**, *807*, 87–92.

[68] Modelli, A.; Jones, D. *J. Phys. Chem. A* **2006**, *110*(34), 10219–10224.

[69] Matxain, J. M.; Asua, J. M.; Ruipérez, F. *Phys. Chem. Chem. Phys.* **2016**, *18*(3), 1758–1770.

[70] Nevejans, S.; Ballard, N.; Miranda, J. I.; Reck, B.; Asua, J. M. *Phys. Chem. Chem. Phys.* **2016**, *18*(39), 27577–27583.

[71] Ruiz de Luzuriaga, A.; Martin, R.; Markaide, N.; Rekondo, A.; Cabañero, G.; Rodríguez, J.; Odriozola, I. *Mater. Horizons* **2016**, *3*(3), 241–247.

[72] Formoso, E.; Asua, J. M.; Matxain, J. M.; Ruipérez, F. *Phys. Chem. Chem. Phys.* **2017**, *19*(28), 18461–18470.

[73] Ruiperez, F. *Int. Rev. Phys. Chem.* **2019**, *38*(3-4), 343–403.

[74] Schrödinger, E. *Ann. Phys.* **1926**, *80*(13), 437–490.

[75] Dirac, P. A. M. *Proc. R. Soc. A Math. Phys. Eng. Sci.* **1927**, *113*(765), 621–641.

[76] Heisenberg, W. *Zeitschrift für Phys.* **1925**, *33*(1), 879–893.

[77] Schrödinger, E. *Ann. Phys.* **1927**, *388*(15), 956–968.

[78] Born, M.; Oppenheimer, R. *Ann. Phys.* **1927**, *84*, 457.

[79] Arrhenius, S. A. *Z. Phys. Chem.* **1889**, *4*, 96.

[80] Eyring, H. *J. Chem. Phys.* **1935**, *3*(2), 107–115.

[81] Hartree, D. R. *Proc. Cambridge Phil. Soc.* **1928**, *24*, 89.

[82] Fock, V. *Z. Phys.* **1930**, *61*, 126.

[83] Szabo, A.; Ostlund, N. S. *Modern Quantum Chemistry. Introduction to Advanced Electronic Structure Theory;* Dover: New York, 1996.

[84] Shavitt, I. *Mol. Phys.* **1998**, *94*(1), 3–17.

[85] David Sherrill, C.; Schaefer, H. F. *Adv. Quantum Chem.* **1999**, *34*, 143–269.

[86] Kutzelnigg, W. *J. Mol. Struct.* **1988**, *181*, 22.

[87] Moller, C.; Plesset, M. S. *Phys. Rev.* **1934**, *46*, 618.

[88] Pople, J. A.; Krishnan, R.; Schlegel, H. B.; Binkley, J. S. *Int. J. Quantum Chem.* **1978**, *14*(5), 545–560.

[89] Bartlett, R. J.; Purvis, G. D. *Int. J. Quantum Chem.* **1978**, *14*(5), 561–581.

[90] Bartlett, R. J.; 1995; pages 1047–1131.

[91] Bartlett, R. J. *Recent Advances in Coupled-Cluster Methods*, Vol. 3 of *Recent Advances in Computational Chemistry;* WORLD SCIENTIFIC, 1997.

[92]

[93] Kryachko, E. S.; LudenÌa, E. V. *Energy Density Functional Theory of Many-Electron Systems;* Springer Netherlands, 1990.

[94] Hohenberg, P.; Kohn, W. *Phys. Rev. B* **1964**, *136*.

[95] Kohn, W.; Sham, L. J. *Phys. Rev.* **1965**, *140*.

[96] Stowasser, R.; Hoffmann, R. **1999**.

[97] Gunnarsson, O.; Lundqvist, B. I.; Wilkins, J. W. *Phys. Rev. B* **1974**, *8*(4).

[98] T. Kar J.G. Angyan, A. B. S. *J. Phys. Chem. A* **2000**, *104*, 9953.

[99] Slater, J. C. *The Self-Consistent Field for Molecules and Solids;* McGraw-Hill, 1974.

[100] Runge, E.; Gross, E. K. U. *Phys. Rev. Lett.* **1984**, *52*(12), 997–1000.

[101] Casida, M. E.; 1995; pages 155–192.

[102] Jamorski, C.; Casida, M. E.; Salahub, D. R. *J. Chem. Phys.* **1998**, *104*(13), 5134.

[103] Petersilka, M.; Gossmann, U. J.; Gross, E. K. U. *Phys. Rev. Lett.* **1996**, *76*(8), 1212–1215.

[104] Petersilka, M.; Gross, E. K. U. *Int. J. Quantum Chem.* (7), 1393–1401.

[105] Bauernschmitt, R.; Ahlrichs, R. *Chem. Phys. Lett.* **1996**, *256*(4-5), 454–464.

[106] Hirata, S.; Head-Gordon, M. *Chem. Phys. Lett.* **1999**, *302*(5-6), 375–382.

[107] Hirata, S.; Lee, T. J.; Head-Gordon, M. nov **1999**, *111*(19), 8904.

[108] Matsuzawa, N. N.; Ishitani, A.; Dixon, D. A.; Uda, T. *American Chemical Society* **2001**.

[109] Cai, Z.-L.; Reimers, J. R. *J. Chem. Phys.* **1999**, *112*(2), 527.

[110] Bauernschmitt, R.; Ahlrichs, R.; Frank H. Hennrich.; .; Kappes, M. M. **1998**.

[111] Gross, E.; Kohn, W. *Adv. Quantum Chem.* **1990**, *21*, 255–291.

[112] Stratmann, R. E.; Scuseria, G. E.; Frisch, M. J. *J. Chem. Phys.* **1998**, *109*(19), 8218.

[113] Casida, M. E.; Jamorski, C.; Casida, K. C.; Salahub, D. R. *J. Chem. Phys.* **1998**, *108*(11), 4439.

[114] Gray, C. G.; Gubbins, K. E.; Joslin, C. G. *Theory of molecular fluids;* Oxford University Press, 1984.

[115] Schatz, G. C. *Rev. Mod. Phys.* **1989**, *61*(3), 669–688.

[116] Sprik, M. *Effective Pair Potentials and Beyond;* Springer Netherlands, 1993.

[117] van Gunsteren, W. F.; Berendsen, H. J. C. *Angew. Chemie Int. Ed. English* **1990**, *29*(9), 992–1023.

[118] Car, R.; Parrinello, M. *Phys. Rev. Lett.* **1985**, *55*(22), 2471–2474.

[119] Nose, S. *J. Chem. Phys.* **1984**, *81*(1), 511–519.

[120] Hoover, W. G. **1985**, *31*(3), 1695–1697.

[121] Torrie, G. M.; Valleau, J. P. *Chem. Phys. Lett.* **1974**.

[122] Ferrenberg, A. M.; Swendsen, R. H. *Phys. Rev. Lett.* **1989**.

[123] Valleau, J. P. *ChemInform* **2010**.

[124] Metropolis, N.; Rosenbluth, A. W.; Rosenbluth, M. N.; Teller, A. H.; Teller, E. *J. Chem. Phys.* **1953**.

[125] McCammon, J. A.; Gelin, B. R.; Karplus, M. *Nature* **1977**.

[126] Scott, R.; Allen, M. P.; Tildesley, D. J. *Math. Comput.* **1991**.

[127] Allen, M. P. *Comput. Soft Matter From Synth. Polym. to Proteins, Lect. Notes* **2004**.

[128] Slater, J. C. *Phys. Rev.* **1930**, *36*(1), 57–64.

[129] Boys, S. F. *Proc. R. Soc. A Math. Phys. Eng. Sci.* **1950**, *200*(1063), 542–554.

[130] Rekondo, A.; Martin, R.; Ruiz de Luzuriaga, A.; Cabañero, G.; Grande, H. J.; Odriozola, I. *Mater. Horiz.* **2014**, *1*(2), 237–240.

[131] *ChemistryOpen* **2018**, *7*(3), 248–255.

[132] Chai, J.-D.; Head-Gordon, M. *Phys. Chem. Chem. Phys.* **2008**, *10*, 6615.

[133] Hehre, W. J.; Ditchfield, R.; Pople, J. A. *J. Chem. Phys.* **1972**, *2257*.

[134] Krishnan, R.; Binkley, J. S.; Seeger, R.; Pople, J. A. *J. Chem. Phys.* **1980**, *650*.

[135] Gaussian16 {R}evision {C}.01. Frisch, M. J.; Trucks, G. W.; Schlegel, H. B.; Scuseria, G. E.; Robb, M. A.; Cheeseman, J. R.; Scalmani, G.; Barone, V.; Petersson, G. A.; Nakatsuji, H.; Li, X.; Caricato, M.; Marenich, A. V.; Bloino, J.; Janesko, B. G.; Gomperts, R.; Mennucci, B.; Hratchian, H. P.; Ortiz, J. V.; Izmaylov, A. F.; Sonnenberg, J. L.; Williams-Young, D.; Ding, F.; Lipparini, F.; Egidi, F.; Goings, J.; Peng, B.; Petrone, A.; Henderson, T.; Ranasinghe, D.; Zakrzewski, V. G.; Gao, J.; Rega, N.; Zheng, G.; Liang, W.; Hada, M.; Ehara, M.; Toyota, K.; Fukuda, R.; Hasegawa, J.; Ishida, M.; Nakajima, T.; Honda, Y.; Kitao, O.; Nakai, H.; Vreven, T.; Throssell, K.; Montgomery Jr., J. A.; Peralta, J. E.; Ogliaro, F.; Bearpark, M. J.; Heyd, J. J.; Brothers, E. N.; Kudin, K. N.; Staroverov, V. N.; Keith, T. A.; Kobayashi, R.; Normand, J.; Raghavachari, K.; Rendell, A. P.; Burant, J. C.; Iyengar, S. S.; Tomasi, J.; Cossi, M.; Millam, J. M.; Klene, M.; Adamo, C.; Cammi, R.; Ochterski, J. W.; Martin, R. L.; Morokuma, K.; Farkas, O.; Foresman, J. B.; Fox, D. J. **2016**.

[136] Perdew, J. P.; Burke, K.; Ernerhof, H. *Phys.$\$Rev.$\$Lett.***1996**, 77, 3865.

[137] Perdew, J. P.; Burke, K.; Ernerhof, H. *Phys.\ Rev.\ Lett.* **1997**, *78*, 1396.

[138] Deglmann, P.; May, K.; Furche, F.; Ahlrichs, R. *Chem. Phys. Lett.* **2004**, *384*, 103.

[139] K. Eichkorn, O Treutler, A. R. *Chem. Phys. Lett.* **1995**, *240*, 283.

[140] Sierka, A.; Hogekamp, A.; Ahlrichs, R. *J. Chem. Phys.* **2003**, *118*, 9136.

[141] version 6.6 a development of University of Karlsruhe, T.; Forschungszentrum Karlsruhe GmbH, 1989-2007, T. G. s. . a. f. h.

[142] Reed, A. E.; Weinhold, F. **1985**, *1736*(May 2013).

[143] Reed, A. E.; Weinhold, F. **1985**, *735*.

[144] Reed, A. E.; Curtiss, L. A.; Weinhold, F. *Chem. Rev.* **1988**, *88*(6), 899–926.

[145] Evans, M. G.; Polanyi, M. *Trans. Faraday Soc.* **1935**, *31*(0), 875.

[146] Irigoyen, M.; Fernández, A.; Ruiz, A.; Ruipérez, F.; Matxain, J. *J. Org. Chem.* **2019**, *84*(7).

[147] Maier, J. A.; Martinez, C.; Kasavajhala, K.; Wickstrom, L.; Hauser, K. E.; Simmerling, C. *J. Chem. Theory Comput.* **2015**, *11*(8), 3696–3713.

[148] AMBER 14. Case, D. A.; Babin, V.; Berryman, J. T.; Betz, R. M.; Cai, Q.; Cerutti, D. S.; Cheatham III, T. E.; Darden, T. A.; Duke, R. E.; Gohlke, H.; Goetz, A. W.; Gusarov, S.; Homeyer, N.; Janowski, P.; Kaus, J.; Kolossvï¿œry, I.; Kovalenko, A.; Lee, T. S.; LeGrand, S.; Luchko, T.; Luo, R.; Madej, B.; Merz, K. M.; Paesani, F.; Roe, D. R.; Roitberg, A.; Sagui, C.; Salomon-Ferrer, R.; Seabra, G.; Simmerling, C. L.; Smith, W.; Swails, J.; Walker, R. C.; Wang, J.; Wolf, R. M.; Wu, X.; Kollman, P. A. **2014**.

[149] Torsello, M.; Pimenta, A. C.; Wolters, L. P.; Moreira, I. S.; Orian, L.; Polimeno, A. *J. Phys. Chem. A* **2016**, *120*(25), 4389–4400.

[150] Bayly, C. I.; Cieplak, P.; Cornell, W. D.; Kollman, P. A. *J. Phys. Chem.* **1993**, *97*(40), 10269–10280.

[151] Irigoyen, M.; Matxain, J. M.; Ruipérez, F. *Polymers (Basel).* **2019**, *11*(12), 1960.

[152] Reed, A. E.; Weinstock, R. B.; Weinhold, F. *J. Chem. Phys.* **1985**, *83*, 735.

[153] Savin.; A.. *On degeneracy, near-degeneracy and density functional theory;* 1997.

[154] Vosko, S. H.; Wilk, L.; Nusair, M. *Can. J. Phys.* **1980**, *58*(8), 1200–1211.

[155] Becke, A. D. *J. Chem. Phys.* **1986**, *84*(8), 4524–4529.

[156] Lee, C.; Yang, W.; Parr, R. G. *Phys. Rev. B* **1988**, *37*(2), 785–789.

[157] Tao, J.; Perdew, J. P.; Staroverov, V. N.; Scuseria, G. E. *Phys. Rev. Lett.* **2003**, *91*(14), 146401.

[158] Zhao, Y.; Truhlar, D. G. *J. Chem. Phys.* **2006**, *125*(19), 194101.

[159] Becke, A. D. *J.Chem. Phys.* **1993**, *98*, 5648.

[160] Iikura, H.; Tsuneda, T.; Yanai, T.; Hirao, K. *J. Chem. Phys.* **2001**, *115*(8), 3540–3544.

[161] Gill, P. M.; Adamson, R. D.; Pople, J. A. **1996**, *88*(4), 1005–1009.

[162] Head-gordon, M. *Phys. Chem. Chem. Phys.* **2008**, pages 6615–6620.

[163] Becke, A. D. *J. Chem. Phys.* **1998**, *107*(20), 8554.

[164] Dobson, J. F.; McLennan, K.; Rubio, A.; Wang, J.; Gould, T.; Le, H. M.; Dinte, B. P. *Aust. J. Chem.* **2001**, *54*(8), 513.

[165] Kristyán, S.; Pulay, P. *Chem. Phys. Lett.* **1994**, *229*(3), 175–180.

Appendix I: Density Functional Approximations

Although the Kohn-Sham formalism is, in principle, exact E_{xc} and V_{xc} are unknown, except for the case of the uniform electron gas. Thus, approximations have to be made.

Local Density Approximation (LDA)

The first approximation was the so-called Local Density Approximation (LDA) [153], where each volume element with local density $\rho(\vec{r})$ is considered to be a homogeneus electron gas. This approximation would be accurate if the density varies slowly in the space. The form of the exchange-correlation functional is:

$$E_{xc}^{LDA}[\rho] = \int \rho(\vec{r})\varepsilon_{xc}(\rho)d\vec{r} \tag{12.1}$$

where $\varepsilon_{xc}(\rho)$ is the exchange plus correlation energy per electron in a homogeneus electron gas with electron density ρ. An accurate expression $\varepsilon_{xc}(\rho)$ was provided by Vosko, Wilk and Nusair [154]. For open-shell systems, the Local Spin Density Approximation (LSDA) is defined by replacing the density ρ by ρ^{α} and ρ^{β}, for electrons with different spins.

Generalized Gradient Approximation (GGA)

Since ρ is far from being homogeneus, more sophisticated methods have been designed to improve the LDA approach. In order to account for the inhomogeneous character of the electron density, the variation of ρ with the distance as a gradient ($\nabla\rho(r)$) is introduced:

$$E_{xc}^{GGA}[\rho] = \int f(\rho, \nabla\rho)dr \tag{12.2}$$

These methods are called generalized gradient (GGA) approximations, and are of great importance in the study of molecules, where the electron density

can not be considered homogeneous. Usually, E_{xc}^{GGA} is split into exchange and correlation contributions:

$$E_{xc}^{GGA} = E_x^{GGA} + E_C^{GGA} \tag{12.3}$$

Many exchange functionals use the following expression for E_x^{GGA}:

$$E_x^{GGA} = E_x^{LDA} + E_x^{NLDA} = E_x^{LDA} + \int f(s)\rho^{\frac{4}{3}} dr \tag{12.4}$$

where $f(s)$ is a function of the reduced density gradient: $s = \frac{|\nabla\rho|}{\rho^{\frac{4}{3}}}$. In this way, s, which is an adimensional parameter, takes into account the inhomogeneous nature of the electron density. So, in order to construct an exchange-correlation functional, one may select the exchange functional, for example one of Becke (B86 [155], and B88 [**?**] and the correlation functional, like the one of Parr [156] and combine them.

GGA functionals are sometimes referred to as non-local functionals, which is incorrect since they are as local as LDA itself. Even so, GGA is a more accurate LDA, and its correlation-exchange functionals are in general accurate enough for most chemical applications. It was the development of the GGAs which made DFT a new player in the field of computational chemistry.

Meta-Generalized Gradient Approximation (mGGA)

In addition to the density and its gradient, GGA methods can be further improved by introducing the Laplacian of the density, $\nabla^2\rho(r)$, and/or the local kinetic energy density, defined as:

$$\tau(r) = \frac{1}{2}\sum_{i=1}^{N_{occ}} |\nabla\psi_i(r)|^2 \tag{12.5}$$

where ψ_i are the Kohn-Sham orbitals. These functionals are called meta-GGA (mGGA) and read:

$$E_{xc}^{meta-GGA}[\rho] = \int f(\rho, \nabla\rho, \nabla^2\rho) dr \tag{12.6}$$

Popular meta-GGA functionals are TPSS [157] and M06L [158].

Hybrid Functionals

Since the exchange energy is crucial for the correct description of the molecular system, the so-called hybrid functionals are based on a combination of Hartree-Fock exchange and DFT correlation. This approach is based in the so-called adiabatic connection [159]. Thus, two limiting systems, in this case the non-interacting (Kohn-Sham) system and the real system, are connected by the coupling parameter λ, which operates on the electron interaction as:

$$\hat{H}^{\lambda} = \sum_{i=1}^{N} -\frac{1}{2}\nabla_i^2 + \sum_{i=1}^{N} \hat{v}_S^{\lambda}(i) + \sum_{i=1}^{N}\sum_{j>i}^{N} \frac{\lambda}{r_i - r_j} \tag{12.7}$$

where, $\lambda = 0$ for the non-interacting system and $\lambda = 1$ for the real system. For intermediate values of λ, the effective external potential $\hat{v}_S^{\lambda}$ changes accordingly so that the density is always the real density of the system ($\rho(r)$ is independent of λ). Thus, the λ parameter softly connects both systems by simulating a continuous of partially interacting systems.

One of the most popular hybrid functionals combines the Becke's exchange [**?**] with the correlation functional Lee-Yang-Parr (LYP) [156], and the obtained functional is known as B3LYP, which is expressed as:

$$(1 - a_0)E_x^{LSDA} + a_0 E_x^{HF} + a_x E_x^{B88} + a_c E_c^{LYP} + (1 - a_c)E_c^{VWN} \tag{12.8}$$

where $a_0 = 0.20$, $a_x = 0.72$ and $a_c = 0.81$.

Appendix II: Long Range Corrected Desnity Functional Theory.

The exchange-correlation functionals have been represented by using only local quantities at a reference point, such as the electron density. It is, therefore, presumed that those functionals overestimate local contributions and underestimate non-local contributions, such as van der Waals interactions, charge-transfer processes or Rydberg excitations. The most significant non-local contribution may be the long-range electron-electron exchange interaction, because it may be impossible to represent this interaction as a functional of a one-electron quantity.

In 1996, Savin suggested a long-range correction scheme for LDA [153], where the two-electron operator, $\frac{1}{r_{12}}$, is split into the short-range and long-range terms naturally by using the standard error function:

$$\frac{1}{r_{12}} = \frac{1 - erf(\omega r_{12})}{r_{12}} + \frac{erf(\omega r_{12})}{r_{12}} \tag{12.9}$$

where $r_{12} = |r_1 - r_2|$ and ω is a parameter that determines the ratio of these parts. However, Savin's scheme is inapplicable to conventional GGA functionals. Later in 2001, Iikura et. al. [160] proposed a simplified long-range corrected (LC) hybrid scheme where the long-range (LR) exchange is treated exactly by HF theory while the short-range (SR) exchange is approximated by means of density functional approximations, such as LSDA, and the correlation functional remains the same as that of the full Coulomb interaction:

$$E_{xc}^{LC} = E_x^{LR} + E_x^{SR} + E_c \tag{12.10}$$

Thus, for the simplest LC hybrid functional, the local spin density approximation is used for the SR exchange interaction, while the LR is described using the HF exchange integral as:

$$E_x^{LR-HF} = -\frac{1}{2}\sum_{\sigma}\sum_{i,j}^{occ}\int\int \psi_{i\sigma}^*(r_1)\psi_{j\sigma}^*(r_2)\frac{erf(\omega r_{12})}{r_{12}}\psi_{j\sigma}(r_1)\psi_{i\sigma}(r_2)dr_1dr_2 \tag{12.11}$$

where $\psi_{i\sigma}$ is the i-th σ-spin orthonormal MO. On the other hand, the analytical form of the SR-LSDA exchange functional can be obtained by integration of the square of the LSDA density matrix with the SR operator [153, 161]:

$$E_x^{SR-LSDA} = \sum_\sigma \int e_{x\sigma}^{SR-LSDA}(\rho_\sigma) dr \tag{12.12}$$

Here, $e_{x\sigma}^{SR-LSDA}(\rho_\sigma)$ is the short-range LSDA exchange energy density for σ-spin,

$$e_{x\sigma}^{SR-LSDA}(\rho_\sigma) = -\frac{3}{2}\left(\frac{3}{4\pi}\right)^{\frac{1}{3}} \rho^{\frac{4}{3}}(r) F(a_\sigma) \tag{12.13}$$

where $a_\sigma \equiv \frac{\omega}{2K_{F\sigma}}$ is a dimensionless parameter that controls the values of the attenuation function $F(a_\sigma)$.

As was stated in Eq. 12.9, the parameter ω modulates the ratio between long and short-range terms, in such a way that the smaller the value of ω is, the longer ranged the short-range operator will be. As a result, the use of small values of ω in LC functionals implies that the SR exchange, which is actually not so short-ranged, is approximated by spatially-localized density functional approximations (DFA). Since the DFA exchange hole is semi-local, for relatively small ω values, the non-locality of the exchange hole should be important and may not be adequately described by SR exchange alone.

To remedy this, Head Gordon and Chai [162] suggested that introducing a small amount of the SR Hartree-Fock exchange could be helpful, and proposed a new expression for LC hybrid functionals:

$$E_{xc}^{LC-DFA} = E_x^{LR-HF} + c_x E_x^{SR-HF} + E_x^{SR-DFA} + E_c^{DFA} \tag{12.14}$$

where c_x is a fractional paramter and E_x^{SR-HF} is the short-range HF exchange, reading:

$$E_x^{SR-HF} = -\frac{1}{2}\sum_\sigma \sum_{i,j}^{occ} \int\int \psi_{i\sigma}^*(r_1)\psi_{j\sigma}^*(r_2) x \frac{erfc(\omega r_{12})}{r_{12}} \psi_{j\sigma}(r_1)\psi_{i\sigma}(r_2) dr_1 dr_2 \tag{12.15}$$

Following this scheme, and in conjunction with the BP97b [163] exchange functional, they proposed two new functionals, ωB97 and ωB97X, with the X on the latter referring to the inclusion of short range HF exchange. However, problems related to the lack of non-locality of the correlation hole, such as the lack of dispersion interactions (London forces), still remained, as the semi-local correlation functionals cannot capture long-range correlation effects [164, 165].

However, given that an empirical atom-atom dispersion potential can be added to an existing density functional, the same autors developed a new functional, namely ωB97X-D [162], based on the ones mentioned above and the DFT-D (density functional theory with empirical dispersion corrections) scheme, which reads:

$$E_{tot} = E_{KS-DFT} + E_{disp} \tag{12.16}$$

where, in this case, the E_{KS-DFT} was computed using the ωB97X functional, and the following empirical dispersion correction is used:

$$E_{disp} = -\sum_{i=1}^{N_{at}-1} \sum_{j=i+1}^{N_{at}} \frac{c_{ij}^6}{R_{ij}^6} f_{damp}(R_{ij}) \tag{12.17}$$

where N_{at} is the number of atoms of the system, c_{ij}^6 is the dispersion coefficient for atom pair ij, and R_{ij} is the interatomic distance. The conditions of zero dispersion at short interatomic distances and the asymptotic behavior are enforced by introducing a damping function:

$$f_{damp}(R_{ij}) = \frac{1}{1 - a(R_{ij}/R_r)^{-12}} \tag{12.18}$$

which reduces to one at large interatomic distances, while vanishing fast enough to prevent divergence of the undamped van der Waals potentials at small R_{ij}. R_r stands for the sum of van der Waals radii of the atomic pair r_{ij}, and the only non-linear parameter, a, controls the strength of dispersion corrections.

Appendix III: Natural Bond Orbital analysis.

Natural Bond Orbital (NBO) [144]analysis transforms the input basis set $\{\chi_i\}$ to various localized basis sets (natual atomic orbitals, NAOs, hybrid orbitlas, NHOs, and localized molecular orbitlas, NLMOs)

$$input \rightarrow basis \rightarrow NAOs \rightarrow NHOs \rightarrow NBOs \rightarrow NLMOs$$

The localized sets may be subsequently transformed to delocalized natural orbitals (NOs) or canonical molecular orbitals (MOs). Each step of the above sequence involves an orthonormal set that spans the full space of the input basis sets and can be used to give an exact representation of the calculated wavefunction and the expectation values of the selected operators (properties) of the system.

The NAO orbitals allow the calculation of an improved Natural Population Analysis correcting some of the Mulliken population analysis deficiencies. Once the NAOs are evaluated, the core orbitals (with occupancies > 1.999 e^-) are set. Following, among the one-center blocks, the lone-pairs (with occupancies > 1.90 e^-) are defined, and finally, the bond-vectors (occupancy < 1.90 e^-) are located among the two-center blocks. In this way, a "natural Lewis Structure" is obtained.

In this context, the σ_{AB} localized NBO bond is formed from the h_A and h_B NAOs.

$$\sigma_{AB} = c_A h_A + c_B h_B \tag{12.19}$$

Such natural localized functions require simoultaneously *orthonormality* and *maximum occupancy* leading to compact expressions for atomic and

bond properties. *ab initio* wave functions are found to be in good agreement with Lewis structure concepts and with the basic Pauling-Slater-Coulson picture of bond hybridization and polarization. The filled NBOs, σ_{AB}, of the "natural Lewis structure" are therefore well adapted to describe covalency effects in molecules.

The NBOs also describe the non-covalency effects like the antibonds σ^*_{AB}

$$\sigma^*_{AB} = c_B h_A - c_A h_B \tag{12.20}$$

which arise from the same set of atomic valence-shell hybrids that unite to form the bond functions σ_{AB}.

The antibonding orbital contribution to the energy, $E_{\sigma\sigma^*}$, is typically much less than 1% of the covalent contribution, reflecting the dominance of the Lewis-type component of the bonding. These corrections to the Lewis picture are usually so small as to be well approximated by simple second-order perturbative expressions.

The interaction of a filled orbital σ of the normal Lewis structure with one of the unfilled antibonding orbitals σ^* to give the second-order energy lowering, $\Delta E^{(2)}_{\sigma\sigma^*}$, in SCF-MO theory, is given by the formula,

$$\Delta E^{(2)}_{\sigma\sigma^*} = -2\frac{< \sigma|\hat{F}|\sigma^* >^2}{\epsilon_{\sigma^*} - \epsilon_\sigma} \tag{12.21}$$

where $\hat{F}$ is the Fock operator and ϵ_σ and ϵ_{σ^*} are the NBO orbital energies. The NBO perturbative framework permits one to apply qualitative concepts of valence theory to describe the non-covalent energy lowering.

Since the non-covalent delocalization effects are associated with $\sigma \rightarrow \sigma^*$interactions between filled (donor) and empty (acceptor) orbitals, it is natural to describe them as being of "donor-acceptor", "charge-transfer" or generalized "Lewis base-Lewis acid" type.

For a good and illustrative review of NBO and its applications, see the review article by Reed, Curtis and Weinhold [144].

Appendix IV: Theoretical protocol

Based on these two works, the authors proposed a new theoretical protocol to estimate the self-healing capacity of disulfide-based materials, depending on three parameters directly related to the previously discussed features. Thus, the first parameter is the probability to generate sulfenyl radicals (ρ), which is governed by the dissociation of the S-S bond:

$$\rho = \frac{N_{S-S}}{N_{Tot}} \tag{22}$$

This parameter is calculated from quantum molecular dynamics, and is defined as the number of simulation steps where the S-S bond distance is longer than 2.3 Å (N_{S-S}), a value for which, in disulfide-based materials, the bond may be considered dissociated (and the radical formed), divided by the total number of simulation steps, N_{tot}.

The second parameter is the exchange reaction rate constant (k), which is estimated according to the Wigner, Eyring, Polanyi and Evans formulation of the Transition State Theory [145, 80]:

$$k = \frac{k_B T}{h} e^{-\Delta G/RT} \tag{23}$$

where R, k_B and h are the ideal gas, Boltzmann and Planck constants, respectively, and ΔG is the activation energy.

The third parameter is related to the influence of the hydrogen bonding in the mobility of the chains, in such a way that the generated sulfenyl radical may attack another neighboring disulfide bond. Thus, this parameter is

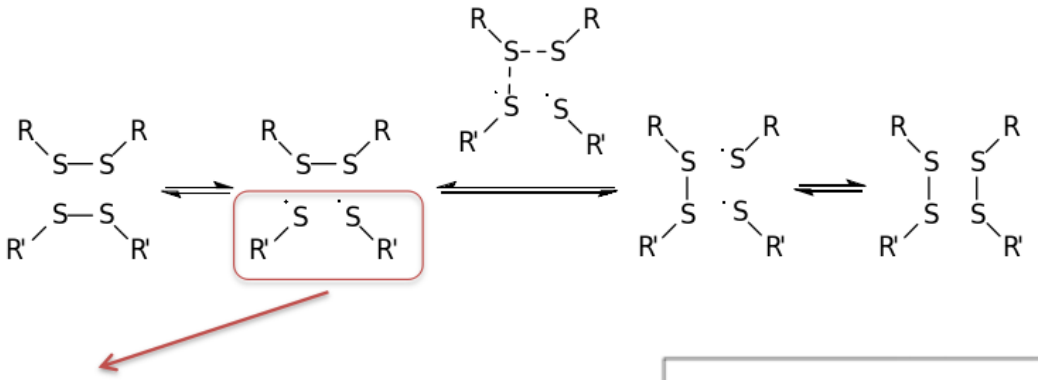

• Probability of radicals to be formed thermally

$$\rho = \frac{N_{S\text{-}S}}{N_{tot}}$$

- $N_{S\text{-}S}$: number of simulation steps where SS bonds larger than the selected threshold are found.
- N_{tot} : total number of simulation steps.

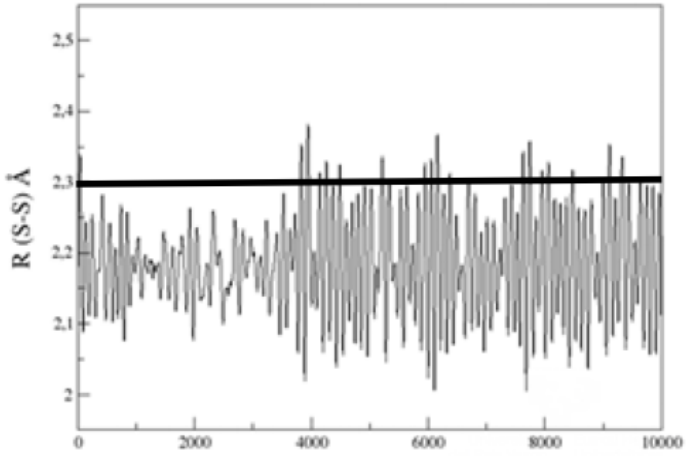

Figure 1: Graphical explanation of how ρ is calculated by means of *ab initio* molecular dynamics.

based on the distance between disulfides and three regions are defined: i) the reacting region, where disulfides are close enough to undergo the exchange reaction (R $\leq$ 4.5 Å), ii) the neighboring region, where disulfides are far to react but with a non-negligible probability to approach the reacting region (4.5 $<$ R$<$ 20 Å), and iii) the external region, where disulfides are neglected (R $>$ 20 Å). Certainly, the size of the third region is dependent on the size of the system considered, while the first two regions are system-independent for large enough chains. The amount of sulfur atoms located in each region is calculated by integration of the radial distribution function within the limits defined above. The authors denote this integral values as I_i, I_{ii} and I_{iii}, in regions i, ii and iii, respectively. With this information, the parameter ω is defined as the number of disulfides that lie inside the reacting region. In this way, the percentage of disulfides that would be close enough for the exchange reaction can be estimated according to the following equation:

$$\omega = \frac{I_i}{I_i + I_{ii}} \tag{24}$$

Larger values of ω denote larger probability for disulfides to be in the reacting region, that is, larger values of ω may indicate larger theoretical self-healing capacity. Still, the size of the mentioned regions may only be valid for disulfides, and other regions may be selected for systems with different sizes.

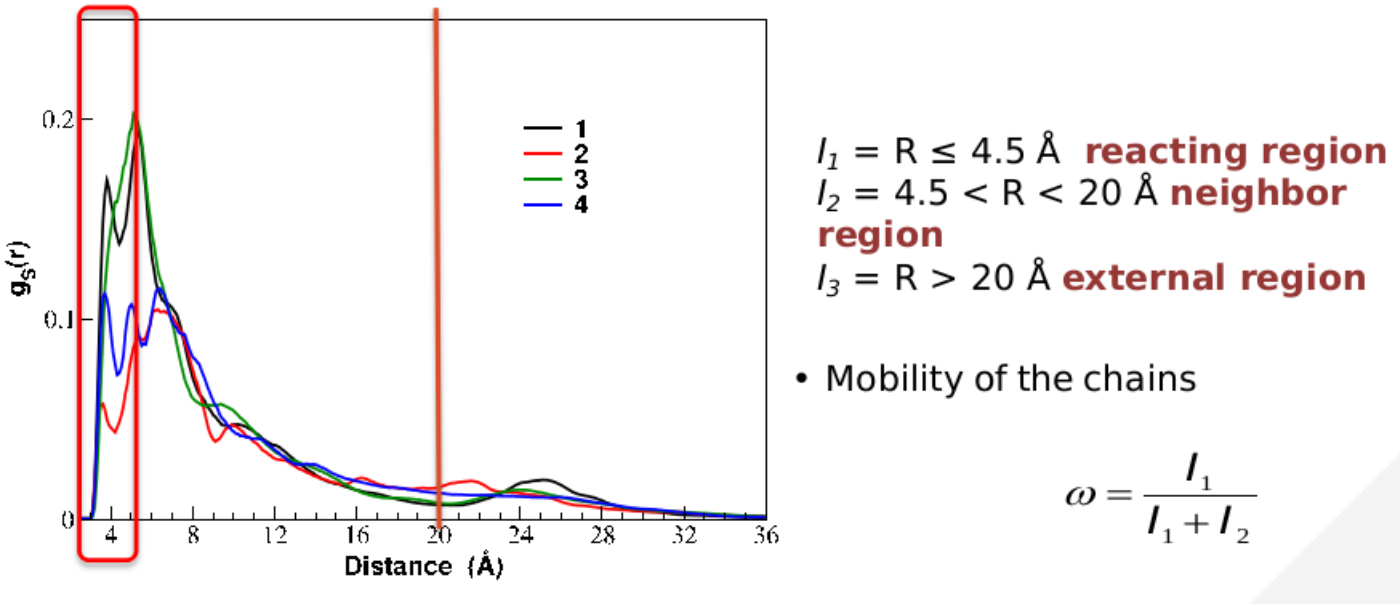

Figure 2: Graphical description of how ω is calculated by integration of different regions of the radial distribution function of the sulfur atoms

Appendix V: Supporting Information for Chapter 3

Table 1: Nature of the $S_0 \rightarrow S_1$ transition, vertical absorption wavelength (λ), in nm, and oscillator strength (f), calculated at the ωB97XD/6-311++G(2df,2p)//ωB97XD/6-31+G(d,p) level of theory.

		S-S			Se-Se			Se-S		
Model	R	$S_0 \rightarrow S_1$	λ	f	$S_0 \rightarrow S_1$	λ	f	$S_0 \rightarrow S_1$	λ	f
PD-XX	R_1	$\pi \rightarrow \sigma^*$	359.9	0.0102	$\pi \rightarrow \sigma^*$	411.4	0.0066	$\pi \rightarrow \sigma^*$	347.0	0.0091
	R_2	$\pi \rightarrow \sigma^*$	357.1	0.0070	$\pi \rightarrow \sigma^*$	412.4	0.0049	$\pi \rightarrow \sigma^*$	386.2	0.0052
	R_3	$\pi \rightarrow \sigma^*$	321.2	0.0204	$\pi \rightarrow \sigma^*$	380.3	0.0074	$\pi \rightarrow \sigma^*$	357.1	0.0114
	R_4	$\pi \rightarrow \sigma^*$	344.5	0.0103	$\pi \rightarrow \sigma^*$	428.9	0.0041	$\pi \rightarrow \sigma^*$	363.8	0.0114
	R_5	$\pi \rightarrow \sigma^*$	319.2	0.0129	$\pi \rightarrow \sigma^*$	396.9	0.0053	$\pi \rightarrow \sigma^*$	369.1	0.0114
	R_6	$\pi \rightarrow \sigma^*$	325.3	0.0150	$\pi \rightarrow \sigma^*$	427.4	0.0040	$\pi \rightarrow \sigma^*$	350.0	0.0112
	R_7	$\pi \rightarrow \sigma^*$	319.6	0.0228	$\pi \rightarrow \sigma^*$	373.2	0.0076	$\pi \rightarrow \sigma^*$	353.2	0.0089
PA-XX	R_1	$\pi \rightarrow \sigma^*$	292.5	0.1508	$\pi \rightarrow \sigma^*$	316.0	0.1428	$\pi \rightarrow \sigma^*$	298.7	0.6170
	R_2	$\pi \rightarrow \sigma^*$	282.9	0.1730	$\pi \rightarrow \sigma^*$	318.7	0.0440	$\pi \rightarrow \sigma^*$	289.0	0.0761
	R_3	$\pi \rightarrow \sigma^*$	286.4	0.1369	$\pi \rightarrow \sigma^*$	311.0	0.1574	$\pi \rightarrow \sigma^*$	297.5	0.1105
	R_4	$\pi \rightarrow \sigma^*$	286.4	0.1263	$\pi \rightarrow \sigma^*$	352.3	0.0349	$\pi \rightarrow \sigma^*$	313.6	0.1214
	R_5	$\pi \rightarrow \sigma^*$	289.0	0.1333	$\pi \rightarrow \sigma^*$	311.6	0.1573	$\pi \rightarrow \sigma^*$	278.3	0.0220
	R_6	$\pi \rightarrow \sigma^*$	290.7	0.1569	$\pi \rightarrow \sigma^*$	322.4	0.0314	$\pi \rightarrow \sigma^*$	304.0	0.0892
	R_7	$\pi \rightarrow \sigma^*$	286.2	0.7544	$\pi \rightarrow \sigma^*$	321.0	0.0331	$\pi \rightarrow \sigma^*$	299.1	0.0928
PF-XX	R_1	$\sigma \rightarrow \sigma^*$	239.0	0.0340	$\sigma \rightarrow \sigma^*$	278.4	0.0202	$\sigma \rightarrow \sigma^*$	269.5	0.0065
	R_2	$\sigma \rightarrow \sigma^*$	232.1	0.0000	$\sigma \rightarrow \sigma^*$	288.3	0.0043	$\sigma \rightarrow \sigma^*$	282.7	0.0018
	R_3	$\sigma \rightarrow \sigma^*$	228.3	0.0056	$\sigma \rightarrow \sigma^*$	286.1	0.0027	$\sigma \rightarrow \sigma^*$	258.7	0.0038
	R_4	$\sigma \rightarrow \sigma^*$	229.5	0.0057	$\sigma \rightarrow \sigma^*$	282.9	0.0028	$\sigma \rightarrow \sigma^*$	262.3	0.0044
	R_5	$\sigma \rightarrow \sigma^*$	232.0	0.0234	$\sigma \rightarrow \sigma^*$	291.2	0.0040	$\sigma \rightarrow \sigma^*$	254.3	0.0054
	R_6	$\sigma \rightarrow \sigma^*$	237.8	0.0013	$\sigma \rightarrow \sigma^*$	270.7	0.0176	$\sigma \rightarrow \sigma^*$	267.2	0.0067
	R_7	$\sigma \rightarrow \sigma^*$	237.6	0.0102	$\sigma \rightarrow \sigma^*$	271.6	0.0225	$\sigma \rightarrow \sigma^*$	266.7	0.0077

[H] Table S1 Spin density on chalcogen atom (ρ_X), occupation numbers for the antibonding orbitals and bond order (BO) of the dichalcogenide bonds.

		S-S				Se-Se				Se-S				
Model	R	ρ_S	$\eta(\sigma_{SS})$	$\eta(\sigma^*_{SS})$	BO(σ_{SS})	ρ_{Se}	$\eta(\sigma_{SeSe})$	$\eta(\sigma^*_{SeSe})$	BO(σ_{SeSe})	ρ_{Se}	ρ_S	$\eta(\sigma_{SeS})$	$\eta(\sigma^*_{SeS})$	BO(σ_{SeS})
PD-XX	R_1	0.769	1.960	0.058	0.951	0.842	1.958	0.058	0.953	0.769	0.835	1.96	0.060	0.950
	R_2	0.804	1.961	0.052	0.955	0.872	1.959	0.049	0.955	0.804	0.860	1.959	0.055	0.952
	R_3	0.725	1.962	0.070	0.946	0.812	1.960	0.066	0.947	0.725	0.812	1.960	0.069	0.945
	R_4	0.722	1.979	0.023	0.978	0.809	1.959	0.077	0.941	0.722	0.809	1.960	0.071	0.945
	R_5	0.726	1.958	0.087	0.936	0.812	1.960	0.070	0.945	0.726	0.812	1.960	0.071	0.944
	R_6	0.779	1.962	0.061	0.950	0.847	1.957	0.061	0.948	0.779	0.847	1.960	0.058	0.951
	R_7	0.778	1.962	0.040	0.961	0.842	1.959	0.058	0.951	0.778	0.842	1.960	0.061	0.949
PA-XX	R_1	0.667	1.9758	0.145	0.913	0.687	1.975	0.129	0.923	0.668	0.717	1.978	0.148	0.915
	R_2	0.679	1.9759	0.145	0.916	0.705	1.973	0.136	0.919	0.684	0.711	1.976	0.132	0.922
	R_3	0.652	1.9767	0.142	0.918	0.672	1.975	0.127	0.924	0.656	0.672	1.975	0.159	0.908
	R_4	0.650	1.9762	0.143	0.917	0.669	1.971	0.143	0.914	0.654	0.669	1.975	0.167	0.904
	R_5	0.652	1.9766	0.143	0.917	0.671	1.975	0.129	0.923	0.656	0.671	1.974	0.146	0.914
	R_6	0.679	1.9761	0.146	0.914	0.703	1.973	0.138	0.918	0.679	0.703	1.976	0.152	0.912
	R_7	0.674	1.9761	0.159	0.901	0.697	1.973	0.137	0.918	0.674	0.697	1.975	0.158	0.909
PF-XX	R_1	0.804	1.9774	0.117	0.930	0.846	1.977	0.101	0.938	0.804	0.846	1.979	0.113	0.933
	R_2	0.868	1.9776	0.079	0.949	0.927	1.977	0.061	0.958	0.868	0.896	1.978	0.066	0.957
	R_3	0.760	1.9810	0.123	0.929	0.794	1.980	0.051	0.964	0.760	0.794	1.978	0.149	0.914
	R_4	0.751	1.9805	0.124	0.928	0.743	1.980	0.107	0.936	0.725	0.743	1.977	0.153	0.912
	R_5	0.736	1.9793	0.135	0.922	0.796	1.979	0.099	0.940	0.760	0.796	1.977	0.135	0.921
	R_6	0.820	1.9779	0.101	0.939	0.865	1.978	0.084	0.947	0.820	0.865	1.978	0.089	0.945
	R_7	0.810	1.9777	0.098	0.940	0.857	1.978	0.088	0.945	0.810	0.857	1.978	0.093	0.942

Appendix VI: Supporting Information for Chapter 5

Figure 3: Small model structrues for quantum simulations

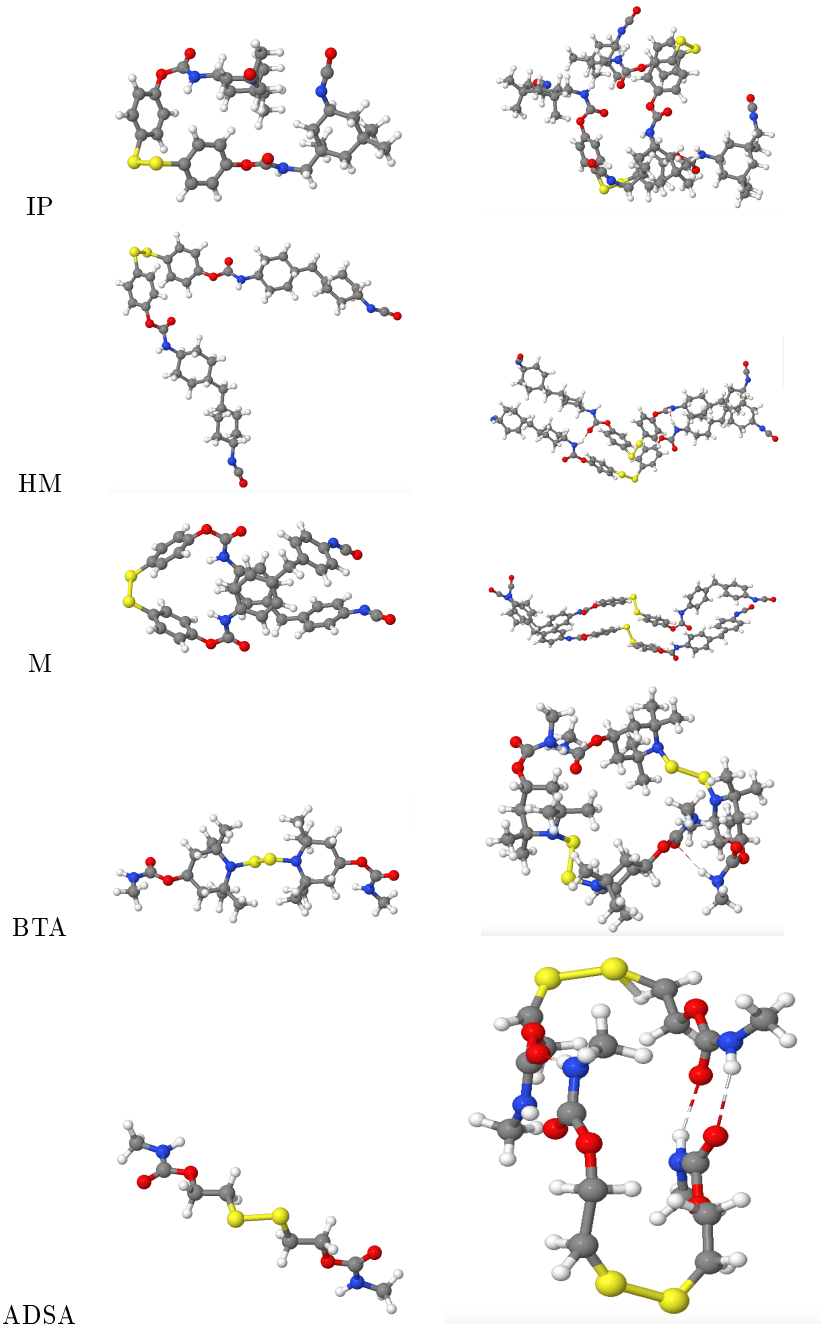

Figure 4: Single-chain models and simulation boxes used for Molecular Dynamics simulations.